

Institut für Technische Mechanik  
Abteilung Dynamik

## Dissertation

# On Modeling, Analysis and Nonlinear Control of Hydraulic Systems

Dipl.Wirtsch.-Ing. Marius Alexander  
Köster



# **On Modeling, Analysis and Nonlinear Control of Hydraulic Systems**

---

Zur Erlangung des akademischen Grades

**Doktor der Ingenieurwissenschaften**

der  
Fakultät für Maschinenbau  
Karlsruher Institut für Technologie (KIT)

genehmigte  
**Dissertation**

von

**Dipl.Wirtsch.-Ing. Marius Alexander Köster**  
aus Königstein/Ts.

---

Tag der mündlichen Prüfung:

13.04.2017

Hauptreferent:

Prof. Dr.-Ing. habil. Alexander Fidlin

Korreferent:

Univ. Prof. Dipl.-Ing. Dr. techn. Stefan Jakubek



# Abstract

Hydraulic circuits are widely featured in engineering systems of various kinds. Despite their long history and important role in technology advances, analysis of hydraulic systems from a dynamics point of view has remained poorly covered by research. Therefore, questions of hydraulic modeling, analysis and control are treated in the present thesis.

In the first part of this thesis, an elaborate minimal model of a translatory-type variable displacement vane pump is derived. The model is a physical model based on the nonlinear kinematics of the pump. It provides detailed insight into the relationship between pump cam ring eccentricity, load pressure and internal pump forces resulting from internal pressure distribution within the pump.

Building on the minimal model of such a pump, a classic hydraulic circuit variable displacement pumps are frequently used in is then modeled. Due to switching properties of the passive regulator valve used in such circuits, the aggregate system model features switched system behavior. In order to make the system accessible by eigenvalue-based stability analysis, the system model is regularized by taking into account leakage flow in the regulator valve for which a minimal model is derived, too. Equilibrium stability under variation of system pressure, load flow and viscosity are then discussed. The stability discussion is prepared by stability analysis of a simplified pressure regulator valve.

Motivated by loss of equilibrium stability under certain operating conditions, a model-based nonlinear control approach for the volume flow provided by a variable displacement vane pump is derived in the second part of the thesis. By replacing the passive regulator valve with a (active) servo valve and appropriately modeling the resulting aggregate system, the system can be subjected to feedback linearization in spite of switched system behavior. The feedback linearization concept is extensively discussed with respect to stability and extended to output feedback concepts by application of high-gain and tracking observers.

Ultimately, feasibility of the control concept in the multiple-input-multiple-output context of automotive clutch actuation is demonstrated. The concept is extended by observer concepts specific to clutch actuation.



# Contents

Abstract . . . . .	V
Danksagung . . . . .	XI
<b>Introduction</b>	<b>1</b>
<b>Motivation</b>	<b>1</b>
<b>State of Research</b>	<b>3</b>
Analysis of Hydraulic Systems . . . . .	3
Variable Displacement Vane Pumps . . . . .	4
Control of Hydraulic Systems . . . . .	5
Non-Smooth Dynamics . . . . .	5
<b>Thesis Purpose</b>	<b>7</b>
<b>Thesis Structure</b>	<b>7</b>
<b>I Modeling and Analysis of Hydraulic Systems</b>	<b>9</b>
<b>1 Fundamentals of Hydraulic Modeling</b>	<b>11</b>
1.1 Capacitances and Hydraulic Stiffness . . . . .	11
1.2 Hydraulic Resistances . . . . .	13
1.2.1 Orifice . . . . .	13
1.2.2 Throttle . . . . .	14
1.3 Damping in Hydraulic Elements . . . . .	15
1.4 Hydraulic Inductance and Flow Forces . . . . .	16
<b>2 Modeling Control Edge Flow</b>	<b>17</b>
2.1 Background . . . . .	17
2.2 Generic Leakage Flow Model . . . . .	18
2.3 Geometry-specific Leakage Flow Models . . . . .	20
2.3.1 Rectangular Notch . . . . .	20
2.3.2 Triangular Notch . . . . .	22
2.3.3 Circular Notch . . . . .	26
2.4 Flow Direction, Overlap and Opening Direction Transformations . . . . .	28

2.5	Intermediate Conclusion . . . . .	28
<b>3</b>	<b>Modeling and Analysis of a Pressure Control Valve</b>	<b>31</b>
3.1	Background . . . . .	31
3.2	System Description . . . . .	32
3.3	System Model . . . . .	33
3.4	Stability Analysis . . . . .	33
3.4.1	Non-Dimensionalization . . . . .	34
3.4.2	Stability Analysis for Non-Zero Load Flow . . . . .	36
3.4.3	Stability Analysis for Zero Load Flow . . . . .	40
3.5	Forced Response of the Pressure Control Valve . . . . .	44
3.6	Optimality Properties of the Pressure Control Valve . . . . .	47
3.7	Intermediate Conclusion . . . . .	51
<b>4</b>	<b>Modeling and Simulating Clutch Actuation in an Automatic Transmission</b>	<b>53</b>
4.1	Background . . . . .	53
4.2	System Description . . . . .	53
4.3	System Model . . . . .	56
4.4	Simulation Results . . . . .	59
4.5	Intermediate Conclusion . . . . .	60
<b>5</b>	<b>Modeling of a Variable Displacement Vane Pump</b>	<b>65</b>
5.1	Background . . . . .	65
5.2	Pump Description . . . . .	66
5.3	Pump Model . . . . .	68
5.3.1	Pump Kinematics . . . . .	68
5.3.2	Pump Forces . . . . .	69
5.3.3	Pump Volume Flow . . . . .	83
5.4	Intermediate Conclusion . . . . .	84
<b>6</b>	<b>Modeling and Analysis of a Variable Displacement Vane Pump System</b>	<b>87</b>
6.1	Background . . . . .	87
6.2	System Description . . . . .	87
6.3	System Model . . . . .	88
6.4	Simulation Results and Stability Analysis . . . . .	91
6.4.1	Non-Dimensionalization . . . . .	92
6.4.2	Simulation Results . . . . .	93
6.4.3	Stability Analysis . . . . .	94
6.5	Intermediate Conclusion . . . . .	103

<b>II</b>	<b>Nonlinear Control of Hydraulic Systems</b>	<b>105</b>
<b>7</b>	<b>Fundamentals of Feedback-Linearizing Control</b>	<b>107</b>
7.1	Fundamentals of Single-Input-Single-Output Feedback-Linearizing Control . . . . .	107
7.2	Fundamentals of Multiple-Input-Multiple-Output Feedback-Linearizing Control . . . . .	114
<b>8</b>	<b>Nonlinear Volume Flow Control of a Variable Displacement Vane Pump</b>	<b>119</b>
8.1	Background . . . . .	119
8.2	System Description . . . . .	120
8.3	SISO Model . . . . .	120
8.4	Feedback-Linearizing Control . . . . .	122
8.4.1	Control Synthesis for a Drop in Volume Flow . . . . .	123
8.4.2	Control Synthesis for a Rise in Volume Flow . . . . .	128
8.4.3	Boundedness of Tracking . . . . .	132
8.4.4	Simulation Results . . . . .	135
8.5	Adaptive Feedback-Linearizing Control . . . . .	137
8.6	Nonlinear Observer Design . . . . .	143
8.6.1	High Gain Observer . . . . .	143
8.6.2	Nonlinear Local Observer . . . . .	156
8.7	Feedforward-Linearizing Control . . . . .	166
8.8	Intermediate Conclusion . . . . .	169
<b>9</b>	<b>Nonlinear Control of a Transmission Featuring a Variable Displacement Vane Pump</b>	<b>171</b>
9.1	Background . . . . .	171
9.2	System Description . . . . .	171
9.3	MIMO Model . . . . .	173
9.4	Feedback-Linearizing Control . . . . .	176
9.4.1	Control Synthesis . . . . .	176
9.4.2	Simulation Results . . . . .	180
9.5	Observer Designs for Clutch Actuation . . . . .	183
9.5.1	Disturbance Observer . . . . .	184
9.5.2	<i>PI</i> -Observer . . . . .	186
9.6	Intermediate Conclusion . . . . .	190
<b>10</b>	<b>Identification of a Hydraulic Consumer</b>	<b>191</b>
10.1	Background . . . . .	191
10.2	System Description . . . . .	194
10.3	System Model . . . . .	195
10.4	Identification Approach . . . . .	196
10.4.1	Identification of the System Capacitance . . . . .	196

10.4.2	Identifcation of the Clutch . . . . .	196
10.4.3	Identification of the Valve . . . . .	198
10.5	Intermediate Conclusion . . . . .	205
	<b>Conclusion and Outlook</b>	<b>207</b>
	<b>Appendix</b>	<b>213</b>
	<b>A Theorems</b>	<b>213</b>
	<b>Bibliography</b>	<b>215</b>
	<b>Publications</b>	<b>225</b>
	<b>Supervision of student thesis assignments</b>	<b>227</b>

# Danksagung

Die vorliegende Arbeit entstand während meiner Tätigkeit als wissenschaftlicher Mitarbeiter am Institut für Technische Mechanik (ITM), Abteilung Dynamik/Mechatronik des Karlsruher Instituts für Technologie (KIT).

An erster Stelle gilt mein Dank Prof. Dr.-Ing. habil. Alexander Fidlin, der dieses Thema angeregt und über die fünf Jahre meiner Institutsangehörigkeit begleitet hat. Während meiner Zeit am Institut hat er mir Gelegenheit gegeben, sehr viel zu lernen und mich weiterzuentwickeln. Mein herzlicher Dank gebührt auch Herrn Univ. Prof. Dipl.-Ing. Dr. techn. Stefan Jakobek von der TU Wien für die freundliche Übernahme des Korreferats zu dieser Arbeit und die produktive Zusammenarbeit im Zusammenhang mit dem FFG-Projekt 850729. Herrn Prof. Dr.-Ing. Peter Elsner vom Institut für Angewandte Materialien des KIT danke ich für die Übernahme des Prüfungsvorsitzes.

Herrn Prof. Dr.-Ing. Wolfgang Seemann danke ich für sein Vertrauen in mich und sein stets offenes Ohr. Herrn Prof. Dr.-Ing. Carsten Proppe danke ich für die jederzeit konstruktive und angenehme Zusammenarbeit am Institut.

Ein besonderes Dankeschön möchte ich den emeritierten Professoren Prof. Dr.-Ing. h.c. Jörg Wauer, Prof. Dr.-Ing. Walter Wedig und Prof. Dr.-Ing. h.c. Jens Wittenburg aussprechen, deren Engagement das Institut anhaltend bereichert. Es sei ihnen für ihr Interesse an und ihre Anmerkungen zu meiner Arbeit sowie zahlreiche interessante Gespräche zu Themen abseits der Mechanik und Systemdynamik gedankt. Herrn Professor Dr.-Ing. h.c. Jörg Wauer möchte ich besonders für sein wohlwollendes Interesse an meiner Arbeit und seine wertvolle und konstruktive Kritik der schriftlichen Ausarbeitung danken.

Vielen Dank an Frau Barbara Windbiel, Frau Gudrun Volz, Frau Sylvia Gelsok und Frau Elke Höllig für Ihre Unterstützung in kleineren und größeren Dingen und auch einfach so.

Ich möchte allen wissenschaftlichen Mitarbeitern des Instituts, deren Zeit am Institut sich mit meiner überschneidet, meinen Dank aussprechen. Die Atmosphäre unter den Kollegen werde ich in bester Erinnerung halten, sowohl in Hinblick auf den fachlichen Austausch als auch auf den persönlichen. Besonders hervorheben möchte ich unter der „älteren“ Generation an dieser Stelle ohne besondere Reihenfolge Heike Vogt, Karolina Bach, Claudia Bellanger und Dominik Kern. Unter „meiner“ Generation von Mitarbeitern fühle ich mich gegenüber Christoph Baum, Jens Deppler, Georg Jehle, Ulrich Römer und Philipp Mall zu besonderem Dank verpflichtet. Ihr stets offenes Ohr für Anliegen aller Art waren wesentlich für meine Zeit hier am Institut. Viele unserer Diskussionen haben Eingang in meine Arbeit gefunden – ich schätze mich glücklich, von und

mit ihnen gelernt zu haben. Georg Jehle sei darüber hinaus besonders gedankt: Es war mir eine Ehre, mit ihm auf einem Projekt zur Parameteridentifikation für die AVL List GmbH, das auch in diese Arbeit eingeflossen ist, sowie auf einem weiteren Industrieprojekt zusammenzuarbeiten.

Auch Prof. Dr.-Ing. Hartmut Hetzler war prägend für meine Zeit am Institut. Sein Weggang ist ein großer Verlust für das ITM und ein großer Gewinn für die Universität Kassel – ihm sei für zahlreiche interessante fachliche und nichtfachliche Gespräche sowie seine stetige Hilfsbereitschaft und Unterstützung gedankt.

Ein herzlicher Dank auch an all die interessierten Studenten, deren Fragen die von mir gehaltenen Lehrveranstaltungen bereichert haben, sowie an meine Abschlussarbeiter. Hier möchte ich vor allem Florian Engelhorn und Simon Schröders nennen, die wertvolle Voruntersuchungen zu manchen der hier behandelten Probleme vorgenommen haben.

Der AVL List GmbH sowie der österreichischen FFG danke ich für die finanzielle Förderung der vorliegenden Arbeit, Frau Helene Gamper aus der Rechtsabteilung für ihr Engagement in den Belangen des KIT und des ITM.

Aus meiner Darmstädter Zeit danke ich der gesamten TU für eine tolle Ausbildung, die mir viel fachlichen Freiraum gelassen und viele Möglichkeiten eröffnet hat. Besonders danken möchte ich Herrn Prof. Dr. Peter Hagedorn für sein hervorragendes Engagement in Forschung, Lehre und internationaler Kooperation, von dem ich nachhaltig profitieren durfte.

Danken möchte ich auch meinen Eltern und meiner Familie, die mich auf meinem Bildungsweg stets gefördert und unterstützt hat. Familie Lüthi aus Richterswil/CH sei für viele schöne Wochenenden in der Zürichsee-Region und ihre Anteilnahme gedankt. Auch Mechthild Gerhard und Harald Lohsse möchte ich für ihr Interesse und ihre Anteilnahme an meinen Geschicken über viele Jahre hinweg danken.

Ohne meinen lieben Freund Christian Kraft hätte ich oft nicht den nötigen Abstand zur Promotion gefunden. Ich danke ihm für die vielen Jahre seiner Freundschaft sowie dafür, in Phasen akuter Unzufriedenheit stets an den Erfolg dieses Projekts geglaubt und mich mit seinem bewährten Humor zerstreut zu haben.

Meiner lieben Therese danke ich für die wunderbaren Jahre an ihrer Seite. Im Kontext unserer Karlsruher Zeit möchte ich ihr besonders für ihren Rückhalt bei meiner Promotion sowie ihre Geduld danken, wenn ich wegen irgendeines Problems im Zusammenhang mit dieser Arbeit wiederholt in Paralleluniversen unterwegs war. Auch unserem kleinen Johann bin ich besonders dankbar: er hat mit seinem Eintritt in Thereses und mein Leben in der Endphase meiner Promotionszeit für einen wunderbaren Ausgleich gesorgt und mich mit tief empfundener Freude und Dankbarkeit erfüllt.

Karlsruhe, den 28.05.2017

Dipl.Wirtsch.-Ing. Marius Alexander Köster

# Introduction

## Motivation

In the modern world's engineering design, hydraulics has been playing a prominent role ever since, the origins of its technical application dating back to the end of the 18th century. Conceived with the idea in mind to have a compressible fluid exert forces onto reaction areas of movable components and to thereby move large loads within short time, the field has found application in numerous solutions to man's practical problems. In the course of engineering history, it was a natural idea to introduce the principles of hydraulic actuation to mobile working machinery and automotive systems as well. Here, large forces have to be exerted under demanding operating conditions and in many cases little mounting space. Amongst others, hydraulic systems are used for servo-steering mechanisms as well as clutch actuation in order for a drivetrain torque to be transferred.

While hydraulic circuits come in a variety of topologies, they all feature an energy source in the form of a hydraulic pump. In order for these systems to work according to specification, it is necessary to control the flow of energy provided by the pump. This is achieved through the utilization of hydraulic resistances that can be varied in such a way that fluid energy is allocated as desired.

The single most important element to control energy flow in a hydraulic circuit is a valve. As hydraulic circuits come in a wide range of topologies, so do valves - their common feature being a movable valve body or spool that is seated in a housing and by being displaced allows a (variable) volume flow to pass through the valve.

Based upon the type of actuation of the flow-controlling valves, hydraulic systems can be distinguished into self-regulating and externally controlled or actuated systems. While a strict distinction cannot always be clearly made and in any circumstance all hydraulic systems have to fulfill a certain control purpose, self-regulating systems shall be understood in the context of this work as systems where hydraulic valves react to changes in volume flow and pressure and by their autonomous behavior control for a certain equilibrium *themselves*. Classical examples here are pressure limitation valves, pressure control valves and volume flow control valves. Such self-regulating hydraulic systems are essentially passive.

This stands in contrast to systems where valves can be actuated through external signals, mainly in the form of a current or voltage input. This input translates into an actuation force displacing the valve spool and opening a flow area inside the valve, thereby allowing for a control of the volume flow through the valve. Prominent examples are systems featuring e.g. servo or proportional valves.

While the underlying physical laws of hydraulic systems have been researched extensively, stability issues with self-regulating hydraulic systems have remained a phenomenon barely touched by research. This should come somewhat surprisingly as oscillation phenomena in hydraulic systems of various kinds are a problem well-known to practitioners.

The reasons for this underrepresentation of hydraulics in dynamics research have different aspects. Firstly, hydraulics are a field with strong practical relevance, indicating that a majority of research is actually conducted in private companies so that generated insight remains undisclosed in many cases. Secondly, the dynamics of hydraulic systems are very complex in the sense that the mathematical tools to analyze idealized hydraulic systems with are not developed to an extent that they can easily be applied to an arbitrary system featuring hydraulic components. Especially within the context of self-regulating hydraulic systems, the underlying idealized dynamics inevitably lead to a non-smooth system formulation. While methods for the stability analysis of non-smooth systems have been conceived, they have not been researched to the extent of general applicability to problems of hydraulics. These problems are often characterized by critically lapped valves so that the non-smoothness of the problem implies a switching behavior innate to the system. The problem related to switching is in many cases aggravated by the circumstance that even a single valve does not necessarily imply a single non-smoothness interacting with one pressure state of the system. Depending on the topology of the system and the system's point in state space, interactions with a varying number of capacitances in one and the same system are often encountered and will also feature in the present work. In addition, for systems with critically lapped valves, the equilibrium position is located on the switching surface in some cases so that in theory, eigenvalues-based stability analysis is an invalid approach. In principle, only Lyapunov-based methods apply for a systematic assessment of the stability properties of a certain system. Because no systematic method to devise Lyapunov function candidates is known to date and even the simplest hydraulic valve involves two states related to the mechanical behavior of the valve and one state related to the system pressure, Lyapunov-based analysis is not feasible in the majority of cases. Thirdly, hydraulic systems typically feature a large number of parameters, making them very difficult to investigate comprehensively. Ultimately, the physical stiffness of hydraulic systems mirrored in numerically stiff equations make a numerical treatment difficult.

Directing one's attention towards the key sources of hydraulic energy, pumps can, for example, be distinguished according to their mode of operation. Fixed displacement pumps operate with a fixed charging volume so that the only possibility to adjust volume flow is to alter the pump's revolution speed. Due to the problem of accelerating the rotating components if the number of revolutions per minute are to be increased or decreased, these pumps may not lend themselves ideally to applications where a dynamically varying volume flow is required. In contrast, this can be achieved by so-called variable displacement pumps where the charging volume is a function of the

displacement of a certain component whose position can be varied according to the requirements of the problem.

One of the most frequently used providers of hydraulic energy in mid-pressure applications are variable displacement vane pumps. In some cases, the pump is to provide a certain volume flow while in other cases a certain pressure shall be held. Each of these concepts is referred to as a control concept. Among the different usage scenarios, variable displacement vane pumps are frequently used in automotive applications, i.e. in transmission systems. Here, they typically are to provide a number of hydraulic consumers with volume flow. The main consumer usually is a clutch while cooling and lubrication circuits are secondary consumers. The control purpose is to ensure a fast pressure increase in the clutch upon clutch actuation. This requires maximum volume flow from the pump. Once this goal is achieved, the pump shall provide the secondary consumers with volume flow. The volume flow required by the secondary consumer(s) lies significantly below the volume flow required for achieving the main control purpose. It is evident that there lies a significant energy saving potential in employing variable displacement pumps in this context.

Considering today's pronounced relevance of energy efficiency for engineering systems in general, control strategies are needed that stably control for energy efficient system behavior. For hydraulic systems, this means stable control of volume flow and pressure. In the past, this was achieved mainly by self-regulating hydraulic control devices. Stability problems with self-regulating control valves aside, the developments in nonlinear control theory in the recent past call for more sophisticated strategies making use of servo control with approaches founded on differential geometry. It is to be seen in how far these approaches allow for a precise control of the desired system outputs.

Therefore, this thesis shall contribute to an improved understanding of dynamic aspects of passive and semi-active hydraulic systems in general and present novel concepts for the design and nonlinear control of hydraulic circuits featuring a variable displacement vane pump.

## **State of Research**

### **Analysis of Hydraulic Systems**

The fundamental laws of hydraulic modeling are presented and discussed in a variety of introductory textbooks, amongst which [4, 23, 70, 73] should be mentioned for the classic approach they take. As for the stability and dynamics of hydraulic systems, in [73] a small section is devoted to the occurrence of limit cycles in hydraulic systems and appropriate countermeasures. The treatment remains qualitative, however, while most other textbooks spare the topic. In the past few decades, a small number of researchers

have contributed to the analysis of the dynamics and stability of hydraulic systems. Among the first publications where stability properties of valves are analyzed, in [102] an analytical model of a safety poppet valve is derived and numerical studies investigating the dynamical behavior under different operating conditions are presented. In [17], limit cycle conditions for a class of electrohydraulic drive systems are established. In the neighboring field of pneumatics, in [74] a model of a pneumatic poppet-type relief valve is set up and fluid structure interaction is investigated in order to uncover destabilizing mechanisms. In [63], a poppet-type pressure relief valve's equilibrium position is investigated and a grazing bifurcation analysis is performed. A bifurcation-based design approach for a classical hydraulic servo system is proposed in [57]. This approach is built upon and extended in [100] where a bifurcation stability analysis of a hydraulic servo system is performed. Drawing on classic systems theory, static and dynamic behavior of different valve types are modeled and discussed in [68, 113, 128]. A comparatively large amount of research has been devoted to the stability of load sensing pump systems featuring swash plate piston pumps. Here, for example [58, 80, 124] are to be mentioned, even though in some of that research the intricacies of non-smooth dynamical behavior is treated with a hands-on mentality and may not in all cases yield dependable insight.

### **Variable Displacement Vane Pumps**

Variable displacement vane pumps can be distinguished by the type of motion they perform when subject to a change in displacement. With pivoting type variable displacement vane pumps, the element determining the pump's charging volume rotates about an attachment point in the pump housing while vane pumps of translatory type feature a purely translational displacement. Unfortunately, literature on the physical modeling of pumps in general and on minimal pump models in particular is scarce. While for piston pumps [71] is a classic publication in the field and has provided the foundation for a series of pump behavior modeling effort and dynamics investigations, an equivalent for pivoting type variable displacement vane pumps can be seen in the work presented by Karmel [45, 46, 48, 49]. This work is built on in e.g. [27], where additional simulation results are presented. Since Karmel's series of papers, the literature in the field has remained stagnant more or less. In [11], a lumped parameter model for a purely translational, linearly displacing variable displacement vane pump is derived. The model's complexity, however, makes it unsuitable to general stability investigations or control design. This observation also holds for [69], where another comprehensive pump model is presented. Neither of the mentioned references yields an autonomous model of the pump dynamics that can easily be integrated in plant models and be utilized for stability analysis and the derivation of suitable control laws. Apart from the pure modeling aspect, several publications touching special issues related to variable displacement pumps exist. For a general understanding of some of those problems, [33, 34, 120] should be mentioned.

## Control of Hydraulic Systems

In the context of hydraulic servo systems and control, [6, 41, 59, 114] are general references frequently drawn onto. The former two focus on linear control strategies, while the latter also cover nonlinear and other advanced concepts and present a comprehensive literature overview. In most cases the goal is hydraulic actuator control, i.e. the system to be controlled is a hydraulic cylinder which is actuated through pressure from hydraulic fluid. In the field of pump control, most efforts have been directed towards axial piston pumps so far. Among others, [58, 126] discuss control approaches based on operating point linearization. In [51], a nonlinear control approach to pressure control of an axial piston pump is given under significant model simplifications. As for variable displacement vane pump systems, the only publications known to this thesis' author are [111, 112] where an optimal controller design based on quantitative feedback theory is suggested. Despite significant advances in the theory of nonlinear control in the past decades, especially with the techniques of exact feedback linearization, linear control approaches continue to dominate the literature. Nevertheless, successful application of feedback-linearizing techniques is documented in some cases, [16, 32, 98, 105, 115].

## Non-smooth Dynamics

As pointed out, the behavior of ideal valves in hydraulic circuits leads to a non-smooth problem formulation when modeled as idealized systems without valve leakage. A significant problem with the treatment of such systems lies in its mathematical foundations that just relatively recently started developing. While the field certainly is rich, an easy-to-apply or practically usable unified treatment of systems whose equilibrium lies on a system's switching boundary is still not known so that in many cases one will have to resort to physically motivated regularization approaches such as leakage smoothing the nonlinear description of the system.

It is not the purpose at this point to provide a thorough overview on non-smooth dynamics and analysis, for these, the reader is referred to [19, 20, 61, 99]. Instead, a much-cited example from [9] shall be drawn on to illustrate some properties that make these problems difficult to assess in general.

If the system

$$\dot{\mathbf{x}} = \mathbf{A}_i \mathbf{x}, \quad i = 1, 2$$

with

$$\mathbf{A}_1 = \begin{bmatrix} -1 & 10 \\ -100 & -1 \end{bmatrix}, \quad \mathbf{A}_2 = \begin{bmatrix} -1 & 100 \\ -10 & -1 \end{bmatrix}$$

is considered for  $i = 1, 2$ , its equilibrium position clearly is  $\mathbf{x} = \mathbf{0}$  which is globally exponentially stable. For a system switching between the two system configurations,

however, system stability depends on the prescribed switching law. For  $A_1$  active in the first and third quadrant and  $A_2$  active in the second and fourth quadrant, the system is stable. In contrast, for  $A_1$  active in the second and fourth quadrant and  $A_2$  in the first and third quadrant, the system has an unstable equilibrium. Stability of a non-smooth or switched system can therefore not be assessed through separate consideration of the stability of its individual subsystems. With the non-smooth modeling of critically lapped valves in hydraulic systems, such switching behavior naturally occurs in many practical cases.

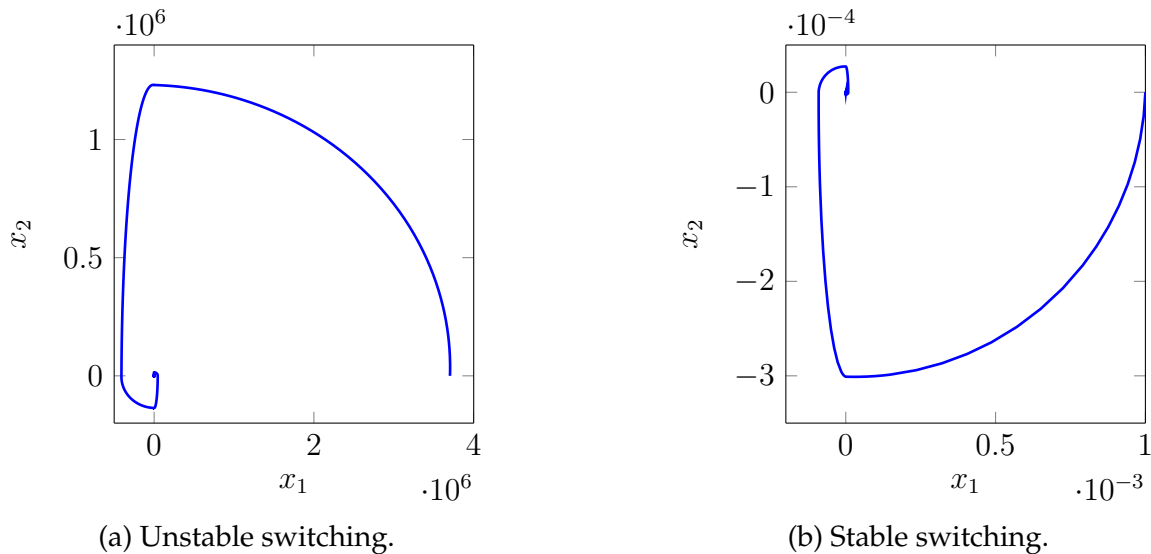


Figure 0.1: Switching of a piecewise linear system.

As for a systematic treatment of such problems, two approaches are most prominently discussed in the literature on nonsmooth dynamics and switched systems [9, 62, 129]. The first approach entails the existence of a so called common Lyapunov function. The line of reasoning is that if a Lyapunov function can be found whose time derivative decreases along any of the trajectories associated with the system for  $i = 1, \dots, j$ , then this function is a common Lyapunov function, implying equilibrium stability.

With the idea of multiple Lyapunov functions attributable to [78], the concept was extended to nonlinear systems and popularized by Branicky [9], see also [99] for an outline of the history of research in the field. Here, the concept is to find Lyapunov functions for each subsystem and to show that the value of each of the Lyapunov functions has decreased upon activation relative to the last time the respective Lyapunov function was active. Evidently, the concept of common Lyapunov function fulfills this requirement. From a practical perspective, the concept of multiple Lyapunov functions is most likely to be used for the design of switching laws (i.e. control design and design of switching point location) ensuring stability of the switched system. In contrast, assessing stability of a system subject to autonomous switching requires showing the decrease of each of the Lyapunov functions relative to the last time of their respective activation and thereby knowledge of the switching times. For autonomously switching systems, these

points in time will only in rare cases be determinable in closed form – thereby making the approach difficult to apply to systems other than those switching at pre-defined points in time.

## **Thesis Purpose**

The literature analysis shows contributions to the state of research can be made in several ways.

In order to improve an understanding of the mechanisms potentially governing instability in hydraulic systems, a series of models with systematically increasing complexity shall be built and discussed with respect to stability, incorporating a regularization approach based on the physics of leakage flow in valves where necessary. This is an effort that has not yet been undertaken systematically. Beginning with the investigation of a simple pressure control valve subject to different operating conditions, a hydraulic actuation topology for an automatic transmission shall be covered, too.

The dynamics of a variable displacement vane pump used in many hydraulic circuits shall then be modeled and assessed with respect to stability within a classic hydraulic circuit in order to generate novel insight into stability problems with such pumps. To this date, no physically and mathematically solid investigation of this problem complex exists.

Building on the modeling of the circuit, a novel control approach for the volume flow of a variable displacement vane pump making use of methods from nonlinear control design shall be investigated. Here, questions regarding observer design are to be addressed, too. The modeling and synthesis are to be performed with application in an automotive transmission context in mind. Automotive transmissions exhibit significant dynamical behavior so that as little simplifications as possible should be made in the derivation of the control approach in order to minimize effects from parasitic dynamics. Building on single-input-single-output volume flow control of the pump, the approach shall then be extended to a multiple-input-multiple-output control design for the actuation of a clutch and the volume flow delivery to secondary consumers in an automotive transmission. In this context, different observer designs for the pressure dynamics within a clutch cylinder shall be devised and tested for applicability.

Ultimately, a novel concept for parameter identification within a clutch actuation context shall be tested for applicability. The approach rests upon Kalman Filtering and shall be tested with virtual measurements generated by simulation.

## **Thesis Structure**

To account for the desired purpose, this thesis is divided into two parts. The first part covers aspects of modeling and stability of passive or semi-active hydraulic systems in chapters 1–6 while in the second part nonlinear control approaches are discussed with

respect to the questions outlined above. The second part extends over chapters 7–10.

As for Part I, chapter 1 provides an overview of elementary physical laws governing the dynamics of hydraulic systems. Starting from there, in chapter 2 a modeling approach for control edges with different notch geometries and physically based control edge flow regularization based on leakage modeling is presented. In chapter 3 the model of a most simple pressure control valve is discussed with respect to system stability under different operating conditions. In chapter 4, the model of a hydraulic clutch actuation circuit is outlined. It features a fixed displacement pump and is to provide a clutch with actuation energy upon valve actuation. Simulation results are interpreted and discussed with respect to the stability findings from chapter 3. With a view towards volume flow adaptive pumps, a minimal model of a variable displacement vane pump of translatory type is presented in chapter 5. The pump model is suitable for control law derivation and elementary stability analysis. Integrating this model into a standard pressure regulation circuit, structural and stability properties of this circuit are treated in chapter 6.

In Part II, fundamental concepts of feedback linearization are briefly reviewed in chapter 7. Building on this, in chapter 8 a model of a variable displacement pump system suitable for nonlinear control actuation through a servo valve is derived and subjected to a feedback-linearization for volume flow control. Within this context, observer and feedforward concepts are discussed, too. The control approach is then extended to a novel concept for clutch actuation in an automatic transmission in chapter 9. Here, problems of clutch observer design are discussed, too. Chapter 10 covers a novel approach for system identification based on Kalman Filtering in the form of a case study within a clutch actuation context.

The thesis then concludes with a summary of the key findings and an outlook on future research questions.

**Part I**

**Modeling and Analysis of Hydraulic  
Systems**



# 1 Fundamentals of Hydraulic Modeling

In this chapter, the most important elements of hydraulic modeling are presented and discussed. The elements presented comprise hydraulic capacitances, hydraulic resistances and hydraulic valves. Finally, damping, inductance and flow forces in hydraulic systems are shortly discussed with respect to their relevance for this work.

## 1.1 Capacitances and Hydraulic Stiffness

Hydraulic capacitances are used to model the pressure dynamics in any volume extant in a hydraulic system. Such volumes may be dead volumes in hydraulic valves, the volumes contained in hydraulic pipes and the volume in pressure cylinders. The approach to model the pressure dynamics in a possibly varying volume is to consider the mass flow balance in such a volume under the assumption that the mass distribution is uniform. This assumption is very common in hydraulic modeling. It should be mentioned, however, that it implies the neglect of fluid dynamics [41, 73, 75].

The fluid mass  $m(t)$  in a time varying volume  $V(t)$  is given by

$$m(t) = \rho(t)V(t) \quad (1.1)$$

with time-dependent fluid density  $\rho(t)$ . In many cases, the volume  $V(t)$  represents a piston volume that can be computed by  $V(t) = V_0 + Ax(t)$  as shown in Figure 1.1.

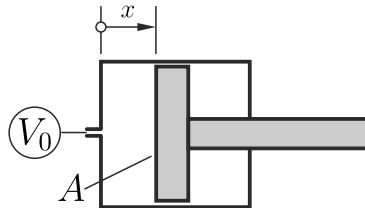


Figure 1.1: Exemplary volume computation for capacitance calculation in a hydraulic cylinder.

Here,  $x(t)$  is the piston displacement and  $A$  the piston area while  $V_0$  represents the so called dead or base volume inherent to a piston with zero displacement. In many practical cases, this dead volume is inevitable due to design considerations. The mass flow in a hydraulic volume can be computed by building the time derivative on both sides of equation (1.1):

$$\dot{m} = \dot{\rho}V + \rho\dot{V}. \quad (1.2)$$

The mass flow into the hydraulic volume under consideration is proportional by fluid density  $\rho$  to the net volume flow into the volume

$$\dot{m} = \rho \sum_i q_i, \quad (1.3)$$

where a positive sign of  $q_i$  represents a volume inflow and a negative sign of  $q_i$  a volume outflow. In what follows, the definition of the hydraulic fluid bulk modulus is needed. Fluid bulk modulus commonly is defined by

$$E_{fl} = -V \frac{dp}{dV} = \rho \frac{dp}{d\rho} \quad (1.4)$$

with fluid pressure  $p$ . Conceptually, the quantity  $E_{fl}$  can be interpreted as hydraulic stiffness and is referred to as the (isothermal) fluid bulk modulus accordingly. It is a material property. Within the scope of this thesis, it is assumed (see [41]) that it can be represented by

$$E_{fl} = E_0 + K_p p. \quad (1.5)$$

Representative values for this model's constants are  $E_0 = 16500\text{bar}$  and  $K_p = 9.558$  [41]. Up to mid-pressure applications, bulk modulus variations thus are comparatively insignificant within this model's scope.

With the bulk modulus definition (1.4), the density's time derivative can be expressed as

$$\dot{\rho} = \frac{d\rho}{dp} \dot{p} = \frac{\rho}{E_{fl}} \dot{p}, \quad (1.6)$$

which, when substituted into equation (1.2) and set equal to the right hand side of (1.3), yields

$$\rho \sum_i q_i = \dot{\rho} V + \rho \dot{V} = \rho \left( \frac{1}{E_{fl}} \dot{p} V + A \dot{x} \right). \quad (1.7)$$

From this, it follows that

$$\frac{V_0 + Ax}{E_{fl}} \dot{p} = \sum_i q_i - A \dot{x}, \quad (1.8)$$

which is the well-known equation governing the pressure dynamics in a varying volume. The expression

$$\frac{V_0 + Ax}{E_{fl}} =: C_h$$

is typically referred to as hydraulic capacitance. It is immediately obvious and intuitively understandable that the magnitude of the capacitance increases proportionally

with the total volume. The bulk modulus  $E_{fl}$ , however, requires further consideration. So far, it has been taken as the bulk modulus of a pure fluid. In practice, one may have to employ an effective bulk modulus, taking into account effects of air contained in the hydraulic fluid [6, 41] and the stiffness effects of the hydraulic chambers, pipelines etc. Generally, air is known to appear in hydraulic systems in three ways [67]:

- free air in the form of trapped air pockets which can be removed from the system through venting,
- entrained air in the form of air bubbles up to a diameter of about 0.6 mm,
- dissolved air which is invisible and assumed to be uniformly distributed between molecules.

While the problems with free air can be resolved through appropriate venting and dissolved air has negligible effects on the bulk modulus [41, 67], the effects of entrained air in hydraulic fluids have considerable effects on the hydraulic bulk modulus. These effects are especially relevant when passing from high system pressure to low pressure. At high pressure values, entrained air is compressed to a small volume and thereby dissolved – at sufficiently low pressure values, the dissolved air expands abruptly into entrained air which has motivated e.g. [7, 81] to approximate the fluid behavior in the respective pressure region by unilateral constraints.

In practical applications, a large amount of effort will be directed at achieving a low level of entrained air. Within the scope of the present thesis, fluid bulk modulus will thus be taken in the form of equation (1.5) if not stated otherwise.

## 1.2 Hydraulic Resistances

In hydraulics, flow across hydraulic resistances is mostly turbulent as it takes place across sharp edges in the majority of cases. Most prominently, one such sharp edge is an orifice where for sufficiently large Reynolds numbers the flow can be modeled sufficiently accurately through a nonlinear function of the pressure difference across the orifice. Another important type of hydraulic resistance is the throttle for which a model is frequently drawn unto which features a linear dependence of the volume flow on the pressure difference across the resistance.

### 1.2.1 Orifice

The flow through a sharp-edged orifice can be derived from the Bernoulli equation known from fluid dynamics (for further study of fluid dynamics, the excellent book by Spurk [106] is recommended). The energy balance for incompressible, stationary flow along a streamline with dissipation reads [6, 29]

$$\frac{1}{2}w_H^2 + \frac{p_H}{\rho} + gh_H = \frac{1}{2}w_L^2 + \frac{p_L}{\rho} + gh_L + \frac{\Delta p_{HL}}{\rho}. \quad (1.9)$$

In the above expression,  $w_i$  denotes the fluid velocity at points  $i = \{H, L\}$  (“high”, “low”) along a stream tube filament,  $p_i$  the corresponding pressure and  $gh_i$  the specific potential energy from gravity. In the context treated here, it is assumed that  $h_0 = h_1$ . Also, for points  $i = \{H, L\}$  sufficiently far away from the orifice,  $w_H = w_L = w$  may be assumed due to continuity.

The term  $\Delta p_{HL}$  represents the specific energy loss from dissipation between points  $H$  and  $L$ . It is commonly described by

$$\frac{\Delta p_{HL}}{\rho} = \frac{1}{2}\zeta w^2, \quad (1.10)$$

where  $\zeta$  is the so-called resistance number. Ultimately, with an effective area of the orifice  $A_{OR}$  it follows that

$$q = A_{OR}w = \sqrt{\frac{2}{\rho\zeta}}A_{OR}\sqrt{p_H - p_L} = \alpha_d\sqrt{\frac{2}{\rho}}A_{OR}\sqrt{p_H - p_L}. \quad (1.11)$$

The resistance number  $\zeta$  is a function of the Reynolds number indicating turbulent flow. The Reynolds number is defined as

$$Re = \frac{wd_H}{\nu}, \quad (1.12)$$

with flow velocity  $w$ , hydraulic diameter  $d_H = 4A/U$  where  $A$  is the area through which the flow passes and  $U$  the area’s circumference and the kinematic viscosity  $\nu$ . The formulation featuring the so called discharge coefficient  $\alpha_d$  is more common and will be used in the remainder of this thesis. Because it will always come alongside the square root of  $2/\rho$ , the following abbreviation will be used throughout this work:

$$\alpha_d\sqrt{\frac{2}{\rho}} =: \gamma_F. \quad (1.13)$$

## 1.2.2 Throttle

The law governing the flow behavior across a sharp-edged orifice is the most important hydraulic nonlinearity. The nonlinearity comes from turbulence-related pressure drops. In some cases, however, flows may be laminar, especially in the case of throttles for which a description via the law of Hagen-Poiseuille is assumed. With  $l$  representing the length of a circular channel of diameter  $D$  through which the fluid is to flow and  $\eta_F$  the dynamic fluid viscosity, the law of Hagen-Poiseuille reads

$$q = \frac{\pi D^4}{128\eta_F l}(p_H - p_L). \quad (1.14)$$

In accordance with the property of laminar flow, the dependence of volume flow  $q$  on the pressure drop across the hydraulic resistance of a throttle is linear. Most importantly in the context of this thesis, the throttle is referred to when modeling leakage

phenomena. Leakage occurs in any hydraulic system. It cannot be avoided completely, but only reduced with increasing manufacturing accuracy. Leakage arises in hydraulic cylinders, valves and any moving component in a hydraulic system which is exposed to pressurized fluid. The reason for leakage phenomena are (radial) clearances between the moving component and its housing which allow fluid to flow from high pressure to low pressure chambers. In many cases, leakage phenomena can be modeled by assuming laminar flow through a throttle. The most prominent example for such purely laminar leakage phenomena is the laminar flow across a moving piston. In general, the geometry of the flow problem naturally plays an important role for the specific leakage behavior of a hydraulic component. For a piston moving within a circular housing of diameter  $D$ , the flow passage area is an annular gap with gap height  $\Delta r$ , leading to volume flow that is commonly modeled with the following laminar (throttle) flow law (e.g. [4, 6, 23, 122]):

$$q = \frac{D\pi\Delta r^3}{12\eta_F l} \left[ 1 + 1.5 \left( \frac{e}{\Delta r} \right)^3 \right] (p_H - p_L). \quad (1.15)$$

In the above relationship,  $e$  represents the eccentricity of the moving component's center relative to the (fixed) circular housing's center. The major problem with leakage is that the quantities constituting its magnitude can barely be determined in most cases, such as the moving component's eccentricity. As a consequence, such models are appropriate only for the qualitative description of systems featuring leakage. For practically accurate predictions, experimental investigation is inevitable.

### 1.3 Damping in Hydraulic Elements

The phenomenon of leakage is closely related to damping phenomena in hydraulic systems. While the intention at this point is not to derive a comprehensive model of viscous damping forces for piston-like bodies moving in an annular gap filled with viscous fluid, it is worthwhile to qualitatively describe the origin of damping in hydraulic systems. With radial clearances between valve spools or pistons and housings, fluid within a radial gap exerts shear stress on a moving valve spool or piston. For Newtonian fluids, this shear stress is proportional to shearing velocity and fluid viscosity so that velocity-proportional forces can be expected for a piston with radial clearance moving in its housing. With fluid viscosity varying with temperature, so will damping. In the present work, however, damping will be modeled as viscous damping described by a lumped damping coefficient. This is well-established practice in hydraulics modeling (e.g. [2, 41, 56, 63, 68, 113]) and also due to the highly complex problem of adequately modeling damping in hydraulic systems, see [2] for a brief discussion of this problem. Since damping in valves is at times purposefully increased through incorporation of a dashpot (see e.g. [4, 122]), a lumped viscous damping coefficient for modeling valve spool damping can be interpreted as a design proxy variable for dashpot

dimensions. Notably, damping effects from a dashpot dominate over damping effects from leakage at control edge openings. If no dashpot is designed for in a specific valve, damping will – besides fluid viscosity and annular gap height – depend on effective gap length within which fluid shear forces act. Then, a lumped viscous damping coefficient can be interpreted to mirror geometric properties of the valve not explicitly modeled. Notably, the approach of modeling valve damping as a lumped parameter has the benefit of allowing for a separate discussion of the effects of damping and leakage on equilibrium stability given in chapter 6. Thereby, recommendations for the design of the valve (i.e. dashpot dimensions, effective leakage gap length etc.) can be deduced that may be difficult to unveil when employing a fully elaborate damping model.

### 1.4 Hydraulic Inductance and Flow Forces

In this chapter, fundamental elements of hydraulic modeling were discussed with their relevance to this thesis in mind. Two aspects of modeling were spared, namely the effect of hydraulic inductance and the effect of flow forces within a hydraulic valve. In the majority of cases within the extant body of research on hydraulic systems, the so called hydraulic inductance of fluid columns is neglected in models. This inductance is typically defined as

$$L = \frac{\rho l}{A} \quad (1.16)$$

with  $l$  representing the fluid column's length and  $A$  its cross-sectional area. The inductance  $L$  captures mass properties of fluid volume – its purpose is to allow for a modeling of the acceleration behavior of a column of fluid. The reason this aspect of fluid dynamics is usually neglected in the context of hydraulic modeling is that the force needed to accelerate a column of fluid is usually much less than the force conveyed through the static pressure within a system [6].

Another aspect not treated in this study are flow forces within a valve. The directional change fluid flow is subjected to when passing into and out of a valve is associated with reaction forces acting on the valve body. These forces can be computed from applying the law of momentum to the fluid control volume within the valve and will depend on the valve geometry. While for many analyses ignoring flow forces is an admissible simplification in system modeling, it is not advisable once the flow through a valve becomes large as for large volume flows, flow forces may be significant. Throughout this thesis, however, it will be assumed that flow forces can be omitted.

## 2 Modeling Control Edge Flow

### 2.1 Background

In order to model and simulate hydraulic systems, a mathematical description of flow across control edges is necessary. Flow across valve control edges is typically modeled as flow through an orifice of varying area. The classical flow geometry for most valves is a rectangular orifice as shown in Figure 2.1a where the area through which flow takes place is proportional to valve spool displacement.

Alternative geometries exist, however. Most prominently, this is a triangular notch geometry shown in Figure 2.1b. In many cases, it is desirable to be able to very finely control the volume flow through a valve – with the help of a triangular notch this can be achieved well. Another advantage of triangular notches is that leakage is minimal for a nominally closed valve. This is due to the overlap inherent to triangular notches. A practical problem with this notch geometry is, however, that they are impossible to manufacture accurately. Therefore, another notch geometry frequently encountered in practice is a circular notch as shown in Figure 2.1c. These are comparatively easy to manufacture and feature the ability to slowly vary flow area upon displacement of the valve spool, too.

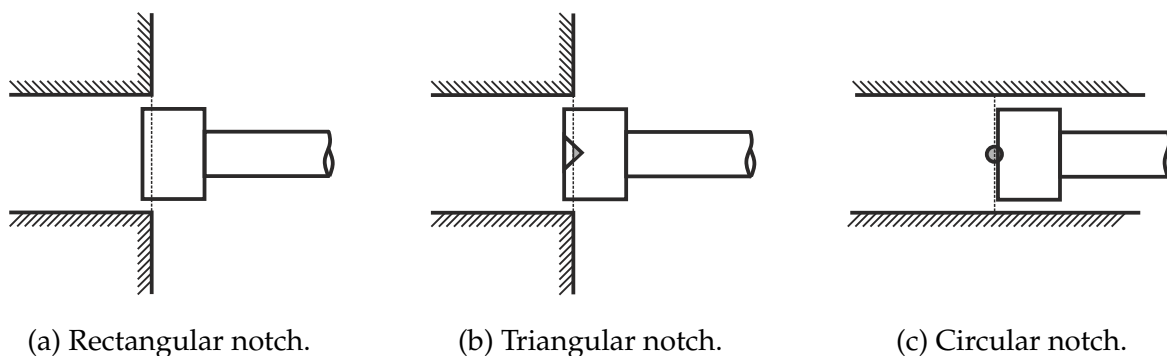


Figure 2.1: Notch geometries. Grey shaded areas in b) and c) represent the nominal valve opening area.

Idealized opening characteristics of valves go in hand with a non-smooth system description for hydraulic systems. With an eye towards real world manufacturing imperfections and accessibility of system models for mathematical analysis, the assumption of ideal, non-smooth valves therefore calls for reconsideration. In practice, even valves designed to be lapped critically will feature an overlap or underlap due to the limitations of manufacturing technology. From an energetic point of view, an overlap is more

feasible than an underlap as underlaps go along with excessive leakage and thereby potentially significant but undesirable fluid drain from the system.

Overlaps, however, are not the only source of manufacturing imperfection. Despite very high standards of manufacturing for hydraulic valves, radial clearance between the valve spool and its housing is inevitable, leading to leakage phenomena and damping mechanisms intrinsic to hydraulic valve design. From a physical viewpoint, leakage in combination with an overlap can be seen as a smoothing mechanism for an otherwise non-smooth opening characteristic. Modeling leakage accordingly therefore yields a system description which allows for the application of eigenvalue-based analysis to systems that feature equilibria on switching surfaces when assuming idealized non-smooth modeling.

Either of the discussed geometries relates to geometry-specific leakage phenomena. In this chapter, a generic leakage model will first be outlined and then specified with respect to different notch geometries. Within this context, also see [136, 147].

## 2.2 Generic Leakage Flow Model

For leakage in hydraulic valves, the flow situation is schematically shown in Figure 2.2. Within the scope of this thesis, leakage flow from high pressure to low pressure regions is assumed to be characterized by a combination of laminar and turbulent flow patterns. Flow within the annular gap region of length  $l_{LL}(x)$ , width  $b_{LL}$  and gap height  $\Delta r$  is assumed to be laminar and thus modeled as a throttle-type resistance while the entry or exit of fluid through an orifice-like valve notch resistance is turbulent and should therefore be modeled as an orifice. The necessity to draw on both elements for modeling leakage also has an intuitive aspect: the laminar-type flow resistance varies with gap length  $l_{LL}(x)$  which is subject to the position of the valve spool. If leakage in a valve were modeled without including an orifice in the model, a singularity for leakage flow would occur once  $l_{LL}(x) = 0$  and the valve starts to uncover its flow passage area, see equation (1.15). In order to account for this, leakage is modeled as a sequential coupling of an annular gap channel and an orifice with the orifice's flow area derived from the specific geometry at hand. For such a sequential coupling of an orifice and a throttle as suggested in Figure 2.2d, the volume flows are given by

$$q_{TL} = \gamma_F A_{TL} \sqrt{p_H - p_{HL}}, \quad q_{LL} = \frac{b_{LL} \Delta r^3}{12 \eta_F l_{LL}(x)} \left[ 1 + 1.5 \left( \frac{e}{\Delta r} \right)^3 \right] (p_{HL} - p_L).$$

Here and in the remainder, index “ $TL$ ”, is to indicate the turbulent leakage component whereas index “ $LL$ ” is to indicate the laminar leakage component. In the above expressions,  $p_{HL}$  is an intermediate pressure between the two hydraulic elements. Under the assumption that no pressure dynamics exist between the two elements, it follows that  $q_{TL} = q_{LL}$ . This allows for solving for the volume flow  $q_{TL} = q_{LL} =: q_L$  as a func-

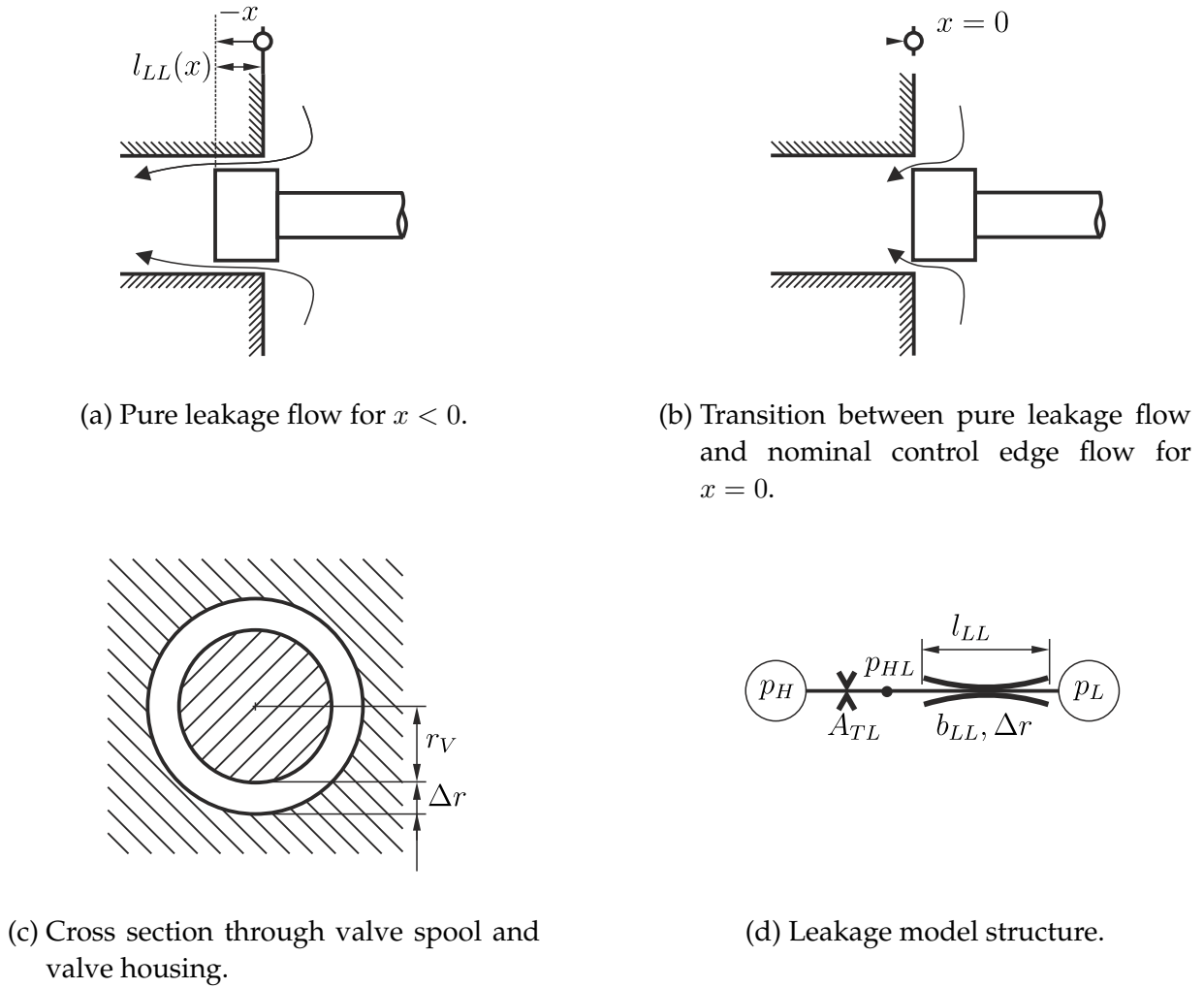


Figure 2.2: Leakage flow model.

tion of pressure difference  $p_H - p_L$ . Performing the necessary manipulations under the simplifying assumption of zero spool eccentricity,  $e = 0$ , then yields

$$q_L(x, p_H, p_L) = -\frac{6\gamma_F^2 A_{TL}^2 \eta_F}{b_{LL} \Delta r^3} l_{LL}(x) + \sqrt{\gamma_F^2 A_{TL}^2 (p_H - p_L) + \left(\frac{6\gamma_F^2 A_{TL}^2 \eta_F}{b_{LL} \Delta r^3}\right)^2 l_{LL}^2(x)}. \quad (2.1)$$

From the above expression, it can clearly be seen that once the length of the annular gap  $l_{LL}(x)$  decreases to zero, the flow  $q_L$  becomes an orifice-type flow with orifice flow area  $A_{TL}$ . Equivalently, overall leakage flow decreases with increasing gap length  $l_{LL}(x)$ , just as one would expect. The above model structurally resembles the approach suggested in [21] (also, see [22] for a discussion of this model). With a view towards experimental validation, a problem with this modeling approach is that it requires system identification of parameters which enter the governing equations in a nonlinear way, thereby

making the identification problem a non-trivial one. Alternate approaches therefore rely on data-driven modeling, see e.g. [107, 125]. In [41, 73], a data-driven approach is recommended, too. In order to qualitatively assess the influence of different parameters governing leakage flow, however, a discrete model as suggested above should be seen as an appropriate approach.

## 2.3 Geometry-specific Leakage Flow Models

Notably, the quantities  $l_{LL}$ ,  $b_{LL}$ ,  $A_{TL}$  needed in the preceding section's generic leakage model will depend on the specific notch geometry at hand and possibly vary with valve spool position, too. For this reason, a specification of these quantities will be made for different notch geometries in the following subsections.

### 2.3.1 Rectangular Notch

For a rectangular notch (index “ $\square$ ”) according to Figure 2.1a with zero overlap and radial clearance, the nominal flow from high pressure  $p_H$  to low pressure  $p_L$  is given by the equation

$$q_{\square}(x, p_H, p_L) = \begin{cases} 0 & \text{for } x < 0, \\ \gamma_F b_{Reg} x \sqrt{p_H - p_L} & \text{for } x \geq 0. \end{cases} \quad (2.2)$$

The quantity  $b_{Reg}$  corresponds to the radius of the valve spool  $r_V$  by  $b_{Reg} = 2\pi r_V$ . When accounting for leakage by introducing an approach such as (2.1) to the model (2.2), different situations need to be considered: First, for negative displacements  $x < 0$  the flow through the valve comes from leakage exclusively. Channel length for the laminar component of leakage then is  $l_{LL\square}(x) = -x$ , channel width is  $b_{LL\square} = b_{Reg}$  and channel height is given by radial clearance  $\Delta r$  as shown in Figures 2.2a, 2.2c.

Once the valve spool is moved up to  $x = 0$ , the flow from leakage has to be blended into the flow defined by (2.2). The situation at  $x = 0$  therefore is critical to the model and defines the area of the orifice  $A_{TL\square}$  modeling the turbulent component of leakage in equation (2.1). Considering the view on the valve spool within the valve cylinder bore at  $x = 0$ , area  $A_{TL\square}$  can be computed from radial clearance  $\Delta r$  and circumference  $b_{Reg}$  of the valve spool approximately as

$$A_{TL\square} = b_{LL\square} \Delta r = b_{Reg} \Delta r. \quad (2.3)$$

In order to have a continuous transition from pure leakage flow in  $x < 0$  into valve flow with leakage for  $x \geq 0$ , the flow area from nominal valve opening (index “VO”) with turbulent flow is modeled as the lateral surface area of a truncated cone as spanned

between the valve spool and the port land at the valve cylinder (see Figure 2.3) which, under the neglect of second order effects from radial clearance, is approximated as

$$A_{VO\Box}(x) = b_{Reg} \sqrt{x^2 + \Delta r^2}. \quad (2.4)$$

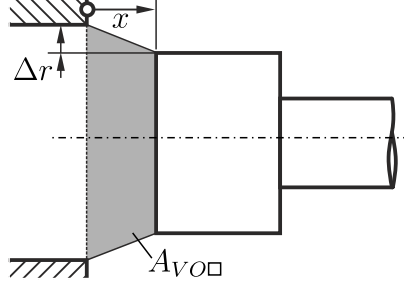


Figure 2.3: Leakage geometry for rectangular notch. The grey-shaded area is the truncated cone surface drawn on for modeling leakage.

Clearly,  $A_{VO\Box}(x = 0) = A_{TL\Box}$  so that the different flow regimes continuously blend into each other when passing  $x = 0$ . Incorporating  $A_{VO\Box}(x)$  into equation (2.2) thus yields

$$q(x, p_H, p_L) = A_{VO\Box}(x) \gamma_F \sqrt{p_H - p_L}. \quad (2.5)$$

It is obvious from equation (2.4) that with increasing spool displacement  $x$  the effect of radial clearance on flow behavior will decrease.

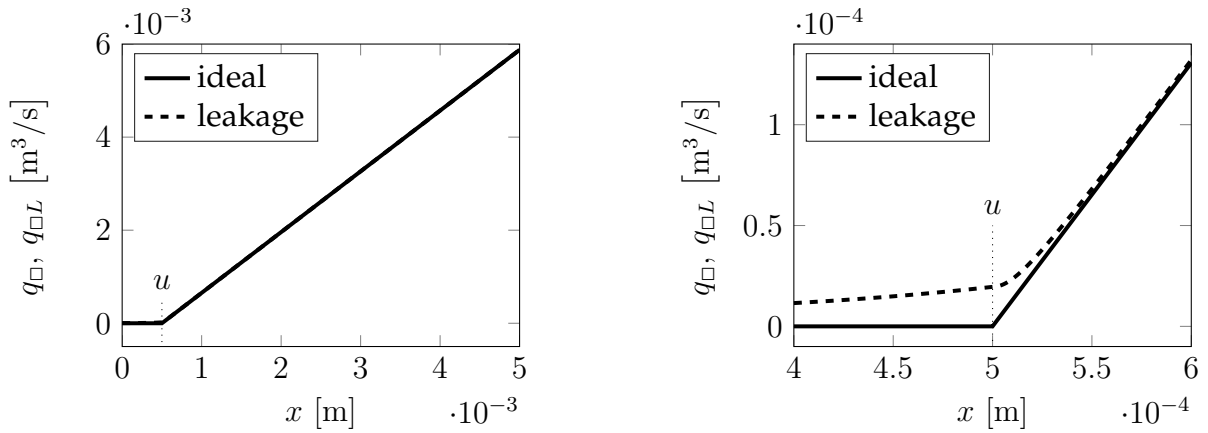
Summarizing, for a valve with rectangular notch featuring leakage flow,

$$q_{L\Box}(x, p_H, p_L) = \frac{6\gamma_F^2 A_{TL\Box}^2 \eta_F}{b_{LL\Box} \Delta r^3} x + \sqrt{\gamma_F^2 A_{TL\Box}^2 (p_H - p_L) + \left( \frac{6\gamma_F^2 A_{TL\Box}^2 \eta_F}{b_{LL\Box} \Delta r^3} \right)^2 x^2}, \quad (2.6)$$

one ultimately obtains

$$q_{\Box L}(x, p_H, p_L) = \begin{cases} q_{L\Box}(x, p_H, p_L) & \text{for } x < 0, \\ A_{VO\Box}(x) \gamma_F \sqrt{p_H - p_L} & \text{for } x \geq 0. \end{cases} \quad (2.7)$$

For  $x \geq 0$  the model resembles a model suggestion briefly touched upon in [127] but discarded in favor of a model fitted to experimental data. Overlaps of magnitude  $u$  can easily be incorporated in the above model by transforming  $x$  with  $x \mapsto x - u$ . In Figures 2.4a and 2.4b, the flow behavior of the valve is shown for representative geometry parameters listed in Table 2.1 and a pressure difference of  $p_H - p_L = 20 \times 10^5$  Pa and an overlap of  $u = 0.0005$  m. In Figure 2.4a it can clearly be seen that the overall effect of leakage is negligible for sufficiently large valve openings  $x$  while Figure 2.4b shows a zoomed configuration revealing that in the vicinity of  $x - u = 0$  leakage has effects on the shape of the flow function.



(a) Flow through rectangular control edge.

(b) Zoomed.

 Figure 2.4: Leakage flow through rectangular notch (featuring overlap  $u$ ).

Table 2.1: Control edge parameters.

Parameter	Symbol	Value	Unit
Valve overlap	$u$	0.0005	m
Diameter of piston bore	$D$	0.01	m
Spool circumference	$b_{Reg}$	$D\pi = 2\pi r_V$	m
Triangular notch width	$b_\Delta$	0.002	m
Triangular notch length	$a_\Delta$	0.002	m
Circular notch radius	$r_o$	0.001	m
Gap height	$\Delta r$	$15 \times 10^{-6}$	m
Fluid viscosity	$\eta_F$	0.01	Pas

### 2.3.2 Triangular Notch

The volume flow behavior of ideal valves with triangular notch (index “ $\Delta$ ”) is governed by two flow regimes as can be seen from Figures 2.1b, 2.5.

For  $x < b_\Delta$ , the flow is characterized by turbulent flow through a triangular orifice of height  $x$ . For  $x \geq b_\Delta$ , the triangular notch is fully uncovered and the total flow area is computed from the full triangle flow area plus the displacement dependent flow area from an ordinary rectangular orifice. Nominally, one obtains

$$q_\Delta(x, p_H, p_L) = \begin{cases} 0 & \text{for } x < 0, \\ \frac{1}{2}\gamma_F n_N \left(\frac{a_\Delta}{b_\Delta}\right) x^2 \sqrt{p_H - p_L} & \text{for } 0 \leq x < b_\Delta, \\ \gamma_F \left(b_{Reg}(x - b_\Delta) + \frac{1}{2}n_N a_\Delta b_\Delta\right) \sqrt{p_H - p_L} & \text{for } x \geq b_\Delta. \end{cases} \quad (2.8)$$

Here,  $n_N$  is the number of notches along the spools circumference. The triangular notch is associated with a comparatively slowly varying flow area which is desirable in many

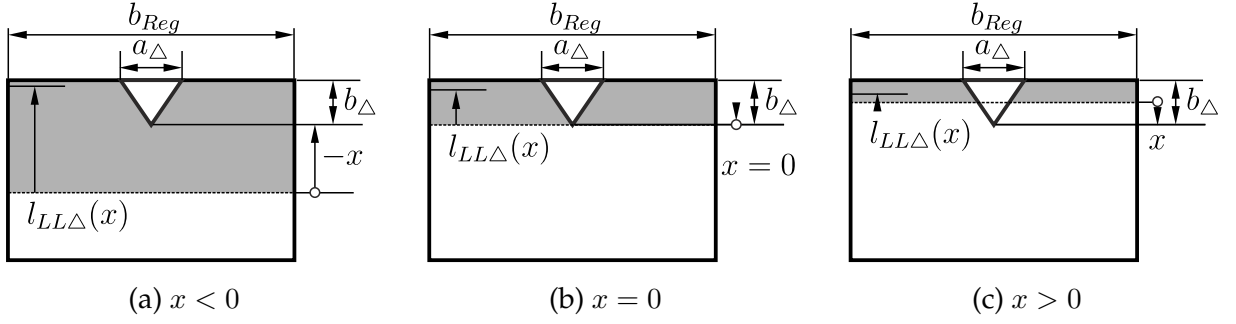


Figure 2.5: Triangular notch geometry parameters and calculation of average throttle length  $l_{LL\Delta}(x)$  – one triangular notch along circumference  $b_{Reg}$ .

practical cases, see e.g. [95] for further reference. Accounting for leakage in this model is more complicated than for a model with rectangular notch because the channel length  $l_{LL\Delta}(x)$  for laminar component of leakage flow will vary along the circumference of the valve spool due to the triangular notches. Thinking of the problem as a planar problem by unwrapping the valve spool allows a conceptualization as shown in Figure 2.5.

For  $x < 0$ , the throttle length for laminar flow is given by  $l_{LL\Delta} = b_{\Delta} - x$  at all points along the circumference of the valve spool except for those points which lie below the triangular notch. The approach taken here is to compute an average throttle length along the circumference. It is assumed that this satisfyingly describes the flow situation. The same line of reasoning is applicable to the situation with  $0 \leq x < b_{\Delta}$ . Performing the respective calculations for the quantities characterizing leakage flow, one gets

$$l_{LL\Delta}(x) = \begin{cases} \frac{(b_{Reg} - n_N a_{\Delta})(b_{\Delta} - x) + n_N a_{\Delta} \left(\frac{b_{\Delta}}{2} - x\right)}{b_{Reg}} & \text{for } x < 0, \\ (b_{\Delta} - x) \frac{b_{Reg} - \frac{n_N}{2} a_{\Delta} \left(1 + \frac{x}{b_{\Delta}}\right)}{b_{Reg} - n_N \left(\frac{a_{\Delta}}{b_{\Delta}}\right) x} & \text{for } 0 \leq x < b_{\Delta}. \end{cases} \quad (2.9)$$

The corresponding channel width for the laminar component of leakage flow  $b_{LL\Delta} = b_{LL\Delta}(x)$  is taken as

$$b_{LL\Delta}(x) = \begin{cases} b_{Reg} & \text{for } x < 0, \\ b_{Reg} - n_N \left(\frac{a_{\Delta}}{b_{\Delta}}\right) x & \text{for } 0 \leq x < b_{\Delta} \end{cases} \quad (2.10)$$

and, resulting from this,

$$A_{TL\Delta}(x) = b_{LL\Delta}(x) \Delta r. \quad (2.11)$$

From (2.9) and (2.10), laminar components of leakage are considered relevant in this model only within  $x < b_{\Delta}$ , i.e. as long as the flow regime for the triangular notch prevails.

Within the interval  $0 \leq x < b_\Delta$ , the nominal flow area of the triangle begins to uncover so that, in addition to leakage flow, the turbulent flow through the uncovered tip of the triangle occurs. Because of radial clearance, this triangle will be inclined as shown in Figure 2.6.

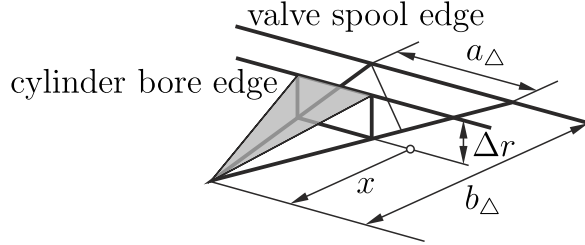


Figure 2.6: Leakage geometry for triangular notch and the  $0 < x < b_\Delta$ . The grey-shaded area is the tilted triangle  $A_{VO\Delta}(x)$  through which flow from nominal valve opening occurs.

The same will be the case for  $x \geq b_\Delta$ . Here, the effective flow area is computed from the sum of the fully opened inclined triangle added to the lateral surface of a truncated cone as in the model for a rectangular notch. The corresponding opening area  $A_{VO\Delta}$  of the valve can thus be stated as

$$A_{VO\Delta}(x) = \begin{cases} 0 & \text{for } x < 0, \\ \frac{1}{2}n_N \left(\frac{a_\Delta}{b_\Delta}\right) x\sqrt{x^2 + \Delta r^2} & \text{for } 0 \leq x < b_\Delta, \\ \frac{1}{2}n_N a_\Delta \sqrt{b_\Delta^2 + \Delta r^2} + n_N a_\Delta (x - b_\Delta) \\ \quad + (b_{Reg} - n_N a_\Delta) \sqrt{(x - b_\Delta)^2 + \Delta r^2} & \text{for } x \geq b_\Delta. \end{cases} \quad (2.12)$$

While for  $x \geq b_\Delta$  the above area computation is not entirely physically consistent in that the tilted triangle area is simply extruded once  $x > b_\Delta$  and added to the truncated cone related to the rectangular notch section, this is deemed acceptable here because firstly the model should be seen as only a rough approximation to the complex flow situation anyways, but secondly because alternative modeling of the effective flow area does barely affect the resulting flow behavior. Thirdly, this difference is not of relevance within the main usage scenario for the model: stability assessment of a system in the proximity of  $x = 0$ . The chosen approach does ensure continuous blending of turbulent regimes at  $x = b_\Delta$ .

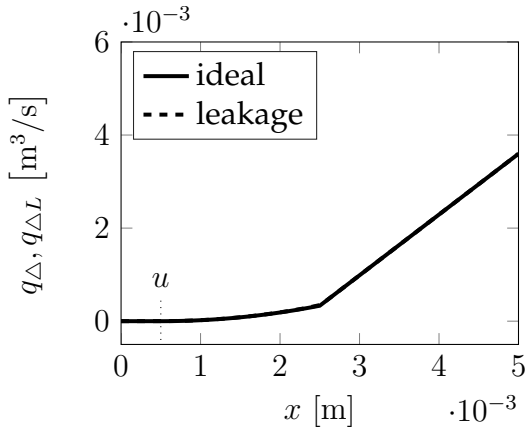
From these considerations, flow through a valve with a triangular notch featuring leakage can be modeled with

$$q_{L\Delta}(x, p_H, p_L) = -\frac{6\gamma_F^2 A_{TL\Delta}^2(x) \eta_F}{b_{LL\Delta}(x) \Delta r^3} l_{LL\Delta}(x) + \sqrt{\gamma_F^2 A_{TL\Delta}^2(x) (p_H - p_L) + \left(\frac{6\gamma_F^2 A_{TL\Delta}^2(x) \eta_F}{b_{LL\Delta}(x) \Delta r^3}\right)^2} l_{LL\Delta}^2(x) \quad (2.13)$$

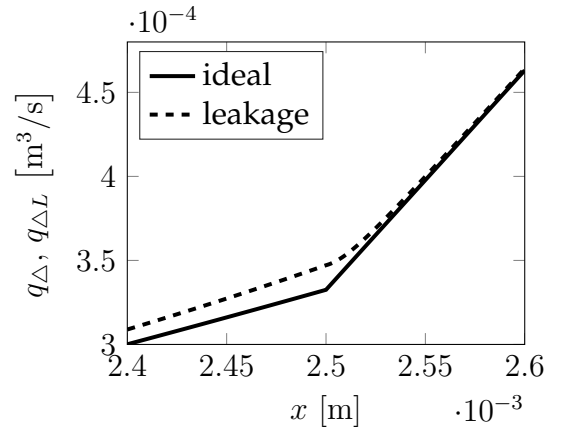
as

$$q_{\Delta L}(x, p_H, p_L) = \begin{cases} q_{L\Delta}(x, p_H, p_L) & \text{for } x < 0, \\ q_{L\Delta}(x, p_H, p_L) + \gamma_F A_{VO\Delta}(x) \sqrt{p_H - p_L} & \text{for } 0 \leq x < b_\Delta, \\ \gamma_F A_{VO\Delta}(x) \sqrt{p_H - p_L} & \text{for } x \geq b_\Delta. \end{cases} \quad (2.14)$$

Representative simulation results are shown in Figures 2.7a, 2.7b.



(a) Flow through triangular notch.



(b) Zoomed.

Figure 2.7: Leakage flow through triangular notch (featuring overlap  $u$ ).

From a macro perspective, the effect of leakage again is not prominent. Only when zooming into the flow Figure at  $x = b_\Delta + u$  (taking into account overlap  $u$ ) differences between the leakage and the non-leakage case becomes noticeable. It is within the interval  $u \leq x < b_\Delta + u$  that the aforementioned advantages of triangular notches with respect to total leakage flow can well be seen. This valve spool displacement is related to the transition between the flow regime from the triangular notch and the succeeding flow regime from the rectangular notch. Accordingly, the differences visible in Figure 2.7b are comparable to those observed in 2.4b.



$$l_{LLo2}(x) = \left( 2(x - r_o)\sqrt{x(2r_o - x)} + 2r_o^2 \arcsin\left(\frac{\sqrt{x(2r_o - x)}}{r_o}\right) - 4r_o(x - r_o) - r_o^2\pi \right) / \left( 4\left(r_o - \sqrt{x(2r_o - x)}\right) \right).$$

The corresponding width of the leakage channel modeled as throttle is given by

$$b_{LLo}(x) = \begin{cases} 2r_o & \text{for } x < 0, \\ 2\left(r_o - \sqrt{x(2r_o - x)}\right) & \text{for } 0 \leq x < r_o, \\ 0 & \text{for } x \geq r_o, \end{cases} \quad (2.18)$$

so that

$$A_{TL0}(x) = b_{LLo}(x)\Delta r \quad (2.19)$$

can easily be computed.

As laid out before, the orifice area from nominal valve opening for  $x > 0$  and  $\Delta r \neq 0$  is a tilted ellipse. Its magnitude is governed by

$$A_{VOo2}(x) = \begin{cases} 0 & \text{for } x < 0, \\ A_{VOo2}(x) & \text{for } 0 \leq x < 2r_o, \\ A_{VOo2}(2r_o) & \text{for } x \geq 2r_o \end{cases} \quad (2.20)$$

with

$$A_{VOo2}(x) = \left( \frac{r_o^2}{x} \arccos\left(1 - \frac{x}{r_o}\right) - \left(\frac{r_o}{x} - 1\right) \sqrt{x(2r_o - x)} \right) \sqrt{x^2 + \Delta r^2}. \quad (2.21)$$

It is worth pointing out that  $A_{VOo2}(x)$  bears a singularity for  $x = 0$  that requires smoothing to prevent from numerical problems with this approach. Results are shown in Figures 2.9a, 2.9b, indicating that for a circular notch, too, leakage has effects on a micro level only.

Ultimately, circular notch leakage flow thus is given by

$$q_{Lo}(x, p_H, p_L) = -\frac{6\gamma_F^2 A_{TL0}^2(x) \eta_F}{b_{LLo}(x) \Delta r^3} l_{LLo}(x) + \sqrt{\gamma_F^2 A_{TL0}^2(x) (p_H - p_L) + \left(\frac{6\gamma_F^2 A_{TL0}^2(x) \eta_F}{b_{LLo}(x) \Delta r^3}\right)^2 l_{LLo}^2(x)}, \quad (2.22)$$

so that circular notch flow with leakage can be stated accordingly:

$$q_{oL}(x, p_H, p_L) = \begin{cases} q_{Lo}(x, p_H, p_L) & \text{for } x < 0, \\ q_{Lo}(x, p_H, p_L) + \gamma_F A_{VOo2}(x) \sqrt{p_H - p_L} & \text{for } 0 \leq x < r_o, \\ \gamma_F A_{VOo2}(x) \sqrt{p_H - p_L} & \text{for } x \geq r_o. \end{cases} \quad (2.23)$$

In case of  $n_N$  notches, the mapping  $q_{oL}(x, p_H, p_L) \mapsto n_N q_{oL}(x, p_H, p_L)$  can be applied.

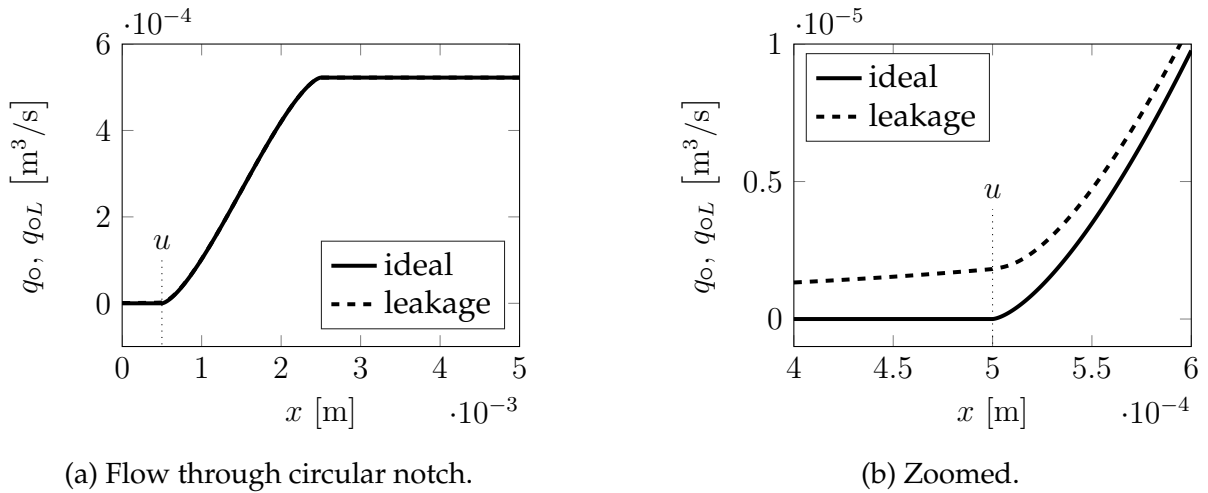


Figure 2.9: Leakage flow through circular notch (featuring overlap  $u$ ).

## 2.4 Flow Direction, Overlap and Opening Direction Transformations

While the above flow laws were derived for a valve opening towards the right hand side, the transformation  $x \mapsto -x - u$  allows using the same laws for a valve opening towards the left hand side with overlap  $u$ .

As for a reversal of flow directions due to a sign change of the pressure difference  $p_H - p_L$ , the transformation  $p_H - p_L \mapsto |p_H - p_L|$  in combination with a subsequent mapping  $q_{iL}(x, p_H, p_L) = q_{iL}(x, p_H - p_L) \mapsto \text{sign}(p_H - p_L)q_{iL}(x, |p_H - p_L|)$  can be applied for all notch geometries  $i = \{\square, \triangle, \circ\}$ .

## 2.5 Intermediate Conclusion

In this chapter, a modeling approach for leakage in hydraulic valves with discrete parameters was presented and refined with respect to notch geometries most commonly encountered in hydraulic systems practice.

With the approach of deriving such a model with discrete parameters, results from this model should be understood in a qualitative sense as the specific flow situation in valves with small radial clearance and small nominal openings is highly complex so that quantitatively accurate results are not to be expected from this model. It does however provide a sensible approach to leakage modeling that can easily be integrated into numerical models of aggregate hydraulic systems.

This is best achieved by implementing the respective flows in a single function which allows for a transformation of the displacement quantities according to the opening direction of the valve.



## 3 Modeling and Analysis of a Pressure Control Valve

### 3.1 Background

Valves are cornerstone elements of hydraulic systems and come in a large variety of functions and designs. The most important functions can be seen in the control of pressure and volume flow. Because of its frequent employment in automotive transmissions, a self-regulating pressure control valve shall be discussed here. The system under investigation (see Figure 3.1) is the simplest configuration of a hydraulic pressure control valve. It is a hybrid system in that it has a mechanical component – the valve spool – coupled with the dynamics of a hydraulic consumer through a piston area  $A$  upon which system pressure acts. This coupling makes the present system representative of hydraulic systems in general. The question of stability of such valves under different operating conditions has not yet been thoroughly investigated and shall therefore be treated here. The discussion here extends the results reported in [39] where a qualitative assessment of phase space properties of this system is given. Within this context, also see [136].

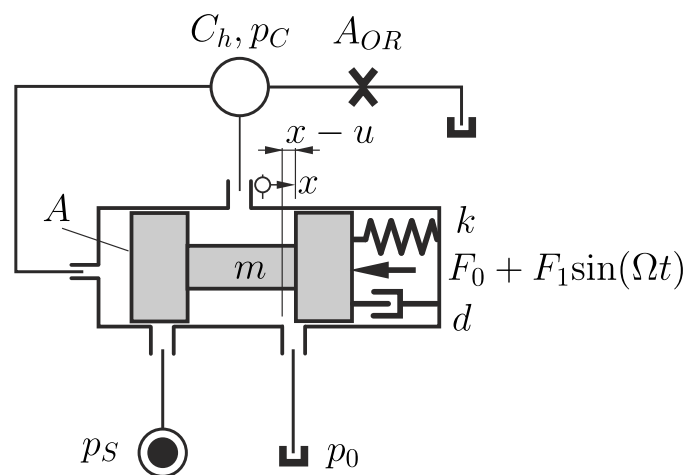


Figure 3.1: Pressure control valve.

## 3.2 System Description

The valve's function is to stabilize a certain set-point pressure level within the hydraulic consumer modeled by a capacitance  $C_h$ . Set-point pressure shall be maintained irrespective of volume out- or inflows from and to the consumer. It is defined by the choice of  $F_0$  and an appropriate level of pre-compression of the spring  $k$ . Through the feedback of the system pressure  $p_C$  on piston area  $A$ , deviations from the desired pressure level defined by  $F_0$  will perturb the force balance of the valve spool, thereby causing the valve to displace accordingly towards either the tank side or the pressure supply side control edge.

While in some situations there is no fluid outflow from  $C_h$ , in principle there may be load flow in the system. Within the scope of the present investigation, this load is modeled by an orifice  $A_{OR}$ . Once load flow across this orifice is positive, pressure within the capacitance drops, causing the valve to open the pressure supply sided control edge and allowing fluid to flow across the control edge and into the system. Thereby, pressure rises up to the desired level until the force balance on the valve spool is restored and the control edge closes. Alternatively, if pressure rises above the desired level, the valve will open towards the tank side, allowing fluid to flow out of the system and thereby restoring the desired pressure level. For non-transient volume in- or outflow to or from  $C_h$ , the valve's equilibrium position will therefore be such that the valve permits fluid flow across its control edges, thereby leveling out net flow within  $C_h$ .

In practical applications, the static component  $F_0$  of the force acting on the valve can come from a variety of sources. For magnetically actuated valves,  $F_0$  will be a magnetic force. In a lot of systems and especially in automotive engineering, the actuating force applied to the valve spool may come from a secondary hydraulic circuit whose purpose is not to transmit mechanical power, but to set the equilibrium position of the respective valve. In addition, the valve spool may be subject to periodic forcing. For hydraulically actuated valves, this may be induced by oscillations in the secondary hydraulic circuit which should not in general be assumed independent from main line pressure. For magnetic forcing, high frequency excitation is sometimes applied to the valve in order to achieve a dithering effect. This is done with the purpose of smoothening stiction behavior of the valve, thereby enhancing responsiveness to pressure changes on its pressure feedback area  $A$ .

The valve treated here features representative nonlinearities inherent to hydraulics: A typical source of nonlinearity besides the orifice dynamics within hydraulic systems are valve overlaps. These may be a design feature with the idea in mind to reduce the effects of leakage, but can also be a consequence of variance in the manufacturing process for nominally critically lapped valves, see the discussion in chapter 2. In either case, the result will be a nonlinear dependence of the valve flow on the valve spool displacement. It is important to note that overlaps directly affect the regulation quality of a pressure valve. For example, in the case of the valve discussed in this chapter, the bigger the overlap, the larger the pressure perturbation in the consumer needs to

be in order to cause a valve spool displacement exceeding valve overlap. For perfect set-point regulation, the valve should, in theory, be critically lapped. Here, however, a nominally overlapped valve shall be considered.

### 3.3 System Model

The equations describing the system behavior mirror the hybrid nature of the present system: by Newton's second law one obtains the equation of motion for the valve and formulating a balance equation for the fluid flow within the hydraulic consumer yields an equation for the hydraulic dynamics of the system coupled with the mechanical behavior by the dependence of the fluid flow on the position and the velocity of the valve spool. A simplified mechanical model of the valve and consumer can be given as

$$m\ddot{x} + d\dot{x} + kx = -F_0 - F_1\sin(\Omega t) + Ap_C, \quad (3.1)$$

with consumer pressure  $p_C = p^* + p$ . The applied force  $F_0$  defines set-point pressure  $p^*$  so that  $p$  represents perturbations from  $p^*$ . Considering the fluid flow balance, one obtains

$$C_h\dot{p} + A\dot{x} = q - \gamma_F A_{OR}\sqrt{p_C}, \quad (3.2)$$

where  $q$  is the fluid flow into capacitance  $C_h$  across the valve:

$$q = q(x, p_S, p_C) = \begin{cases} q_i(-x - u, p_S, p_C, \mathcal{P}_i) & \text{if } x < -u, \\ 0 & \text{if } -u \leq x \leq u, \\ -q_i(x - u, p_C, p_0, \mathcal{P}_i) & \text{if } x > u. \end{cases} \quad (3.3)$$

In the above equation, index  $i = \{\square, \triangle, \circ\}$  and  $u$  is the valve overlap which is assumed to be symmetrical here. The set  $\mathcal{P}_i$  comprises all control-edge related parameters specific to the respective notch geometry as discussed in chapter 2. The components of  $q$  are volume flows from the pressure supply into the system capacitance for  $x < -u$  and from  $C_h$  into the tank for  $x > u$ . As pointed out, the overlap  $u$  in both positive and negative displacement direction implies a dead band region and thereby a non-smooth flow description for an ideal valve. Without loss of generality, load flow is assumed positive in what follows, i.e. a flow out of  $C_h$  is assumed.

### 3.4 Stability Analysis

It is well known from advanced stability theory (see e.g. [79, 121]) that in the vicinity of an equilibrium of a nonlinear dynamical system, the nonlinear system is topologically equivalent to that of its linearization about the respective equilibrium point if none of the linearization's eigenvalues features a zero real part (Hartman-Grobman theorem) –

i.e. if the equilibrium is hyperbolic. The implication of this theorem is that a system's stability can be assessed by consideration of the real parts of its Jacobian's eigenvalues subject to the occurrence of zero real part eigenvalues.

In the following analysis, two situations will be distinguished: firstly, situations where there is non-zero (positive or negative) load flow and secondly situations where no load flow is extant. For the sake of simplicity, it is assumed that  $p_S > p^* + p > p_0 = 0$  at all times.

### 3.4.1 Non-Dimensionalization

Non-dimensionalization with  $x = uX$ ,  $t = T\tau$ ,  $T = \sqrt{m/k}$  and  $p = p(t) = (P^* + P(T\tau))\hat{p} = (P^* + P(\tau))\hat{p}$ , where  $\hat{p} = F_0/A$ , yields

$$X'' + 2D\omega X' + \omega^2 X = -\bar{F}_0 - \bar{F}_1 \sin(\eta\tau) + A_1(P^* + P) \quad (3.4)$$

$$P' = Q - \Gamma_{OR}\sqrt{P^* + P} - A_2X'. \quad (3.5)$$

Here,

$$\omega^2 = \frac{kT^2}{m} = 1, \quad D = \frac{d}{2\sqrt{mk}}, \quad A_1 = \frac{T^2 A}{mu} \hat{p}, \quad \bar{F}_0 = \frac{T^2}{mu} F_0, \quad (3.6)$$

$$\bar{F}_1 = \frac{T^2 F_1}{mu}, \quad \Gamma_{OR} = \frac{T\gamma_F A_{OR}}{C_h \sqrt{\hat{p}}}, \quad A_2 = \frac{Au}{C_h \hat{p}}, \quad \eta = \Omega T \quad (3.7)$$

and  $Q$  is non-dimensionalized control edge flow that will be specified further below. For non-zero load flow indicated by  $\Gamma_{OR} \neq 0$  and no excitation through  $\bar{F}_1$ , the equilibrium position  $X^*$ ,  $P^*$  can be computed from

$$\omega^2 X^* = -\bar{F}_0 + A_1 P^* \quad (3.8)$$

$$0 = Q(X^*, P^*) - \Gamma_{OR}\sqrt{P^*}. \quad (3.9)$$

For positive load  $\Gamma_{OR} > 0$ , the equilibrium for  $X^*$  will fulfill  $X^* < -1$  while for a negative load  $\Gamma_{OR} < 0$  it will hold that  $X^* > 1$ . The valve spool will displace by just as much as to compensate the load flow in order to maintain the pressure level defined by the magnitude of  $\bar{F}_0$ .

For sufficiently large pressure differences across orifices and control edges, linearization in the pressure coordinate is feasible. Assuming an ideal rectangular control edge, the non-dimensional volume flow  $Q$  across the valve can therefore be taken as

$$Q = Q_{\square}(X, P) = \begin{cases} -\Gamma_{\square}(X + 1)\sqrt{P_S - P^*} \left(1 - \frac{1}{2(P_S - P^*)}P\right) & \text{if } X < -1, \\ 0 & \text{if } -1 \leq X \leq 1, \\ -\Gamma_{\square}(X - 1)\sqrt{P^*} \left(1 + \frac{1}{2P^*}P\right) & \text{if } X > 1, \end{cases} \quad (3.10)$$

for which the constant

$$\Gamma_{\square} = \frac{uT\gamma_F b_{Reg}}{C_h \sqrt{\hat{p}}} \quad (3.11)$$

was introduced.

Alternatively, for a valve featuring a triangular notch, the volume flow in the proximity of the dead band can be stated as

$$Q = Q_{\Delta}(X, P) = \begin{cases} \Gamma_{\Delta}(X+1)^2 \sqrt{P_S - P^*} \left(1 - \frac{1}{2(P_S - P^*)} P\right) & \text{if } X < -1, \\ 0 & \text{if } -1 \leq X \leq 1, \\ -\Gamma_{\Delta}(X-1)^2 \sqrt{P^*} \left(1 + \frac{1}{2P^*} P\right) & \text{if } X > 1 \end{cases} \quad (3.12)$$

and

$$\Gamma_{\Delta} = \frac{u^2 T \gamma_F a_{\Delta}}{2 C_h \sqrt{\hat{p}} b_{\Delta}}.$$

Ultimately, for a circular notch, the volume flow linearized in  $P$  is

$$Q = Q_{\circ}(X, P) = \begin{cases} Q_{\circ 1}(X, P) & \text{if } X < -1, \\ 0 & \text{if } -1 \leq X \leq 1, \\ Q_{\circ 3}(X, P) & \text{if } X > 1. \end{cases}$$

Here, the respective flows are

$$Q_{\circ 1}(X, P) = \Gamma_{\circ} \left( -(\chi(X+1) + 1) \sqrt{1 - (\chi(X+1) + 1)^2} + \arcsin(\chi(X+1) + 1) + \frac{\pi}{2} \right) \sqrt{P_S - P^*} \left( 1 - \frac{1}{2(P_S - P^*)} P \right) \quad (3.13)$$

and

$$Q_{\circ 3}(X, P) = \Gamma_{\circ} \left( (\chi(X-1) - 1) \sqrt{1 - (\chi(X-1) - 1)^2} + \arcsin(\chi(X-1) - 1) + \frac{\pi}{2} \right) \sqrt{P^*} \left( 1 + \frac{1}{2P^*} P \right), \quad (3.14)$$

where the following constants were introduced:

$$\Gamma_{\circ} = \frac{r_{\circ}^2 T \gamma_F}{C_h \sqrt{\hat{p}}}, \quad \chi = \frac{u}{r_{\circ}}. \quad (3.15)$$

### 3.4.2 Stability Analysis for Non-Zero Load Flow

In order to gain an elementary understanding of the system behavior, it is sensible to further simplify the system equations by assuming that pressure changes about the equilibrium are dominated by changes in valve displacement. This assumption is also made in [56] for different notch geometries and in [39] for a valve with rectangular notch. While this certainly is a strongly simplifying assumption, it allows for the approximation of the pressure dynamics through a Taylor expansion up to zeroth order, so that ultimately the dead band region becomes the only source of nonlinearity considered in the remainder of this section.

For non-zero load flow it was argued on the foundation of physical reasoning that the valve spool will displace by as much towards the pressure supply side that the pressure drop from load flow will be compensated. With the assumption of constant non-zero load flow for the present analysis, questions of stability therefore arise. With an emphasis on the macro effects from control edge flow and therefore a neglect of leakage flow and first order pressure changes, conditions for the stability of the valve with equilibrium position outside of the dead band can be given analytically in a form that allows an intuitive, physics-based interpretation. The present analysis focuses on the case with  $\Gamma_{OR} > 0$  but is applicable to situations with  $\Gamma_{OR} < 0$ , too. In either case, non-zero load flow  $\Gamma_{OR} \neq 0$  will lead to an equilibrium position located in  $X^* \in (-\infty, -1) \cup (1, \infty)$ .

The general Jacobian for the system about an equilibrium  $\mathbf{X}^* = [P^*, X^*, 0]^T$  is given by

$$\mathbf{J}(\mathbf{X}^*) = \begin{bmatrix} \left. \frac{dQ}{dP} \right|_{(X^*, P^*)} - \frac{\Gamma_{OR}}{2\sqrt{P^*}} & \left. \frac{dQ}{dX} \right|_{(X^*, P^*)} & -A_2 \\ 0 & 0 & 1 \\ A_1 & -\omega^2 & -2D\omega \end{bmatrix}. \quad (3.16)$$

With

$$\left. \frac{dQ}{dP} \right|_{(X^*, P^*)} \ll \left. \frac{dQ}{dX} \right|_{(X^*, P^*)}, \quad (3.17)$$

the observation that

$$\frac{\Gamma_{OR}}{2\sqrt{P^*}} \ll A_1 \quad (3.18)$$

and, thereupon, the neglect of  $dQ/dP \mapsto 0$  and  $\Gamma_{OR}/(2\sqrt{P^*}) \mapsto 0$ , the simplified Jacobian upon which to perform a qualitative stability assessment can be stated as

$$\mathbf{J}(\mathbf{X}^*) = \begin{bmatrix} 0 & \left. \frac{dQ}{dX} \right|_{(X^*, P^*)} & -A_2 \\ 0 & 0 & 1 \\ A_1 & -\omega^2 & -2D\omega \end{bmatrix}. \quad (3.19)$$

The corresponding characteristic equation is

$$\lambda^3 + 2D\omega\lambda^2 + (A_1A_2 + \omega^2)\lambda - A_1 \left. \frac{dQ}{dX} \right|_{(X^*, P^*)} = 0, \quad (3.20)$$

which suggests that the stability properties of the system at equilibrium largely depend on the derivative of the flow function  $Q$  with respect to  $X$  in the equilibrium point for a given set of parameters.

**Stability of the control valve with rectangular notch** Because for a rectangular notch the flow function is linear in  $X$ , stability of the equilibrium position is independent of the location of  $X^* \in (-\infty, -1)$  and therefore independent of the load flow  $\Gamma_{OR}$  when ignoring first order changes in  $P$ . For the flow function's derivative in this case, one obtains

$$\left. \frac{dQ}{dX} \right|_{(X^*, P^*)} = -\Gamma_{\square} \sqrt{P_S - P^*}. \quad (3.21)$$

Substituting parameters in (3.20) and rearranging, after the introduction of the non-dimensional constant

$$\Upsilon = \frac{(C_h k + A^2) d}{\gamma_F m A u \sqrt{\hat{p}}} \quad (3.22)$$

also needed for the discussion of other notch geometries, one finds the maximum allowable pressure difference between supply pressure  $P_S$  and working point pressure  $P^*$  for which equilibrium positions  $X^* \in (-\infty, -1)$  are stable:

$$P_S - P^* < \left( \Upsilon \frac{u}{b_{Reg}} \right)^2. \quad (3.23)$$

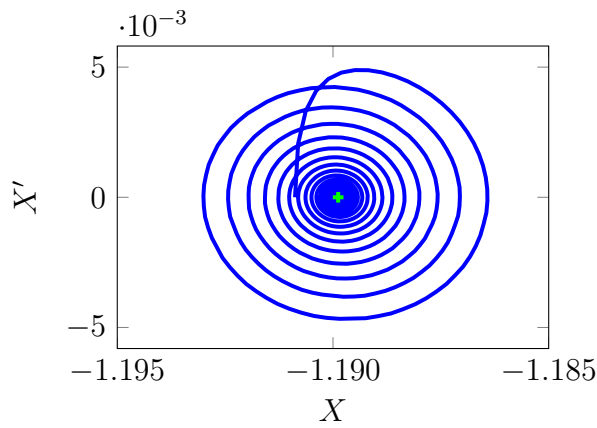
In practice, the working point of pressure control valves easily exceeds the maximum allowable pressure difference as given by (3.23). Under most circumstances, an equilibrium outside of  $X \in [-1, 1]$  will therefore be unstable. In Figure 3.2 two trajectories for the respective situations are shown for positive load flow. In Figure 3.2a a situation where the pressure difference between supply pressure and system working pressure fulfills (3.23) is shown. In contrast to this, Figure 3.2b clearly shows the limit cycles appearing in the system once (3.23) is offended. The different location of the equilibrium position is due to different pressure differences  $P_S - P^*$  between Figures 3.2a and 3.2b.

**Stability of the control valve with triangular notch** For a triangular notch and  $X^* < -1$ , it holds that

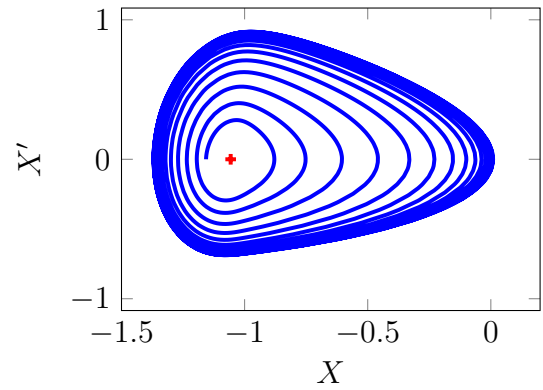
$$\left. \frac{dQ}{dX} \right|_{(X^*, P^*)} = 2\Gamma_{\Delta} (X^* + 1) \sqrt{P_S - P^*}. \quad (3.24)$$

The Hurwitz criterion for equilibrium positions  $X^* \in (-\infty, -1)$  can be rearranged into the region within which  $X^*$  is stable:

$$X^* > -1 - \Upsilon \frac{b_{\Delta}}{a_{\Delta}} \frac{1}{\sqrt{P_S - P^*}}. \quad (3.25)$$



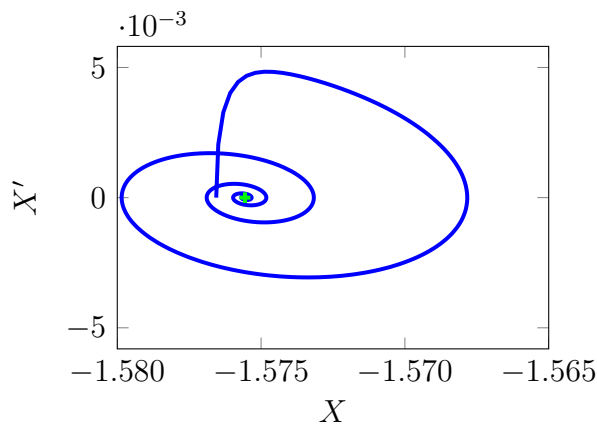
(a) Condition (3.23) fulfilled.



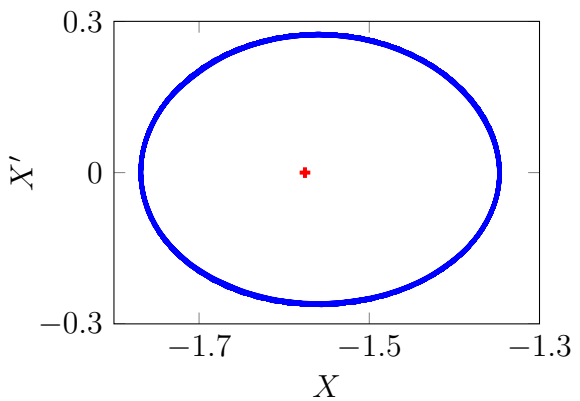
(b) Condition (3.23) offended through too large a pressure difference  $P_S - P^*$ .

Figure 3.2: Trajectories about the equilibrium contingent on condition (3.23). The equilibrium positions are highlighted by a green (stable equilibrium) and red (unstable equilibrium) cross.

For practical parameters, the equilibrium for a triangular notch can possibly remain stable as long as it does not transition into a rectangular opening (see chapter 2, equation (2.8)). In Figure 3.3 simulation results are shown. In Figure 3.3a the stability condition is fulfilled where in 3.3b the condition is offended through decreased damping so that a limit cycle about the equilibrium position occurs.



(a) Condition (3.25) fulfilled.



(b) Condition (3.25) offended through decreased damping - stationary process.

Figure 3.3: Trajectories about the equilibrium contingent on condition (3.25). The equilibrium positions are highlighted by a green (stable equilibrium) and red (unstable equilibrium) cross.

**Stability of the control valve with circular notch** In the case of a circular notch with  $X^* < -1$ , the flow function's derivative can, after some manipulations, be given as

$$\left. \frac{dQ}{dX} \right|_{(X^*, P^*)} = -2\Gamma_0 \chi \sqrt{1 - (\chi(-X^* - 1) - 1)^2} \sqrt{P_S - P^*}. \quad (3.26)$$

From the stability condition, one finds the range of stable equilibria accordingly:

$$X^* > -1 - \frac{r_o}{u} \left( 1 - \sqrt{1 - \left( \Upsilon \frac{u}{2r_o} \frac{1}{\sqrt{P_S - P^*}} \right)^2} \right). \quad (3.27)$$

The implication of the above stability condition is that a valve with circular notch will be stable in some interval in  $(-\infty, -1)$  for non-zero damping. For  $\sqrt{P_S - P^*}$  sufficiently small to yield a negative argument for the outer square root in (3.27), equilibria are stable. Figure 3.4 shows two different system configurations with stable (Figure 3.4a) and unstable (Figure 3.4b) equilibrium. Comparing the resulting limit cycle from Figure 3.2b with the one in Figure 3.4b, the impact of the valve flow increasing progressively with  $-X$  in the case of a circular notch can clearly be seen in the shape of the limit cycle: because for a circle the flow function's derivative with respect to  $X$  (compare equation (3.26)) equals zero as the valve opens at  $X = -1$ , there is no discontinuity in the opening area as the valve displacement crosses the point  $X = -1$ .

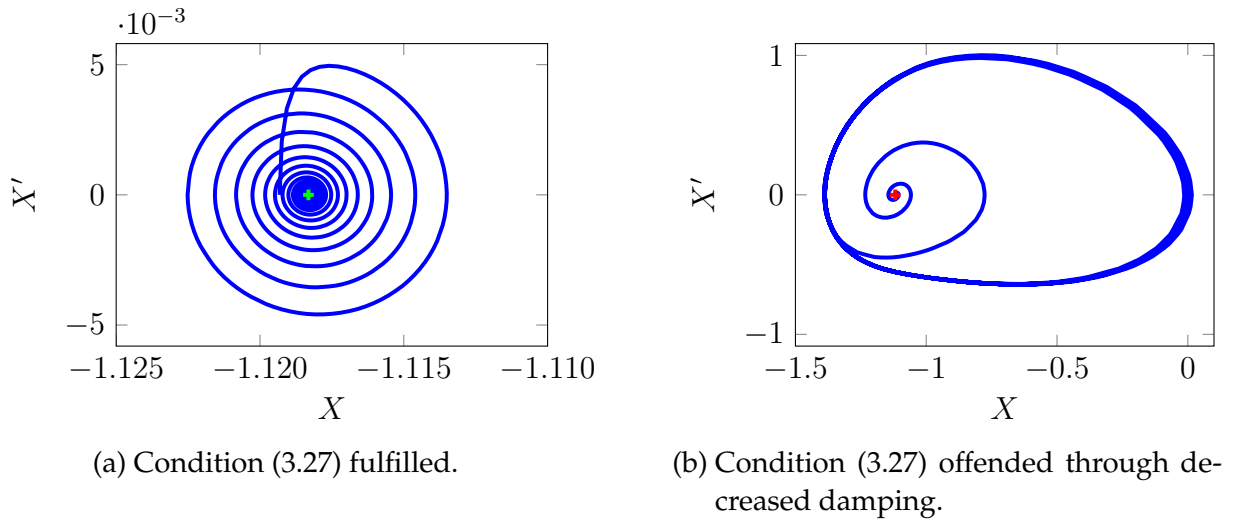


Figure 3.4: Trajectories about the equilibrium contingent on condition (3.27). The equilibrium positions are highlighted by a green (stable equilibrium) and red (unstable equilibrium) cross.

**Notch geometry comparison** The derivations outlined in the previous paragraphs showed that stability of a valve's equilibrium with open control edge depends on the

pressure difference across the control edge, non-dimensional parameter  $\Upsilon$  and non-dimensional geometry parameters  $b_{Reg}/u$ ,  $a_{\Delta}/b_{\Delta}$  and  $r_{\circ}/u$  for  $i = \{\square, \triangle, \circ\}$ , respectively.

Figure 3.5 visualizes the regions of stability for conditions (3.23), (3.25), (3.27) for the parameters listed in Table 3.1.

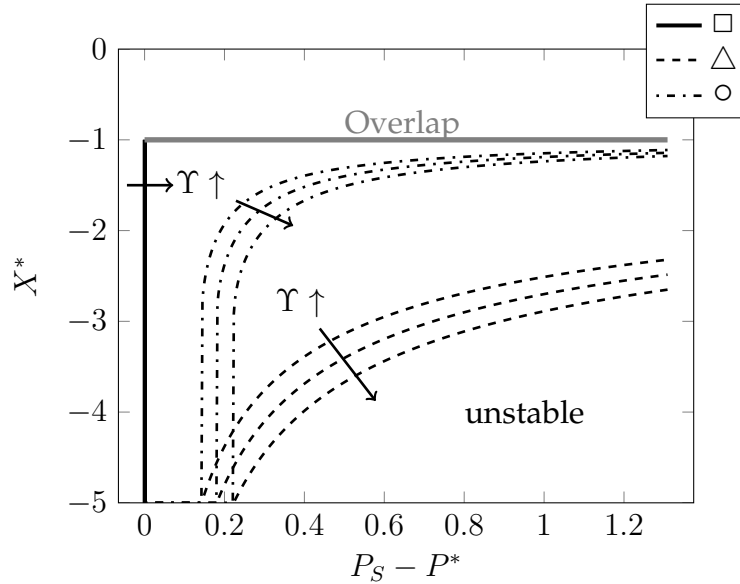


Figure 3.5: Stability map visualizing stability conditions (3.23), (3.25), (3.27).

As pointed out above, the rectangular notch is unstable for the majority of pressure differences – practically, its stable region is negligibly small as the corresponding vertical stability boundary is in close proximity of  $P_S - P^* = 0$  irrespective of variations in  $\Upsilon$ . The map also reveals the qualitative superiority of a triangular notch over a circular notch. As  $\Upsilon$  is increased, the stable regions increase for all geometries.

### 3.4.3 Stability Analysis for Zero Load Flow

For an ideal valve and zero load flow ( $\Gamma_{OR} = 0$ ), the equilibrium position of the valve will be set valued and lie within the interval  $X \in [-1, 1]$  since the flow function has infinitely many zeros: any point  $X^* \in [-1, 1]$  is a zero of the flow function and thus an equilibrium position. This is a feature of the dead region resulting from perfect impermeability when the valve is nominally closed. Equilibria for the resulting (linear) ordinary differential equation lie in the dead region of the ideal valve and are indifferent as the Jacobian

$$\mathbf{J}(\mathbf{X}^*) = \begin{bmatrix} 0 & 0 & -A_2 \\ 0 & 0 & 1 \\ A_1 & -\omega^2 & -2D\omega \end{bmatrix} \quad (3.28)$$

for this situation has the characteristic equation

$$\lambda^3 + 2D\omega\lambda^2 + (A_1A_2 + \omega^2)\lambda = 0 \quad (3.29)$$

and the corresponding eigenvalues

$$\lambda_1 = 0, \quad (3.30)$$

$$\lambda_2 = -D\omega + j\sqrt{\omega^2(1 - D^2) + A_1A_2}, \quad (3.31)$$

$$\lambda_3 = -D\omega - j\sqrt{\omega^2(1 - D^2) + A_1A_2}, \quad (3.32)$$

so that the maximum eigenvalue real part is equal to zero, implying an indifferent equilibrium position.

As discussed in chapter 2, ideal control valves cannot be provided by real-world manufacturing technology. In practice, tolerance errors will always generate leakage flow within the valve. It may therefore be asked in how far leakage affects the stability properties of the valve for zero load flow. For an ideal valve, the equilibrium position is set-valued with any point within the dead region being a possible equilibrium point. Allowing for leakage, the system obtains a unique equilibrium.

It is assumed that leakage flows at two points in the system, namely from pressure supply into the system and from the system into the tank. After non-dimensionalizing, leakage flow for  $i = \{\square, \triangle, \circ\}$  and a valve spool position within the dead band reads

$$\begin{aligned} Q &= Q_{Li}(X, P) \\ &= -q_{L1i}(-X - 1)L_{LLi}(-X - 1) \\ &\quad + \sqrt{(P_S - P^* - P)q_{L2i}(-X - 1) + q_{L1i}^2(-X - 1)L_{LLi}^2(-X - 1)} \\ &\quad + q_{L1i}(X - 1)L_{LLi}(X - 1) \\ &\quad - \sqrt{(P^* + P)q_{L2i}(X - 1) + q_{L1i}^2(X - 1)L_{LLi}^2(X - 1)} \end{aligned} \quad (3.33)$$

with the non-dimensional functions

$$q_{L1i}(X) = 6 \frac{T u \hat{\eta}_F}{C_h \hat{p}} \frac{b_{LLi}(uX)}{\lambda_L D} \Xi \gamma_F^2, \quad q_{L2i}(X) = \frac{T^2}{C_h^2 \hat{p}} \gamma_F^2 b_{LLi}^2(uX) \lambda_L^2 D^2. \quad (3.34)$$

In the above functions, the non-dimensional geometric leakage parameter  $\lambda_L = \Delta r/D$  was introduced and viscosity was scaled by  $\hat{\eta}_F = 1 \text{Pas}$  so that it can be represented by  $\Xi = \eta_F/\hat{\eta}_F$ . The new quantities  $L_{LLi}(X - 1)$ ,  $L_{LLi}(-X - 1)$  are the non-dimensionalized channel lengths for the laminar components of leakage for flow into the tank and from pressure supply into the system, respectively, as computed by equation (2.1) et sqq. for different notch geometries  $i = \{\square, \triangle, \circ\}$ . With this representation of volume flow, the equilibrium position can be computed upon which the Jacobian of the system about this equilibrium may be evaluated. Parameters used for simulation are listed in Table 3.1.

One natural choice of parameters by which to vary the system properties and to compute stability maps are supply pressure  $P_S$  and leakage parameter  $\lambda_L$ . For these, a

Table 3.1: Parameters of the pressure control valve.

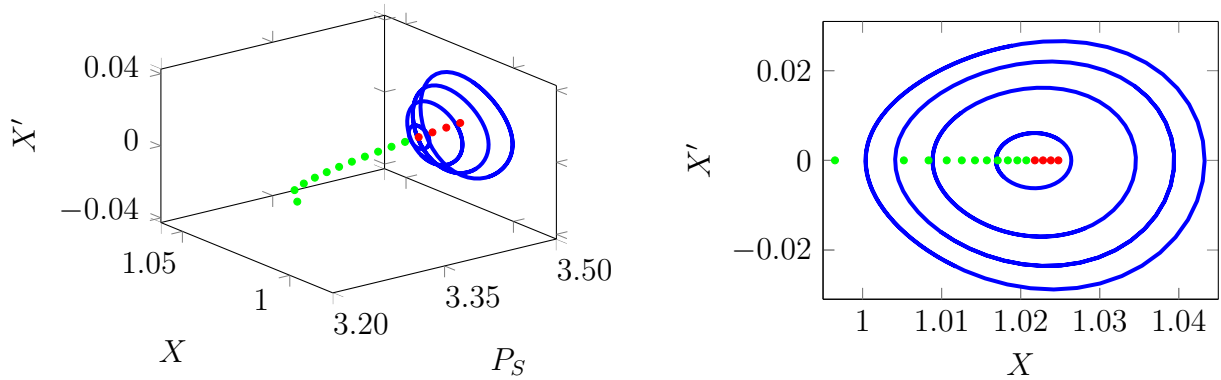
Parameter	Symbol	Value	Unit
Valve mass	$m$	0.015	kg
Damping coefficient	$d$	30	Ns/m
Spring stiffness	$k$	1000	N/m
Force components	$F_0, F_1$	135, 0–1	N
Excitation frequency	$\Omega$	$240\pi$	rad/s
System capacitance	$C_h$	$10^{-11}$	m <sup>3</sup> /bar
Piston area	$A$	$\pi/4 \times 0.01^2$	m <sup>2</sup>
Supplied pressure	$p_S$	20 – 50	bar
Flow coefficient	$\gamma_F$	0.029	$\sqrt{\text{m}^3/\text{kg}}$
Valve overlap	$u$	0.0001 – 0.0015	m
Diameter of piston bore	$D$	0.01	m
Spool circumference	$b_{Reg}$	$D\pi$	m
Triangular notch width	$b_\Delta$	0.002	m
Triangular notch length	$a_\Delta$	0.002	m
Circular notch radius	$r_\circ$	0.001	m
Gap height	$\Delta r$	$15 \times 10^{-6}$	m
Fluid viscosity	$\eta_F$	0.005	Pas

corresponding dimensional range of 20 – 80bar and  $1 \times 10^{-6} - 5 \times 10^{-5}$ m were chosen, respectively. While different system parameters do of course influence the precise location of the equilibrium position within  $-1 \leq X^* \leq 1$ , a numerical analysis reveals that for the majority of parameter constellations investigated the partial derivatives of the volume flow from (3.33) are such that a destabilization of the equilibrium position within  $-1 \leq X^* \leq 1$  does not occur. In these cases, equilibria within  $-1 \leq X^* \leq 1$  are stable irrespective of the notch geometries.

This is most notably due to the overlap  $u$  which for this type of valves typically lies in a range of up to 1.5mm. Because decreasing  $L_{LLi}(-X - 1)$  implies increasing  $L_{LLi}(X - 1)$  (and vice versa), from a certain point onwards in either displacement direction the turbulent component of leakage outflow dominates over its laminar inflow counterpart (and vice versa) as long as valve overlap  $u$  is sufficiently large.

For comparatively small overlaps (e.g. with  $u = 0.5 \times 10^{-3}$ m), however, destabilization through leakage is possible, albeit in a parameter region rarely encountered in practice, i.e. with a very large pressure difference between supply pressure and operating pressure. The mechanism behind this instability is visualized in Figure 3.6.

For increasing supply pressures, leakage into the system increases up to the point where leakage outflow can not compensate leakage inflow anymore: increasing supply pressures shift the equilibrium position towards an open control edge in direction of the tank. As a consequence, the valve begins to open nominally in order to achieve zero net



(a) Equilibrium path and limit cycle evolution for increasing supply pressure  $P_S$ .

(b) View of the  $(X, X')$ -plane.

Figure 3.6: Birth of a stable limit cycle from supply pressure increase as bifurcation parameter. Green dots represent stable, red points unstable equilibria.

fluid flow within the capacitance and to maintain set-pressure. As outlined above and expressed through stability condition (3.23), for a rectangular notch, an open control edge usually yields unstable behavior with limit cycles occurring about the unstable equilibrium. This can well be seen in Figure 3.6b: the equilibria become unstable once they lie in  $X^* > 1 + \varepsilon_i$ , where  $\varepsilon_i > 0$  is a small non-dimensional quantity depending on the leakage characteristic of the geometries  $i = \{\square, \triangle, \circ\}$  at hand. The stable limit cycles about the unstable equilibria therefore essentially are relaxation oscillations. The reason some equilibria remain stable for  $1 \leq X^* \leq 1 + \varepsilon_i$  (i.e. within the very proximity of  $X = 1$ ) is that the flow function gradient blends into an instability-generating gradient  $dQ/dX$  here as visualized in Figure 2.4b.

In Figure 3.7, a corresponding stability map for a rectangular notch for the variation of non-dimensional supply pressure  $P_S$  and non-dimensional leakage gap height  $\lambda_L$  is shown.

It can well be seen that larger gap heights require lower supply pressures for the equilibrium to remain stable. Increasing viscosity increases the stable region – this is intuitive since increasing viscosity decreases total leakage flow, thereby eventually leading to a situation where nominal valve opening is not required anymore to compensate leakage inflow.

For notch geometries other than the rectangular notch, destabilization through leakage is not observed in this parameter range. While it is possible that equilibria are shifted into a region where  $X^* > 1$  holds, stability conditions (3.25) and (3.27) provide the explanation for the persistence of equilibrium stability in spite of a nominally open control edge.

Destabilization effects from leakage within realistic pressure ranges are therefore to be expected mainly in almost critically lapped valves and operating scenarios involving excessively large pressure differences between supply and operating pressure. In chap-

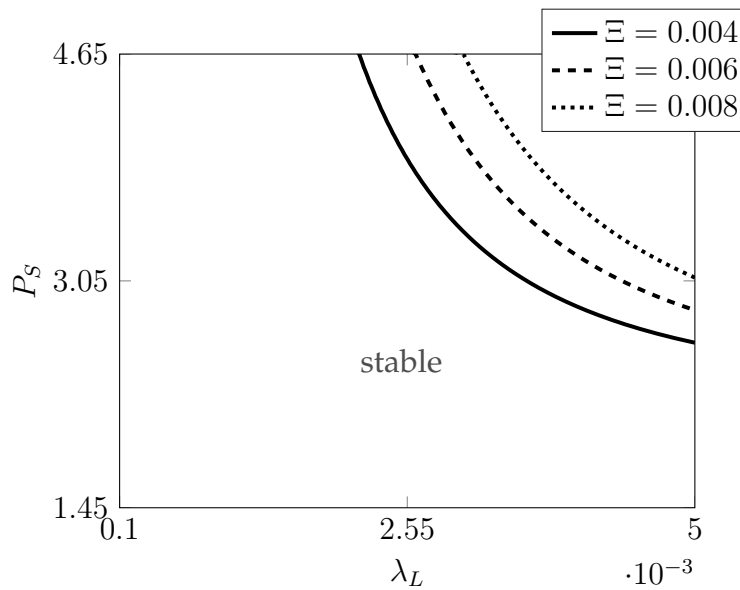


Figure 3.7: Stability map for a rectangular notch.

ter 6 destabilizing effects of leakage in the context of an almost critically lapped valve will be considered further.

### 3.5 Forced Response of the Pressure Control Valve

In practice, certain valve types may be subjected to high-frequency excitation with the purpose of an improved stiction behavior. For low frequency excitation and under simplifying modeling assumptions, it was shown in [39] that the nonlinearities of the present valve bear the potential for chaotic solutions upon periodic excitation. For high-frequency excitation which commonly lies in the range of 100 – 300Hz, the forced response behavior has yet to be investigated.

To do so, a Monte-Carlo approach following e.g. [66, 77] is employed. Here, the system is simulated from a number of random initial conditions up to stationary behavior for which the solutions are then investigated, most commonly in form of a Poincaré section, see [66, 77, 79, 121]. The choice of random initial conditions is motivated by the hope to thereby obtain a large number of and possibly all stable solutions that exist for the system. The approach does however not guarantee completeness, let alone finding unstable solutions.

Figure 3.8 shows the Poincaré sections through stationary solutions  $P_\Sigma$  for different notch geometries and overlaps subject to increasing forcing amplitude  $\bar{F}_1$ .

In order to gain qualitative insight into possible bifurcation scenarios for the system, a forcing range covering excitation force amplitudes not practically encountered in real world settings is investigated. The underlying model is the fully nonlinear model from equations (3.4), (3.5) featuring leakage.

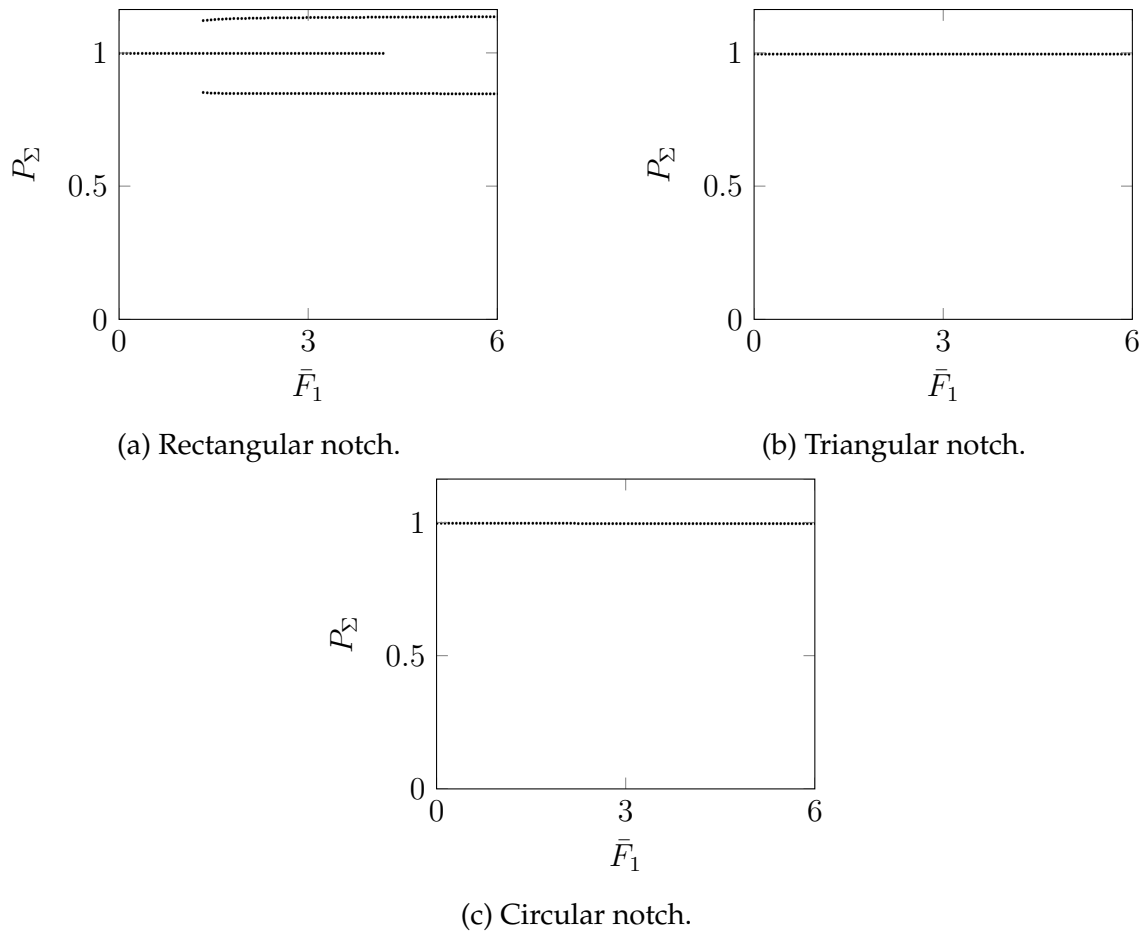


Figure 3.8: Stationary solutions for high frequency excitation,  $u = 0.0005\text{m}$ .

The results indicate that for the parameters in Table 3.1 there is no period-doubling up to quasi-periodicity or chaos for triangular and circular notch. For small overlaps and sufficiently large excitation force, however, the rectangular notch eventually gives rise to a period two solution. Parameters (system capacitance, damping and stiffness) were varied within reasonable ranges to ensure this is not an observation related to the specific choice of parameters – for these alternative parameter constellations similar behavior can be observed. In the context of dithering and high frequency excitation, larger overlaps may thus be preferable over smaller overlaps: Larger overlaps essentially prevent the valve from control edge opening due to dither and thereby from undesired interaction of the pressure regulating autonomous dynamics of the valve and the external forcing.

In [39], it was shown for a simplified model that the system features an unstable limit cycle. This limit cycle is also extant in the model when accounting for fully nonlinear pressure dynamics. Its location in phase space depends, amongst others, on operating and supply pressures. The existence of an unstable limit cycle in this system yields a stable limit cycle surrounding the unstable limit cycle in phase space, see Figure 3.9.

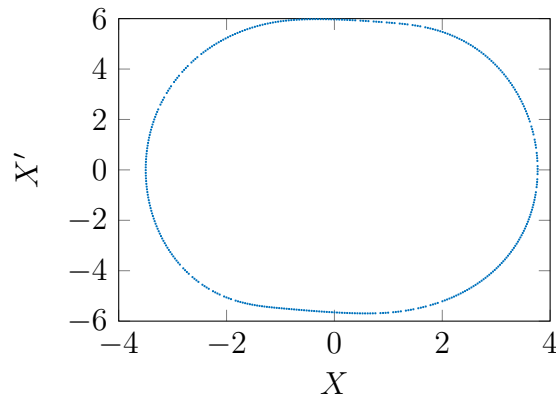
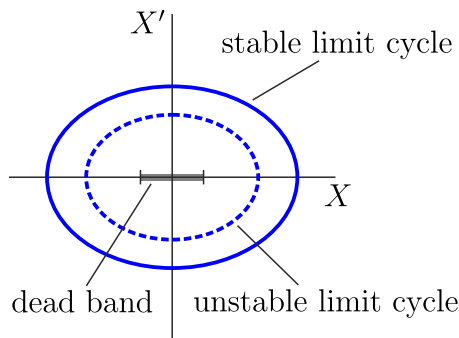


Figure 3.9: Phase space structure, see also [39].

Figure 3.10: Phase plane representation of the system's Poincaré map under high frequency excitation and an unstable limit cycle.

Naturally, once pressures are such that an unstable limit cycle repels the trajectory from its equilibrium and the trajectory is then attracted towards an outer stable limit cycle, quasi-periodic behavior can easily occur when additionally subjecting the valve spool to high-frequency excitation with an excitation frequency different from the (stable) limit cycle's natural frequency. Figure 3.10 illustrates this effect for a rectangular notch. Similar results can be expected when the system has an unstable equilibrium position in  $X^* \in (-\infty, -1) \cup (1, \infty)$ , since here the natural frequency of the stable limit cycle about the unstable equilibrium will likely be incommensurable with the external excitation's frequency.

### 3.6 Optimality Properties of the Pressure Control Valve

The design and topology of valves has – in most cases – evolved around practical questions of hydraulics engineering with solutions found by means of trial and error and engineering intuition. As for the control of (pressure) equilibrium positions, the pressure control valve discussed in this chapter is the elementary device to achieve the control goal of equilibrium regulation.

However, one may wonder if there are meaningful topology alternatives for the regulation of pressure by means of feeding back the physical states of the system to some technical device yet to be conceived. In any case, the existence of a set of control edges allowing for volume inflow and outflow and a displaceable mass allowing to alter the flow area of the pair of control edges upon actuation will be needed to achieve this task, so that an initial system configuration prior to valve design as shown in Figure 3.11 may be assumed.

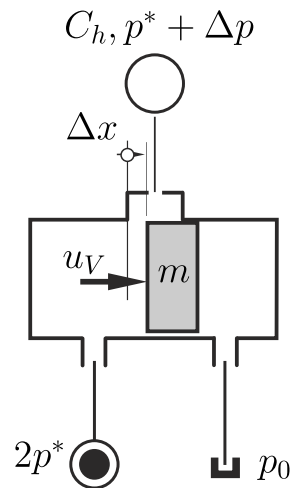


Figure 3.11: Initial valve structure for control valve synthesis.

With control theory providing a systematic approach to problems of set-point regulation, it is worth an effort to investigate if control theory would predict a different design of the pressure regulator from this chapter. The approach drawn onto will be linear quadratic regulation (also referred to as *LQR* both in the literature and in the remainder of this chapter). In order to apply this control approach to the problem of pressure regulation, certain simplifying assumptions have to be made for the system at hand.

The purpose of the valve is to control pressure  $p_C$  within a capacitance  $C_h$  and to level out possible perturbations in pressure  $p^*$ . Rewriting  $p_C = p^* + p = p^* + \Delta p$  with  $p^*$  the desired equilibrium position and  $\Delta p = p$  representing the deviations from this desired equilibrium position, the valve is to regulate  $\Delta p = 0$ . The control task thus is to exert a force upon a valve spool of mass  $m$  so that a volume inflow to and outflow of the capacitance is such that pressure deviations from  $p^*$  vanish. In order to make the problem accessible by *LQR* theory which is an inherently linear control approach, it will be

assumed that  $p_S = 2p^*$  and that no overlap exists, i.e.  $u = 0$ . Leakage is not considered and load flow is assumed to be zero. This leads to a smooth transition between the volume flows  $q_i(-x - u, p_S, p_C, \mathcal{P}_i)$  and  $-q_i(x - u, p_C, p_0, \mathcal{P}_i)$  for perfect set-point regulation to  $p_C = p^*$ :

$$q(x, p_S, p_C) = q(x, p_S, p^* + \Delta p) = \begin{cases} -\gamma_F b_{Reg} x \sqrt{p_S - p^* - \Delta p} & \text{for } x < 0, \\ -\gamma_F b_{Reg} x \sqrt{p^* + \Delta p} & \text{for } x \geq 0. \end{cases} \quad (3.35)$$

Upon linearization in  $x = x^* + \Delta x$  about  $x^* = 0$  and in  $p_C$  about  $p^*$  the *smooth* volume flow approximation reads

$$q \approx \left( \frac{\partial q}{\partial x} \bigg|_{x^*, p^*} \right) \Delta x + \left( \frac{\partial q}{\partial p_C} \bigg|_{x^*, p^*} \right) \Delta p \quad (3.36)$$

$$= -\gamma_F b_{Reg} \Delta x \sqrt{p^*}. \quad (3.37)$$

Here, it is to be noted that

$$\left( \frac{\partial q}{\partial p_C} \bigg|_{x^*=0, p=p^*} \right) = 0 \quad (3.38)$$

due to non-existing valve overlap and thereby  $x^* = 0$ .

With the system at this stage only comprising the valve spool and the capacitance subject to volume flow  $q$ , the system equations read

$$m\ddot{x} = 0, \quad (3.39)$$

$$C_h \dot{p} = q(x, p_S, p_C) \quad (3.40)$$

with  $q(x, p_S, p_C)$  from (3.35).

Approximating linearly through equation (3.37), the perturbed and linearized equations can be written as

$$m\Delta\ddot{x} = 0, \quad (3.41)$$

$$\Delta\dot{p} = -\frac{1}{C_h} \gamma_F b_{Reg} \Delta x \sqrt{p^*}. \quad (3.42)$$

Now, the intention is to derive a state-dependent force  $u_V = u_V(\Delta x, \Delta\dot{x}, \Delta p)$  acting on the valve spool in such a way that the control purpose, i.e. the control for  $\Delta p = 0$ , is fulfilled. The perturbed system (3.41), (3.42) subject to the control input to be devised can thus be stated as

$$m\Delta\ddot{x} = u_V, \quad (3.43)$$

$$\Delta\dot{p} = -\frac{1}{C_h} \gamma_F b_{Reg} \Delta x \sqrt{p^*}. \quad (3.44)$$

In state space formulation, this yields

$$\dot{\mathbf{x}} = \mathbf{A}\mathbf{x} + \mathbf{B}u_V \quad (3.45)$$

with the system or drift matrix  $\mathbf{A}$ , the control input matrix  $\mathbf{B}$  and the state vector  $\mathbf{x} = [x_1 \ x_2 \ x_3]^T = [\Delta x \ \Delta \dot{x} \ \Delta p]^T$  and

$$\mathbf{A} = \begin{bmatrix} 0 & 1 & 0 \\ 0 & 0 & 0 \\ -\frac{1}{C_h} \gamma_F b_{Reg} \sqrt{p^*} & 0 & 0 \end{bmatrix}, \quad \mathbf{B} = \begin{bmatrix} 0 \\ 1/m \\ 0 \end{bmatrix}. \quad (3.46)$$

The pair  $(\mathbf{A}, \mathbf{B})$  has the controllability matrix

$$\mathbf{C}_S = [\mathbf{B} \ \mathbf{A}\mathbf{B} \ \mathbf{A}^2\mathbf{B}] \quad (3.47)$$

with non-zero determinant and thus is controllable so that  $LQR$  is formally admissible. The  $LQR$  approach is based upon the formulation of a cost functional to be minimized by means of  $LQR$  design:

$$J = \int_{t_0}^{t_F} \mathbf{x}^T \mathbf{Q} \mathbf{x} + u_V \mathbf{B}^T \mathbf{R} \mathbf{B} u_V dt. \quad (3.48)$$

This cost functional penalizes deviations from the desired equilibrium  $\mathbf{x} = \mathbf{0}$  through matrix  $\mathbf{Q}$  and makes excessive control effort costly through matrix  $\mathbf{R}$ . The matrices  $\mathbf{Q}$  and  $\mathbf{R}$  contain weighting factors for the final deviation error and the control effort. In order to obtain a finite value for  $J$ ,  $\mathbf{x} \rightarrow \mathbf{0}$  for  $t_F \rightarrow \infty$ . The choice of the weighting factors defining  $\mathbf{Q}$  and  $\mathbf{R}$  is subject to the control design and has to be carefully made as the resulting control law is contingent on the choice of these matrices. Generally, both  $\mathbf{Q}$  and  $\mathbf{R}$  are required to be symmetric and positive definite – this guarantees the existence of a minimum of the cost functional  $J$ . General recommendations on tuning these matrices can be found in e.g. [10, 25, 60, 65].

In the present case, the respective matrices are chosen as

$$\mathbf{Q} = \text{diag} \left( \frac{1}{\Delta x_{max}^2}, \frac{1}{\Delta \dot{x}_{max}^2}, \frac{1}{\Delta p_{max}^2} \right), \quad \mathbf{R} = \frac{1}{F_{max}^2}. \quad (3.49)$$

This choice is motivated by [10] where the choice of individual weights is suggested as the squared inverse of the desired maximum value of the respective states and controls. The maximum force  $F_{max}$  to be exerted on the valve spool is taken as in the range of

$$F_{max} = \mathcal{O}(\Delta p_{max} A_{max}), \quad (3.50)$$

i.e. it is chosen based on the reasoning that the force to be exerted on mass  $m$  should be bounded by the maximum pressure deviation that can be applied to a maximum piston area  $A_{max}$ .

While the *LQR* approach is suitable for time-variant problems too, an optimal solution to time-invariant problems is solved for by setting the upper integration limit in (3.48) to infinity:  $t_F \rightarrow \infty$ . For a time invariant controller, the computation of the control  $u_V$  resulting in the minimization of (3.48) with respect to (3.46) is equivalent to solving the (algebraic) Ricatti equation

$$\mathbf{0} = -\mathbf{S}\mathbf{A} - \mathbf{A}^T\mathbf{S} + \mathbf{S}\mathbf{B}\mathbf{R}^{-1}\mathbf{B}^T\mathbf{S} - \mathbf{Q} \quad (3.51)$$

for the matrix  $\mathbf{S}$ . This is most easily solved by the so-called sweep method, simply by integrating

$$\dot{\mathbf{S}} = -\mathbf{S}\mathbf{A} - \mathbf{A}^T\mathbf{S} + \mathbf{S}\mathbf{B}\mathbf{R}^{-1}\mathbf{B}^T\mathbf{S} - \mathbf{Q}. \quad (3.52)$$

backwards in time from steady state with respect to the boundary condition

$$\mathbf{S}(0) = \mathbf{0}.$$

This yields a solution for  $\mathbf{S}$ , from which the optimal control law follows as

$$u_V = -\mathbf{K}\mathbf{x} \quad (3.53)$$

with

$$\mathbf{K} = -\mathbf{R}^{-1}\mathbf{B}^T\mathbf{S}. \quad (3.54)$$

Performing the respective computations for representative values, one obtains the matrix  $\mathbf{K}$ . It is of the form

$$\mathbf{K} = \begin{bmatrix} k_1 & k_2 & k_3 \end{bmatrix} \quad (3.55)$$

with entries

$$k_1 \in \mathbb{R}^+, k_2 \in \mathbb{R}^+, k_3 \in \mathbb{R}^-. \quad (3.56)$$

This implies the necessity of a displacement-proportional *restoring* force (negative sign of the force via equation (3.53)) as well as a velocity-proportional force acting in opposite direction of the motion and a force proportional to the pressure deviation acting in positive direction (positive sign via (3.53)). In order to implement the optimal control law with purely physical elements, a spring with stiffness  $k = k_1$ , a damper with damping constant  $d = k_2$  and a piston area  $A = k_3$  feeding back the pressure deviation on the valve thus have to be implemented in the system. However, the matrix entry  $k_3 \neq 0$  requires to feed back the pressure deviation  $x_3 = \Delta p$  on the valve spool – with piston area  $A$ , only system pressure  $p$  can be fed back. The feedback of the deviation  $\Delta p$  from desired pressure  $p^*$  can be achieved by feeding back the actual pressure in positive  $x$ -direction on the piston area of the mass. Pre-stressing the spring by a force  $F_0$  then leads to effectively feeding back the pressure difference  $\Delta p = p - F_0/A$  on the piston

area. The spring pre-stress can therefore be interpreted as the means to physically perform a subtraction and to implement the feedback of pressure deviation  $\Delta p$ .

It is remarkable that the quantities obtained for  $k_1$ ,  $k_2$  and  $k_3$  from solving an optimal control problem lie fully in the range of real-world values for a pressure control valve with their respective signs capturing the real world pressure control valve topology. It therefore can be concluded that a real world pressure control valve as treated in this section has certain optimality properties. The flow  $A\dot{x}$  generated from valve spool motion in a real-world valve is not captured in the control design approach, but can be seen as a parasitic effect extant in a real world valve. Naturally, its relevance rises with decreasing capacitance of the consumer. From a theoretical perspective, valve overlaps can be seen as parasitic effects, too – preventing an otherwise perfect set-point regulator from achieving its goal.

### 3.7 Intermediate Conclusion

In this chapter, the model of a simple hydraulic pressure control device was presented and simplified for the needs of stability analysis.

Generally speaking, it was found that equilibria which require an open control edge (towards either side) tend to be destabilized by increasing pressure differences across the control edge. Damping on the other hand increases stability. From a dynamics point of view, low pressure differences across valves ought to be strived for in hydraulic systems. The feedback area  $A$  has the same effect, which is intuitive: positive valve spool velocities in case of excess pressure will induce valve flow  $A\dot{x}$  which reduces pressure in addition to flow across the tank-sided control edge, thereby stabilizing pressure at the set-point. The same reasoning holds for negative velocities in case of a pressure increase.

A comparison of valves with different notch geometries yielded the result that a triangular notch is most advantageous from a stability point of view.

Within the scope of this analysis it also was investigated if leakage can destabilize an equilibrium position. It was found that for certain constellations of gap height, viscosity and pressure-differential between supply and operating pressure, leakage may shift the equilibrium position towards unstable regimes. This observation remained specific to the rectangular notch – for triangular and circular notches no such destabilization through leakage was observed.

The model allows for a physically intuitive assessment of stability conditions. It should be kept in mind, however, that the neglect of pressure changes in the derivation of the stability conditions implies limited prediction quality of the model in quantitative

terms.

Introducing further simplifications with respect to system smoothness, the pressure regulator valve as utilized in many practical instances could be shown to be structurally optimal from an  $LQR$  point of view.

# 4 Modeling and Simulating Clutch Actuation in an Automatic Transmission

## 4.1 Background

Modern automotive transmissions come in a variety of possible designs and specific actuation topologies. Among the foremost design questions, hydraulic system layout and control design eminently determine the dynamics and performance of the transmission and therefore require careful planning – especially with respect to questions of system robustness and stability. In order to achieve the desired dynamic behavior in a transmission, the availability of a theoretical model based on the laws of physics is in many cases inevitable. Such models have remained scarce in the publicly available body of research so far, mostly due to reasons related to questions of intellectual property. In this chapter, a model for the actuation of a clutch in an automatic transmission shall therefore be presented and discussed. Building on and relating to the analysis in chapter 3, a loss of system stability shall be demonstrated.

## 4.2 System Description

In Figure 4.1, a simplified system layout of a clutch actuation circuit for an automatic transmission is shown. In order to keep the model simple, only a single clutch cylinder is modeled. This is without loss of generality and the model can easily be extended to include multiple clutch cylinders.

The system comprises an energy/flow source in the form of the pump providing a volume flow  $q_P(u_P)$  contingent on pump input  $u_P$ . In the system discussed here, the pump is a fixed displacement pump whose volume flow thus depends on the pump capacity and the revolution speed which in this context is taken as the system input.

Main system pressure  $p_{PRV}$  in capacitance  $C_{hPRV}$  is regulated through the piloted regulation valve shown in detail in Figure 4.2. The working principle here is similar to the working principle of the valve discussed in chapter 3. While multiple secondary consumers will be served via a prioritization of control edges in many practical cases (see e.g. [24] for further reference), for modeling purposes and with a view towards test-bed validation, only a single control edge connecting the valve with a tank outlet are assumed here. The pilot solenoid valve shown in the upper half of Figure 4.2 is actuated via an input current which determines valve  $m_{PRV}$ 's actuation pressure  $p_{Y2}(u_{BWMDA})$ .

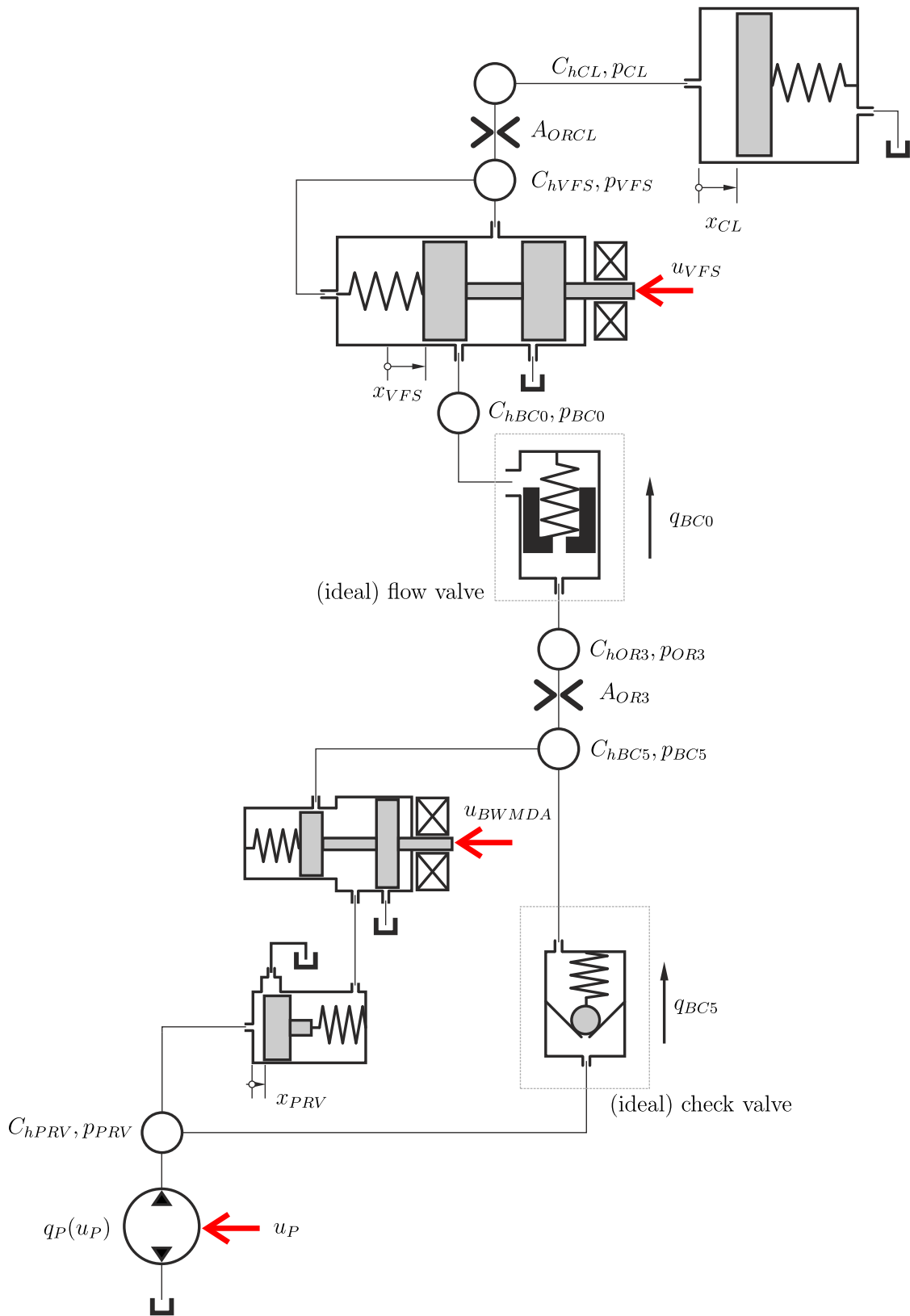


Figure 4.1: Clutch actuation circuit.

Pressure  $p_{Y2}$  is supplied with fluid from capacitance  $C_{hBC5}$  which is separated from main capacitance  $C_{hPRV}$  via a simple check valve.

Moving up further in the topology shown in Figure 4.1, fluid passes a flow valve restricting the volume passing to the clutch. Clutch pressure is largely controlled for through the valve shown in Figure 4.3. The valve controls pressure  $p_{VFS}$  upon valve input  $u_{VFS}$  which, after a pressure drop through orifice  $A_{ORCL}$ , then determines clutch pressure  $p_{CL}$ . The clutch itself is shown in Figure 4.4 and is modeled as a piston pressed against a pre-stressed spring. Parameters for the respective elements are given in Tables 4.1 – 4.4.

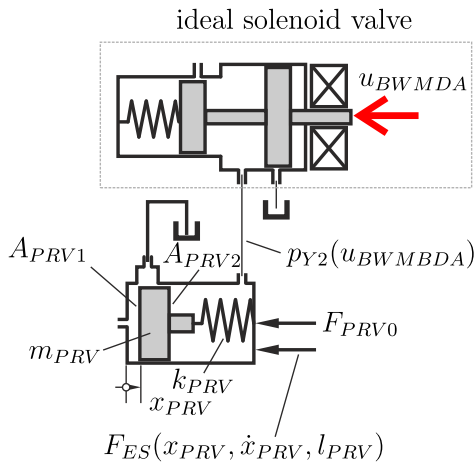


Figure 4.2: Pressure valve.

Parameter	Symbol	Value	Unit
Piston area	$A_{PRV1}$	$\frac{\pi}{4} \times 0.01^2$	m <sup>2</sup>
Piston area	$A_{PRV2}$	$\frac{\pi}{4} \times 0.015^2$	m <sup>2</sup>
Piston mass	$m_{PRV}$	0.015	kg
Valve damping	$d_{PRV}$	5 – 20	Ns/m
Spring stiffness	$k_{PRV}$	1000	N/m
Spring pre-stress	$F_{PRV0}$	10	N
Channel length	$l_{PRV}$	0.005	m
Outlet width	$l_{RegPRV}$	0.003	m
Valve overlap	$u_{PRV}$	0.001	m

Table 4.1: Pressure valve parameters.

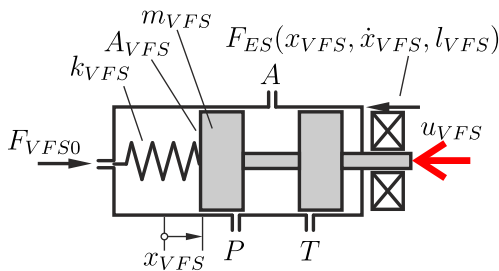


Figure 4.3: Clutch valve.

Parameter	Symbol	Value	Unit
Piston area	$A_{VFS}$	$\frac{\pi}{4} \times 0.005^2$	m <sup>2</sup>
Piston mass	$m_{VFS}$	0.015	kg
Valve damping	$d_{VFS}$	10	Ns/m
Spring stiffness	$k_{VFS}$	1000	N/m
Spring pre-stress	$F_{VFS0}$	10	N
Channel length	$l_{VFS}$	0.01	m
Outlet width	$l_{RegVFS}$	0.003	m
Valve overlap PA	$u_{VFS_{PA}}$	0.001	m
Valve overlap AT	$u_{VFS_{AT}}$	0.001	m

Table 4.2: Clutch valve parameters.

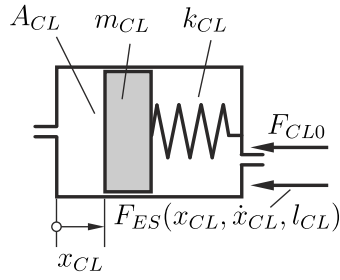


Figure 4.4: Clutch cylinder.

Parameter	Symbol	Value	Unit
Clutch area	$A_{CL}$	$\frac{\pi}{4} \times 0.04^2$	$\text{m}^2$
Clutch mass	$m_{CL}$	3	kg
Clutch damping	$d_{CL}$	20	Ns/m
Clutch stiffness	$k_{CL}$	$10^6$	N/m
Clutch pre-stress	$F_{CL0}$	200	N

Table 4.3: Clutch cylinder parameters.

Table 4.4: Miscellaneous parameters.

Parameter	Symbol	Value	Unit
Orifice area	$A_{OR3}$	$\frac{\pi}{4} \times 0.002^2$	$\text{m}^2$
Check valve orifice area	$A_{ORBC5}$	$\frac{\pi}{4} \times 0.002^2$	$\text{m}^2$
Orifice area	$A_{ORCL}$	$\frac{\pi}{4} \times 0.002^2$	$\text{m}^2$
Base volume	$V_{PRV0}$	$1 \times 10^{-4}$	$\text{m}^3$
Base volume	$V_{BC50}$	$1 \times 10^{-4}$	$\text{m}^3$
Base volume	$V_{OR30}$	$1 \times 10^{-4}$	$\text{m}^3$
Base volume	$V_{BC00}$	$1 \times 10^{-4}$	$\text{m}^3$
Base volume	$V_{VFS0}$	$1 \times 10^{-4}$	$\text{m}^3$
Base volume	$V_{CL0}$	$1 \times 10^{-4}$	$\text{m}^3$

### 4.3 System Model

The system is modeled with discrete parameters neglecting leakage effects. Because in many cases specific parameter knowledge for the system valves will not be available, simplifying assumptions for the dynamics of some of the valves governing the pressure dynamics in the transmission system need to be made. Mostly, valves are modeled as static (i.e. ideal) elements even in models of sophisticated hydraulic circuits. The assumption of static valve behavior neglects the dynamics of the valve itself, i.e. oscillatory behavior that may occur. While transfer functions of valves may be obtained from system identification, the assumption of static valves can be made in many cases with insignificant loss of model accuracy. For the model derived here, the check valve and flow valve limiting volume flow towards the clutch cylinder are assumed as ideal. The implication of ideal check valve behavior is a decoupling of the dynamics for main pressure  $p_{PRV}$  from the rest of the circuit. In a sense, this is beneficial for system functionality from a stability point of view.

In addition, the pilot valve governing pressure  $p_{Y2}$  is assumed to exhibit ideal dynamics. Along with this,  $p_{Y2}$  is taken as a linear function of solenoid valve input  $u_{BWMDA}$

due to ideal solenoid behavior. This assumption is justified by a negligibly small pilot actuation capacitance for  $m_{PRV}$  with volume flows across the solenoid valve control edges insignificant to the pressure dynamics in  $C_{hBC5}$ .

While the simplifying assumptions outlined above do certainly not represent the ideal approach to modeling a highly dynamic system such as an automotive transmission, they serve as a sensible starting point for further model refinement in accordance with test-bed measurements.

The system equations for the mechanical degrees of freedom

$$\mathbf{x}_m = [x_{PRV} \quad x_{VFS} \quad x_{CL}] \quad (4.1)$$

thus are

$$m_{PRV}\ddot{x}_{PRV} + d_{PRV}\dot{x}_{PRV} + k_{PRV}x_{PRV} = -F_{PRV0} - F_{ES}(x_{PRV}, \dot{x}_{PRV}, l_{PRV}) + p_{PRV}A_{PRV1} - p_{Y2}(u_{BWMDA})A_{PRV2}, \quad (4.2)$$

$$m_{VFS}\ddot{x}_{VFS} + d_{VFS}\dot{x}_{VFS} + k_{VFS}x_{VFS} = F_{VFS0} - F_{ES}(x_{VFS}, \dot{x}_{VFS}, l_{VFS}) + p_{VFS}A_{VFS} - u_{VFS}, \quad (4.3)$$

$$m_{CL}\ddot{x}_{CL} + d_{CL}\dot{x}_{CL} + k_{CL}x_{CL} = -F_{CL0} - F_{ES}(x_{CL}, \dot{x}_{CL}, l_{CL}) + p_{CL}A_{CL}. \quad (4.4)$$

In these equations, end-stop forces are modeled with a regularization approach:

$$F_{ES}(x, \dot{x}, l) = \begin{cases} xk_{ES} + d_{ES}\min(\dot{x}, 0) & \text{if } x < 0, \\ 0 & \text{if } 0 \leq x \leq l, \\ (x - l)k_{ES} + d_{ES}\max(\dot{x}, 0) & \text{if } x > l. \end{cases} \quad (4.5)$$

Here,  $k_{ES}$  and  $d_{ES}$  are regularization parameters physically motivated by a real world's end stop stiffness and damping. In the above force formulation, it is assumed that coordinates are introduced relative to the left end stop of a mass.

The general hydraulic balance equations are

$$\mathbf{C}_h \dot{\mathbf{p}} = \mathbf{Q}\mathbf{q} + \mathbf{A}\dot{\mathbf{x}}_m \quad (4.6)$$

with the hydraulic states

$$\mathbf{p} = [p_{PRV} \quad p_{BC5} \quad p_{OR3} \quad p_{BC0} \quad p_{VFS} \quad p_{CL}] \quad (4.7)$$

for this system and with

$$\mathbf{C}_h = \mathbf{diag}([C_{hPRV} \quad C_{hBC5} \quad C_{hOR3} \quad C_{hBC0} \quad C_{hVFS} \quad C_{hCL}]) \quad (4.8)$$

for which

$$C_{hPRV} = \frac{V_{PRV0} + x_{PRV}A_{PRV1}}{E_{fl}}, \quad C_{hBC5} = \frac{V_{BC50}}{E_{fl}}, \quad (4.9)$$

$$C_{hOR3} = \frac{V_{OR30}}{E_{fl}}, \quad C_{hBC0} = \frac{V_{BC00}}{E_{fl}}, \quad (4.10)$$

$$C_{hVFS} = \frac{V_{VFS0} + x_{VFS}A_{VFS}}{E_{fl}}, \quad C_{hCL} = \frac{V_{CL0} + x_{CL}A_{CL}}{E_{fl}}. \quad (4.11)$$

The system volume flows are collected in vector  $\mathbf{q}$  with

$$\mathbf{q} = [q_P \quad q_{PRV} \quad q_{BC5} \quad q_{OR3} \quad q_{BC0} \quad q_{VFS_{PA}} \quad q_{VFS_{AT}} \quad q_{ORCL}]. \quad (4.12)$$

Here,

$$q_P = q_P(u_P), \quad (4.13)$$

$$q_{PRV} = q_{PRV}(x_{PRV}, p_{PRV}, p_0, \mathcal{P}_{PRV}), \quad (4.14)$$

$$q_{BC5} = \begin{cases} \gamma_F A_{ORBC5} \sqrt{p_{PRV} - p_{BC5}} & \text{if } p_{PRV} > p_{BC5}, \\ 0 & \text{else,} \end{cases} \quad (4.15)$$

$$q_{OR3} = \text{sign}(p_{BC5} - p_{OR3}) \gamma_F A_{OR3} \sqrt{|p_{BC5} - p_{OR3}|}, \quad (4.16)$$

$$q_{BC0} = \begin{cases} \tilde{q}_{BC0} & \text{if } \tilde{q}_{BC0} < \hat{q}_{BC0}, \\ \hat{q}_{BC0} & \text{else,} \end{cases} \quad (4.17)$$

$$\tilde{q}_{BC0} = \text{sign}(p_{OR3} - p_{BC0}) \gamma_F A_{BC0} \sqrt{|p_{OR3} - p_{BC0}|}, \quad (4.18)$$

$$q_{VFS_{PA}} = q_{VFS_{PA}}(x_{VFS}, p_{BC0}, p_{VFS}, \mathcal{P}_{VFS_{PA}}), \quad (4.19)$$

$$q_{VFS_{AT}} = q_{VFS_{AT}}(x_{VFS}, p_{VFS}, p_0, \mathcal{P}_{VFS_{AT}}), \quad (4.20)$$

$$q_{ORCL} = \text{sign}(p_{VFS} - p_{CL}) \gamma_F A_{ORCL} \sqrt{|p_{VFS} - p_{CL}|} \quad (4.21)$$

with  $\mathcal{P}_{PRV}$ ,  $\mathcal{P}_{VFS_{PA}}$  and  $\mathcal{P}_{VFS_{AT}}$  collecting the geometry parameters for the respective control edges. Clearly, equation (4.15) represents the assumption of an ideal check valve where equation (4.17) makes the ideal flow valve assumption mathematically explicit through a flow restriction by a maximum admissible volume flow  $\hat{q}_{BC0}$ . The matrices  $\mathbf{Q}$  and  $\mathbf{A}$  connecting the system volume flows and mechanical piston velocities with the pressure dynamics in the system capacitances are

$$\mathbf{Q} = \begin{bmatrix} 1 & -1 & -1 & 0 & 0 & 0 & 0 & 0 \\ 0 & 0 & 1 & -1 & 0 & 0 & 0 & 0 \\ 0 & 0 & 0 & 1 & -1 & 0 & 0 & 0 \\ 0 & 0 & 0 & 0 & 1 & -1 & 0 & 0 \\ 0 & 0 & 0 & 0 & 0 & 1 & -1 & -1 \\ 0 & 0 & 0 & 0 & 0 & 0 & 0 & 1 \end{bmatrix}, \quad \mathbf{A} = \begin{bmatrix} -A_{PRV} & 0 & 0 \\ 0 & 0 & 0 \\ 0 & 0 & 0 \\ 0 & 0 & 0 \\ 0 & -A_{VFS} & 0 \\ 0 & 0 & -A_{CL} \end{bmatrix}. \quad (4.22)$$

With this model, the system can be seen as an example of a top-down circuit which is common in hydraulic systems design: An energy source delivers volume flow which is allocated to consumers downward. Structurally, this is mirrored in the diagonal structure of  $\mathbf{Q}$ . Non-top down systems would not allow for a largely diagonal matrix representation of the volume flow allocation to the capacitances. Notably, this top-down structure is related to the neglect of pressure dynamics and volume flow balances for  $p_{Y2}$ . Since  $p_{Y2}$  is fed from  $p_{BC5}$ , a model taking these dynamics into account would result in a non-top-down system model. Topologically, this non-top-down property can be seen from the loop between  $C_{hPRV}$  and  $C_{hPBC5}$  and the valve components in between in Figure 4.1. By neglecting pressure dynamics for  $p_{Y2}$  and the corresponding volume flow balance, this loop structure is ignored, thus yielding the present top-down system model.

## 4.4 Simulation Results

In Figure 4.5 the system inputs used for system simulation are visualized. For the sake of an illustrative simulation, a constant pump input yielding a constant revolution speed and thus a constant pump volume flow are assumed. Pump volume flow is chosen so that it exceeds the level needed for operating the circuit at the desired pressure level  $p_{PRV}$  as defined by the choice of  $u_{BWMDA}$ . Consequentially, the valve has to open the tank-sided control edge, letting excess fluid pass into the tank and thereby bound pressure  $p_{PRV}$ . As for the main pressure actuation force, the input  $u_{BWMDA}$  is chosen to yield a force jump at  $t = 0.25s$  and a force drop at  $t = 0.75s$  to a level below the initial force input. This choice translates into a jump and a drop for  $p_{PRV}$ , accordingly. Ultimately, the clutch is to be actuated at  $t = 0.5s$  as is evident from Figure 4.5c where the clutch valve actuation force is shown. Here, from  $t = 0.75s$  onwards, clutch actuation pressure shall be reduced and kept at a non-zero level.

Figure 4.6 shows the simulation results for the system states in the case of a physically unstable scenario. With the plentitude of parameters in this system, such instabilities can easily occur – as in real world systems, too. The results clearly illustrate the decoupling properties of the (ideal) check-valve through which  $q_{BC5}$  passes. Instabilities occurring in the pressure control of  $p_{PRV}$  are largely eliminated through this valve, therefore not showing in the subsequent pressure and mechanical states.

With a view towards the findings from chapter 3, the instability occurring upon induced main pressure increase at  $t = 0.25s$  can be interpreted from the viewpoint of an excessive pressure difference across the main pressure regulation valve. In chapter 3 it was shown that larger pressure differences across valve edges eventually leads to a loss of stability. The findings also allow to implement a suitable countermeasure: By increasing damping, the instability can be prevented from appearing, see Figure 4.7 where the only difference to Figure 4.6 is an increased damping  $d_{PRV}$ . It should be kept in mind, however, that this interpretation is admissible mainly due to the decoupling property of the circuit's check valve and ideal pressure dynamics for  $p_{Y2}$ .

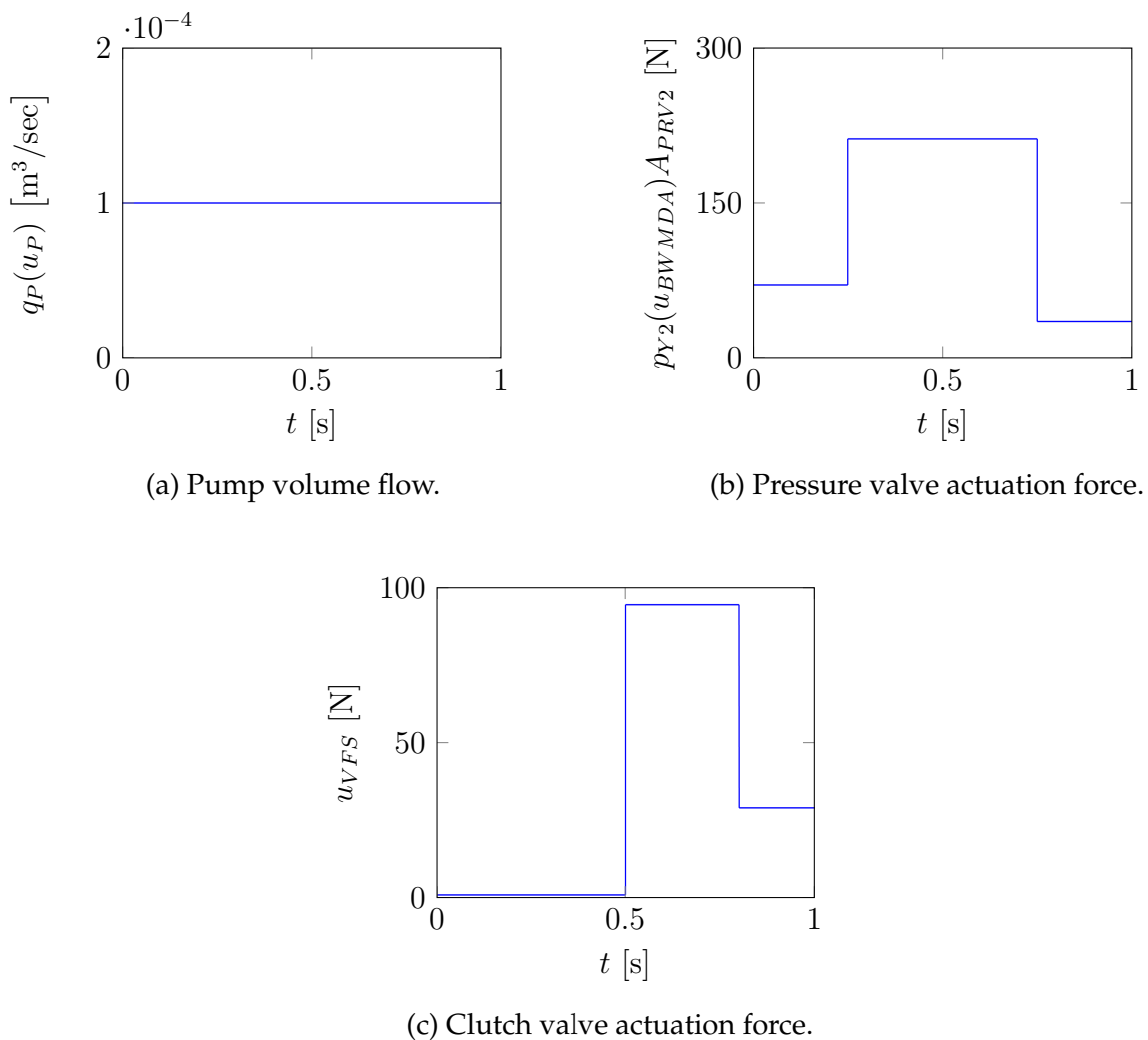


Figure 4.5: System inputs.

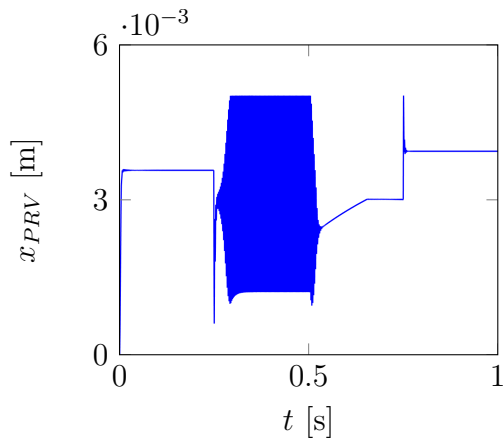
## 4.5 Intermediate Conclusion

In this chapter, the physical model of a hydraulic circuit employed in clutch actuation for an automatic transmission was presented.

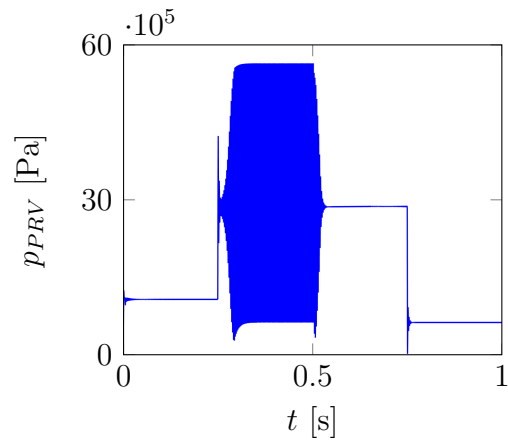
A stable and an unstable operating regime were discussed and interpreted against the background findings from chapter 3. Insight from the dynamical behavior of an isolated pressure regulation valve was drawn on to explain instability in the aggregate system and to derive appropriate countermeasures in order to eliminate the problem. Too large a pressure difference over the main pressure valve control edge in combination with insufficient valve damping were demonstrated to determine unstable system behavior. The effects from the respective instability within the aggregate system is alleviated, however, by a pressure decoupling check-valve, thereby only yielding sub-

optimal energetic and not physically dysfunctional circuit performance.

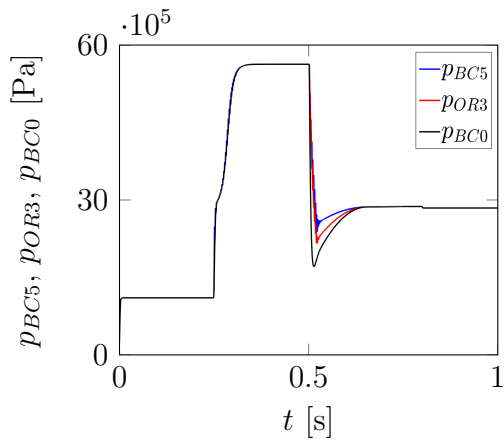
The model outlined in this chapter lends itself to in-depth stability analysis and to the application of identification and control techniques as frequently applied in automotive engineering. In the context within which this model was developed – FFG project 850729, jointly conducted with ITM/KIT, TU Vienna and AVL List GmbH Graz, Austria – this is measurement-based hybrid modeling and systematic and advanced system identification for energy-efficient actuation, employing methods investigated in the research group of Univ. Prof. DI. Dr. Stefan Jakubek at TU Vienna, Austria. The application of these techniques to this hydraulic circuit will be the focus of subsequent research effort for which the present model builds a foundation.



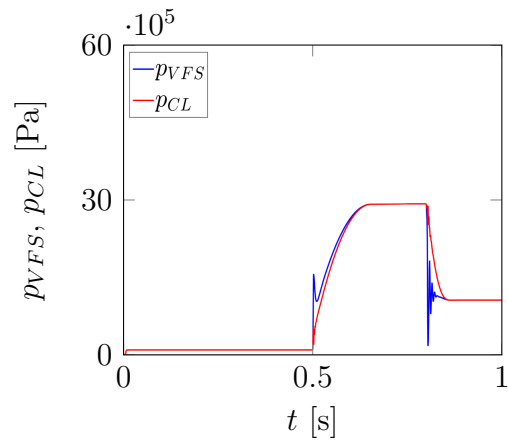
(a) Main pressure valve displacement.



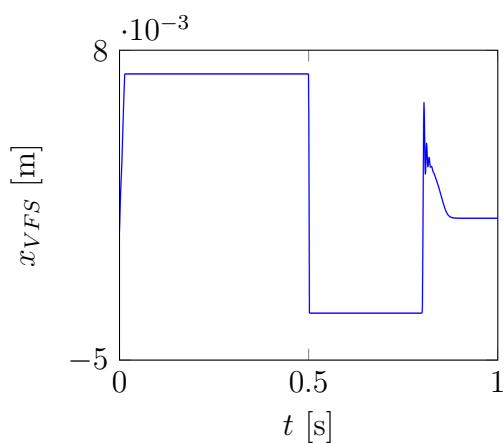
(b) Main pressure.



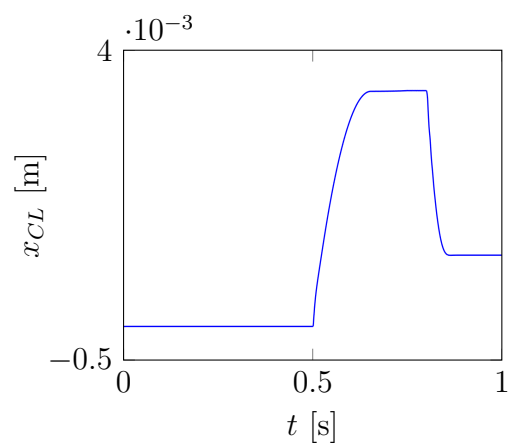
(c) Intermediate system pressures.



(d) Solenoid and clutch pressures.

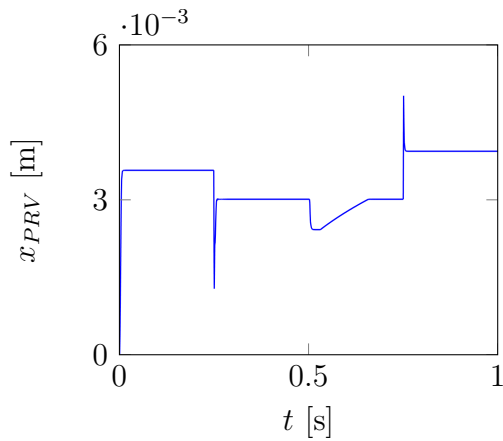


(e) Solenoid valve displacement.

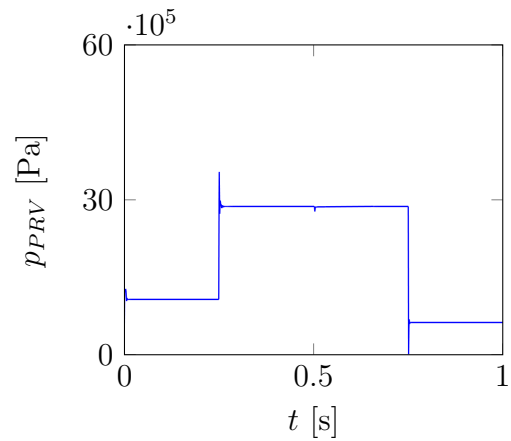


(f) Clutch displacement.

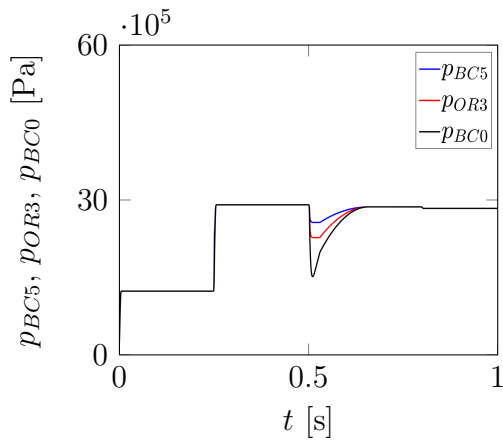
Figure 4.6: Unstable scenario.



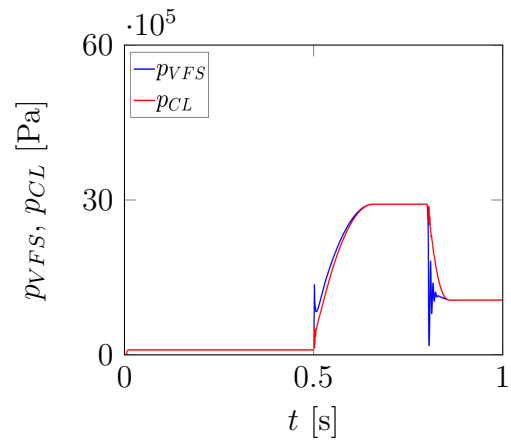
(a) Main pressure valve displacement.



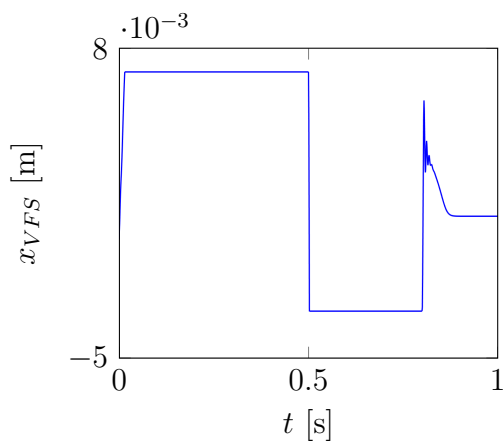
(b) Main pressure.



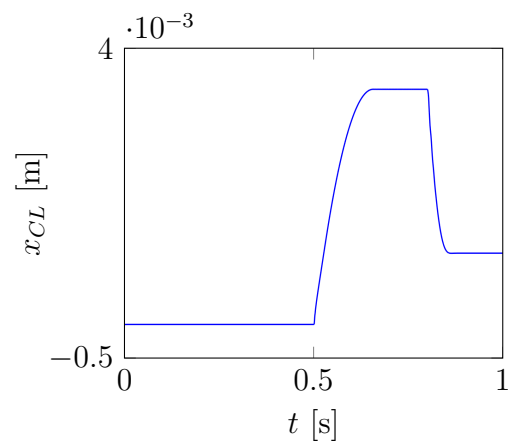
(c) Intermediate system pressures.



(d) Solenoid and clutch pressure.



(e) Solenoid valve displacement.



(f) Clutch displacement.

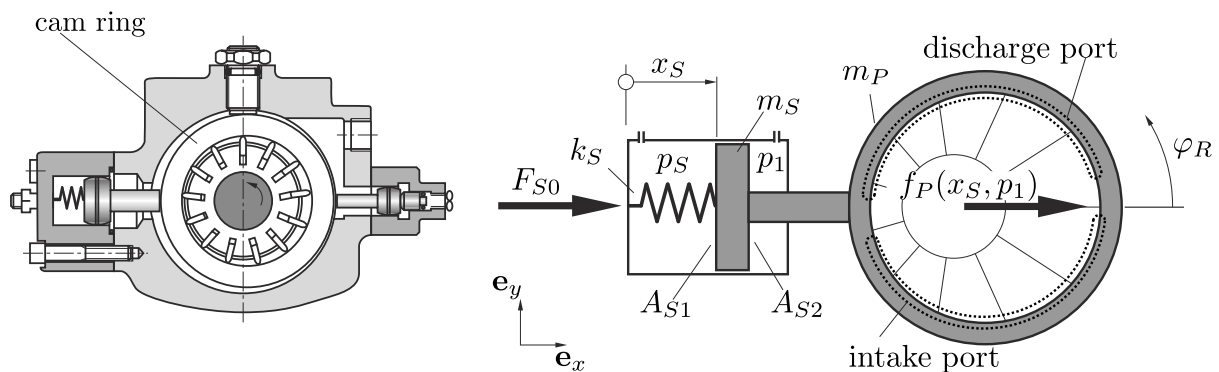
Figure 4.7: Stable scenario.



# 5 Modeling of a Variable Displacement Vane Pump

## 5.1 Background

Variable displacement pumps are used in a variety of applications. In contrast to fixed-displacement pumps, they allow for an adjustment of the volume flow provided by the pump to different requirements in a hydraulic circuit, most prominently volume flow or pressure control. Changes in pump volume flow according to the control purpose are achieved by displacing components of the pump that determine the pump's delivery volume. In the case of the variable displacement vane pump of translational type (see Figures 5.1a, 5.1b ) to be discussed here, this is the so-called cam ring along whose geometry the vanes of the pump slide and which can be displaced in horizontal direction.



(a) Pump construction, following [8]. (b) Cam ring with actuation components: Parameters and forces acting on the cam ring (end stop forces not shown).

Figure 5.1: Variable displacement vane pump.

For non-zero volume flow, this cam ring has to be displaced relative to the rotor bearing the vanes, thereby changing the chamber volumes they enclose during a revolution. This change of chamber volume leads to a compression and expansion of the enclosed fluid over a revolution of the pump. The fluid is discharged into the line once connection of a vane chamber with the line via the so-called discharge port is established. In contrast, volume expansion leads to fluid intake while passing the so-called intake port.

Because any pump exhibits an internal force evolution resulting from internal pressure dynamics, the displacement of the cam ring can only be achieved by overcoming the internal forces of the pump. Especially in mid- to high-pressure applications, the internal forces in a pump can easily become so large that a displacement based on external actuation through servo-mechanisms is inappropriate from an energetic point of view. For this reason, the actuation force usually comes from a hydraulic actuation mechanism. In order to devise suitable actuation strategies for different control purposes or to investigate the stability of systems featuring a variable displacement vane pump, an autonomous model of the internal pump dynamics and the resulting internal pump forces therefore is needed. It is the purpose of this section to derive such a model.

This will be achieved by taking relevant dynamical effects intrinsic to the working principle of the pump into account and by averaging the corresponding internal forces of the pump with respect to the revolution period. Averaging time-variant quantities is an approach commonly used in the assessment of hydraulic systems (see e.g. [6, 50, 54, 71, 94, 128, 130] ) and considered valid in the case of pumps if the chamber (= vane) frequency is larger than the undamped eigenfrequency of the cam ring [45] (and in the context of axial piston pumps [50]). While this line of reasoning can only be a rough assessment for the admissibility of such an approach in general, it will be deemed feasible here, too. The resulting pump model should therefore be considered as an idealization in that volume flow pulsation and internal force pulsation are averaged out. In many cases, the need for considering averaged quantities is further motivated by computation speed considerations, see e.g. [6, 45]. Within this chapter's context, also see [142, 143].

## 5.2 Pump Description

As briefly outlined in the preceding section, the working principle of the variable displacement vane pump is fluid intake and discharge during a revolution upon chamber expansion and contraction. In order to achieve chamber expansion and contraction over pump revolution, eccentricity of the cam ring's center  $O_C$  relative to the rotor center  $O_R$  (see Figure 5.2) is necessary. This eccentricity comprises two components: vertical and horizontal. While vertical eccentricity remains fixed during operation, the horizontal component of eccentricity corresponds to so-called cam ring displacement  $x_S$  which is variable and subject to cam ring actuation via hydraulic pistons of areas  $A_{S1}, A_{S2}$ , see Figure 5.1b.

The internal dynamics of the pump significantly depend on system or line pressure and the actual kinematic configuration of the displaced cam ring relative to the fixed rotor bearing the vanes. This kinematic configuration is firstly determined by discharge port angles  $\alpha_R^{L0}, \alpha_R^{L1}$  and intake port angles  $\alpha_R^{T0}, \alpha_R^{T1}$  as introduced in Figure 5.2. These angles are defined relative to the rotor (subscript "R") and are fixed quantities relative to the rotor. Secondly, cam ring eccentricity in vertical and horizontal direction affect the

change in chamber volumes upon revolution and thereby the internal pressure dynamics. These dynamics are modeled in this chapter taking into account three effects.

The first effect that is considered relevant for a model of the pump is related to the line pressure exposure of the vane chambers. As can be seen from Figure 5.2, as a vane chamber enters the pressure port region a uniform pressure equal to line pressure  $p_1$  is assumed to immediately manifest itself in the respective chamber. The pressure dynamics in the chambers thereby are assumed infinitely fast due to the high stiffness of the hydraulic fluid and the small chamber volumes, essentially yielding very fast and therefore negligible pressure dynamics. While this assumption neglects the pressure build-up or reduction phase in the chamber volume as a chamber enters the pressure port region, this effect is considered of no significant qualitative relevance; see also [90] and [45], where this assumption is made, too.

The second (and third) effect taken into account is related to the forces generated within distinct compression (and expansion) zones along the circumference of the cam ring which are referred to as dead volume zones in the remainder of this chapter. These zones are a result of port angle design: The working principle of the pump necessitates the existence of two dead zones within which contraction (and expansion) of the chamber volumes occur while passing from the tank port to the line port (and from the line port to the tank port). The necessity of compression (and expansion) dead volume zones derives from the need to separate intake and discharge port from another while a chamber moves between these – in case no such separation were designed for, fluid could flow from line to tank, resulting in hydraulic shortcut.

Another reason for these zones is that in many circumstances, pre-compression of the chamber volumes before entering the discharge port region is necessary. Most ideally, the chamber pressure of a vane entering the discharge port region would equal line pressure. If the pressure at the end of the dead volume compression phase is below line pressure, this will result in an impact-like rise in chamber pressure as soon as connection to the discharge port is established. This is a consequence of the fast dynamics of chamber pressure: the impact-like rise in chamber pressure results from oil-backflow from line to the vane chamber. This in turn is often related to undesired noise. In order to reduce such noise, the pump chambers may be subjected to pre-compression while passing through the compression dead volume zone with the pre-compression effect augmented by fixed vertical eccentricity of the cam ring. In the interest of a consistent derivation of the underlying kinematic relationships, the Figures in this chapter show positive vertical displacements where in real applications it assumes negative values in order to achieve the desired pre-compression effect.

Despite their significantly nonlinear nature, it will be demonstrated that averaging of the pump forces resulting from line pressure exposure surprisingly will result in a purely analytical model. As for pump forces from chamber compression and expansion, comparatively simple approximations will be shown to allow averaging of the respective forces, yielding satisfactory results.

## 5.3 Pump Model

### 5.3.1 Pump Kinematics

The major problem in deriving a minimal vane pump model is the circumstance that the pressure ports determining all relevant angles in the formulation of the force computation problem are fixed relative to the rotor bearing the vanes. However, forces resulting from pressure and acting on the cam ring are to be computed, thereby either a mapping between rotor-fixed geometrical quantities and cam-ring-fixed geometrical quantities is needed or the problem has to be formulated in such a way that the necessity of this mapping is circumvented. As it turns out, this mapping indeed is not required if the approach presented here is taken.

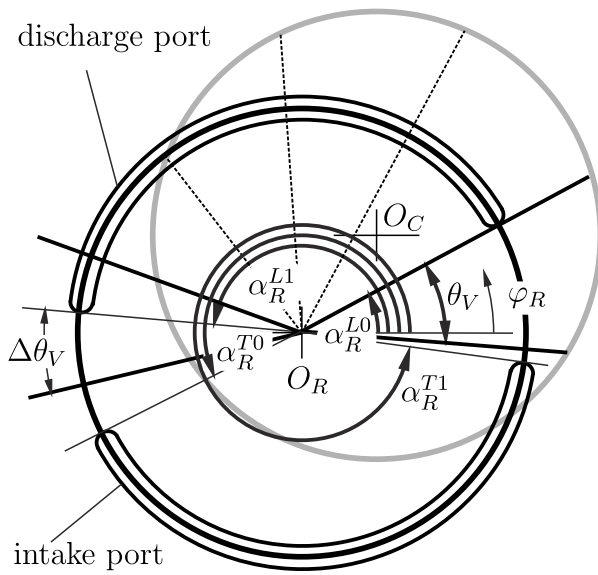


Figure 5.2: Vane pump kinematics: relevant angles.

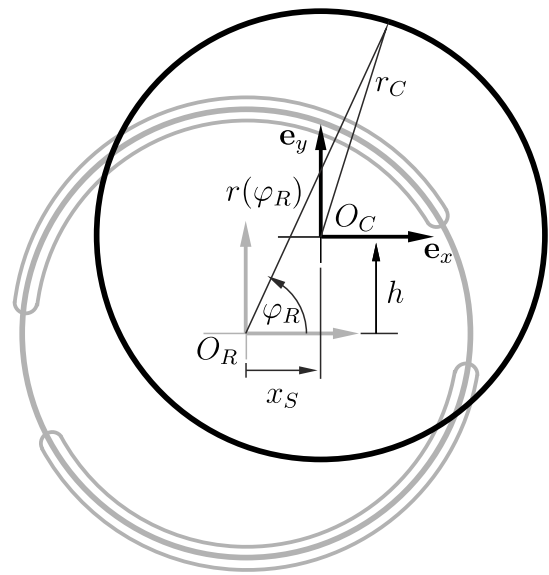


Figure 5.3: Vector ray.

From Figure 5.3, the vector ray connecting the center of the rotor  $O_R$  with an arbitrary point on the cam ring parameterized by  $\varphi_R$  has a length  $r(\varphi_R)$  that is given by

$$\psi_0 = \arctan\left(\frac{h}{x_S}\right),$$

$$r(\varphi_R) = \sqrt{x_S^2 + h^2} \cos(\varphi_R - \psi_0) + \sqrt{(x_S^2 + h^2) \cos^2(\varphi_R - \psi_0) - h^2 - x_S^2 + r_C^2}.$$

From here onwards,  $\varphi_R$  will be taken as the first vane chamber's leading vane's angle. This decision is arbitrary and does not alter the results of the analysis. It should be noted that  $r(\varphi_R)$  is a function of the cam-ring displacement  $x_S$  as well. In order to keep the notation simple, however, this functional dependence will not always be explicitly stated in what follows. Wherever relevant, dependence on  $x_S$  will be noted explicitly.

### 5.3.2 Pump Forces

Since pressure acts hydrostatically, forces from pressure in  $e_x$ - or  $e_y$ -direction can be computed by considering the effective area in the respective direction the pressure is acting on as shown in Figure 5.4 for the  $i$ -th vane chamber's pressure acting on cam ring in  $e_x$ -direction.

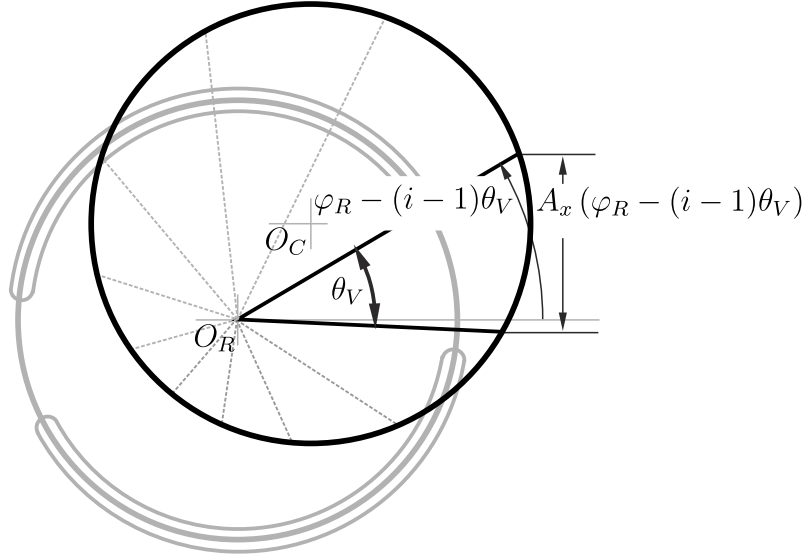


Figure 5.4: Effective area for force from a single chamber.

As the cam ring is displaced in  $e_x$ -direction, the general representation of the force from internal pressure in  $e_x$ -direction within the  $i$ -th single vane chamber (subscript "SC") undergoing a revolution quantified by the first chamber's leading vane's rotation angle  $\varphi_R$  can be stated as

$$\begin{aligned}
 F_{P,SC}(\varphi_R - (i-1)\theta_V) &= A_x(\varphi_R - (i-1)\theta_V)p(\varphi_R - (i-1)\theta_V) \\
 &= h_P \left[ r(\varphi_R - (i-1)\theta_V) \sin(\varphi_R - (i-1)\theta_V) \right. \\
 &\quad \left. - r(\varphi_R - i\theta_V) \sin(\varphi_R - i\theta_V) \right] p(\varphi_R - (i-1)\theta_V)
 \end{aligned} \tag{5.1}$$

where  $h_P$  is pump width and  $\theta_V$  the vane angle. The vane angle is determined by  $2\pi/n_{CH}$  with the number of vane chambers  $n_{CH}$ . The pump force's period thus is  $\theta_V$ , accordingly.

Now, because for the average force  $f_P(x_S, p_1)$  from the pump's internal pressure distribution the following holds

$$f_P(x_S, p_1) = \frac{1}{\theta_V} \int_0^{\theta_V} \sum_{i=1}^{n_{CH}} F_{P,SC}(\varphi_R - (i-1)\theta_V) d\varphi_R \tag{5.2}$$

$$= \frac{1}{\theta_V} \sum_{i=1}^{n_{CH}} \int_0^{\theta_V} F_{P,SC}(\varphi_R - (i-1)\theta_V) d\varphi_R. \tag{5.3}$$

Then, with the substitution  $\Phi = \varphi_R - (i - 1)\theta_V$ ,

$$f_P(x_S, p_1) = \frac{1}{\theta_V} \sum_{i=1}^{n_{CH}} \int_{-(i-1)\theta_V}^{-(i-1)\theta_V + \theta_V} F_{P,SC}(\Phi) d\Phi = \frac{1}{\theta_V} \int_0^{2\pi} F_{P,SC}(\Phi) d\Phi, \quad (5.4)$$

i.e. the average force from all pump chambers acting on the cam ring in  $e_x$ -direction over one period is equal to the average force from the pressure within a single vane chamber while passing from  $0 \leq \varphi_R < 2\pi$ .

For the sake of simplicity, the calculation is performed for the first vane chamber here. Since the derivations hold for any chamber  $i$ , the distinction between  $\Phi$  and  $\varphi_R$  will be made void in what follows and only  $\varphi_R$  will be used.

### 5.3.2.1 Forces from Line Pressure Exposure

Noting that generally the angular difference  $\alpha_R^{L1} - \alpha_R^{L0}$  is no natural number multiple of  $\theta_V$ , it becomes evident that the force from line pressure exposure of all exposed chambers exhibits a jump after a revolution angle of  $\theta_V - \Delta\theta_V$  where  $\Delta\theta_V$ , according to Figure 5.2, is

$$\Delta\theta_V = \theta_V \cdot \text{ceil} \left( \left( \alpha_R^{L1} - \alpha_R^{L0} \right) / \theta_V \right) - \left( \alpha_R^{L1} - \alpha_R^{L0} \right). \quad (5.5)$$

The force  $F_{LPE}$  from all chambers exposed to line pressure  $p_1$  (subscript "LPE") can then be given by

$$F_{LPE}(x_S, p_1, \varphi_R) = \begin{cases} p_1 h_P \left( r(\Theta_1(\varphi_R)) \sin(\Theta_1(\varphi_R)) \right. \\ \quad \left. - r(\Theta_0(\varphi_R)) \sin(\Theta_0(\varphi_R)) \right) & \text{for } 0 \leq \varphi_R < \theta_V - \Delta\theta_V, \\ p_1 h_P \left( r(\Theta_2(\varphi_R)) \sin(\Theta_2(\varphi_R)) \right. \\ \quad \left. - r(\Theta_0(\varphi_R)) \sin(\Theta_0(\varphi_R)) \right) & \text{for } \theta_V - \Delta\theta_V \leq \varphi_R < \theta_V \end{cases} \quad (5.6)$$

with

$$\Theta_0(\varphi_R) = \alpha_R^{L0} - \theta_V + \varphi_R, \quad (5.7)$$

$$\Theta_1(\varphi_R) = \alpha_R^{L1} + \Delta\theta_V + \varphi_R, \quad (5.8)$$

$$\Theta_2(\varphi_R) = \alpha_R^{L1} - (\theta_V - \Delta\theta_V) + \varphi_R. \quad (5.9)$$

For the parameters in Table 5.1, the force assumes the variation in revolution angle (proportional to time) shown in Figure 5.5.

With the considerations in equation (5.2) et sqq., the average force resulting from chamber exposure to line pressure can however be computed simply by averaging the force on the cam ring over period  $\theta_V$  for an individual chamber traversing the interval between  $\varphi_R = \alpha_R^{L0}$  and  $\varphi_R = \alpha_R^{L1} + \theta_V$ . This is the interval within which the respective vane chamber has connection with the discharge port. Thereby, the necessity to take the

Table 5.1: Vane pump parameters.

Parameter	Symbol	Value	Unit
Rotor radius	$r_R$	0.0445	m
Cam ring radius	$r_C$	0.048	m
Number of vane chambers	$n_{CH}$	11	
Vane chamber angle	$\theta_V$	$\frac{2\pi}{n_{CH}}$	rad
Vertical cam eccentricity	$h$	-0.001	m
Pump width	$h_P$	0.02	m
Pump revolution speed	$n_P$	900	rpm
Pump revolution frequency	$\Omega_P$	$2\pi n_P/60$	rad/s
Angle defining the beginning of discharge port	$\alpha_R^{L0}$	28	deg
Angle defining the end of discharge port	$\alpha_R^{L1}$	173	deg
Angle defining the beginning of tank port	$\alpha_R^{T0}$	208	deg
Angle defining the end of tank port	$\alpha_R^{T1}$	353	deg
Leakage parameter	$\gamma_1$	$1.5 \times 10^{-12}$	$\text{m}^4\text{s}/\text{kg}$
Leakage parameter multiple	$\kappa$	1	-
Line pressure	$p_1$	30	bar

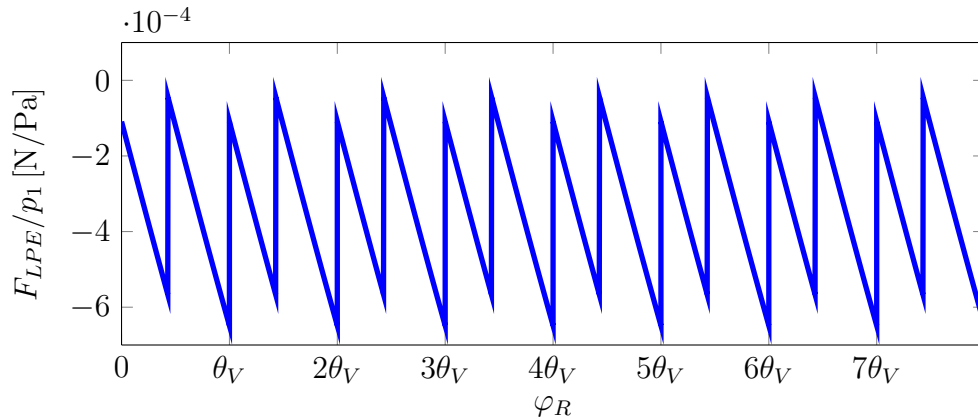


Figure 5.5: Force from line pressure exposure over revolution angle  $\varphi_R$  and  $x_S = 0.001\text{m}$ .

jump condition in (5.6) into consideration is spared. The average force in  $e_x$ -direction from line pressure exposure can thus be written as

$$f_{LPE}(x_S, p_1) = p_1 \overbrace{\frac{h_P}{\theta_V} \int_{\alpha_R^{L_0}}^{\alpha_R^{L_1} + \theta_V} [r(\varphi_R) \sin(\varphi_R) - r(\varphi_R - \theta_V) \sin(\varphi_R - \theta_V)] d\varphi_R}^{=: f_{P1}(x_S)}. \quad (5.10)$$

Before continuing, a closer look at the integrand reveals the need for one further transformation. If, for example, the first part of the integrand is considered and one introduces the abbreviation  $e_{hx_S} = \sqrt{x_S^2 + h^2}$ , one finds

$$r(\varphi_R) \sin(\varphi_R) = \left[ e_{hx_S} \cos(\varphi_R - \psi_0) + \sqrt{r_C^2 - e_{hx_S}^2 \sin^2(\varphi_R - \psi_0)} \right] \sin \varphi_R.$$

The subtraction of  $\psi_0$  in the arguments of the cos- and sin-functions makes the problem of finding an antiderivative unwieldy. Therefore, it is purposeful to introduce the transformation

$$\psi = \varphi_R - \psi_0. \quad (5.11)$$

Hence,

$$r(\varphi_R) \rightarrow r(\psi) = e_{hx_S} \cos(\psi) + \sqrt{r_C^2 - e_{hx_S}^2 \sin^2 \psi}. \quad (5.12)$$

Geometrically speaking, this corresponds to counting angle  $\varphi_R$  from a different position, i.e. the angle  $\varphi_R$  is shifted by  $\psi_0$  so that the force  $F_{P,SC}$  acting in  $e_x$ -direction can be interpreted as a projection of the components of a force in a  $(e_\xi, e_\eta)$  coordinate system rotated by  $\psi_0$  relative to the original coordinate system, see Figure 5.6.

According to Figures 5.6 and 5.7, the effective area the dead volume pressure acts on in  $e_x$ -direction can thus be decomposed into two effective areas in  $e_\xi$ - and  $e_\eta$ -directions, respectively:

$$A_\xi = -r(\psi) \cos(\psi) + r(\psi - \theta_V) \cos(\psi - \theta_V), \quad (5.13)$$

$$A_\eta = r(\psi) \sin(\psi) - r(\psi - \theta_V) \sin(\psi - \theta_V). \quad (5.14)$$

The corresponding force components in the respective directions therefore are

$$F_{P,SC\xi} = -p_1 h_P [r(\psi) \cos(\psi) - r(\psi - \theta_V) \cos(\psi - \theta_V)], \quad (5.15)$$

$$F_{P,SC\eta} = p_1 h_P [r(\psi) \sin(\psi) - r(\psi - \theta_V) \sin(\psi - \theta_V)]. \quad (5.16)$$

With

$$\mathbf{e}_x = \cos(\psi_0) \mathbf{e}_\xi - \sin(\psi_0) \mathbf{e}_\eta, \quad (5.17)$$

$$\mathbf{e}_y = \sin(\psi_0) \mathbf{e}_\xi + \cos(\psi_0) \mathbf{e}_\eta, \quad (5.18)$$

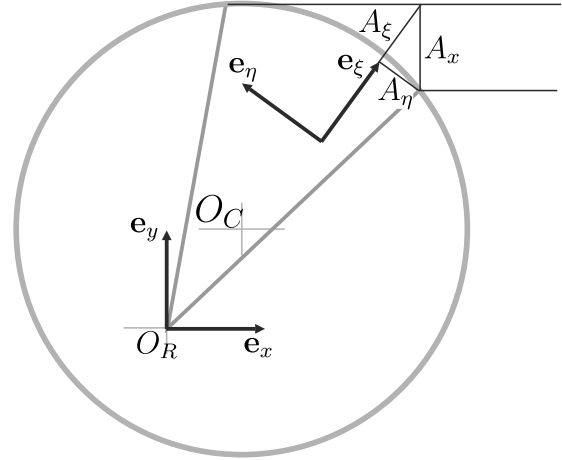
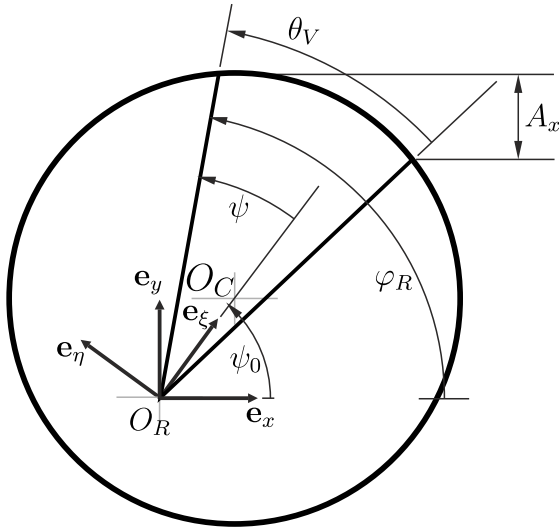


Figure 5.6: Kinematics of coordinate transformation (5.11). Figure 5.7: Pressure area decomposition.

the force from line pressure exposure in a single chamber  $\mathbf{F} = F_{P,SC\xi}\mathbf{e}_\xi + F_{P,SC\eta}\mathbf{e}_\eta$  can be projected onto the  $\mathbf{e}_x$ -direction:

$$F_{P,SC} = \mathbf{F} \cdot \mathbf{e}_x \quad (5.19)$$

$$= F_{P,SC\xi}\mathbf{e}_\xi \cdot \mathbf{e}_x + F_{P,SC\eta}\mathbf{e}_\eta \cdot \mathbf{e}_x \quad (5.20)$$

$$= F_{P,SC\xi} \cos(\psi_0) - F_{P,SC\eta} \sin(\psi_0). \quad (5.21)$$

By applying this transformation, the force in an individual chamber whose position is characterized by  $\alpha_R^{L0} - \psi_0 \leq \psi \leq \alpha_R^{L1} + \theta_V - \psi_0$  can ultimately be given as

$$\begin{aligned} F_{P,SC}(x_S, p_1, \psi) = & p_1 h_P \left[ \frac{h}{e_{hx_S}} \left( \left( e_{hx_S} \cos \psi + \sqrt{r_C^2 - e_{hx_S}^2 \sin^2 \psi} \right) \cos \psi \right. \right. \\ & - \left. \left( e_{hx_S} \cos(\psi - \theta_V) + \sqrt{r_C^2 - e_{hx_S}^2 \sin^2(\psi - \theta_V)} \right) \cos(\psi - \theta_V) \right) \\ & + \frac{x_S}{e_{hx_S}} \left( \left( e_{hx_S} \cos \psi + \sqrt{r_C^2 - e_{hx_S}^2 \sin^2 \psi} \right) \sin \psi \right. \\ & \left. \left. - \left( e_{hx_S} \cos(\psi - \theta_V) + \sqrt{r_C^2 - e_{hx_S}^2 \sin^2(\psi - \theta_V)} \right) \sin(\psi - \theta_V) \right) \right]. \end{aligned} \quad (5.22)$$

Then, the average force from line pressure exposure is given by (compare to (5.10))

$$f_{LPE}(x_S, p_1) = \frac{1}{\theta_V} \int_{\alpha_R^{L0} - \psi_0}^{\alpha_R^{L1} - \psi_0 + \theta_V} F_{P,SC}(x_S, p_1, \psi) d\psi = p_1 f_{P1}(x_S), \quad (5.23)$$

for which a closed form solution of manageable size exists for  $f_{P1}(x_S)$  that can be evaluated with the help of computer algebra systems such as MAPLE. It is remarkable that in contrast to alternative ways of deriving the above force-displacement-relationship, neither linearization of the kinematical relationships nor piecewise integration as a consequence of jump conditions as implied by equation (5.6) for the number of chambers exposed to line pressure are necessary.

Performing the respective calculations with the parameters from Table 5.1, the results for  $f_{P1}(x_S)$  are shown in Figure 5.8.

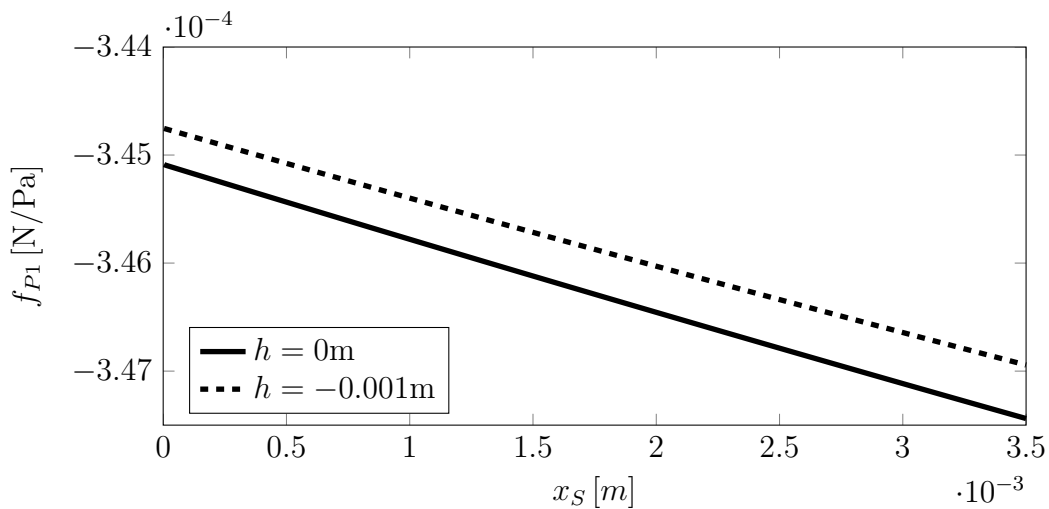


Figure 5.8: Average force area from line pressure exposure.

### 5.3.2.2 Forces from Dead Volume Compression

The second force effect taken into account is due to compression and expansion effects in the dead volumes, see Figure 5.9.

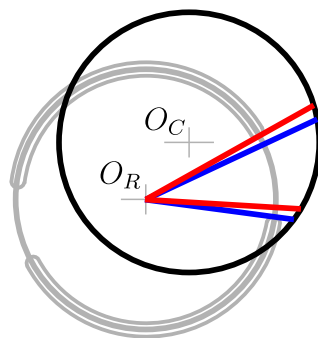


Figure 5.9: Dead volume compression: volume with intake pressure  $p_0 = 0$  (blue) and compressed volume (red).

Forces acting on the cam ring in dead volume regions result from compression and expansion and can be modeled as functions of the compression and expansion geometry. As in the calculation of the forces resulting from line pressure expansion of the vane chambers, an averaging approach with respect to vane chamber revolution will be utilized.

The starting point of the force computation again is the vector ray in Figure 5.3 describing the kinematics of the pump. By integration, one finds the chamber volume  $V(\varphi_R)$  for a specific position  $\varphi_R$  of the leading vane

$$\begin{aligned}
 V(\varphi_R) &= \frac{1}{2} h_P \int_{\varphi_R - \theta_V}^{\varphi_R} (r^2(\varphi_R) - r_R^2) d\varphi_R \\
 &= \frac{1}{4} h_P e_{hxS}^2 (\sin(2(\varphi_R - \psi_0)) - \sin(2(\varphi_R - \theta_V - \psi_0))) \\
 &\quad + \frac{1}{2} h_P r_C^2 \left[ \arctan \left( \frac{e_{hxS} \sin(\varphi_R - \psi_0)}{\sqrt{r_C^2 - e_{hxS}^2 \sin^2(\varphi_R - \psi_0)}} \right) \right. \\
 &\quad \quad \left. - \arctan \left( \frac{e_{hxS} \sin(\varphi_R - \theta_V - \psi_0)}{\sqrt{r_C^2 - e_{hxS}^2 \sin^2(\varphi_R - \theta_V - \psi_0)}} \right) \right] \\
 &\quad + \frac{1}{2} h_P e_{hxS} \left[ \sin(\varphi_R - \psi_0) \sqrt{r_C^2 - e_{hxS}^2 \sin^2(\varphi_R - \psi_0)} \right. \\
 &\quad \quad \left. - \sin(\varphi_R - \theta_V - \psi_0) \sqrt{r_C^2 - e_{hxS}^2 \sin^2(\varphi_R - \theta_V - \psi_0)} \right] + \frac{1}{2} h_P (r_C^2 - r_R^2) \theta_V.
 \end{aligned} \tag{5.24}$$

Knowing the volume as a function of revolution angle  $\varphi_R$ , pressure within a chamber in dead volume region can be computed from

$$dp = -E_{fl} \frac{dV}{V(\varphi_R)}. \tag{5.25}$$

Under the assumption of a constant bulk modulus  $E_{fl}$  this translates into a pressure evolution governed by

$$p(\varphi_R) = p_{R0} + E_{fl} \ln \left( \frac{V(\varphi_{R0})}{V(\varphi_R)} \right), \tag{5.26}$$

where  $p_{R0}$  is an integration constant representing the initial chamber pressure corresponding to  $\varphi_R = \varphi_{R0}$ . For the compression dead volume,  $\varphi_{R0} = \alpha_R^{T1} + \theta_V$  as this is the angle where the representative vane chamber just disconnects from the intake port.

For the averaging procedure, the consideration of the revolution of a single chamber in  $\alpha_R^{T1} + \theta_V \leq \varphi_R \leq \alpha_R^{L0}$  renders expression (5.1) into

$$F_{DVc}(x_S, \varphi_R) = F_{P,SC}(x_S, \alpha_R^{T1} + \theta_V \leq \varphi_R \leq \alpha_R^{L0}) \quad (5.27)$$

$$= p(\varphi_R)h_P \left[ r(\varphi_R) \sin(\varphi_R) - r(\varphi_R - \theta_V) \sin(\varphi_R - \theta_V) \right]. \quad (5.28)$$

From this, the average force from dead volume can be computed as

$$f_{P2}(x_S) := \frac{1}{\theta_V} \int_{\alpha_R^{T1} + \theta_V}^{\alpha_R^{L0}} F_{DVc}(x_S, \varphi_R) d\varphi_R. \quad (5.29)$$

It is to be emphasized here that the averaging takes place with respect to  $\theta_V$ , the period of all relevant forces – forces from line pressure exposure *and* dead volume compression (and expansion) – but that compression dead volume forces are only active during a fraction of the period, i.e. in the range  $\alpha_R^{T1} + \theta_V \leq \varphi_R \leq \alpha_R^{L0}$ .

Equation (5.29) cannot be solved analytically anymore due to the formally highly non-linear character of the function  $p(\varphi_R)$ . In order to perform an averaging with respect to revolution angle  $\varphi_R$  over a period of  $\theta_V$ , pressure  $p(\varphi_R)$  can be Taylor-expanded with respect to  $\varphi_R$

$$p(\varphi_R) \approx p(\alpha_R^{T1} + \theta_V) + \left. \frac{dp}{d\varphi_R} \right|_{\alpha_R^{T1} + \theta_V} \left( \varphi_R - (\alpha_R^{T1} + \theta_V) \right) \quad (5.30)$$

$$+ \left. \frac{1}{2} \frac{d^2p}{d\varphi_R^2} \right|_{\alpha_R^{T1} + \theta_V} \left( \varphi_R - (\alpha_R^{T1} + \theta_V) \right)^2 + \dots, \quad (5.31)$$

leading to an approximate representation of dead volume pressure and thereby an integrable expression. The Taylor-expansion approach is justified by noting that the force from dead volume compression is only active within the small angular range  $\alpha_R^{T1} + \theta_V \leq \varphi_R \leq \alpha_R^{L0}$  – resulting in an almost linear pressure evolution. Figures 5.10a and 5.10b show representative results for the evolution of dead volume pressure at different values of  $x_S$  and  $h$  featuring a visualization of the associated Taylor expansions of dead volume pressure. Corresponding results for average forces from dead volume compression are shown in Figure 5.11.

The above pressure computations were performed under the assumption of an ideal pump with perfectly sealed vane chambers. No leakage was assumed, hence the pressure evolution in the dead volume region is a result of pure geometric compression and expansion. In case leakage is introduced to the model, the pressure differential equation for a vane chamber can be given as

$$\frac{dp}{dt} = \frac{E_{fl}}{V} \left( -\frac{dV}{dt} - \gamma_1(p - p_1) - \gamma_2(p - p_0) \right). \quad (5.32)$$

In the above equation, leakage takes place in two directions as illustrated in Figure 5.12: firstly, leakage passes from the chamber with pressure  $p$  to the line with load pressure  $p_1$  or vice versa, depending on the sign of the pressure difference between the two. The second source of leakage flow is the pressure difference between the vane chamber and tank pressure  $p_0$ .

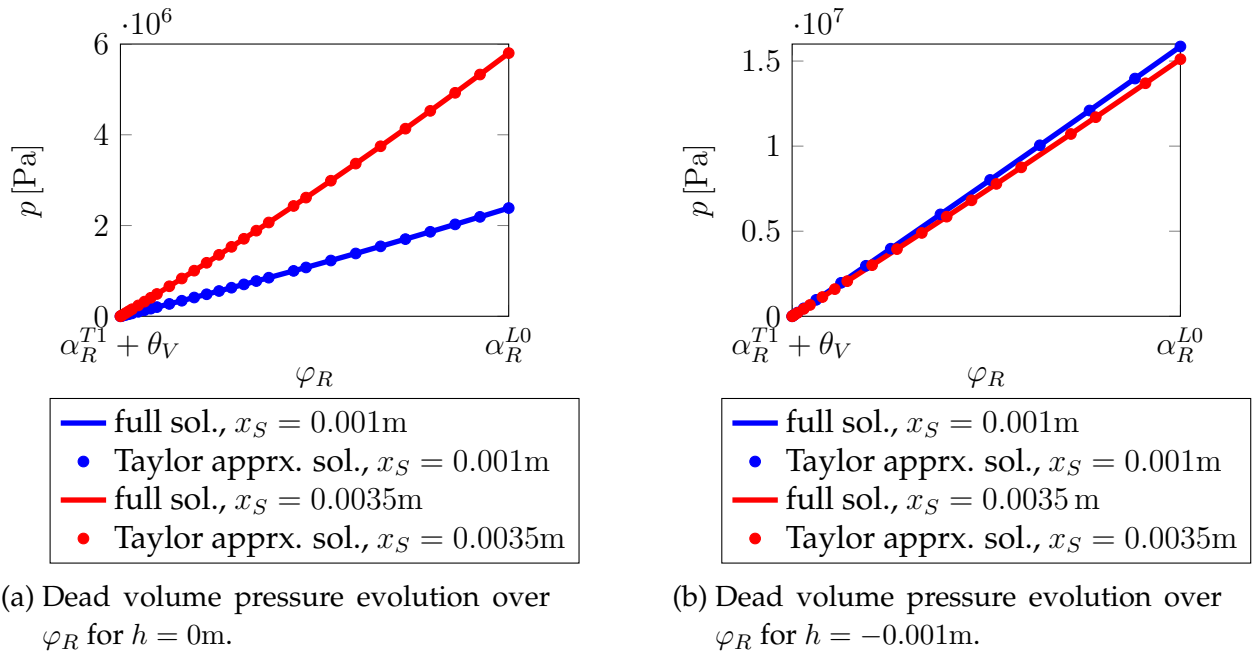
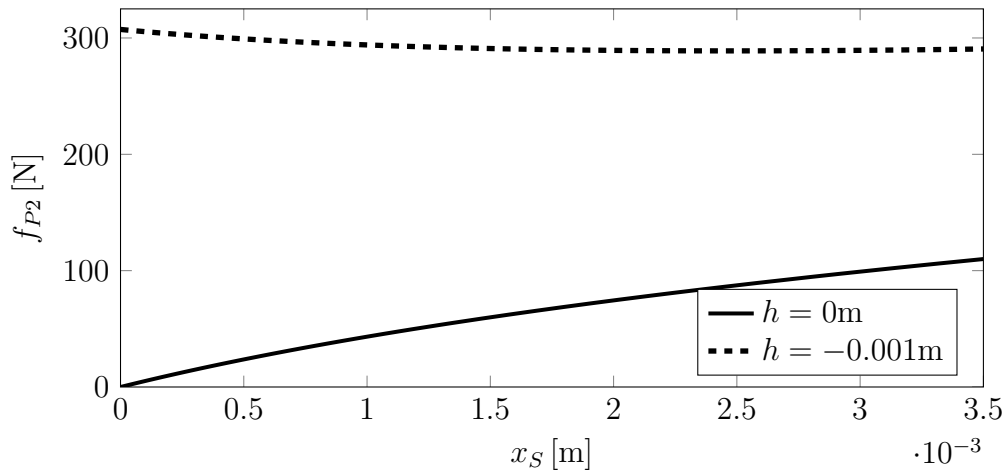


Figure 5.10: Validity of the Taylor approximation (5.30).


 Figure 5.11: Average force from dead volume compression over  $x_S$ .

In equation (5.32),

$$\gamma_1 = \frac{bh_L^3}{12l\eta_F}, \quad \gamma_2 = \kappa\gamma_1, \quad (5.33)$$

with  $\kappa$  a multiple between  $\gamma_1$  and  $\gamma_2$  so that  $\gamma_1$  can be understood as a leakage flow coefficient that depends on leakage gap height  $h_L$ , slot width  $b$ , channel length  $l$  and fluid viscosity  $\eta_F$ . In the following,  $\gamma_1$  and  $\gamma_2$  will be taken as a lumped parameter and varied according to possible ranges of their constituents. This is motivated by the fact that under operating conditions, neither of its constituents can be determined precisely.

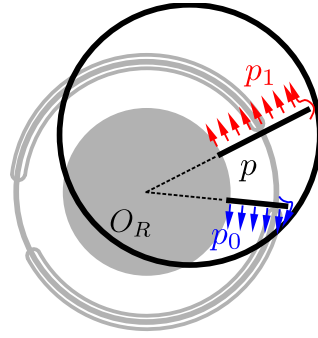


Figure 5.12: Leakage flows from a vane chamber in the compression dead volume region. Leakage flow towards line pressure  $p_1$  is red, leakage flow towards the tank pressure  $p_0$  is blue.

For constant revolution speeds, it holds that  $\varphi_R = \Omega_P t$  and thus

$$\Omega_P \frac{dp}{d\varphi_R} = \frac{E_{fl}}{V} \left( -\Omega_P \frac{dV}{d\varphi_R} - \gamma_1(p - p_1) - \gamma_2(p - p_0) \right), \quad (5.34)$$

$$\frac{dp}{d\varphi_R} = -\frac{E_{fl}}{V} \frac{dV}{d\varphi_R} - \frac{\gamma_1 E_{fl}}{\Omega_P V} (p - p_1) - \frac{\gamma_2 E_{fl}}{\Omega_P V} (p - p_0). \quad (5.35)$$

This form of the differential equation for the chamber pressure reveals the perturbation character of the leakage volume flow. Taking

$$\varepsilon = \frac{\gamma_1 E_{fl}}{\Omega_P} \quad (5.36)$$

it can be seen that the leakage perturbation increases with gap height and width while it decreases with revolution speed, viscosity and gap length.

The pressure equation thus reads

$$p' = -\frac{E_{fl}}{V} V' - \varepsilon \frac{1}{V} (p - p_1) - \kappa \varepsilon \frac{1}{V} (p - p_0) \quad (5.37)$$

with the prime symbol denoting the derivative with respect to pump revolution angle  $\varphi_R$ .

The inverse dependence of leakage on the revolution speed captures the intuitive notion that for the purely geometric compression and expansion of the chamber, time or revolution speed does not play any role as volume change and thus pressure does only depend on the angular position of the vane chamber. However, the slower the process of dead volume compression and decompression take place, the more time leakage has to flow into and out of the system, thereby changing the pressure of the vane chamber. While equation (5.37) is linear in  $p$  and therefore analytically solvable via a variation of constants approach, the results obtained do not lend themselves ideally to an averaging approach over  $\theta_V$ . In order to investigate the effect of leakage, a simple perturbation ansatz for the pressure is therefore assumed:

$$p = p_{as0} + \varepsilon p_{as1} + \varepsilon^2 p_{as2} + \dots \quad (5.38)$$

This approach qualitatively emphasizes the perturbation character of leakage and also allows for an extension to possible nonlinear models of pump leakage. Substituting the expansion into the pressure differential equation yields

$$p'_{as0} + \varepsilon p'_{as1} + \varepsilon^2 p'_{as2} + \dots = -\frac{E_{fl}}{V} V' - \varepsilon \frac{1}{V} (p_{as0} + \varepsilon p_{as1} + \varepsilon^2 p_{as2} + \dots - p_1) - \kappa \varepsilon \frac{1}{V} (p_{as0} + \varepsilon p_{as1} + \varepsilon^2 p_{as2} + \dots - p_0). \quad (5.39)$$

Collecting identical orders of  $\varepsilon$  yields the following recursively solvable system of differential equations:

$$\underline{\varepsilon^0}: \quad p'_{as0} = -\frac{E_{fl}}{V} V', \quad (5.40)$$

$$\underline{\varepsilon^1}: \quad p'_{as1} = -(1 + \kappa) \frac{1}{V} p_{as0} + \frac{1}{V} (p_1 + \kappa p_0), \quad (5.41)$$

$$\underline{\varepsilon^2}: \quad p'_{as2} = -(1 + \kappa) \frac{1}{V} p_{as1}, \quad (5.42)$$

$\vdots$

$$\underline{\varepsilon^n}: \quad p'_{asn} = -(1 + \kappa) \frac{1}{V} p_{as(n-1)}. \quad (5.43)$$

The solution for the unperturbed problem  $p_{as0}$  is given by (5.26), so that higher order approximations can be computed recursively. In order to do so, however, it is necessary to find expressions integrable in  $\varphi_R$  for  $1/V(\varphi_R)$  and for  $p_{as0}$ . As before, this is achieved by approximating the relevant expressions as Taylor-series about  $\varphi_R^* = \alpha_R^{T1} + \theta_V$ , so that

$$1/V(\varphi_R) \approx \frac{1}{V} \Big|_{\varphi_R^*} - \frac{1}{V^2} \frac{dV}{d\varphi_R} \Big|_{\varphi_R^*} (\varphi_R - \varphi_R^*) + \frac{1}{2} \left( \frac{1}{V^3} \left( \frac{dV}{d\varphi_R} \right)^2 - \frac{1}{V^2} \frac{d^2V}{d\varphi_R^2} \right) \Big|_{\varphi_R^*} (\varphi_R - \varphi_R^*)^2 + \dots \quad (5.44)$$

$$=: c_{V0} + c_{V1} \varphi_R + c_{V2} \varphi_R^2 + \dots \quad (5.45)$$

$$p_{as0} \approx c_{pas00} + c_{pas01} \varphi_R + c_{pas02} \varphi_R^2 + \dots \quad (5.46)$$

A solution for  $p_{as1}$  then is of the form

$$p_{as1} \approx c_{pas10} + c_{pas11} \varphi_R + c_{pas12} \varphi_R^2 + c_{pas13} \varphi_R^3 + c_{pas14} \varphi_R^4 + \dots \quad (5.47)$$

from which higher order solutions can be computed in a similar fashion. While there is no limitation to the order of approximation conceptually due to the repetitive nature of the equation structure in the recursively defined system of equations, evaluation of approximations of order higher than  $\varepsilon^6$  become excessively time-consuming in MAPLE. This is, however, not a problem as approximation quality is very good for expansions up to third order in  $\varepsilon$ , as can be seen in Figures 5.13 and 5.14 where pressure evolutions

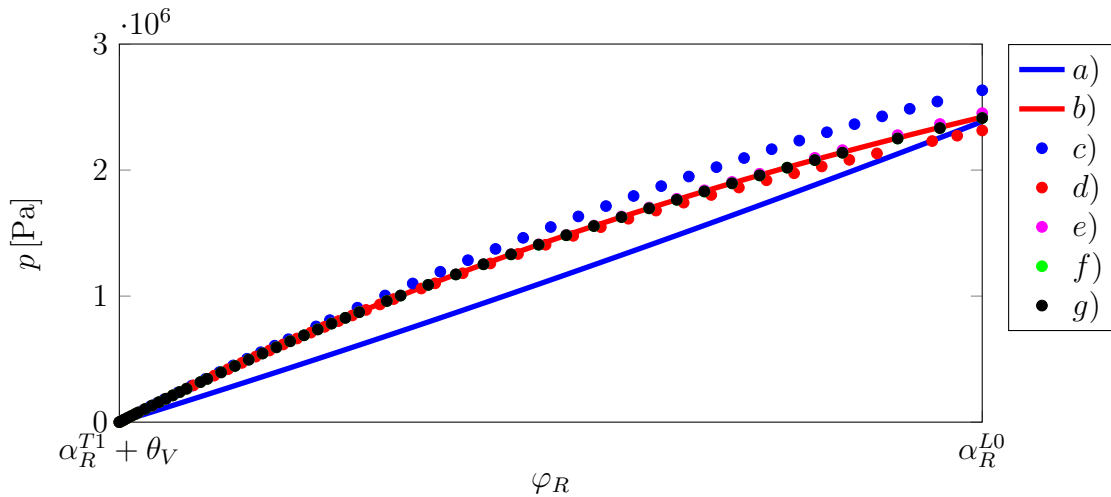


Figure 5.13: Dead volume pressure evolution over  $\varphi_R$  at a line pressure of 30bar,  $h = 0\text{m}$ ,  $x_S = 0.001\text{m}$ . Cases *a)* no leakage, *b)* leakage, analytical solution, *c)* first order approximation to pressure evolution with leakage through asymptotic series, *d)* second order approximation, *e)* third order approximation, *f)* fourth order approximation, *g)* fifth order approximation.

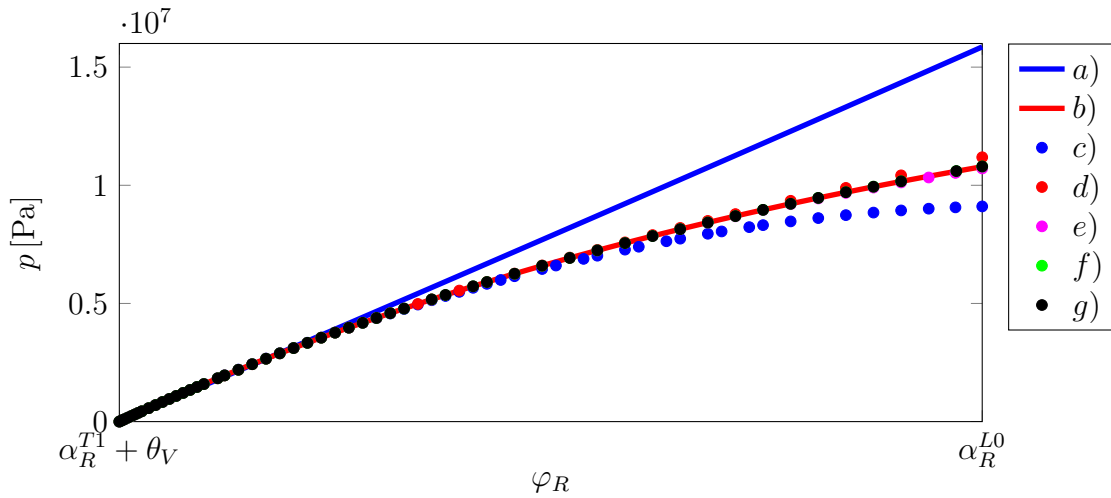


Figure 5.14: Dead volume pressure evolution over  $\varphi_R$  at a line pressure of 30bar,  $h = -0.001\text{m}$ ,  $x_S = 0.001\text{m}$ . Cases *a)* no leakage, *b)* leakage, analytical solution, *c)* first order approximation to pressure evolution with leakage through asymptotic series, *d)* second order approximation, *e)* third order approximation, *f)* fourth order approximation, *g)* fifth order approximation.

are shown for a comparatively large leakage parameter  $\gamma_1 = 1.5 \times 10^{-12}\text{m}^4\text{s/kg}$  and  $x_S = 0.001\text{m}$ .

These Figures very well illustrate the effects of leakage on dead volume chamber pressure evolution: For zero vertical eccentricity and thereby no chamber volume pre-

compression, the pressure evolution in the chamber is such that the chamber pressure does not reach line pressure  $p_1 = 30\text{bar}$  within the dead volume region. As a consequence, leakage flows from the line into the chamber, leading to an increased pressure within the chamber when compared to the non-leakage flow situation. Because leakage flow towards the tank simultaneously takes place, the slope of the pressure evolution with leakage is decreasing: Increasing chamber pressure will shift the net balance of leakage flow towards the tank-directed leakage flow over  $\varphi_R$ .

Equivalently, for a situation with chamber pre-compression through  $h = -0.001\text{m}$ , as long as chamber pressure is below line pressure, leakage overall increases chamber pressure above the pressure level that would persist would no leakage be present. Once the chamber pressure exceeds line pressure, the overall effect of leakage is the reduction of pressure below the level of the no leakage scenario. The extent of the effect described above is contingent on pump displacement  $x_S$  which explains why in Figure 5.15 even for  $h = 0\text{m}$  the dead volume force without leakage may exceed the dead volume force with leakage for large enough  $x_S$ . In Figure 5.16, results are shown for a vertical eccentricity  $h = -0.001\text{m}$ .

With the perturbation approach outlined above, overall compression dead volume forces can be averaged over a revolution period of the pump, yielding

$$f_{P2} = f_{P2}(x_S, p_1), \quad (5.48)$$

where, in contrast to (5.29), the force from dead volume compression now also is a function of line pressure  $p_1$ .

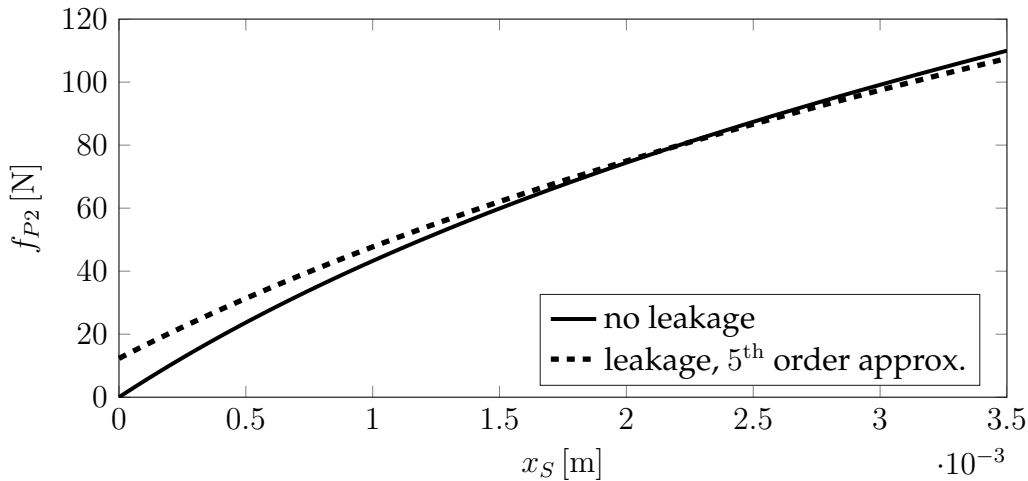


Figure 5.15: Compression dead volume force,  $h = 0\text{m}$ .

### 5.3.2.3 Forces from Dead Volume Expansion

Besides the compression dead volume between tank and discharge port, there is a second dead volume between discharge port and tank where the fluid volume remaining

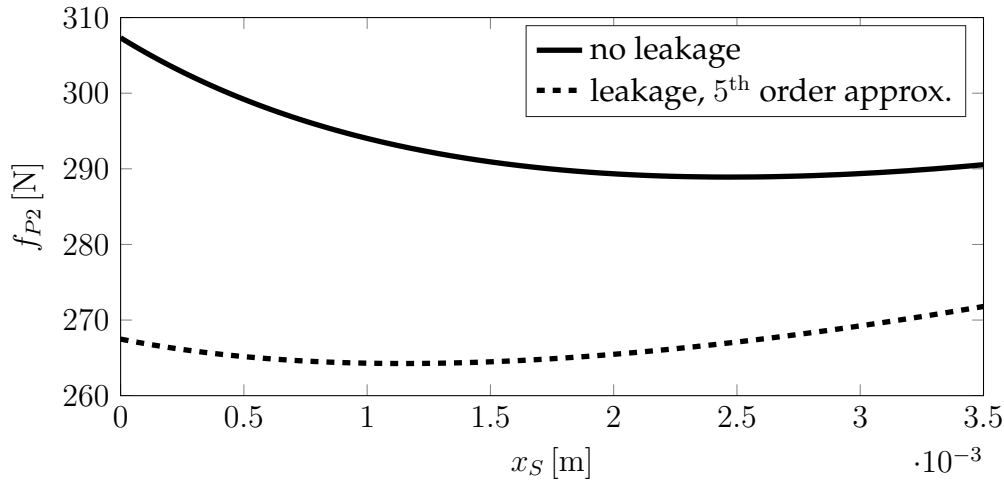


Figure 5.16: Compression dead volume force,  $h = -0.001\text{m}$ .

in a chamber after passing the discharge port is expanded. The volume expansion goes in hand with a pressure reduction, yielding forces  $f_{P3}(x_S, p_1)$  from the expansion dead volume. As in Karmel [45], this pressure reduction is modeled such that pressure drops below atmospheric  $p_0 = 0$  level are neglected. The pressure reduction, too, is governed by equation (5.25), simply with the initial conditions

$$\varphi_{R0} = \alpha_R^{L1} + \theta_V \quad (5.49)$$

$$p_{R0} = p_1, \quad (5.50)$$

from which the force from expansion dead volume pressure  $F_{DVe}(x_S, p_1, \varphi_R)$  and thus

$$f_{P3}(x_S, p_1) = \frac{1}{\theta_V} \int_{\alpha_R^{L1} + \theta_V}^{\alpha_R^{T0}} F_{DVe}(x_S, \varphi_R, p_1) d\varphi_R \quad (5.51)$$

can be computed. The computation of these is identical with those from the compression dead volume.

Due to the stiffness of the fluid, chamber pressure is typically reduced to zero pressure after a very small angle of rotation in the case of non-zero vertical eccentricity  $h$ . For this scenario, averaging the corresponding forces on the cam ring over a revolution period  $\theta_V$  therefore shows only minor influence of forces from dead volume expansion relative to the forces from line-pressure exposure, which by far exceed those from dead volume expansion. As a practical consequence, this force component can be neglected without significantly affecting model quality. The case with zero vertical eccentricity may, however, lead to a somewhat significant contribution of expansion dead volume forces, as can be seen from Figure 5.17, at least for small horizontal eccentricities  $x_S$ . Since in the majority of usage scenarios, vane pumps will be subject to vertical eccentricity, this is of little practical concern.

For very large line pressures and/or zero vertical eccentricity, a simplifying approximation can be made by virtually taking  $\alpha_R^{L1} \mapsto \alpha_R^{T0} - \theta_V$ , i.e. by virtually extending the

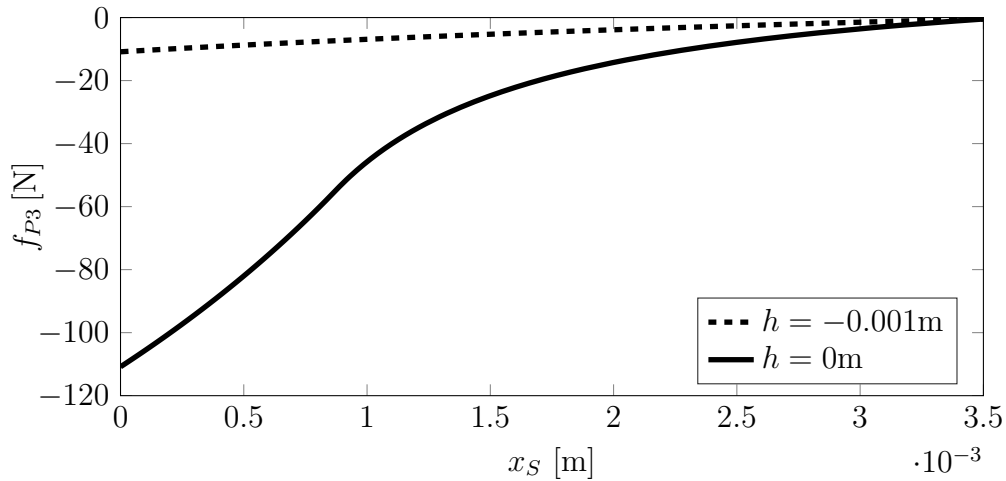


Figure 5.17: Average dead volume expansion forces for different vertical eccentricities at a line pressure of 30bar.

discharge port to the intake port so that the region within which chambers are exposed to line pressure is increased in order to get an estimate for the forces from dead volume expansion.

### 5.3.3 Pump Volume Flow

In classic pump modeling theory, the volume flow provided by a pump is typically computed from purely geometric considerations, see e.g. [120, 123]. Essentially, the theoretical volume flow can be computed from the difference in fluid volume a vane chamber carries when moving from  $\varphi_R = \alpha_R^{L0}$  to  $\varphi_R = \alpha_R^{L1} + \theta_V$ :

$$q_P = n_{CH} \frac{\Omega_P}{2\pi} \left( V(\alpha_R^{L0}) - V(\alpha_R^{L1} + \theta_V) \right). \quad (5.52)$$

It is evident from equation (5.24) that the vertical eccentricity of the cam ring  $h$  affects the volume and thereby the pressure evolution within a chamber. As pointed out before,  $h$  is typically chosen negative with the goal of pump noise reduction in mind. This has the interesting consequence that, from equation (5.52) as visualized in Figure 5.19, with  $h \neq 0$  pump volume flow can eventually become negative for sufficiently low  $x_S$ . In practice, the pump displacement thus has to exceed a certain threshold value to deliver positive volume flow. This is a phenomenon common to pivoting-type variable displacement pumps with cam offset, too, and known from [47]. Apart from this offset, pump volume flow varies approximately in a linear fashion with pump displacement  $x_S$  so that in the remainder of the present thesis, a fitted curve represented by

$$q_P = (x_S - x_S^{offset}) \hat{q}_P \quad (5.53)$$

shall be used to describe pump volume flow.

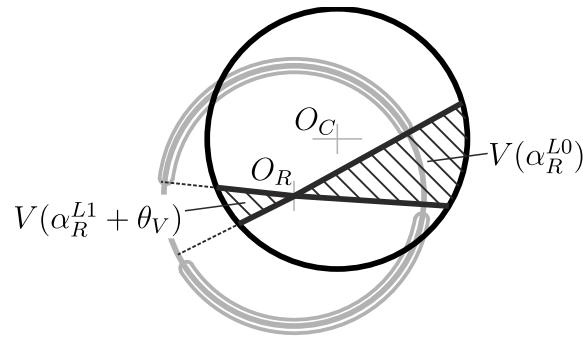


Figure 5.18: Geometric volume flow from chamber volume difference.

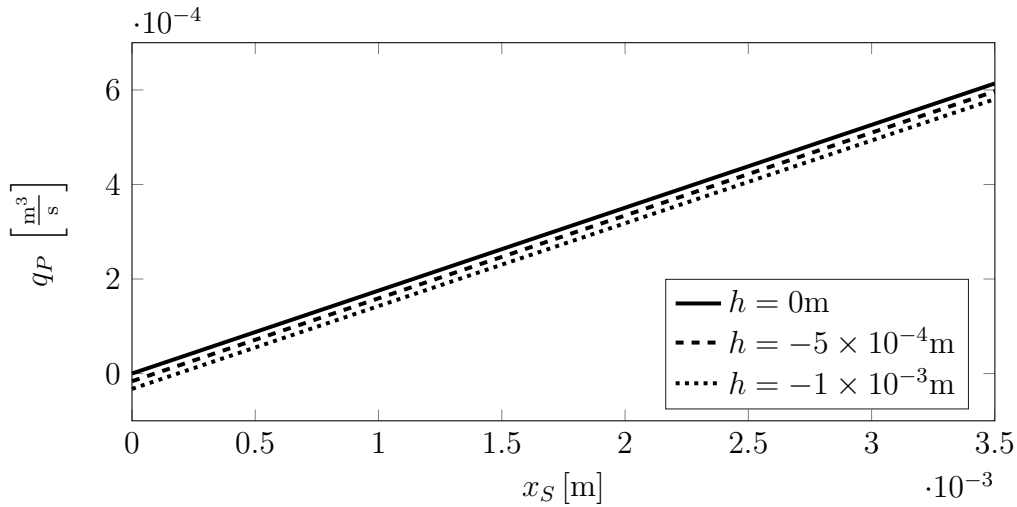


Figure 5.19: Pump volume flow over pump displacement.

## 5.4 Intermediate Conclusion

In this chapter, a minimal model for a variable displacement vane pump was derived.

The model builds on elementary kinematic considerations and internal pump forces acting on the cam ring are averaged over the revolution period of the pump. Within the model's scope, three components of the force on the cam ring were modeled: forces due to line pressure exposure of vane chambers while passing the discharge port, dead volume compression forces and dead volume expansion forces.

For an ideal pump without leakage, the total force on the cam ring can be represented by

$$f_P^I(x_S, p_1) = p_1 f_{P1}(x_S) + f_{P2}(x_S) + f_{P3}(x_S, p_1). \quad (5.54)$$

The model was extended for compression dead volume leakage, yielding

$$f_{PL}^I(x_S, p_1) = p_1 f_{P1}(x_S) + f_{P2}(x_S, p_1) + f_{P3}(x_S, p_1) \quad (5.55)$$

and incorporating line-pressure-depending leakage flow effects through  $f_{P2}(x_S, p_1)$  with  $f_{P2}$  then a function of  $p_1$ , too. Because the expansion dead volume force contribution to total cam ring force is small relative to the other force components, a simplified model

$$f_P^{II}(x_S, p_1) = p_1 f_{P1}(x_S) + f_{P2}(x_S) \quad \text{or} \quad f_{PL}^{II}(x_S, p_1) = p_1 f_{P1}(x_S) + f_{P2}(x_S, p_1) \quad (5.56)$$

will in many cases be sufficient to describe total cam ring force.

Ultimately, based on kinematic considerations, a simplified model for the volume flow provided by the pump was derived which is linear in cam ring displacement  $x_S$ .

The pump model obtained allows for a simple integration into complex hydraulic circuits for dynamic investigations and derivation of control laws for the vane pump.

While the assumption of a constant bulk modulus should be the first step for every model of a hydraulic structure, it is worth pointing out that the approach presented in this chapter can also be made for some models of bulk modulus varying with pressure. For example, the model for the effective bulk modulus proposed in [37] is

$$E_{eff}(p) = E_{max} \left[ 1 - e^{k_1 + k_2 p} \right] \quad (5.57)$$

with  $E_{max} = 1.8 \times 10^9$  Pa,  $k_1 = -0.4$  and  $k_2 = -2 \times 10^{-7}$  /Pa. This approach results in the following model for the pressure evolution in a dead volume

$$p(\varphi_R) = p_{R0} + E_{max} \ln \left( \frac{V(\varphi_{R0})}{V(\varphi_R)} \right) - \frac{1}{k_2} \ln \left( \left( \left( \frac{V(\varphi_{R0})}{V(\varphi_R)} \right)^{k_2 E_{max}} - 1 \right) e^{k_1 + k_2 p_{R0}} + 1 \right). \quad (5.58)$$

Obviously, the possibility of an analytical solution of equation (5.25) depends on the bulk modulus model.



# 6 Modeling and Analysis of a Variable Displacement Vane Pump System

## 6.1 Background

In many practical circumstances, pumps are to provide a volume flow in order to maintain a specific system pressure. It is in these application scenarios that variable displacement pumps provide an advantage over fixed displacement pumps as the volume flow can be adapted to the pressure requirement. Building on the minimal model for a variable displacement vane pump of linearly displacing type derived in chapter 5, in this chapter a model of a classic hydraulic system topology featuring a variable displacement vane pump is presented. The aggregate system model shall be used to discuss relevant aspects of equilibrium stability of the system after incorporating leakage effects through the model derived in chapter 2. Within this context, also see [147] for a stability discussion of the circuit with a simplified pump model.

## 6.2 System Description

In Figure 6.1, the system under consideration is shown. It features a variable displacement vane pump actuated through piston areas  $A_{S1}$ ,  $A_{S2}$  (also, see Figure 5.1b) and a pressure regulating valve with close resemblance to the valve treated in chapter 3. The valve is – at least in theory – critically lapped in order to ensure satisfactory set-point regulation.

The system's purpose is to maintain pressure  $p_1$  independently from the hydraulic load, i.e. how much fluid passes towards the hydraulic consumer. The load the pump provides with volume flow is modeled as a simple orifice with area  $A_{OR}$ . Hence, load volume flow depends linearly on load orifice area  $A_{OR}$ .

There are two scenarios to which the regulator valve responds. If system pressure is below the pressure specified by the spring pre-stress  $F_{R0}$ , the valve will open towards the system side and establish connection between system capacitance  $C_{h1}$  and secondary capacitance  $C_{hS}$ . As a consequence, pressure  $p_S$  acting on the pump actuation cylinder through area  $A_{S1}$  increases and causes a positive cam ring displacement which goes in hand with an increase of the pump's volume flow and thereby system pressure  $p_1$ . The opposite scenario is a decrease in pump volume flow when system pressure  $p_1$  exceeds the set pressure. If this is the case, the regulator valve will open towards the tank side, connecting capacitance  $C_{hS}$  with the tank and thereby decrease  $p_S$  through fluid

outflow in  $C_{hS}$ . This translates into a cam ring displacement in negative direction. As a consequence, volume flow is reduced so that  $p_1$  decreases to the point where force equilibrium on the valve spool is restored and the valve control edges are closed.

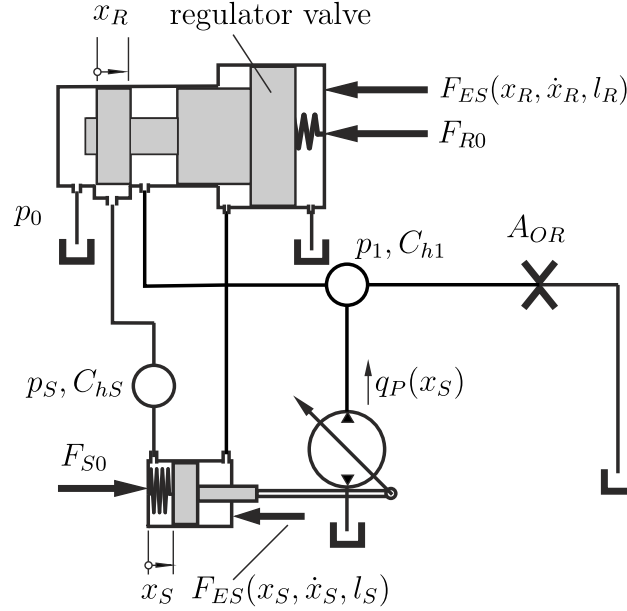


Figure 6.1: System model.

### 6.3 System Model

The system is modeled by means of the methodology already employed in previous chapters. Pump forces acting on the cam ring are taken from chapter 5 as

$$f_P(x_S, p_1) = f_{PL}^I(x_S, p_1) = p_1 f_{P1}(x_S) + f_{P2}(x_S, p_1) + f_{P3}(x_S, p_1). \quad (6.1)$$

The cam ring's equation of motion is

$$m_{PS}\ddot{x}_S + d_{PS}\dot{x}_S + k_S x_S = p_S A_{S1} - p_1 A_{S2} + f_P(x_S, p_1) + F_{S0} + k_S l_S - F_{ES}(x_S, \dot{x}_S, l_S). \quad (6.2)$$

where  $m_{PS}$  is the combined mass of actuation cylinder and pump cam ring and  $d_{PS}$  the corresponding viscous damping coefficient.

For the regulator valve's dynamics, the following differential equation can be given (also, see Figure 6.2b):

$$m_R\ddot{x}_R + d_R\dot{x}_R + k_R x_R = p_1 A_R - F_{R0} - F_{ES}(x_R, \dot{x}_R, l_R). \quad (6.3)$$

The end stop forces acting on the pump actuation cylinder and the regulation valve are modeled with a regularization approach as described by equation (4.5).

The hydraulic balance equations the mechanical components are coupled with can be given as:

$$\mathbf{C}_h \dot{\mathbf{p}} = \mathbf{Q}\mathbf{q} + \mathbf{A}\dot{\mathbf{x}}_m \quad (6.4)$$

with

$$\mathbf{C}_h = \begin{bmatrix} C_{h1} & 0 \\ 0 & C_{hS} \end{bmatrix}, \quad \mathbf{Q} = \begin{bmatrix} 1 & -1 & 0 & -1 \\ 0 & 1 & -1 & 0 \end{bmatrix}, \quad \mathbf{A} = \begin{bmatrix} A_{S2} & -A_R \\ -A_{S1} & 0 \end{bmatrix}, \quad (6.5)$$

the mechanical and hydraulic states

$$\mathbf{x}_m = \begin{bmatrix} x_S & x_R \end{bmatrix}^T, \quad \mathbf{p} = \begin{bmatrix} p_1 & p_S \end{bmatrix}^T \quad (6.6)$$

and

$$\mathbf{q} = \begin{bmatrix} q_P & q_R & q_T & q_{OR} \end{bmatrix}^T. \quad (6.7)$$

In the above equations, the capacitances are computed as follows:

$$C_{h1} = \frac{V_1(x_S, x_R)}{E_{fl}} = \frac{V_{10} + x_R A_R + (l_S - x_S) A_{S2}}{E_{fl}}, \quad (6.8)$$

$$C_{hS} = \frac{V_S(x_S)}{E_{fl}} = \frac{V_{S0} + x_S A_{S1}}{E_{fl}}. \quad (6.9)$$

While for  $q_P$  the volume flow is given by equation (5.53), the other volume flows in (6.7) are those associated with the different notch geometries when regularized by leakage (index "L"):

$$q_R = q_{iL}(-x_R + l_{Reg}, p_1, p_S, \mathcal{P}_i), \quad i = \{\square, \circ\}, \quad (6.10)$$

$$q_T = q_{iL}(x_R - l_{Reg} - 2u, p_S, p_0, \mathcal{P}_i), \quad i = \{\square, \circ\} \quad (6.11)$$

in case of a rectangular or circular notch geometry and

$$q_R = q_{\Delta L}(-x_R + l_{Reg} + b_{\Delta}, p_1, p_S, \mathcal{P}_{\Delta}), \quad (6.12)$$

$$q_T = q_{\Delta L}(x_R - l_{Reg} - b_{\Delta} - 2u, p_S, p_0, \mathcal{P}_{\Delta}) \quad (6.13)$$

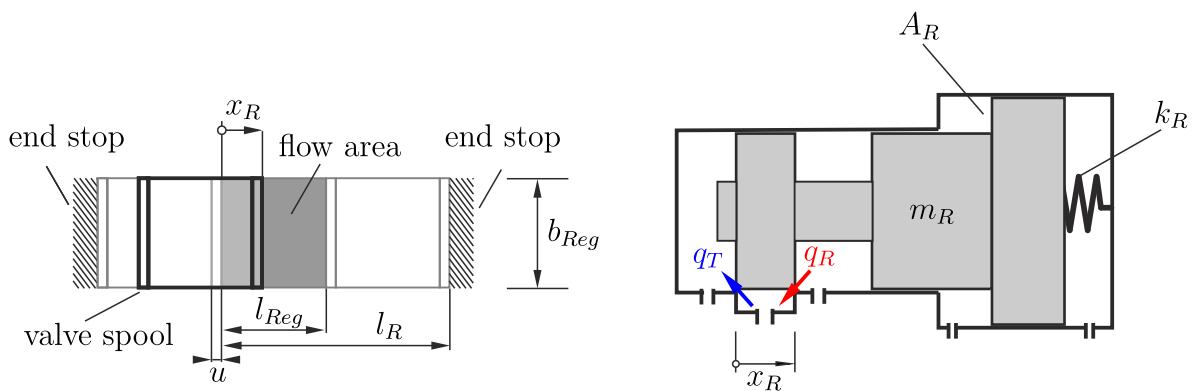
for a triangular notch. The respective notch geometry parameters are collected in  $\mathcal{P}_i$ , see Table 6.1.

For the sake of a simplified notation, the respective transformations in equations (6.10)-(6.13) for the  $x_R$ -coordinate will not be written explicitly from here onwards.

Nominally, the valve is critically lapped. In order to account for leakage effects and to make the problem accessible to numerical investigation at all, leakage is taken into account, too. Notably, the modeling of leakage assumes an overlap  $u$  (see Figure 6.2a) in each opening direction.

Table 6.1: Notch geometry parameters  $\mathcal{P}_i$ .

Parameter	Symbol	Value	Unit
Spool / Flow passage circumference	$b_{Reg}$	0.01	m
Flow passage area length	$l_{Reg}$	0.004	m
Triangular notch height	$b_{\Delta}$	0.0015	m
Triangular notch width	$a_{\Delta}$	0.0015	m
Circular notch radius	$r_o$	0.001	m
Gap height	$\Delta r$	$15 \times 10^{-6}$	m
Number of notches	$n_N$	4	-



(a) Regulator valve: flow passage area geometry and notation for rectangular notch.

(b) Regulator valve design.

Figure 6.2: Regulator valve model. The valve's nominal range of motion is  $0 \leq x_R \leq l_R$  as restricted by the end stops which are modeled through equation (4.5). The valve spool (bold) features an overlap  $u$  on either side.

For load flow,

$$q_{OR} = \gamma_F A_{OR} \sqrt{p_1} \quad (6.14)$$

is assumed.

Structurally, this system can be seen as an example of a non-top-down topology: the main reason for this is that pressure  $p_S$  for displacing the pump cam ring is fed from system pressure  $p_1$  – which itself is governed indirectly by cam ring displacement. In Figure 6.1, this can be seen from the loop between  $C_{hs}$  and  $C_{h1}$  and the valve in between.

## 6.4 Simulation Results and Stability Analysis

An analytical treatment of this system is clearly not feasible. Its general nonlinear structure and the fact that it features six states make an analytical approach unattractive. Notably, even when physically based regularization via leakage is introduced to the model, non-smoothness remains a system characteristic on macro scale, see Figures 2.4, 2.7, 2.9.

Actually, the system's non-smoothness is uncommon due to its lack of symmetry: When the regulator valve establishes connection between  $C_{h1}$  into  $C_{hS}$ , the volume flow balances of the two corresponding pressure dynamics are affected while for a tank-sided valve opening only the fluid balance in  $C_{hS}$  will be affected when fluid is discharged into the tank.

A numerical assessment, however, is non-standard, too, due to an exceptionally large number of parameters the model features (over thirty) and because the numerical properties of the system are those of a highly stiff problem (see Tables 6.2, 6.1), making it a challenge to compute solutions. In order to ease numerical analysis, a non-dimensionalization therefore is to be performed before investigating stability.

Table 6.2: Base system parameters.

Parameter	Symbol	Value	Unit
Regulator valve mass	$m_R$	0.015	kg
Regulator valve damping	$d_R$	20	Ns/m
Regulator valve spring stiffness	$k_R$	16000	N/m
Regulator valve spring pre-stress force	$F_{R0}$	29	N
Regulator valve piston area	$A_R$	$5 \times 10^{-5}$	m
Regulator valve channel length	$l_R$	0.0082 – 0.0114	m
Pump and actuator mass	$m_{PS}$	0.32	kg
Pump damping	$d_{PS}$	10	Ns/m
Pump actuator spring stiffness	$k_S$	5000	N/m
Pump actuator spring pre-stress force	$F_{S0}$	25	N
Actuator reaction area	$A_{S1}$	$\pi/4 \times 0.05^2$	m <sup>2</sup>
Actuator reaction area	$A_{S2}$	$0.7A_{S1}$	m <sup>2</sup>
Actuator channel length	$l_S$	0.0035	m
Actuator base volume	$V_{S0}$	0.0001	m <sup>3</sup>
Line base volume	$V_{10}$	0.001	m <sup>3</sup>
Valve overlap	$u$	$1.2 - 4.8 \times 10^{-4}$	m

### 6.4.1 Non-Dimensionalization

The system equations can be non-dimensionalized by the transformations

$$x_S = l_S X_S, \quad x_R = l_R X_R, \quad p_1 = \hat{p} P_1, \quad p_S = \hat{p} P_S, \quad t = T\tau, \quad (6.15)$$

with

$$\hat{p} = \frac{F_{S0}}{A_{S1}}, \quad T = \sqrt{m_{PS}/k_S}. \quad (6.16)$$

Thus,

$$X_S'' + D_S X_S' + K_S X_S = \bar{A}_{S1} P_S - \bar{A}_{S2} P_1 + \bar{F}_{S0} + \bar{F}_0 + F_P(X_S, P_1) - F_{ES}^S(X_S, X_S', 1), \quad (6.17)$$

$$X_R'' + D_R X_R' + K_R X_R = \bar{A}_R P_1 - \bar{F}_{R0} - F_{ES}^R(X_R, X_R', 1) \quad (6.18)$$

for the mechanical part and

$$P_1' = \frac{\frac{E_0}{\hat{p}} \left(1 + K_p \frac{\hat{p}}{E_0} P_1\right)}{1 + \bar{A}_R X_R - \bar{A}_{S2} X_S} \left( Q_P(X_S) - Q_R(X_R, P_1, P_S, \mathcal{P}_i) - \bar{A}_R X_R' + \bar{A}_{S2} X_S' - \bar{A}_{OR} \sqrt{P_1} \right), \quad (6.19)$$

$$P_S' = \frac{\frac{E_0}{\hat{p}} \left(1 + K_p \frac{\hat{p}}{E_0} P_S\right)}{1 + \bar{A}_{S1} X_S} \left( Q_R(X_R, P_1, P_S, \mathcal{P}_i) \frac{V_{10}}{V_{S0}} - Q_T(X_R, P_S, P_0, \mathcal{P}_i) - \bar{A}_{S1} X_S' \right) \quad (6.20)$$

for the hydraulic balance equations. In the above representation of the system dynamics, the following non-dimensional constants were introduced:

$$\begin{aligned} D_S &= \frac{d_{PS} T}{m_{PS}}, & K_S &= \frac{k_S T^2}{m_{PS}} = 1, & D_R &= \frac{d_R T}{m_R}, & K_R &= \frac{k_R T^2}{m_R}, \\ \kappa &= \frac{A_{S2}}{A_{S1}}, & \bar{A}_{S1} &= \frac{A_{S1} \hat{p} T^2}{m_{PS} l_S}, & \bar{A}_{S2} &= \kappa \bar{A}_{S1}, & \bar{A}_R &= \frac{A_R \hat{p} T^2}{m_R l_R}, \\ \bar{F}_{S0} &= \frac{F_{S0} T^2}{m_{PS} l_S}, & \bar{F}_0 &= \frac{k_S l_S T^2}{m_{PS} l_S}, & \bar{F}_{R0} &= \frac{F_{R0} T^2}{m_R l_R}, \\ \bar{A}_{S1} &= \frac{A_{S1} l_S}{V_{S0}}, & \bar{A}_{S2} &= \kappa \frac{A_{S1} l_S}{V_{10}}, & \bar{A}_R &= \frac{A_R l_R}{V_{10}}, & \bar{A}_{OR} &= \frac{\gamma_F \sqrt{\hat{p}} T A_{OR}}{V_{10}}. \end{aligned}$$

Along with this, system functions were non-dimensionalized as follows:

$$\begin{aligned} F_{ES}^R(X_R, X_R', 1) &= \frac{T^2}{m_R l_R} F_{ES}(l_R X_R, \left(\frac{l_R}{T}\right) X_R', l_R), \\ F_{ES}^S(X_S, X_S', 1) &= \frac{T^2}{m_{PS} l_S} F_{ES}(l_S X_S, \left(\frac{l_S}{T}\right) X_S', l_S), \end{aligned}$$

$$\begin{aligned}
 F_P(X_S, P_1) &= \frac{T^2}{m_{PS}l_S} f_P(l_S X_S, \hat{p}P_1), \\
 Q_P(X_S) &= \frac{T}{V_{10}} q_P(l_S X_S), \\
 Q_R(X_R, P_1, P_S, P_i) &= \frac{T}{V_{10}} q_R(l_R X_R, \hat{p}P_1, \hat{p}P_S, P_i), \\
 Q_T(X_R, P_S, P_0, P_i) &= \frac{T}{V_{S0}} q_T(l_R X_R, \hat{p}P_S, \hat{p}P_0, P_i).
 \end{aligned}$$

Key non-dimensional parameters are given in Table 6.3.

Table 6.3: Reference non-dimensional system parameters used for analysis if not stated otherwise.

Parameter	Symbol	Value
Non-dimensional regulator valve damping	$D_R$	10.66
Non-dimensional regulator valve stiffness	$K_R$	68.25
Non-dimensional regulator valve piston area	$\bar{A}_R$	0.33
Non-dimensional regulator valve pre-stress force	$\bar{F}_{R0}$	15
Non-dimensional pump damping	$D_S$	0.25
Non-dimensional pump actuator spring stiffness	$K_S$	1
Non-dimensional pre-stress force	$\bar{F}_0$	1
Non-dimensional pre-stress force	$\bar{F}_{S0}$	1.43
Non-dimensional actuator reaction area	$\bar{A}_{S1}$	1.43
Non-dimensional piston flow area	$\bar{A}_R$	$4.14 \times 10^{-4}$
Non-dimensional piston flow area	$\bar{\bar{A}}_{S1}$	0.0687
Non-dimensional piston flow area	$\bar{\bar{A}}_{S2}$	0.0048
Force scaling factor	$T^2/(m_R l_R)$	0.5178 /N
Force scaling factor	$T^2/(m_{PS} l_S)$	0.0571 /N
Volume flow scaling factor	$T/V_{10}$	8 s/m <sup>3</sup>
Volume flow scaling factor	$T/V_{S0}$	80 s/m <sup>3</sup>

## 6.4.2 Simulation Results

Simulation results for a run-up simulation are shown in Figures 6.3, 6.4. Here, the system runs up from maximum pump displacement induced by pre-stress force  $F_{S0}$  at zero system pressure, rapidly building pressure within the system up to set-point pressure for  $p_1$ . This causes the regulator valve spool to displace in positive direction from  $X_R = 0$  at  $t = 0$ s and thereby to close the load-sided control edge. Along with this, pump flow decreases accordingly. At  $t = 1$ s, the area of  $\bar{\bar{A}}_{OR}$  is multiplied by a factor of 10, simulating a load increase by a factor of 10. The system responds by increasing volume flow accordingly: The volume flow provided by the pump after the load jump

is increased by a factor of 10, too, while pressure  $p_1$  remains approximately equal to the pre-load-change situation.

The simulation results in Figure 6.3 reveal the effects of overlap  $u$  on set-point regulation: as briefly noted already in chapter 3, larger overlaps induce higher set-point pressure deviation since for a non-leaking valve any position within the overlap dead band is a possible equilibrium position. In principle, this also holds for systems with leaking valves even though the effect is less significant, see Figure 6.4. For valves with major leakage flow, the location of the unique equilibrium position of the regulator valve will, however, depend on leakage parameters and thereby be subject to variations over the operation period. Figure 6.4 shows that larger overlaps make the system with leaking valve slower in terms of time needed for load adaption.

The results illustrate the superior performance of hydraulic systems in terms of dynamic fastness: both run-up time and reaction time for the load change remain well below 100ms for a system with little or no leakage. However, such systems are known to be prone to stability issues which is why an assessment of stability properties of this system will be presented in the subsequent section.

### 6.4.3 Stability Analysis

#### 6.4.3.1 Equilibrium Computation

With respect to an assessment of the system's stability under different operating conditions and parameter configurations, the system dynamics need to be linearized about the equilibrium points.

For the non-smooth case with perfectly critically lapped regulator valve, the equilibrium position is uniquely determined by

$$Q_P(X_S) - \bar{A}_{OR}\sqrt{P_1^*} = 0 \quad (6.21)$$

where  $P_1^*$  is determined from the zero-flow condition

$$Q_R(X_R, P_1, P_S, P_i) = Q_T(X_R, P_S, P_0, P_i) = 0, \quad (6.22)$$

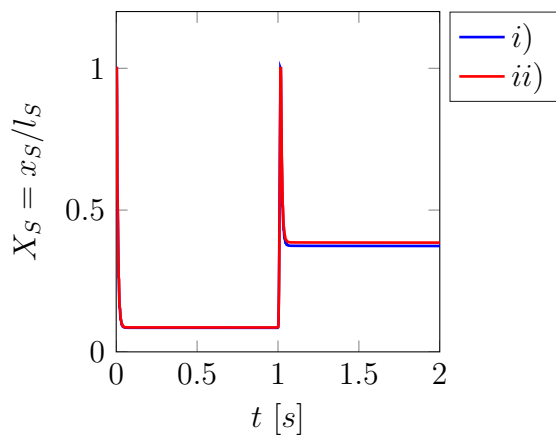
which requires

$$X_R^* = \frac{l_{Reg} + \delta_{\Delta} b_{\Delta}}{l_R} \quad (6.23)$$

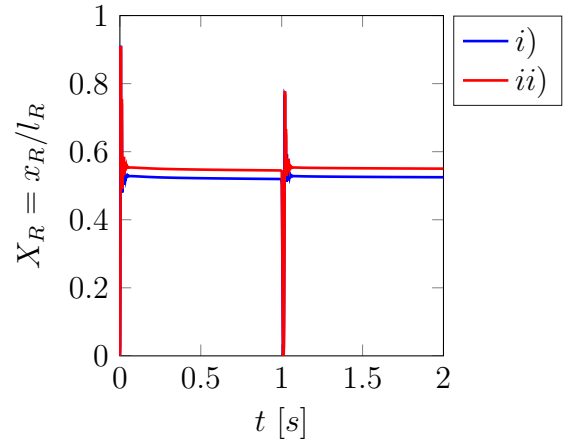
with  $\delta_{\Delta} = 1$  in case of a triangular notch and  $\delta_{\Delta} = 0$  in case of a rectangular or circular notch. From this, with the corresponding force balance of the regulator valve, it follows that

$$P_1^* = \frac{k_R(l_{Reg} + \delta_{\Delta} b_{\Delta}) + F_{R0}}{A_R \hat{p}}. \quad (6.24)$$

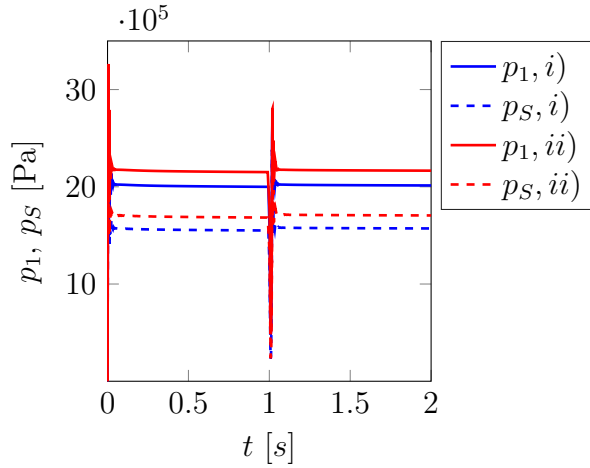
In contrast, when considering the system featuring leakage and overlap  $u$ , the equilibrium needs to be computed from two equations. Because of the overlap  $u$  introduced



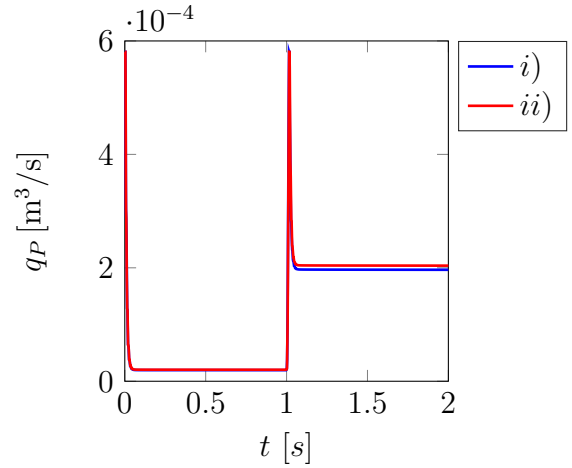
(a) Pump displacement, normalized by maximum pump displacement.



(b) Regulator position, normalized by maximum valve displacement.



(c) Main pressure and actuator capacitance pressure.



(d) Pump volume flow.

Figure 6.3: Run-up simulation with load change at  $t = 1$ s.  $i) u = 2.4 \times 10^{-4}$ m,  $ii) u = 4.8 \times 10^{-4}$ m, minor valve leakage (for illustrating purposes only) with  $\Delta r = 1.5 \times 10^{-6}$ m.

in the model along with leakage, equation (6.23) is not necessarily the equilibrium condition for the regulator anymore. The equilibrium conditions for the system's flow balance now read

$$0 = Q_P(X_S^*) - \bar{A}_{OR} \sqrt{P_1^*} - Q_R(X_R^*, P_1^*, P_S^*, P_i), \quad (6.25)$$

$$0 = Q_R(X_R^*, P_1^*, P_S^*, P_i) - Q_T(X_R^*, P_S^*, P_0, P_i). \quad (6.26)$$

Taking into account

$$P_1^* = \frac{k_R l_R X_R^* + F_{R0}}{A_R \hat{p}}, \quad (6.27)$$

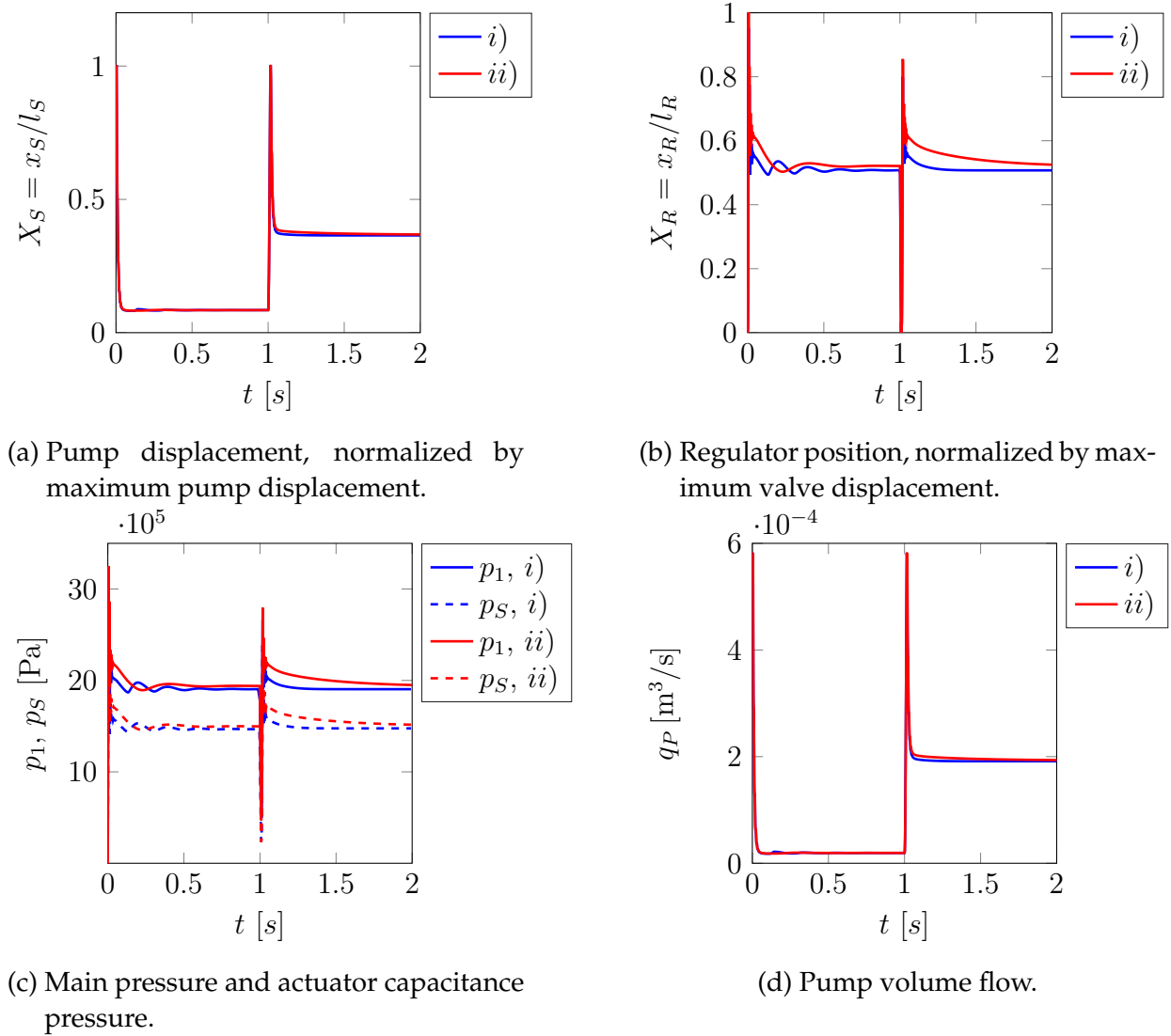


Figure 6.4: Run-up simulation with load change at  $t = 1$  s.  $i)$   $u = 2.4 \times 10^{-4}$  m,  $ii)$   $u = 4.8 \times 10^{-4}$  m, major valve leakage with  $\Delta r = 15 \times 10^{-6}$  m.

$$P_S^* = \frac{1}{A_{S1}\hat{p}} (\hat{p}P_1^*A_{S2} + k_S l_S (X_S^* - 1) - F_{S0} - f_P(l_S X_S^*, \hat{p}P_1^*)) \quad (6.28)$$

and substituting these into (6.25), (6.26), the equilibrium conditions essentially are two coupled nonlinear equations in the non-dimensional displacement variables  $X_R$  and  $X_S$ . These two equations can readily be solved by numerical computing packages such as MATLAB, providing the `fsolve` routine for such problems.

#### 6.4.3.2 Stability Maps

Due to the dependence of the system's capacitances on both pressures and displacements, the Jacobian upon which to perform the stability analysis is of significant size

and complexity and can not sensibly be given explicitly. In addition, the governing laws for leakage flow through valves with different notch geometries further complicate an explicit statement of the Jacobian.

With a view on the large number of parameters the system features the question of which of these to investigate with respect to equilibrium stability is raised. In hydraulic systems, the most important operating parameters are hydraulic load and system pressure. Therefore, it is purposeful to investigate equilibrium stability with respect to these two quantities. In terms of parameters of the system model, they are determined by both load orifice area  $\bar{A}_{OR}$  and spring stiffness  $K_R$  or pre-stress  $\bar{F}_{RO}$ .

In order to cover large system operating pressures, the stability maps in Figures 6.5, 6.6 feature spring-stiffness as a proxy for operating pressure since a variation of system pressure through spring pre-stress may be confined to comparatively small pressure intervals.

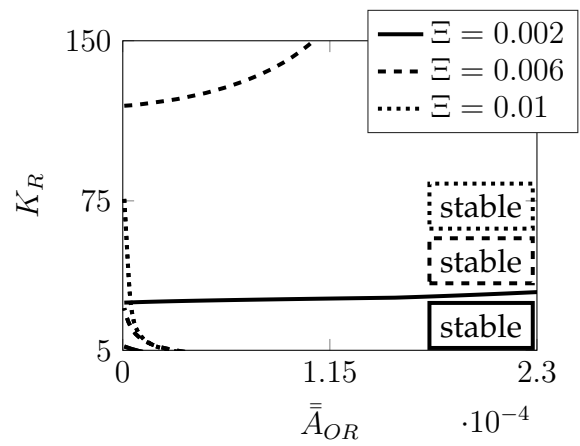
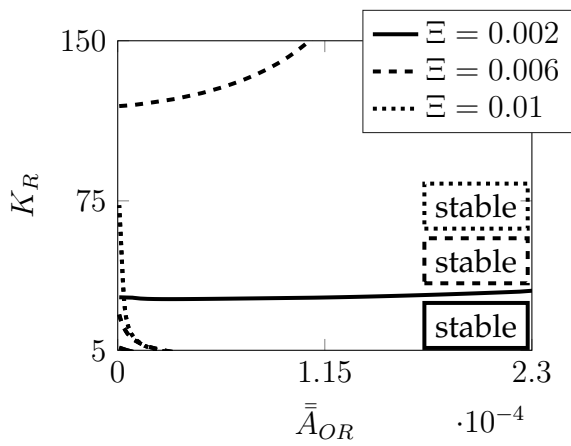
Another parameter of significant importance that is likely to change during operation is the system's viscosity. This parameter strongly varies with temperature. For this reason, stability maps shall be computed for varying levels of fluid viscosity  $\eta_F$  which for a non-dimensional consideration shall be varied in the form of  $\Xi = \eta_F / (1\text{Pas})$ . This parameter mainly determines leakage behavior which for very small overlaps as featured in this system strongly influences equilibrium stability.

Figures 6.5, 6.6 and 6.7, 6.8 show the stability maps for the system with different notch geometries, different pump models and different regulator valve dampings  $D_R$ . Figure 6.5 shows the stability map results for an ideally sealed pump (i.e.  $f_P(x_S, p_1) = f_P^I(x_S, p_1)$ ) while Figure 6.6 shows the corresponding maps with a pump allowing for leakage (i.e.  $f_P(x_S, p_1) = f_{PL}^I(x_S, p_1)$ ). Figures 6.7 and 6.8 replicate the results for a regulator valve damping  $D_R$  multiplied by a factor of two.

In terms of local stability, the rectangular notch yields the least advantageous results of all three notch geometries: For low viscosities, the region within which the system is stable is comparatively small. This is alleviated with increasing viscosity. For higher viscosity, the upper stability boundary is shifted towards higher stiffnesses (i.e. operating pressures), thereby increasing the stable parameter region. Triangular notch and circular notch yield comparable stability regions.

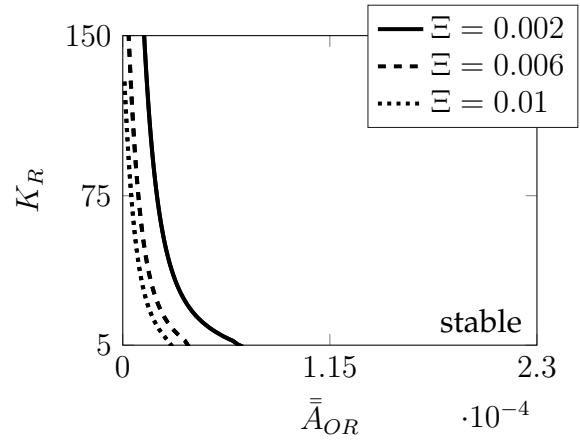
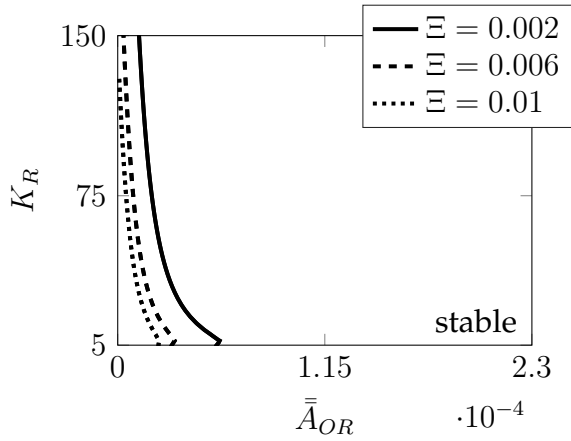
As for the impact of pump leakage on stability, the findings suggest that pump leakage does not significantly affect system stability. The differences between the stability maps in Figure 6.5 and 6.6 are marginal with pump leakage negligibly increasing unstable parameter regions. The same holds true when regulator valve damping is increased by a factor of two. Upon reconsideration of Figures 5.15, 5.16, this may be explained by the circumstance that pump leakage does not significantly alter the gradient of force component  $f_{P2}(x_S)$ .

Contrary to intuition, a comparison between Figures 6.5, 6.7 and 6.6, 6.8 reveals that increasing regulator valve damping actually increases the unstable operating regions for all notch geometries. These findings are in line with the analysis in [147] conducted for the simplified pump model  $f_P(x_S, p_1) = f_P^I(x_S, p_1)$ .



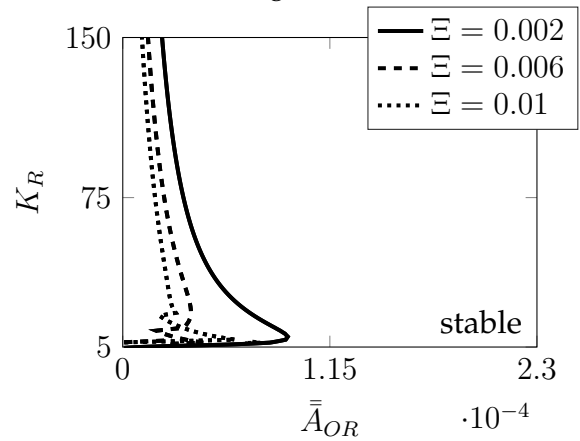
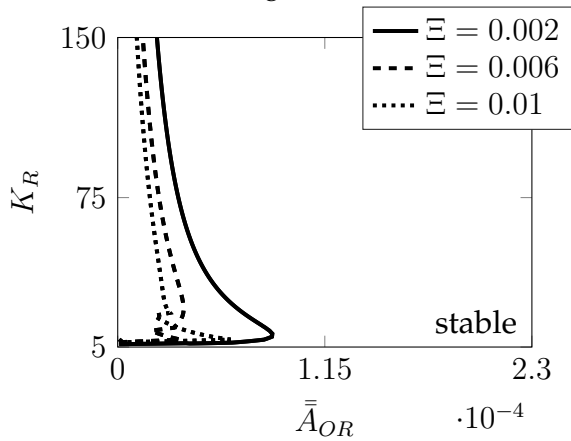
(a) Rectangular notch.

(a) Rectangular notch.



(b) Triangular notch.

(b) Triangular notch.

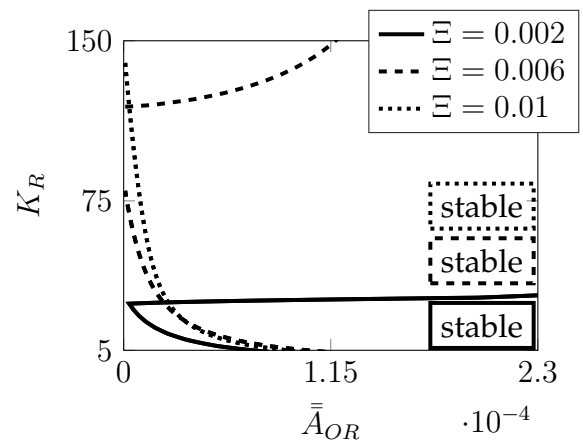
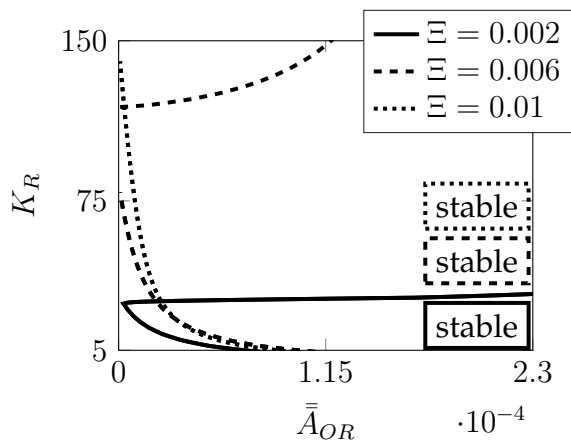


(c) Circular notch.

(c) Circular notch.

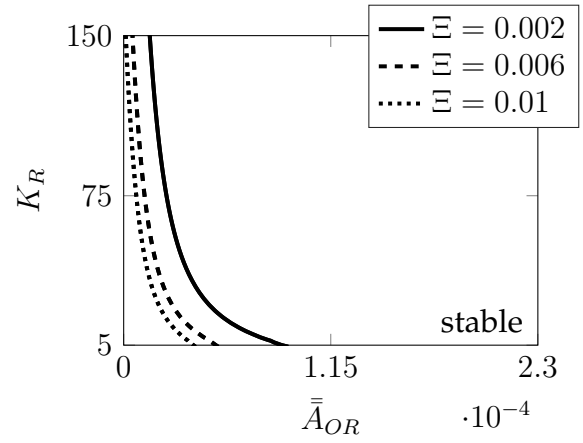
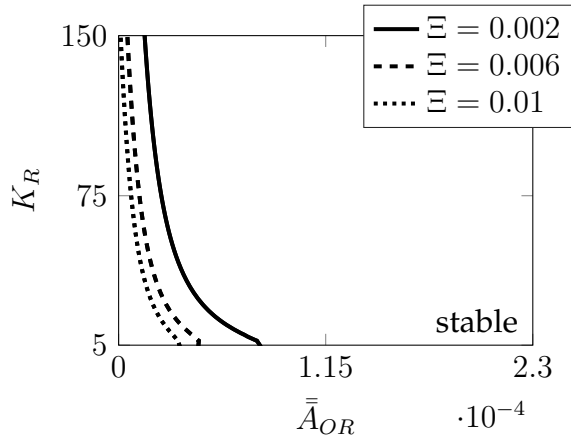
Figure 6.5: Stability maps: sealed pump. Damping  $D_R = 5.33$ .

Figure 6.6: Stability maps: leaking pump. Damping  $D_R = 5.33$ .



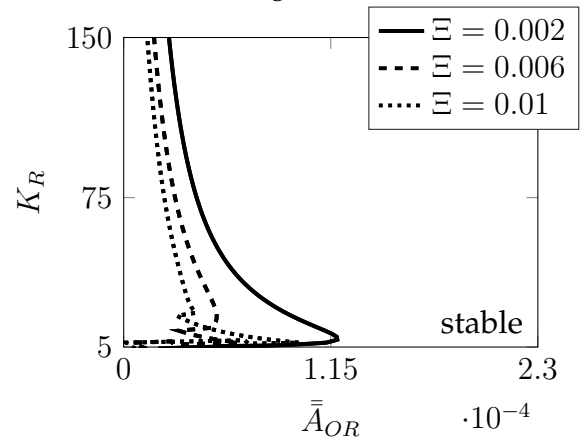
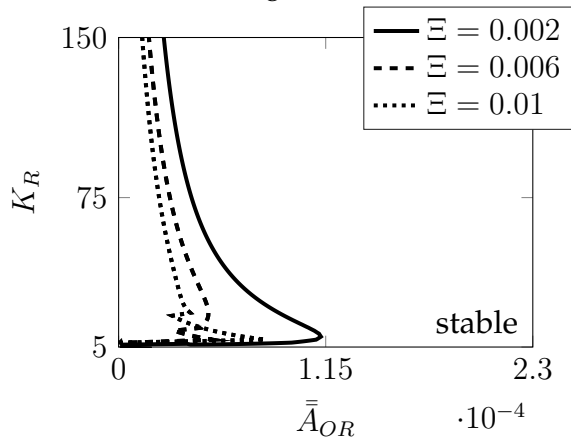
(a) Rectangular notch.

(a) Rectangular notch.



(b) Triangular notch.

(b) Triangular notch.



(c) Circular notch.

(c) Circular notch.

Figure 6.7: Stability maps: sealed pump. Damping  $D_R = 10.66$ .

Figure 6.8: Stability maps: leaking pump. Damping  $D_R = 10.66$ .

In Figure 6.9, a representative root locus is shown, indicating a Hopf-type loss of stability.

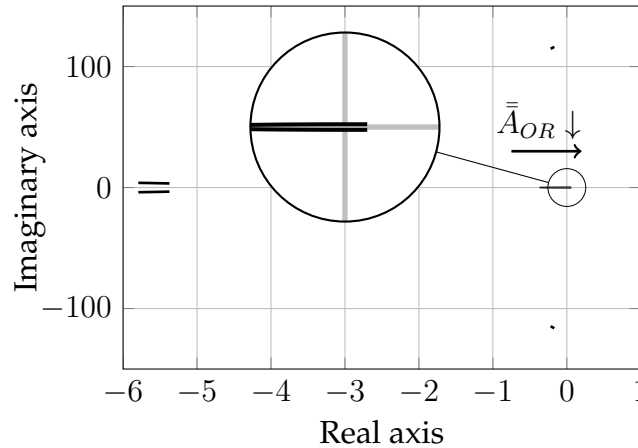


Figure 6.9: Representative (non-dimensional) root locus for variation of  $\bar{A}_{OR}$ , indicating a Hopf-type loss of stability.

The overall indication of stability analysis within the scope of the present model is that low operating pressures related to low regulator stiffnesses and small hydraulic loads tend to negatively affect system stability. Considering a variation of spring pre-stress  $\bar{F}_{RO}$ , Figure 6.10 shows that larger operating pressures induced by increased regulator spring pre-stress increases the unstable regions. It should thus be strived for governing system operating pressure largely by regulator spring stiffness and not by spring pre-stress.

Concluding, the results indicate that valve leakage is a major determinant in pump equilibrium stability.

#### 6.4.3.3 Phase Space Structure

Equilibrium stability is a necessary condition for a functional system. Because its evaluation through eigenvalues is an essentially local approach, the concept of equilibrium stability does not permit a statement about the magnitude of an equilibrium's basin of attraction in the case of a nonlinear system. While an equilibrium may be stable, its basin of attraction can possibly be so small that equilibrium stability is of little practical relevance. Thus, a sufficient criterion for a functional pump regulation system is equilibrium attractiveness over the full operating range in addition to a stable equilibrium. In the context of the present system, an insufficiently small basin of attraction of the equilibrium is associated with an unstable limit cycle that prevents the system from reaching its equilibrium position so that system functionality is jeopardized.

In order to make dependable inferences about the structure of phase space, a Monte-Carlo-like approach similar to that outlined in section 3.5 is employed. More specifically, this means that the system is simulated from a variety of initial conditions and

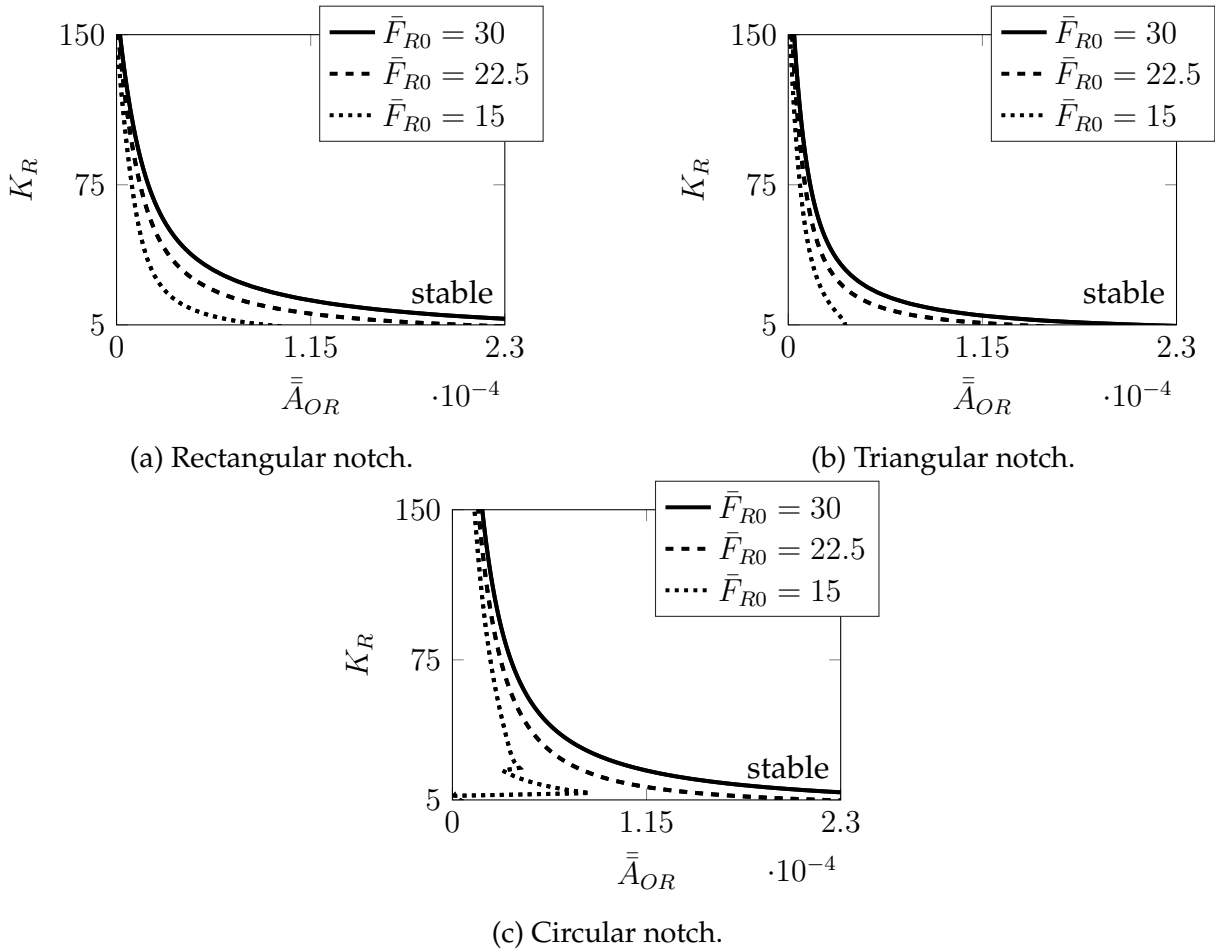


Figure 6.10: Stability maps: sealed pump. Damping  $D_R = 10.66$ , viscosity  $\Xi = 0.01$ .

stationary solutions are then investigated with respect to their qualitative characteristics. The initial conditions are firstly those associated with a classical run-up situation, i.e.  $X_S(\tau = 0) = 1$  and zero initial conditions for all other states, and secondly lightly perturbed equilibrium initial conditions. While for stable equilibria the stationary solution upon small perturbation is expected to result in the equilibrium solution, the run-up situation may yield a stable limit cycle centered about the equilibrium position which in turn implies an unstable limit cycle in-between the stable equilibrium position and the (outer) stable limit cycle.

Figure 6.11 shows simulation results for the three notch geometries discussed in this work. Notably, stable solutions for the  $X_S$ -coordinate are shown as a Poincaré section through  $X'_S = 0$ . For these simulations, valve overlap was chosen  $u = 3.6 \times 10^{-4}$  m so that all equilibria are locally stable, i.e. possible instability effects from leakage are ruled out.

The results demonstrate that an unstable limit cycle can be a system property irrespective of the valve's notch geometry. For rectangular and triangular notch geometries, the system's unstable limit cycle leads to stable periodic solutions whose magnitude for

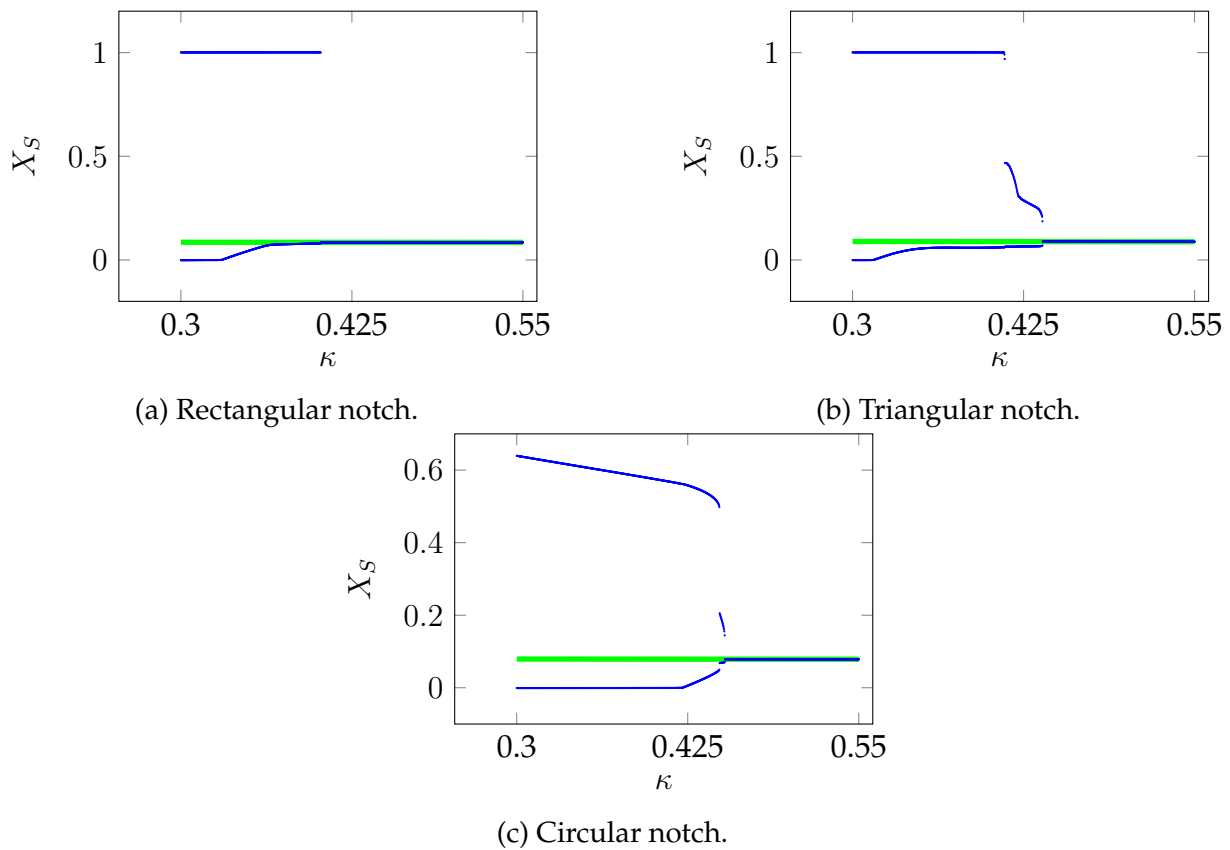


Figure 6.11: Phase space structure for different notch geometries: stable solutions. Equilibria are plotted green, stable limit cycle maxima and minima ( $X'_S = 0$ ) in blue.

some  $\kappa$  is restricted by the end stops at  $X_S = 0$  and  $X_S = 1$ . Representative results for limit stable limit cycle oscillations about the equilibrium are shown in Figure 6.12. The unstable limit cycle identified in the system by an inverse inference can be attributed to the switching nonlinearity introduced through the regulator valve. An unstable limit cycle can be observed for the simple pressure regulation valve in chapter 3 and was discussed under simplifying assumptions in [39], see also Figure 3.9. Notably for the pump system, all geometries feature the possibility of an unstable limit cycle, potentially preventing the system from operating as desired. This suggests that for practical implementations of this system type, parameters have to very carefully be chosen in order to avoid this undesired phenomenon.

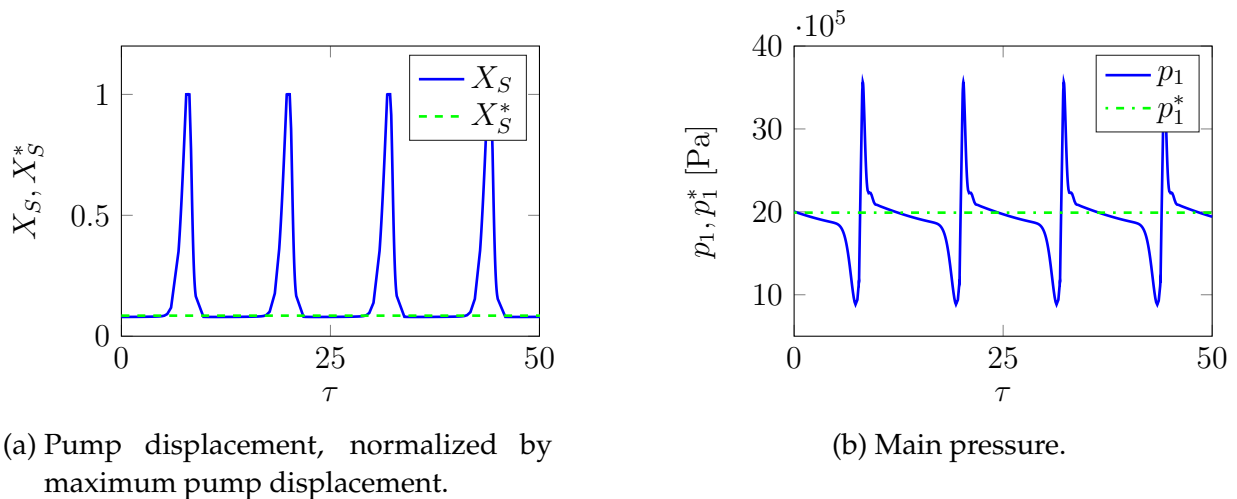


Figure 6.12: Representative stable limit cycle oscillations about the (stable) equilibrium position, relating to Figure 6.11.

## 6.5 Intermediate Conclusion

In this chapter, the model of a classic hydraulic circuit featuring a variable displacement vane pump was developed. Relevant stability properties were discussed for an almost critically lapped valve design.

For all notch geometries investigated, the findings suggest that small regulator spring stiffness and small hydraulic loads may render the system's equilibrium position unstable. Increasing operating pressure through increased regulator spring pre-stress is detrimental to stability, too.

Loss of stability due to decreased load is practically relevant in that the pump is to provide reduced volume flow for reduced demand: when demand falls short of a certain level, the system eventually becomes unstable. Increased valve leakage (via decreased viscosity) increases unstable regions. When set-point regulation accuracy and load adaption time is less of a concern, local instabilities from (valve) leakage can in any case be avoided by deliberately choosing large enough a valve overlap  $u$ . Pump leakage, in contrast, barely affects equilibrium stability.

A wide-reaching finding is the existence of an unstable limit cycle within the system that can be attributed to the macro non-smooth behavior of the regulator valve (even when regularized by leakage on a micro level). While this is a structural property related to valve design, careful parameter choice may alleviate the problem of trajectory rejection from an unstable limit cycle. Regrettably, general statements with respect to which parameter determines the location of the limit cycle in parameter space can not be made as it strongly depends on the specific parameter constellation at hand. The

system shows pronounced sensitivity with respect to parameter choice, so extensive simulations remain a necessity.

It stands to reason that the occurrence of an unstable limit cycle is a phenomenon that is structurally related to control valves featuring two control edges in other settings, too. Given their wide application in technical systems, this points to a novel interpretation of instabilities in hydraulic systems confronting practitioners.

**Part II**

**Nonlinear Control of Hydraulic  
Systems**



# 7 Fundamentals of Feedback-Linearizing Control

Within the recent past, control theory has seen significant contributions and extensions in the field of nonlinear control problems. While still far from having access to generally applicable methodology, one of the major developments can be seen in geometrically motivated nonlinear control. With the advent of these methods, a systematic approach for a comparatively large class of nonlinear problems with significant practical relevance was found. Most prominent and well-known, the feedback-linearizing control technique has marked its relevance in these contexts. For general reference here, see e.g. [40, 53, 91, 103].

With the notion of feedback-linearization effectively covering the methods of both input-output linearization and full-state linearization – ultimately, these terms sometimes are used interchangeably at times – a short explanation of these concepts shall be given in this chapter with a view on single input-single-output as well as multiple-input-multiple-output systems.

## 7.1 Fundamentals of Single-Input-Single-Output Feedback-Linearizing Control

Input-output linearization is a control strategy applicable to a variety of nonlinear systems. Its core idea is to transform the general nonlinear single input, single output (SISO) system with  $n$  states

$$\dot{\mathbf{x}} = \mathbf{f}(\mathbf{x}, u) = \mathbf{f}_d(\mathbf{x}) + \mathbf{g}(\mathbf{x})u, \quad (7.1)$$

$$y = h(\mathbf{x}) \quad (7.2)$$

by a number of nonlinear state transformations in such a way that a control law can be derived that makes the input-output map of the system linear. In the above representation of the system dynamics,  $\mathbf{f}_d(\mathbf{x})$  is the so-called drift term. This nomenclature stems from the notion that in the absence of a control  $u$  being applied to the system through the control input matrix  $\mathbf{g}(\mathbf{x})$ , the system will drift along its trajectory according to the dynamics defined by  $\mathbf{f}_d(\mathbf{x})$ .

While fairly general in its approach, input-output linearization is considered feasible only under certain conditions. Conditions for the applicability of input-output-linearization commonly named are:

- availability of an accurate model of the system to be controlled,
- so-called bilinear or affine control input,
- smoothness of the system function  $\mathbf{f}_d(\mathbf{x})$ ,
- availability of the system states for feedback.

The first condition needs to be fulfilled by the majority of control strategies available except for special techniques from robust control where model uncertainties are included in the control design. In practice, a majority of systems will also feature affine control inputs.

The input-output-linearization approach essentially comprises the following steps:

- determination of the relative degree of the system,
- definition of a nonlinear state transformation specific to the problem at hand,
- transformation of the system and investigation of internal dynamics,
- synthesis of the input-output linearizing control law.

With feedback-linearization belonging to the class of geometrically motivated control strategies, Lie derivatives require introduction in order to make use of the method.

Differentiating the scalar function  $h(\mathbf{x})$  with respect to time along a trajectory of a particle whose dynamics are governed by (7.1) – that is, building the gradient of  $h(\mathbf{x})$  along  $\mathbf{f}_d(\mathbf{x}, t) + \mathbf{g}(\mathbf{x})u$  – the time derivative can be obtained by building the scalar product of the gradient of  $h(\mathbf{x})$  and  $\mathbf{f}_d(\mathbf{x})$ :

$$\frac{dh(\mathbf{x})}{dt} = \frac{\partial h(\mathbf{x})}{\partial \mathbf{x}} \cdot \dot{\mathbf{x}} \quad (7.3)$$

$$= \nabla h(\mathbf{x}) \cdot (\mathbf{f}_d(\mathbf{x}) + \mathbf{g}(\mathbf{x})u) \quad (7.4)$$

$$= \mathcal{L}_{\mathbf{f}_d} h(\mathbf{x}) + \mathcal{L}_{\mathbf{g}} h(\mathbf{x})u, \quad (7.5)$$

where the Lie operators

$$\mathcal{L}_{\mathbf{f}_d}(\cdot) = \nabla(\cdot) \cdot \mathbf{f}_d(\mathbf{x}), \quad (7.6)$$

$$\mathcal{L}_{\mathbf{g}}(\cdot) = \nabla(\cdot) \cdot \mathbf{g}(\mathbf{x}) \quad (7.7)$$

were introduced to allow for a simplified notation.

Repeated derivation of  $h(\mathbf{x})$  along a vector field  $\mathbf{f}_d(\mathbf{x})$  or  $\mathbf{g}(\mathbf{x})$  can be written as

$$\mathcal{L}_{\mathbf{f}_d}^i(\cdot) = \nabla \mathcal{L}_{\mathbf{f}_d}^{i-1}(\cdot) \cdot \mathbf{f}_d(\mathbf{x}), \quad \mathcal{L}_{\mathbf{g}}^i(\cdot) = \nabla \mathcal{L}_{\mathbf{g}}^{i-1}(\cdot) \cdot \mathbf{g}(\mathbf{x}). \quad (7.8)$$

With the major mathematical tool now at hand, the input-output-linearization routine can be outlined in what follows.

**Determining the relative degree of a SISO system** As in linear systems control theory there exists the notion of a relative degree for nonlinear systems control theory. While in the case of a linear system the relative degree is simply the excess of a system's transfer function's poles over its zeros [108], in the nonlinear case the definition is more involved and requires the application of the Lie derivatives defined above.

To obtain the relative degree of a nonlinear system as defined by (7.1), the output equation  $y = h(\mathbf{x})$  is derived with respect to time along the trajectories of (7.1) as many times as needed until the system input  $u$  appears explicitly in the respective time derivative of  $h(\mathbf{x})$ :

$$y = h(\mathbf{x}), \quad (7.9)$$

$$\begin{aligned} \dot{y} &= \nabla h(\mathbf{x}) \cdot (\mathbf{f}_d(\mathbf{x}) + \mathbf{g}(\mathbf{x})u) \\ &= \mathcal{L}_{\mathbf{f}_d} h(\mathbf{x}) + \underbrace{\mathcal{L}_{\mathbf{g}} h(\mathbf{x})}_{=0} u, \end{aligned} \quad (7.10)$$

$$\begin{aligned} \ddot{y} &= \nabla \mathcal{L}_{\mathbf{f}_d} h(\mathbf{x}) \cdot (\mathbf{f}_d(\mathbf{x}) + \mathbf{g}(\mathbf{x})u), \\ &= \mathcal{L}_{\mathbf{f}_d}^2 h(\mathbf{x}) + \underbrace{\mathcal{L}_{\mathbf{g}} \mathcal{L}_{\mathbf{f}_d} h(\mathbf{x})}_{=0} u \end{aligned} \quad (7.11)$$

$$\begin{aligned} &\vdots \\ y^{(r)} &= \mathcal{L}_{\mathbf{f}_d}^r h(\mathbf{x}) + \underbrace{\mathcal{L}_{\mathbf{g}} \mathcal{L}_{\mathbf{f}_d}^{r-1} h(\mathbf{x})}_{\neq 0} u. \end{aligned} \quad (7.12)$$

That is, the relative degree  $r$  of system (7.1) is determined by the lowest natural number  $r$  for which

$$\mathcal{L}_{\mathbf{g}} \mathcal{L}_{\mathbf{f}_d}^{r-1} h(\mathbf{x}) \neq 0 \quad (7.13)$$

holds. In order for the relative degree computed from the above procedure to be a well-defined relative degree, equation (7.13) must hold in the entire operating space  $\mathcal{D} \subset \mathbb{R}^n$  of the system.

**Transforming a SISO system into normal form** As state descriptions of a system's dynamics are not unique, the description of a system's dynamics based on the laws of physics may be transformed to other representations with less intuitive character. As stated in Proposition 4.1.3. in [40], a system's output's derivatives along the trajectories of the respective system as outlined above define one such coordinate transformation (partly for  $r < n$ ), at least locally. As for input-output linearization, these time derivatives of the output are drawn on to define a (partial) set of new coordinates and to bring the system to a state space representation that is suitable for the derivation of nonlinearity-compensating control laws. The most general corresponding normal form to which a system may in some cases be transformed is the so-called Byrnes-Isidori normal form. It not only allows for the simple derivation of the desired control laws but also a simplified investigation of relevant stability properties of the system. Hence, the

Byrnes-Isidori normal form will typically be strived for when devising control strategies for a system. Due to the non-uniqueness of state space representations of a system's dynamics, it does not, however, need to be the only form a system may be transformed to. There are two possible cases for the relative degree  $r$ , which shall be explained briefly with respect to their relevance for the Byrnes-Isidori normal form.

In case that the relative degree of the system equals the system order,  $r = n$ , the output  $y = h(\mathbf{x})$  is referred to as a differentially flat output and so called full-state linearization in the stricter sense of meaning can be performed. Under these circumstances, trajectory design and tracking form a control task that can easily and elegantly be solved because all states of the system can be algebraized by the system output and its  $n - 1$  derivatives. The state transformation from  $\mathbf{x}$  to the new states  $\boldsymbol{\xi}$  allowing to synthesize the desired control law is then given by

$$\boldsymbol{\xi} = \begin{bmatrix} \xi_1 \\ \xi_2 \\ \vdots \\ \xi_{n-1} \\ \xi_n \end{bmatrix} = \boldsymbol{\Phi}(\mathbf{x}) = \begin{bmatrix} h(\mathbf{x}) \\ \mathcal{L}_{f_d} h(\mathbf{x}) \\ \vdots \\ \mathcal{L}_{f_d}^{n-2} h(\mathbf{x}) \\ \mathcal{L}_{f_d}^{n-1} h(\mathbf{x}) \end{bmatrix}. \quad (7.14)$$

According to Proposition 4.1.3. in [40], the time derivatives up to  $r - 1$ th order of the output equation constitute diffeomorphism between  $\boldsymbol{\xi}$  and  $\mathbf{x}$  and guarantee that  $\boldsymbol{\xi} = \boldsymbol{\Phi}(\mathbf{x})$  is invertible with  $\mathbf{x} = \boldsymbol{\Phi}^{-1}(\boldsymbol{\xi})$ , again at least locally. For a system with full relative degree,  $r = n$ , the Byrnes-Isidori normal form becomes the nonlinear control normal form. Because for systems with full relative degree (i.e. flat systems) the output allows for an algebraization of the system through the output and its derivatives only, it is of interest to find such an output that can possibly be a virtual output by which the concrete output of interest can then be represented, too.

In case the relative degree  $r$  of the system is not equal to the system order (i.e.  $r < n$ ) which by far is the more common case, one speaks of input-output-linearization. With this situation, a diffeomorphism transforming between  $\mathbf{x}$  and a set of new coordinates  $\boldsymbol{\xi}, \boldsymbol{\eta}$  can be constructed by

$$\mathbf{z} = \begin{bmatrix} \boldsymbol{\xi} \\ \boldsymbol{\eta} \end{bmatrix} = \begin{bmatrix} \xi_1 \\ \xi_2 \\ \vdots \\ \xi_r \\ \eta_1 \\ \vdots \\ \eta_{n-r} \end{bmatrix} = \boldsymbol{\Phi}(\mathbf{x}) = \begin{bmatrix} h(\mathbf{x}) \\ \mathcal{L}_{f_d} h(\mathbf{x}) \\ \vdots \\ \mathcal{L}_{f_d}^{r-1} h(\mathbf{x}) \\ \Phi_{r+1}(\mathbf{x}) \\ \vdots \\ \Phi_n(\mathbf{x}) \end{bmatrix}, \quad (7.15)$$

where  $\Phi_{r+1}(\mathbf{x}) \dots \Phi_n(\mathbf{x})$  can be chosen arbitrarily but in such a way that  $[\boldsymbol{\xi} \ \boldsymbol{\eta}]^T = \boldsymbol{\Phi}(\mathbf{x})$  is a diffeomorphism, that is

$$\det \frac{\partial \Phi}{\partial \mathbf{x}} \neq 0. \quad (7.16)$$

In the context of input-output-linearization, the  $\boldsymbol{\eta}$  coordinates are the so-called internal coordinates. After performing an input-output-linearization, these coordinates cannot be observed from the system output anymore and are required to possess stable dynamics in order for input-output-linearization to be feasible, even though elaborated techniques exist to also cope with unstable internal dynamics, see e.g. [36] and [91] for further reference. Stability of the internal dynamics can most straightforwardly be assessed if one succeeds in transforming the system into Byrnes-Isidori normal form. For systems with non-full relative degree, this normal form is characterized by the absence of the system input  $u$  in the dynamics for the internal coordinates so that the internal coordinates are decoupled from system input  $u$ . In order to obtain a system's Byrnes-Isidori normal form in this case, the internal coordinates  $\eta_i = \Phi_{r+i}, i = 1, \dots, n-r$  have to be chosen in such a way that for the  $\Phi_{r+i}$  in equation (7.15)

$$\frac{\partial \Phi_{r+i}(\mathbf{x})}{\partial \mathbf{x}} \cdot \mathbf{g}(\mathbf{x}) = 0 \quad \text{for } i = 1 \dots n-r \quad (7.17)$$

is fulfilled. In many cases, one will have to confine oneself to a choice of  $\boldsymbol{\eta}$  subject to condition (7.16) due to the mathematical intricacies one encounters when solving (7.17). For the general case of  $r \neq n$  and (7.17) not fulfilled, the state transformation (7.15) then leads to the following dynamics

$$\dot{\mathbf{z}} = \begin{bmatrix} \dot{\boldsymbol{\xi}} \\ \dot{\boldsymbol{\eta}} \end{bmatrix} = \begin{bmatrix} \dot{\xi}_1 \\ \dot{\xi}_2 \\ \vdots \\ \dot{\xi}_r \\ \dot{\eta}_1 \\ \vdots \\ \dot{\eta}_{n-r} \end{bmatrix} = \begin{bmatrix} \xi_2 \\ \xi_3 \\ \vdots \\ \alpha(\boldsymbol{\xi}, \boldsymbol{\eta}) + \beta(\boldsymbol{\xi}, \boldsymbol{\eta})u \\ q_1(\boldsymbol{\xi}, \boldsymbol{\eta}) + p_1(\boldsymbol{\xi}, \boldsymbol{\eta})u \\ \vdots \\ q_{n-r}(\boldsymbol{\xi}, \boldsymbol{\eta}) + p_{n-r}(\boldsymbol{\xi}, \boldsymbol{\eta})u \end{bmatrix}, \quad (7.18)$$

$$y = \xi_1 \quad (7.19)$$

in the new coordinates  $\boldsymbol{\xi}, \boldsymbol{\eta}$ . In equation (7.18),

$$\alpha(\boldsymbol{\xi}, \boldsymbol{\eta}) = \mathcal{L}_{\mathbf{f}_d}^r h(\Phi^{-1}(\boldsymbol{\xi}, \boldsymbol{\eta})), \quad (7.20)$$

$$\beta(\boldsymbol{\xi}, \boldsymbol{\eta}) = \mathcal{L}_{\mathbf{g}} \mathcal{L}_{\mathbf{f}_d}^{r-1} h(\Phi^{-1}(\boldsymbol{\xi}, \boldsymbol{\eta})) \quad (7.21)$$

with

$$h(\Phi^{-1}(\boldsymbol{\xi}, \boldsymbol{\eta})) = y.$$

If the Byrnes-Isidori normal form is obtained, then

$$\dot{\eta}_1 = q_1(\boldsymbol{\xi}, \boldsymbol{\eta}), \quad (7.22)$$

$$\begin{aligned} & \vdots \\ \dot{\eta}_{n-r} &= q_{n-r}(\boldsymbol{\xi}, \boldsymbol{\eta}), \end{aligned} \quad (7.23)$$

that is, the input  $u$  does not appear in any of the dynamics for  $\eta_i$ ,  $i = 1, \dots, n-r$  by the choice of  $\eta_i$  fulfilling (7.17). The transformed dynamics (7.18) consist of two parts. The first part constitutes a chain of integrators for the external coordinates  $\boldsymbol{\xi}$ . The second part constitutes the internal dynamics of the system. They are a consequence of both the system structure and the chosen output  $y$ . As pointed out before, the states  $\eta_1 \dots \eta_{n-r}$  are unobservable from the system output for an input-output-linearizing control law so that, as a consequence, the internal dynamics cannot be controlled for by the system input  $u$  either and therefore have to be stable or at least bounded to yield feasible control.

**Synthesizing the control law** Drawing on the transformed system representation (7.18), a controller yielding a linear map between the system input  $u$  and the system output  $y = h(\Phi^{-1}(\boldsymbol{\xi}, \boldsymbol{\eta}))$  can be synthesized easily. A prescription of the control law

$$u = \frac{\nu - \alpha(\boldsymbol{\xi}, \boldsymbol{\eta})}{\beta(\boldsymbol{\xi}, \boldsymbol{\eta})} \quad (7.24)$$

with the new input  $\nu$  that can be chosen according to the situation's needs leads to a cancellation of the nonlinear terms in the integrator chain of (7.18). Conceptually,  $\alpha(\boldsymbol{\xi}, \boldsymbol{\eta})$  can be interpreted as the drift-term or plan-nonlinearity-compensating component of the control while  $\beta(\boldsymbol{\xi}, \boldsymbol{\eta})$  is to compensate for control-input nonlinearities. Applying the control law (7.24) to (7.18) yields

$$\dot{\mathbf{z}} = \begin{bmatrix} \dot{\boldsymbol{\xi}} \\ \dot{\boldsymbol{\eta}} \end{bmatrix} = \begin{bmatrix} \dot{\xi}_1 \\ \dot{\xi}_2 \\ \vdots \\ \dot{\xi}_r \\ \dot{\eta}_1 \\ \vdots \\ \dot{\eta}_{n-r} \end{bmatrix} = \begin{bmatrix} \xi_2 \\ \xi_3 \\ \vdots \\ \nu \\ q_1(\boldsymbol{\xi}, \boldsymbol{\eta}) + p_1(\boldsymbol{\xi}, \boldsymbol{\eta})u \\ \vdots \\ q_{n-r}(\boldsymbol{\xi}, \boldsymbol{\eta}) + p_{n-r}(\boldsymbol{\xi}, \boldsymbol{\eta})u \end{bmatrix}. \quad (7.25)$$

The linear input-output map in (7.25) allows for prescribing the desired behavior of the output and controlling for it by means of linear feedback theory. If, for example, trajectory tracking of a desired output trajectory  $y^*(t) = \xi_1^*$  is intended, then

$$\begin{aligned} \dot{\xi}_r &= \nu \\ &= y^{*,(r)} - k_r(\xi_r - y^{*,(r-1)}) - k_{r-1}(\xi_{r-1} - y^{*,(r-2)}) - \dots - k_1(\xi_1 - y^*) \end{aligned} \quad (7.26)$$

can be interpreted as an integrator chain  $\dot{\xi}_r = y^{*,(r)}$  complemented by a linear trajectory error feedback controller  $-k_r(\xi_r - y^{*,(r-1)}) - k_{r-1}(\xi_{r-1} - y^{*,(r-2)}) - \dots - k_1(\xi_1 - y^*)$  ensuring

that the desired trajectory is to be tracked. The coefficients  $k_1, k_2, \dots, k_r$  can be derived from pole placement techniques. It is to be noted that this approach requires the desired trajectory to have smooth derivatives  $\dot{y}^*, \ddot{y}^*, \dots, y^{*,(r)}$ .

**Investigating the zero dynamics** In classical regulation problems, an equilibrium  $\xi = \mathbf{0}$  is to be stabilized. This leads to the so called output-zeroing problem where an input  $u$  has to be devised such that the equilibrium is stabilized. What remains then are the dynamics of the internal coordinates, i.e. the internal dynamics. For a system transformed to Byrnes-Isidori normal form, setting all external states  $\xi$  equal to zero in the equations for the internal dynamics leads to the zero dynamics

$$\dot{\eta}_1 = q_1(\mathbf{0}, \boldsymbol{\eta}), \quad (7.27)$$

⋮

$$\dot{\eta}_{n-r} = q_{n-r}(\mathbf{0}, \boldsymbol{\eta}) \quad (7.28)$$

of the problem. For a system not in Byrnes-Isidori normal form, the zero dynamics can be obtained from substituting

$$u = -\frac{\alpha(\mathbf{0}, \boldsymbol{\eta})}{\beta(\mathbf{0}, \boldsymbol{\eta})} \quad (7.29)$$

into

$$\dot{\boldsymbol{\eta}} = \mathbf{q}(\mathbf{0}, \boldsymbol{\eta}) - \mathbf{p}(\mathbf{0}, \boldsymbol{\eta}) \frac{\alpha(\mathbf{0}, \boldsymbol{\eta})}{\beta(\mathbf{0}, \boldsymbol{\eta})}, \quad (7.30)$$

see also [40, 91] for further reference. In either case, the zero dynamics' equilibrium's stability is a *sufficient* condition for stability of the internal dynamics as excited by the external dynamics, however not a necessary one [40, 119].

**Generating the desired trajectory** The control approach discussed above is applicable to different types of tracking signals. Most typically, however, a change in operating points of the system will be desired. This change of operating points for a system with relative degree  $r = 3$  implies a certain type of desired trajectory  $y^*(t)$  that is most easily described by a polynomial of third order

$$y^*(t) = a_0 + a_1 t + a_2 t^2 + a_3 t^3 \quad (7.31)$$

is an appropriate ansatz-function with smooth derivatives. This ansatz allows for a smooth transition between operating points. If the change of operating point is from  $y_0$  to  $y_T$  during a transition time  $t_T$ , i.e. during a time interval  $t \in [t_0, t_0 + t_T]$ , the conditions

$$y^*(t_0) = y_0, \quad \dot{y}^*(t_0) = 0, \quad (7.32)$$

$$y^*(t_0 + t_T) = y_T, \quad \dot{y}^*(t_0 + t_T) = 0 \quad (7.33)$$

have to be fulfilled by (7.31). Conditions  $\dot{y}^*(t_0) = 0$  and  $\dot{y}^*(t_0 + t_T) = 0$  impose the smoothness requirement on (7.31), while  $y^*(t_0) = y_0$  and  $y^*(t_0 + t_T) = y_T$  simply command the change of operating points.

Substituting (7.31) into (7.33) and solving for the unknown coefficients  $a_0, a_1, a_2, a_3$ , the

$$y^*(t) = y_0 + 3 \frac{y_T - y_0}{(t_T - t_0)^2} (t - t_0)^2 - 2 \frac{y_T - y_0}{(t_T - t_0)^3} (t - t_0)^3 \quad (7.34)$$

function is obtained. While this is the most easily implementable trajectory type for the present control problem, more sophisticated trajectory generation approaches may solve for an optimal trajectory with respect to a certain criterion, e.g. control effort for problems where this is of concern.

## 7.2 Fundamentals of Multiple-Input-Multiple-Output Feedback-Linearizing Control

As for multiple-input-multiple-output (MIMO) problems, a generic formulation of an affine input MIMO control problem with  $m$  inputs and outputs is given by

$$\begin{aligned} \dot{\mathbf{x}} &= \mathbf{f}_d(\mathbf{x}, t) + \sum_{j=1}^m \mathbf{g}_j(\mathbf{x}) u_j, \\ y_1 &= h_1(\mathbf{x}), \\ &\vdots \\ y_m &= h_m(\mathbf{x}), \end{aligned} \quad (7.35)$$

which can be seen as a simple extension of the SISO description through additional inputs  $\mathbf{g}_j(\mathbf{x})$  and outputs  $h_j(\mathbf{x})$  with  $j = 2, \dots, m$ .

Below, the respective concepts from SISO feedback linearization control are extended to the notion of MIMO systems where necessary. Structurally, the steps in MIMO feedback linearization control synthesis are identical with the procedure in SISO systems.

**Determining the relative degree of a MIMO system** The notion of a system's relative degree can easily be extended to MIMO systems. Instead of a scalar relative degree as in the case of a SISO system, one speaks of a vectorial relative degree in the case of a MIMO system. The main idea is to apply the concept of a single output's relative degree to each of the  $m$  MIMO system's outputs individually. If an output  $h_j(\mathbf{x})$  has the relative degree  $r_j$ , then the vectorial relative degree of system (7.35) is given by

$$\mathbf{r} = \{r_1, r_2, \dots, r_m\}. \quad (7.36)$$

As in the SISO case, the relative degree is necessarily restricted by the system order,  $r = \sum_{j=1}^m r_j \leq n$ . The relative degree is well-defined in a set  $\mathbf{x} \in \mathcal{D}$ , if firstly

$$\mathcal{L}_{\mathbf{g}_j} \mathcal{L}_{\mathbf{f}_d}^k h_i(\mathbf{x}) = 0, \quad j = 1, \dots, m, i = 1, \dots, m, k = 0, \dots, r_i - 2 \quad (7.37)$$

for all  $\mathbf{x} \in \mathcal{D}$  and secondly the so-called decoupling matrix

$$\mathbf{B}(\mathbf{x}) = \begin{bmatrix} \mathcal{L}_{\mathbf{g}_1} \mathcal{L}_{\mathbf{f}_d}^{r_1-1} h_1(\mathbf{x}) & \mathcal{L}_{\mathbf{g}_2} \mathcal{L}_{\mathbf{f}_d}^{r_1-1} h_1(\mathbf{x}) & \dots & \mathcal{L}_{\mathbf{g}_m} \mathcal{L}_{\mathbf{f}_d}^{r_1-1} h_1(\mathbf{x}) \\ \mathcal{L}_{\mathbf{g}_1} \mathcal{L}_{\mathbf{f}_d}^{r_2-1} h_2(\mathbf{x}) & \mathcal{L}_{\mathbf{g}_2} \mathcal{L}_{\mathbf{f}_d}^{r_2-1} h_2(\mathbf{x}) & \dots & \mathcal{L}_{\mathbf{g}_m} \mathcal{L}_{\mathbf{f}_d}^{r_2-1} h_2(\mathbf{x}) \\ \vdots & \vdots & \ddots & \vdots \\ \mathcal{L}_{\mathbf{g}_1} \mathcal{L}_{\mathbf{f}_d}^{r_m-1} h_m(\mathbf{x}) & \mathcal{L}_{\mathbf{g}_2} \mathcal{L}_{\mathbf{f}_d}^{r_m-1} h_m(\mathbf{x}) & \dots & \mathcal{L}_{\mathbf{g}_m} \mathcal{L}_{\mathbf{f}_d}^{r_m-1} h_m(\mathbf{x}) \end{bmatrix} \quad (7.38)$$

is regular in  $\mathcal{D}$ . Note that  $\mathbf{B}(\mathbf{x})$  is an  $(m \times m)$  square matrix. Clearly,  $\mathbf{B}(\mathbf{x})$  is the equivalent matrix formulation of  $\beta(\mathbf{x})$  as defined by equation (7.21) – the invertibility requirement for  $\mathbf{B}(\mathbf{x})$  therefore captures the analogous intuition of the non-zero requirement for  $\beta(\mathbf{x})$ .

From the definition of (7.38) it follows that system output  $i$  and its time derivatives are given by

$$\begin{aligned} y_j &= h_j(\mathbf{x}), \\ \dot{y}_j &= \mathcal{L}_{\mathbf{f}_d} h_j(\mathbf{x}) + \underbrace{\mathcal{L}_{\mathbf{g}_1} h_j(\mathbf{x})}_{=0} u_1 + \dots + \underbrace{\mathcal{L}_{\mathbf{g}_m} h_j(\mathbf{x})}_{=0} u_m, \\ \ddot{y}_j &= \mathcal{L}_{\mathbf{f}_d}^2 h_j(\mathbf{x}) + \underbrace{\mathcal{L}_{\mathbf{g}_1} \mathcal{L}_{\mathbf{f}_d} h_j(\mathbf{x})}_{=0} u_1 + \dots + \underbrace{\mathcal{L}_{\mathbf{g}_m} \mathcal{L}_{\mathbf{f}_d} h_j(\mathbf{x})}_{=0} u_m, \\ &\vdots \\ y_j^{(r_j-1)} &= \mathcal{L}_{\mathbf{f}_d}^{r_j-1} h_j(\mathbf{x}) + \underbrace{\mathcal{L}_{\mathbf{g}_1} \mathcal{L}_{\mathbf{f}_d}^{(r_j-2)} h_j(\mathbf{x})}_{=0} u_1 + \dots + \underbrace{\mathcal{L}_{\mathbf{g}_m} \mathcal{L}_{\mathbf{f}_d}^{(r_j-2)} h_j(\mathbf{x})}_{=0} u_m, \\ y_j^{(r_j)} &= \mathcal{L}_{\mathbf{f}_d}^{r_j} h_j(\mathbf{x}) + \mathcal{L}_{\mathbf{g}_1} \mathcal{L}_{\mathbf{f}_d}^{(r_j-1)} h_j(\mathbf{x}) u_1 + \dots + \mathcal{L}_{\mathbf{g}_m} \mathcal{L}_{\mathbf{f}_d}^{(r_j-1)} h_j(\mathbf{x}) u_m \end{aligned} \quad (7.39)$$

with  $r_j$  the smallest integer such that at least one of the  $\mathcal{L}_{\mathbf{g}_i} \mathcal{L}_{\mathbf{f}_d}^{(r_j-1)} h_j(\mathbf{x}) \neq 0$  for  $i = 1, \dots, m$  and some  $\mathbf{x}$ . In matrix notation, the respective  $r_j$ -th time derivative of the  $m$  system outputs then are given by

$$\begin{bmatrix} y_1^{(r_1)} \\ \vdots \\ y_{m-1}^{(r_{m-1})} \\ y_m^{(r_m)} \end{bmatrix} = \underbrace{\begin{bmatrix} \mathcal{L}_{\mathbf{f}_d}^{r_1} h_1(\mathbf{x}) \\ \vdots \\ \mathcal{L}_{\mathbf{f}_d}^{r_{m-1}} h_{m-1}(\mathbf{x}) \\ \mathcal{L}_{\mathbf{f}_d}^{r_m} h_m(\mathbf{x}) \end{bmatrix}}_{=: \mathbf{a}(\mathbf{x})} + \mathbf{B}(\mathbf{x}) \underbrace{\begin{bmatrix} u_1 \\ \vdots \\ u_{m-1} \\ u_m \end{bmatrix}}_{=: \mathbf{u}}. \quad (7.40)$$

**Transforming a MIMO system into normal form** In parallel to the procedure for SISO systems, a diffeomorphism transforming the original state variables  $\mathbf{x}$  to new state variables  $\mathbf{z}$  for a MIMO system can be constructed and is of the form

$$\mathbf{z} = \begin{bmatrix} z_1 \\ z_2 \\ \vdots \\ z_n \end{bmatrix} = \begin{bmatrix} \boldsymbol{\xi} \\ \boldsymbol{\eta} \end{bmatrix} = \begin{bmatrix} \xi_{1,1} \\ \vdots \\ \xi_{1,r_1} \\ \xi_{2,1} \\ \vdots \\ \xi_{2,r_2} \\ \vdots \\ \xi_{m,1} \\ \vdots \\ \xi_{m,r_m} \\ \eta_1 \\ \vdots \\ \eta_{n-r} \end{bmatrix} = \boldsymbol{\Phi}(\mathbf{x}) = \begin{bmatrix} h_1(\mathbf{x}) \\ \vdots \\ \mathcal{L}_{\mathbf{f}_d}^{r_1-1} h_1(\mathbf{x}) \\ h_2(\mathbf{x}) \\ \vdots \\ \mathcal{L}_{\mathbf{f}_d}^{r_2-1} h_2(\mathbf{x}) \\ \vdots \\ h_m(\mathbf{x}) \\ \vdots \\ \mathcal{L}_{\mathbf{f}_d}^{r_m-1} h_m(\mathbf{x}) \\ \Phi_{r+1}(\mathbf{x}) \\ \vdots \\ \Phi_n(\mathbf{x}) \end{bmatrix}. \quad (7.41)$$

As for SISO systems, the variables  $\Phi_{r+1}(\mathbf{x}) \dots \Phi_n(\mathbf{x})$  again represent the internal dynamics of the system which are associated with the zero dynamics upon input-output-linearization. In contrast to the SISO system case, they can be chosen to yield  $\mathcal{L}_{\mathbf{g}_j} \Phi_k(\mathbf{x}) = 0$ ,  $j = 1, \dots, m$ ,  $k = r + 1, \dots, n$  only if the span of  $\{\mathbf{g}_1, \dots, \mathbf{g}_m\}$  is involutive, see [91] for further treatment of this topic. In order for (7.41) to constitute a diffeomorphism, condition (7.16) has to be fulfilled.

Applying the transformation then yields the dynamics

$$\dot{\mathbf{z}} = \begin{bmatrix} \dot{\xi}_{1,1} \\ \dot{\xi}_{1,2} \\ \vdots \\ \dot{\xi}_{1,r_1} \\ \vdots \\ \vdots \\ \dot{\xi}_{m,1} \\ \dot{\xi}_{m,2} \\ \vdots \\ \dot{\xi}_{m,r_m} \\ \dot{\eta}_1 \\ \vdots \\ \dot{\eta}_{n-r} \end{bmatrix} = \begin{bmatrix} \xi_{1,2} \\ \xi_{1,3} \\ \vdots \\ a_1(\boldsymbol{\Phi}^{-1}(\boldsymbol{\xi}, \boldsymbol{\eta})) + \sum_{j=1}^m B_{1j}(\boldsymbol{\Phi}^{-1}(\boldsymbol{\xi}, \boldsymbol{\eta}))u_j \\ \vdots \\ \vdots \\ \xi_{m,2} \\ \xi_{m,3} \\ \vdots \\ a_m(\boldsymbol{\Phi}^{-1}(\boldsymbol{\xi}, \boldsymbol{\eta})) + \sum_{j=1}^m B_{mj}(\boldsymbol{\Phi}^{-1}(\boldsymbol{\xi}, \boldsymbol{\eta}))u_j \\ q_1(\boldsymbol{\xi}, \boldsymbol{\eta}) + \sum_{j=1}^m p_{1,m}(\boldsymbol{\xi}, \boldsymbol{\eta})u_j \\ \vdots \\ q_{n-r}(\boldsymbol{\xi}, \boldsymbol{\eta}) + \sum_{j=1}^m p_{n-r,m}(\boldsymbol{\xi}, \boldsymbol{\eta})u_j \end{bmatrix}. \quad (7.42)$$

Here, the  $a_i$  and  $B_{ij}$  are the entries of matrix  $\mathbf{a}$  and  $\mathbf{B}$ , respectively. In case a suitable transformation can be found, the system may also be transformed to Byrnes-Isidori normal form. For this system representation,

$$p_{i,j} = 0 \quad \text{for } i = 1, \dots, n - r, \quad j = 1, \dots, m. \quad (7.43)$$

**Synthesizing the control law** A control law input-output linearizing the system in Byrnes-Isidori normal form (7.42) can be found from (7.40). The control law immediately presents itself as

$$\mathbf{u} = \mathbf{B}^{-1}(\Phi^{-1}(\boldsymbol{\xi}, \boldsymbol{\eta}))(\boldsymbol{\nu} - \mathbf{a}(\Phi^{-1}(\boldsymbol{\xi}, \boldsymbol{\eta}))) \quad (7.44)$$

with the vector-type new input  $\boldsymbol{\nu}$  subject to control design. The matrix  $\mathbf{B}^{-1}(\Phi^{-1}(\boldsymbol{\xi}, \boldsymbol{\eta}))$  can be understood as a means to invert the nonlinearities of the different control input matrices. As noted earlier, the invertibility of  $\mathbf{B}(\Phi^{-1}(\boldsymbol{\xi}, \boldsymbol{\eta}))$  is crucial to the functioning of the control strategy as devised here. The result is a system with  $m$  decoupled integrator chains of orders  $r_1, \dots, r_m$  respectively.



# 8 Nonlinear Volume Flow Control of a Variable Displacement Vane Pump

## 8.1 Background

The self-regulating vane pump system discussed in chapter 6 is one means to provide a system with volume flow. Its natural advantage lies in the fact that it can by itself adapt to varying consumer loads. The results show, however, that stability problems may occur. In practice, instabilities in the context of such systems are well-known so that it is worthwhile to investigate alternative ways of controlling volume flow in a vane pump system. One option is to replace the self-regulating valve with a servo valve actuated by a prescribed control input voltage or current. Here, instabilities from valve oscillations are largely prevented due to stable actuation of the servo valve. The governing law for the valve input will then be subject to control design. Therefore, in this chapter, a control approach based on nonlinear control theory shall be proposed and discussed for a variable displacement vane pump system featuring a servo valve. Within this context, also see [140, 141].

The approach of choice is the feedback linearization method outlined in the previous chapter. While a common objection to feedback linearization is a potentially large or costly control effort needed to implement the control laws, one of its advantages can be seen in its applicability to a comparatively large class of nonlinear systems where control theory otherwise falls short of providing a general approach to for a systematic treatment. The control effort argument against feedback linearization rests upon the reasoning that the associated control laws suppress rather than make use of the natural dynamics of the underlying system – especially in the manipulation of robotic systems this may lead to “costly” control due to large inertia within such systems. In the case of hydraulic systems, however, the argument does not apply. This is rooted in the amplifier property inherent to valves (see e.g. [4, 23] for a discussion of this property): in some instances the output power of a valve can be up to  $10^6$  times the input power needed for valve actuation. As a consequence, physical control effort when employing servo valves as actuation elements is very small so that especially in the context of hydraulic servo systems, feedback linearization is a feasible means.

Alternative approaches that have established their relevance in the field of hydraulics control are surveyed in [41]. The classification comprises classic and state techniques, adaptive control, feedforward and variable structure control, fuzzy and neuro-control and even – given the physical stiffness of such systems – predictive control approaches.

## 8.2 System Description

The system is identical to the system described in chapter 6 except for the servo valve replacing the self-regulating valve, see Figure 8.1. The servo valve is actuated by an input current or voltage input and will respond to this input by valve spool displacement. It is assumed to be critically lapped (see e.g. [30, 32]) which is commonly seen as an appropriate assumption even though in practical cases, servo valves may feature a (negligible) underlap.

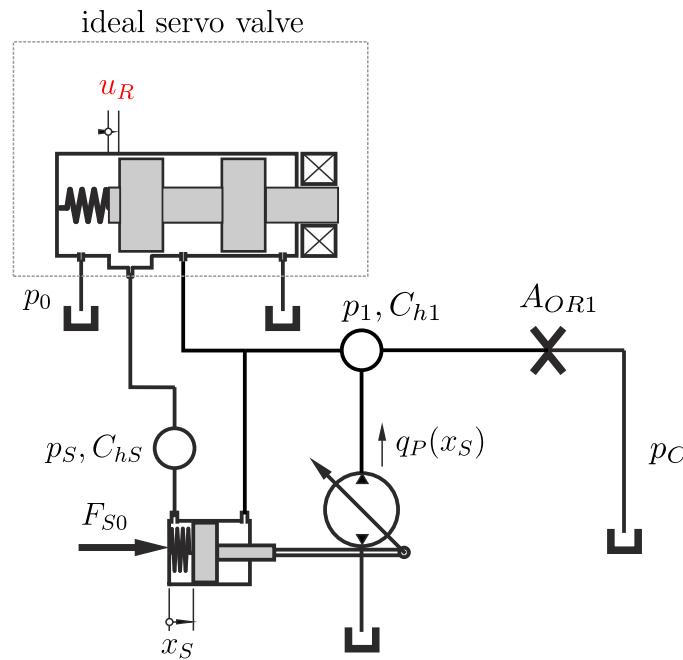


Figure 8.1: Variable displacement vane pump system with servo valve.

## 8.3 SISO Model

In applications featuring hydraulic (servo-)systems, it is common to model systems with hydraulic elements by assuming that (servo) valves operate infinitely fast and do not exhibit relevant dynamic behavior. From a practical viewpoint, this assumption holds for modern servo-valves in many cases and greatly simplifies the resulting control laws, see e.g. [30, 32] for further reference. The reasoning of "ideal" or, equivalently, static valve dynamics is attributed to the low mass of valves and relatively high stiffness of valve springs compared to the mass and stiffness of control pistons or pump units. In most cases, servo valves are modeled as ideal  $PT2$  elements, governed by

$$\ddot{x}_v + 2D_v\omega_v\dot{x}_v + \omega_v^2x_v = \tilde{K}_v\omega_v^2x_{v,max}u. \quad (8.1)$$

Here,  $x_v$  is the actual valve opening. The parameter  $\omega_v$  is the so-called valve limit frequency. Modern servo valves can reach up to 400Hz [18], for the simulations in this chapter however, a valve with 250Hz is assumed. Damping  $D_v$  is typically close to 1 and thus critical damping within the valve is achieved. The valve gain  $\tilde{K}_v$  characterizes the translation of a voltage input  $u$  to the valve in a corresponding normalized valve opening. Servo valves are designed such that this parameter is close to 1, too. Practically, this model can also be written as

$$\ddot{x}_v + 2D_v\omega_v\dot{x}_v + \omega_v^2x_v = K_v\omega_v^2x_{v,nom}, \quad (8.2)$$

where now the nominal valve opening  $x_{v,nom}$  is considered as a control input. With the assumption of a static valve and  $K_v = 1$ ,

$$x_v = x_{v,nom}. \quad (8.3)$$

This then allows the derivation of control laws in  $x_{v,nom}$  representing the nominal valve opening needed to achieve the control purpose at hand. Since the regulator valve from chapter 6 is now replaced by a servo valve,  $x_R = x_v$  and for an ideal valve,  $x_R = x_v = x_{v,nom} =: u_R$ .

Introducing the states

$$x_1 = x_S, \quad x_2 = \dot{x}_S, \quad x_3 = p_1, \quad x_4 = p_S, \quad (8.4)$$

the state  $\mathbf{x}$  of the system under the assumption of a static valve is represented by

$$\mathbf{x} = [x_1 \quad x_2 \quad x_3 \quad x_4]^T. \quad (8.5)$$

In state space, the dynamics of the vane pump system with an ideal servo valve can then be expressed as

$$\dot{\mathbf{x}} = \begin{bmatrix} f_1(\mathbf{x}, u_R) \\ f_2(\mathbf{x}, u_R) \\ f_3(\mathbf{x}, u_R) \\ f_4(\mathbf{x}, u_R) \end{bmatrix} \quad (8.6)$$

with

$$f_1(\mathbf{x}, u_R) = x_2, \quad (8.7)$$

$$f_2(\mathbf{x}, u_R) = \frac{1}{m_{PS}} \left[ -k_S x_1 - d_{PS} x_2 - A_{S2} x_3 + A_{S1} x_4 + f_P(x_1, x_3) + k_S l_S + F_{S0} - F_{ES}(x_1, x_2, l_S) \right], \quad (8.8)$$

$$f_3(\mathbf{x}, u_R) = \frac{1}{C_{h1}} \left[ \hat{q}_P(x_1 - x_S^{offset}) - \text{sign}(x_3 - p_C) \gamma_F A_{OR1} \sqrt{|x_3 - p_C|} - q_R(u_R, x_3, x_4) + A_{S2} x_2 \right], \quad (8.9)$$

$$f_4(\mathbf{x}, u_R) = \frac{1}{C_{hS}} \left[ -A_{S1}x_2 + q_R(u_R, x_3, x_4) - q_T(u_R, x_4, p_0) \right], \quad (8.10)$$

where

$$q_R = \begin{cases} 0 & \text{for } u_R \geq 0, \\ \text{sign}(x_3 - x_4) \gamma_F b_{Reg} |u_R| \sqrt{|x_3 - x_4|} & \text{else,} \end{cases} \quad (8.11)$$

$$q_T = \begin{cases} \text{sign}(x_4 - p_0) \gamma_F b_{Reg} |u_R| \sqrt{|x_4 - p_0|} & \text{for } u_R \geq 0, \\ 0 & \text{else.} \end{cases} \quad (8.12)$$

This is the model of the SISO system that shall be drawn onto for the control design. In what follows, the following assumptions will be made for the sake of a simplified analysis:

- Capacitances  $C_{hS}$  and  $C_{h1}$  are treated constant in the analysis of the obtained control laws. Implementation in the numerical model of the system will, however, includes variations of the system capacitances with the system state  $\mathbf{x}$  as modeled by

$$C_{h1} = \frac{V_{10} + (l_S - x_1)A_{S2}}{E_{fl}}, \quad C_{hS} = \frac{V_{S0} + x_1A_{S1}}{E_{fl}}. \quad (8.13)$$

- Neglecting pump forces from dead volume expansion and the influence of leakage on dead volume pressure, pump force  $f_P(x_1, x_3)$  will be represented as the sum of

$$f_P(x_1, x_3) = f_P^{II}(x_1, x_3) = x_3 f_{P1}(x_1) + f_{P2}(x_1), \quad (8.14)$$

i.e. as the sum of a purely displacement-dependent component  $f_{P2}(x_1)$  and the product of system pressure  $x_3$  multiplied by a displacement-dependent effective area function  $f_{P1}(x_1)$ . The results from chapter 5 show that the force from dead volume expansion and the effect of leakage on total pump force is not significant relative to the force contributions from  $x_3 f_{P1}(x_1)$ ,  $f_{P2}(x_1)$  so that the simplifications related to a choice of  $f_P(x_1, x_3) = f_P^{II}(x_1, x_3)$  are not crucial to the derivation of the resulting control laws. Ultimately, this allows for an analytical discussion of aspects of stability and boundedness of the proposed control approach.

## 8.4 Feedback-Linearizing Control

From the system representation (8.6), the standard input-affine representation

$$\dot{\mathbf{x}} = \mathbf{f}_d(\mathbf{x}) + \mathbf{g}_R(\mathbf{x})u_R$$

needed for feedback linearization can be derived. Because this representation is contingent on whether  $u_R \geq 0$ , i.e. whether the system is in what shall further be referred to as the tank-sided operating condition or whether  $u_R < 0$  so that the system is in so-called load-sided operating condition, these representations will be derived separately in the following two subsections, so that

$$\mathbf{g}_R(\mathbf{x}) = \begin{cases} \mathbf{g}_{RT} & \text{if } u_R \geq 0, \\ \mathbf{g}_{RL} & \text{if } u_R < 0. \end{cases} \quad (8.15)$$

Intuitively,  $u_R > 0$  is related to a decrease in pump volume flow since a pressure decrease in  $C_{hS}$  related to this operating condition will cause the cam ring to displace to the left and thereby reduce pump volume flow. Accordingly, for  $u_R < 0$ , pressure in  $C_{hS}$  will increase, thereby displacing the cam ring to the right.

In order for input-output linearization to be applicable to a certain control problem, smoothness of the system dynamics has to be ensured. In the case at hand, there is a right hand side with the non-smooth functions  $q_R$  and  $q_T$ . Yet, the functions are smooth piecewise, potentially allowing for a piecewise synthesis of a suitable control strategy. It will be seen that this goes in hand with identical external coordinates for both operating conditions.

### 8.4.1 Control Synthesis for a Drop in Volume Flow

As mentioned above, a drop in volume flow requires  $u_R \geq 0$  and thereby

$$q_R = 0, \quad (8.16)$$

$$q_T = \text{sign}(x_4 - p_0) \gamma_F b_{Reg} u_R \sqrt{|x_4 - p_0|}. \quad (8.17)$$

Thus, upon substitution of the above relationships into (8.6) the control system in affine form

$$\dot{\mathbf{x}} = \begin{bmatrix} f_{d1}(\mathbf{x}) \\ f_{d2}(\mathbf{x}) \\ f_{d3}(\mathbf{x}) \\ f_{d4}(\mathbf{x}) \end{bmatrix} + \underbrace{\begin{bmatrix} 0 \\ 0 \\ 0 \\ -\frac{\text{sign}(x_4 - p_0) b_{Reg}}{C_{hS}} \gamma_F \sqrt{|x_4 - p_0|} \end{bmatrix}}_{=: \mathbf{g}_{RT}(\mathbf{x})} u_R \quad (8.18)$$

is obtained, where

$$f_{d1}(\mathbf{x}) = x_2, \quad (8.19)$$

$$f_{d2}(\mathbf{x}) = \frac{1}{m_{PS}} \left[ -k_S x_1 - d_{PS} x_2 - A_{S2} x_3 + A_{S1} x_4 + f_P(x_1, x_3) + k_S l_S + F_{S0} \right], \quad (8.20)$$

$$f_{d3}(\mathbf{x}) = \frac{1}{C_{h1}} \left[ \hat{q}_P(x_1 - x_S^{offset}) - \text{sign}(x_3 - p_C) \gamma_F A_{OR1} \sqrt{|x_3 - p_C|} + A_{S2} x_2 \right], \quad (8.21)$$

$$f_{d4}(\mathbf{x}) = -\frac{A_{S1}}{C_{hS}}x_2. \quad (8.22)$$

In the above system description, the end-stop forces acting on the lumped pump and cylinder mass  $m_{PS}$  are assumed equal to zero which implies that the control to be devised shall only act within the natural operating range  $\mathcal{D}$  of the system. For a concrete pump run at a certain pump revolution speed, this operating range is to the largest part determined by the pump end stops with  $0 \leq x_S \leq l_S$ . With (8.18), the system now is in a form that allows for synthesizing a nonlinear controller by input-output-linearization.

**Determining the relative degree** The output of the system for pump volume flow control is given by the pump displacement variable  $h(\mathbf{x}) = x_1 = x_S$ . Accounting for the possible volume flow offset due to vertical cam ring eccentricity  $h \neq 0$  as outlined in section 5.3.3, the system output thus is

$$h(\mathbf{x}) = x_1 - x_S^{offset}. \quad (8.23)$$

Building the successive Lie derivatives

$$h(\mathbf{x}) = x_1 - x_S^{offset}, \quad (8.24)$$

$$\mathcal{L}_{\mathbf{g}_R} h(\mathbf{x}) = 0, \quad (8.25)$$

$$\mathcal{L}_{\mathbf{f}_d} h(\mathbf{x}) = x_2, \quad (8.26)$$

$$\mathcal{L}_{\mathbf{g}_R} \mathcal{L}_{\mathbf{f}_d} h(\mathbf{x}) = 0, \quad (8.27)$$

$$\begin{aligned} \mathcal{L}_{\mathbf{f}_d}^2 h(\mathbf{x}) = & -\frac{1}{m_{PS}}(k_S x_1 - A_{S1} x_4 + A_{S2} x_3 \\ & + d_{PS} x_2 - x_3 f_{P1}(x_1) - f_{P2}(x_1) - k_S l_S - F_{S0}), \end{aligned} \quad (8.28)$$

$$\mathcal{L}_{\mathbf{g}_R} \mathcal{L}_{\mathbf{f}_d}^2 h(\mathbf{x}) = -\frac{A_{S1}}{m_{PS} C_{hS}} \text{sign}(x_4 - p_0) \gamma_F b_{Reg} \sqrt{|x_4 - p_0|} \quad (8.29)$$

shows that the relative degree of the system defined by (8.18) and (8.23) is  $r = 3$  which implies first order internal and zero dynamics. The relative degree is well defined in state space  $\mathbf{x} \in \mathcal{D}$  except for the case when  $x_4 = p_S = p_0 = 0$ . This does not pose a problem for the control law to be designed practically as the control shall not act in a way that reduces the volume flow of the pump to zero in an equilibrium position. Yet, for non-zero  $p_C$ , this would be the only circumstance under which  $x_4$  could become equal to the tank pressure.

**Transforming into normal form** In order to transform the system (8.18) into Byrnes-Isidori normal form, a fourth state variable  $\eta$  representing the internal state of the system has to be defined in such a way that the matrix  $\Phi(\mathbf{x})$  yields an invertible map between the new coordinates  $\mathbf{z} = [\xi \ \eta]^T$  and  $\mathbf{x}$ . In accordance with the notation used so far, for the tank-sided operating condition  $\eta = \eta_T$ . As discussed in the theoretical outline of

feedback-linearization in section 7.1, this fourth state variable can either be determined freely subject to invertibility of the state transformation matrix demanded by equation (7.16) or it can be computed as the solution of the partial differential equation given by (7.17).

Considering the system dynamics at hand, the fourth state transformation can be defined as

$$\eta_T = x_3 - p_C. \quad (8.30)$$

It is easily seen that this choice for the internal coordinate fulfills (7.17) so that the system can be transformed into Byrnes-Isidori normal form by the choice of (8.30). The full state transformation then reads

$$\begin{aligned} \mathbf{z} = \Phi(\mathbf{x}) &= \begin{bmatrix} h(\mathbf{x}) \\ \mathcal{L}_{f_d} h(\mathbf{x}) \\ \mathcal{L}_{f_d}^2 h(\mathbf{x}) \\ x_3 - p_C \end{bmatrix} \\ &= \begin{bmatrix} x_1 - x_S^{offset} \\ x_2 \\ -\frac{1}{m_{PS}}(k_S x_1 - A_{S1} x_4 + A_{S2} x_3 + d_{PS} x_2 - x_3 f_{P1}(x_1) - f_{P2}(x_1) - k_S l_S - F_{S0}) \\ x_3 - p_C \end{bmatrix}. \end{aligned} \quad (8.31)$$

(8.32)

Building the Jacobian of the transformation yields

$$\frac{\partial \Phi}{\partial \mathbf{x}} = \begin{bmatrix} 1 & 0 & 0 & 0 \\ 0 & 1 & 0 & 0 \\ -\frac{k_S - x_3}{m_{PS}} \frac{\partial f_{P1}}{\partial x_1} - \frac{\partial f_{P2}}{\partial x_1} & -\frac{d_{PS}}{m_{PS}} & -\frac{A_{S2} - f_{P1}}{m_{PS}} & \frac{A_{S1}}{m_{PS}} \\ 0 & 0 & 1 & 0 \end{bmatrix}. \quad (8.33)$$

Clearly, since  $\det \frac{\partial \Phi}{\partial \mathbf{x}} = -A_{S1}/m_{PS}$  condition (7.16) holds irrespective of the current system state so that (8.32) constitutes a diffeomorphism.

Conceptually, from the choice of  $\eta$ , the internal dynamics for the tank-side flow condition  $u_R > 0$  are the volume flow balance of volume  $V_1$  and have to yield stable zero dynamics.

Applying the transformation defined by (8.32), the Byrnes-Isidori normal form of (8.18) reads

$$\begin{bmatrix} \dot{\xi}_1 \\ \dot{\xi}_2 \\ \dot{\xi}_3 \\ \dot{\eta}_T \end{bmatrix} = \begin{bmatrix} \xi_2 \\ \xi_3 \\ \alpha(\boldsymbol{\xi}, \eta_T) + \beta(\boldsymbol{\xi}, \eta_T) u_R \\ q_T(\boldsymbol{\xi}, \eta_T) \end{bmatrix}, \quad (8.34)$$

$$y = \xi_1. \quad (8.35)$$

The above form of the system dynamics immediately reveals the structure for the control input  $u_R$  that is needed in order to compensate the control input nonlinearity and the drift system nonlinearities. In physical coordinates  $\mathbf{x}$ , the nonlinearity-compensating components of the control law can be given as

$$\begin{aligned} \alpha(\boldsymbol{\xi}, \eta_T) &= \mathcal{L}_{\mathbf{f}_d}^3 h(\Phi^{-1}(\boldsymbol{\xi}, \eta_T)) = \mathcal{L}_{\mathbf{f}_d}^3 h(\mathbf{x}) \\ &= \frac{1}{m_{PS}} \left[ -\frac{d_{PS}(k_S l_S + F_{S0})}{m_{PS}} + \frac{d_{PS} k_S}{m_{PS}} x_1 - \frac{A_{S2}}{C_{h1}} \hat{q}_P (x_1 - x_S^{offset}) \right. \\ &\quad + \left( \frac{d_{PS}^2}{m_{PS}} - k_S - \frac{A_{S1}^2}{C_{hS}} - \frac{A_{S2}^2}{C_{h1}} \right) x_2 + \frac{d_{PS}}{m_{PS}} (A_{S2} x_3 - A_{S1} x_4) \\ &\quad + \left( \frac{A_{S2}}{C_{h1}} - \frac{f_{P1}(x_1)}{C_{h1}} \right) \text{sign}(x_3 - p_C) \gamma_F A_{OR1} \sqrt{|x_3 - p_C|} \\ &\quad + \frac{\hat{q}_P}{C_{h1}} (x_1 - x_S^{offset}) f_{P1}(x_1) + \frac{A_{S2}}{C_{h1}} f_{P1}(x_1) x_2 \\ &\quad \left. - \frac{d_{PS}}{m_{PS}} (x_3 f_{P1}(x_1) + f_{P2}(x_1)) + x_2 \left( x_3 \frac{\partial f_{P1}(x_1)}{\partial x_1} + \frac{\partial f_{P2}(x_1)}{\partial x_1} \right) \right], \end{aligned} \quad (8.36)$$

$$\begin{aligned} \beta(\boldsymbol{\xi}, \eta_T) &= \mathcal{L}_{\mathbf{g}_R} \mathcal{L}_{\mathbf{f}_d}^2 h(\Phi^{-1}(\boldsymbol{\xi}, \eta_T)) = \mathcal{L}_{\mathbf{g}_R} \mathcal{L}_{\mathbf{f}_d}^2 h(\mathbf{x}) \\ &= -\frac{A_{S1}}{C_{hS}} \text{sign}(x_4 - p_0) \gamma_F \frac{b_{Reg}}{m_{PS}} \sqrt{|x_4 - p_0|}. \end{aligned} \quad (8.37)$$

**Synthesizing the control law** As outlined in chapter 7, a control law linearizing the input-output relationship in physical coordinates  $\mathbf{x}$  is given by

$$u_R = \frac{\nu - \alpha(\boldsymbol{\xi}, \eta_T)}{\beta(\boldsymbol{\xi}, \eta_T)}$$

with  $\alpha(\boldsymbol{\xi}, \eta_T)$  and  $\beta(\boldsymbol{\xi}, \eta_T)$  from equations (8.36) and (8.37). The new input  $\nu$  is chosen to be

$$\nu = -k_1(\xi_1 - \xi_1^*) - k_2(\xi_2 - \dot{\xi}_1^*) - k_3(\xi_3 - \ddot{\xi}_1^*) + \ddot{\xi}_1^* \quad (8.38)$$

$$= [k_1 \quad k_2 \quad k_3] \mathbf{e} + \ddot{\xi}_1^*, \quad (8.39)$$

feeding back the components of the trajectory tracking error  $\mathbf{e} = \boldsymbol{\xi}^* - \boldsymbol{\xi}$  with weights  $k_1$ ,  $k_2$  and  $k_3$  such that the error system is stable and the system dynamics stably track the desired trajectory  $\xi_1^*$ . The controller structure is visualized in Figure 8.2.

**Investigating the zero dynamics** As for the internal dynamics,

$$\dot{\eta}_T = q_T(\boldsymbol{\xi}, \eta_T) = \frac{1}{C_{h1}} \left( \hat{q}_P \xi_1 + A_{S2} \xi_2 - \text{sign}(\eta_T) \gamma_F A_{OR1} \sqrt{|\eta_T|} \right). \quad (8.40)$$

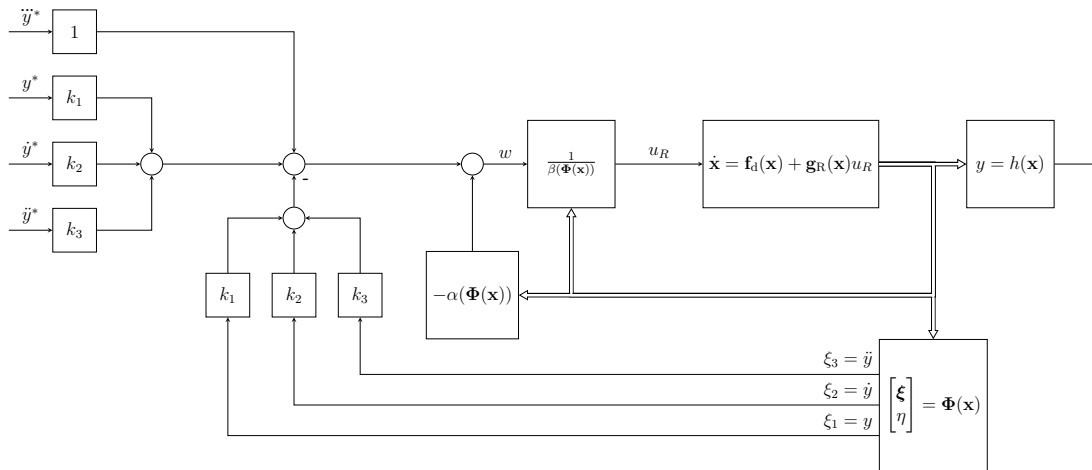


Figure 8.2: Feedback-linearizing control approach.

The corresponding first order zero dynamics resulting hence are obtained from setting  $\xi = \mathbf{0}$ , so that

$$\dot{\eta}_T(\xi = \mathbf{0}, \eta_T) = -\frac{\gamma_F A_{OR1}}{C_{h1}} \text{sign}(\eta_T) \sqrt{|\eta_T|}. \quad (8.41)$$

To prove asymptotic stability of the above zero dynamics, it is necessary to draw on Lyapunov stability theory. A Lyapunov function candidate is chosen as

$$V = \frac{1}{2} C_{h1} \eta_T^2, \quad (8.42)$$

which is positive definite in an arbitrary neighborhood of  $\eta_T = 0$ .

The Lyapunov candidate's derivative along trajectories of  $\eta_T$  then is

$$\dot{V} = C_{h1} \eta_T \dot{\eta}_T \quad (8.43)$$

$$= -\eta_T \text{sign}(\eta_T) \sqrt{|\eta_T|} \gamma_F A_{OR1} \quad (8.44)$$

$$= -|\eta_T| \sqrt{|\eta_T|} \gamma_F A_{OR1}, \quad (8.45)$$

which is negative definite as  $\dot{V}$  can only become zero for  $\eta_T = 0$ . Therefore the zero dynamics are asymptotically stable.

Equation (8.41) does have a unique equilibrium at  $\eta_T = 0$ , so all solutions starting from  $\eta_{T0} \in \mathbb{R}$  converge to zero so that the system is asymptotically stable and input-output-linearization can be performed for this system configuration. With a view on theorems on bounded tracking of trajectories, however, the zero dynamics indeed are only asymptotically, but not globally exponentially stable, as can be seen from consideration of the closed solution of the zero dynamics. If, for example, the case where the sign-function in the zero dynamics yields a positive value, is considered, one finds that

$$\eta_T > 0: \quad \dot{\eta}_T = -\frac{\gamma_F A_{OR1}}{C_{h1}} \sqrt{\eta_T} \quad (8.46)$$

$$\Rightarrow \eta_T = \left( \sqrt{\eta_{T0}} - 2 \frac{\gamma_F A_{OR1}}{C_{h1}} (t - t_0) \right)^2. \quad (8.47)$$

So the convergence speed to the stable equilibrium solution is of second order which implies that a relationship

$$|\eta_T(t)| \leq |\eta_{T0}| m e^{-\alpha(t-t_0)} \quad (8.48)$$

as required for exponential stability in [91] with  $\alpha > 0$  as the rate of convergence and  $m > 0$  a positive constant is not fulfilled for all  $\eta_{T0} \in \mathbb{R}^+$  by the zero dynamics' solution. While some theorems for bounded/asymptotic trajectory tracking control work with converse Lyapunov theorems based on (global) exponential stability, non-global exponential stability of the zero dynamics in this case is not an obstacle to the method, as in [40] a theorem for bounded trajectory tracking is presented. However, especially in the field of adaptive control, global exponential stability is desirable since most convergence proofs rely on converse Lyapunov theorems requiring (global) exponential stability. From an engineering point of view, global exponential stability of the zero dynamics can be associated with a robustness to perturbations.

### 8.4.2 Control Synthesis for a Rise in Volume Flow

In case a rise in pump volume flow is required, the system operates under the condition that  $u_R < 0$  and thereby

$$q_T = 0, \quad (8.49)$$

$$q_R = \text{sign}(x_3 - x_4) \gamma_F b_{Reg} |u_R| \sqrt{|x_3 - x_4|}. \quad (8.50)$$

Substituting these relationships into the system equation (8.6), the system equations in input-affine form for this operating condition are

$$\dot{\mathbf{x}} = \begin{bmatrix} f_{d1}(\mathbf{x}) \\ f_{d2}(\mathbf{x}) \\ f_{d3}(\mathbf{x}) \\ f_{d4}(\mathbf{x}) \end{bmatrix} + \underbrace{\begin{bmatrix} 0 \\ 0 \\ \frac{\text{sign}(x_3 - x_4) b_{Reg}}{C_{h1}} \gamma_F \sqrt{|x_3 - x_4|} \\ -\frac{\text{sign}(x_3 - x_4) b_{Reg}}{C_{hS}} \gamma_F \sqrt{|x_3 - x_4|} \end{bmatrix}}_{=: \mathbf{g}_{RL}(\mathbf{x})} u_R. \quad (8.51)$$

It needs to be emphasized that the input  $u_R$  now appears in two state equations through the structure of  $\mathbf{g}_{RL}(\mathbf{x})$ . Since the drift term  $\mathbf{f}_d(\mathbf{x})$  remains unaffected from the change in the control input matrix,  $f_{d1}(\mathbf{x})$ ,  $f_{d2}(\mathbf{x})$ ,  $f_{d3}(\mathbf{x})$  and  $f_{d4}(\mathbf{x})$  are given by (8.19), (8.20), (8.21) and (8.22), respectively.

**Determining the relative degree** Again assuming the system output to be given by (8.23), the output and its first two time derivatives are identical with (8.24) to (8.28), respectively. However, due to the structurally different input vector, for  $\mathcal{L}_{g_R} \mathcal{L}_{f_d}^2 h(\mathbf{x})$  one obtains

$$\mathcal{L}_{g_R} \mathcal{L}_{f_d}^2 h(\mathbf{x}) = - \left( \frac{A_{S2} - f_{P1}(x_1)}{C_{h1}} + \frac{A_{S1}}{C_{hS}} \right) \text{sign}(x_3 - x_4) \gamma_F \frac{b_{Reg}}{m_{PS}} \sqrt{|x_3 - x_4|}. \quad (8.52)$$

The relative degree is  $r = 3$  for  $x_3 \neq x_4$  and thereby the same in the operating condition where a decrease in pump volume flow is required.

**Transforming into normal form** The state transformation for the external coordinates is defined by the output and its time derivatives up to  $r-1$ -th order. These quantities are identical with those obtained for  $u_R \geq 0$ , so that the external coordinates are identical for the two operating conditions. Finding an appropriate coordinate transformation for the internal dynamics remains a question to be treated, as the obvious candidates  $\eta_L = x_3$  and  $\eta_L = x_4$  can easily be shown to result in internal dynamics depending on the system input  $u_R$ . While this is no major drawback in general, it does complicate the investigation of the stability of the internal dynamics for the load-sided flow condition. For this not to be the case, a solution of (7.17) has to be found.

Formulating the equation for the problem at hand, one obtains

$$\left[ \frac{1}{C_{h1}} \frac{\partial \Phi_4}{\partial x_3} - \frac{1}{C_{hS}} \frac{\partial \Phi_4}{\partial x_4} \right] \left( b_{Reg} \gamma_F \sqrt{|x_3 - x_4|} \right) = 0. \quad (8.53)$$

A solution candidate for this equation is given by

$$\tilde{\Phi}_4 = \tilde{\eta}_L = C_{h1}x_3 + C_{hS}x_4. \quad (8.54)$$

Scaling the above solution candidate by a factor  $\Psi_1$  and adding a constant  $\Psi_2$  will not structurally alter the solution property of the thus obtained result for the partial differential equation in (8.53), so that  $\Phi_4$  is chosen to be

$$\Phi_4 = \eta_L = \Psi_1(C_{h1}x_3 + C_{hS}x_4) + \Psi_2. \quad (8.55)$$

With respect to obtaining the simplest expression for the zero dynamics with an equilibrium located at zero, it is purposeful to choose

$$\Psi_1 = \frac{A_{S1}}{A_{S1}C_{h1} + A_{S2}C_{hS} - C_{hS}f_{P1}(x_S^{offset})}, \quad (8.56)$$

$$\Psi_2 = C_{hS} \frac{F_{S0} + k_S(l_S - x_S^{offset}) + f_{P2}(x_S^{offset})}{A_{S1}C_{h1} + A_{S2}C_{hS} - C_{hS}f_{P1}(x_S^{offset})} - p_C. \quad (8.57)$$

Due to  $f_{P1}(\xi_1 + x_S^{offset}) \leq 0$  for the whole operating range of  $\xi_1$  ( see Figure 5.8), it follows that  $\Psi_1 > 0$ . The full state transformation then reads

$$\mathbf{z} = \Phi(\mathbf{x}) = \begin{bmatrix} h(\mathbf{x}) \\ \mathcal{L}_{f_d} h(\mathbf{x}) \\ \mathcal{L}_{f_d}^2 h(\mathbf{x}) \\ \Psi_1 (C_{h1}x_3 + C_{hS}x_4) + \Psi_2 \end{bmatrix}$$

$$= \begin{bmatrix} x_1 - x_S^{offset} \\ x_2 \\ -\frac{1}{m_{PS}}(k_S x_1 - A_{S1} x_4 + A_{S2} x_3 + d_{PS} x_2 - x_3 f_{P1}(x_1) - f_{P2}(x_1) - k_S l_S - F_{S0}) \\ \Psi_1(C_{h1} x_3 + C_{hS} x_4) + \Psi_2 \end{bmatrix}. \quad (8.58)$$

As in the case of the valve opening in the tank-sided direction, the Jacobian of the system

$$\frac{\partial \Phi}{\partial \mathbf{x}} = \begin{bmatrix} 1 & 0 & 0 & 0 \\ 0 & 1 & 0 & 0 \\ -\frac{k_S - x_3}{m_{PS}} \frac{\partial f_{P1}}{\partial x_1} - \frac{\partial f_{P2}}{\partial x_1} & -\frac{d_{PS}}{m_{PS}} & -\frac{A_{S2} - f_{P1}}{m_{PS}} & \frac{A_{S1}}{m_{PS}} \\ 0 & 0 & \Psi_1 C_{h1} & \Psi_1 C_{hS} \end{bmatrix} \quad (8.59)$$

is regular for all states  $\mathbf{x} \in \mathbb{R}^4$  so that the transformation suggested by (8.58) constitutes a diffeomorphism.

With the transformation derived above, the Byrnes-Isidori normal form follows as

$$\begin{bmatrix} \dot{\xi}_1 \\ \dot{\xi}_2 \\ \dot{\xi}_3 \\ \dot{\eta}_L \end{bmatrix} = \begin{bmatrix} \xi_2 \\ \xi_3 \\ \alpha(\boldsymbol{\xi}, \eta_L) + \beta(\boldsymbol{\xi}, \eta_L) u_R \\ q_L(\boldsymbol{\xi}, \eta_L) \end{bmatrix}, \quad (8.60)$$

$$y = \xi_1. \quad (8.61)$$

**Synthesizing the control law** The control law leading to a linear input output relationship again is

$$u_R = \frac{\nu - \alpha(\boldsymbol{\xi}, \eta_L)}{\beta(\boldsymbol{\xi}, \eta_L)} \quad (8.62)$$

with  $\alpha(\boldsymbol{\xi}, \eta_L)$  given by (8.36) and  $\beta(\boldsymbol{\xi}, \eta_L)$  given by (8.52) accordingly. The new input  $\nu$  is again given by (8.38) as there is no switching behavior for the external variables  $\boldsymbol{\xi}$ .

In order to obtain stable trajectory tracking, the new input  $\nu$  is chosen to be the same as for the tank-sided flow condition, i.e. as in equation (8.38). Since for both flow conditions the external coordinates are the same, choosing  $\nu$  to be identical for tank- and load-sided flow conditions will yield asymptotic tracking in the external coordinates  $\boldsymbol{\xi}$  irrespective of the system's switching behavior.

**Investigating the zero dynamics** The first order internal dynamics again can physically be interpreted as a net fluid flow balance in the system with the main capacitance  $C_{h1}$  now connected with the secondary capacitance  $C_{hS}$ :

$$\dot{\eta}_L = \Psi_1 \left( \hat{q}_P \xi_1 + (A_{S2} - A_{S1}) \xi_2 - \text{sign}(\Psi_3(\boldsymbol{\xi}, \eta_L)) \gamma_F A_{OR1} \sqrt{|\Psi_3(\boldsymbol{\xi}, \eta_L)|} \right) \quad (8.63)$$

with

$$\begin{aligned} \Psi_3(\boldsymbol{\xi}, \eta_L) = & \frac{C_{hS} \left( -d_{PS}\xi_2 + k_S l_S + F_{S0} - k_S(\xi_1 + x_S^{offset}) \right)}{A_{S1}C_{h1} + A_{S2}C_{hS} - C_{hS}f_{P1}(\xi_1 + x_S^{offset})} \\ & + \frac{-m_{PS}\xi_3 + f_{P2}(\xi_1 + x_S^{offset})}{A_{S1}C_{h1} + A_{S2}C_{hS} - C_{hS}f_{P1}(\xi_1 + x_S^{offset})} \\ & + \frac{A_{S1}\eta_L - A_{S1}\Psi_2}{\left( A_{S1}C_{h1} + A_{S2}C_{hS} - C_{hS}f_{P1}(\xi_1 + x_S^{offset}) \right) \Psi_1} - p_C \end{aligned} \quad (8.64)$$

$$= \Psi_{3\xi}(\boldsymbol{\xi}) + \Psi_{3\eta_L}(\boldsymbol{\xi})\eta_L. \quad (8.65)$$

Here, it should be noted that

$$\Psi_{3\eta_L}(\boldsymbol{\xi}) > 0 \quad \forall t, \quad (8.66)$$

since again  $f_{P1}(\xi_1 + x_S^{offset}) \leq 0$ .

Setting  $\boldsymbol{\xi} = \mathbf{0}$  yields the zero dynamics of the system:

$$\dot{\eta}_L(\boldsymbol{\xi} = \mathbf{0}, \eta_L) = -\text{sign}(\eta_L)\Psi_1\gamma_F A_{OR1}\sqrt{|\eta_L|}. \quad (8.67)$$

This representation of the zero dynamics motivated the transformation as suggested in (8.55) – had another transformation been chosen, the resulting internal and corresponding zero dynamics would have yielded a more complicated form with non-zero equilibrium position. With (8.67), from a physical point of view the zero dynamics are very similar to the zero dynamics of the valve opening towards the tank-side, essentially representing a volume flow balance in the main capacitance now connected with the actuator capacitance  $C_{hS}$ . With  $\Psi_1 > 0$ , a nonlinear stability analysis as presented in equation (8.42) et sqq. reveals that the zero dynamics are asymptotically stable.

It is of note that the most obvious alternative coordinate transformation, namely the transformation suggested for the tank-sided flow condition expressed in (8.30), would have led to a representation of the zero dynamics of the kind expressed in equation (7.30), i.e.

$$\begin{aligned} \dot{\eta}_T(\mathbf{0}, \eta_T) = & \frac{1}{C_{h1}} \left( -\text{sign}(\eta_T)\gamma_F A_{OR1}\sqrt{|\eta_T|} \right. \\ & \left. - |u_R(\mathbf{0}, \eta_T)|\text{sign}(x_3(\mathbf{0}, \eta_T) - x_4(\mathbf{0}, \eta_T))\gamma_F b_{Reg}\sqrt{|x_3(\mathbf{0}, \eta_T) - x_4(\mathbf{0}, \eta_T)|} \right), \end{aligned} \quad (8.68)$$

which upon manipulation can be converted into

$$\dot{\eta}_T(\mathbf{0}, \eta_T) = -\text{sign}(\eta_T)\Psi_1\gamma_F A_{OR1}\sqrt{|\eta_T|}. \quad (8.69)$$

Because stability of internal dynamics is a structural property that does not depend on the chosen coordinate transformation, stability is given for (8.68) as well. Then (8.42) can be taken as a common Lyapunov function for both flow conditions whose time derivative is negative along trajectories for both flow conditions, showing the internal dynamics to be asymptotically stable irrespective of the flow condition, see [99] for further background on common Lyapunov functions. This implies that the system with switched internal dynamics is stable.

Interpreting this from a physical perspective, a stable control of output  $y = h(\mathbf{x})$  implies a stably controlled pump as energy source within the system so that the internal dynamics do not have an energy source to draw on for potentially unstable behavior since the pump behavior is prescribed through control. Even though the capacitances  $C_{h1}$  and  $C_{hS}$  provide an interacting set of capacitances potentially allowing for pressure oscillations between each other, pressure oscillations in hydraulic systems are typically related to instabilities of the control valve – because the control valve by assumption is a stably actuated servo valve, no such instabilities are to be expected within this system.

### 8.4.3 Boundedness of Tracking

Applying the control strategy presented in this chapter separates the state variables  $\mathbf{x}$  into observable transformed state variables  $\boldsymbol{\xi}$  and unobservable state variables  $\boldsymbol{\eta} = \{\eta_T, \eta_L\}$ . The latter correspond to internal dynamics and zero dynamics associated with these internal dynamics under the assumptions of the output-zeroing problem. While for the external dynamics asymptotic tracking is achieved by means of nonlinearity compensation and appropriate pole-placement, the boundedness of the full state  $\mathbf{x}$  is a requirement for the control strategy to be feasible. Since the state  $\mathbf{x}$  is obtained from the internal variables  $\boldsymbol{\xi}$  and  $\boldsymbol{\eta}$  through the inverse of  $\Phi(\mathbf{x})$ , once the internal variables lack stability, they possibly become unbounded, thereby rendering the state  $\mathbf{x}$  unbounded. This evidently is a problem because from a certain point onwards, the nonlinearity compensation will become impossible due to physical bounds on the input required to compensate nonlinearities featuring unbounded states. It therefore remains to be shown that the system yields bounded states for the two possible configurations of the control input matrix  $\mathbf{g}_R$ .

In this section, it will be shown that the suggested control approach leads to the desired outcome. The approach relies on a theorem suggested in [40]. Because for input-output linearization (i.e. systems with non-full relative degree) it is not asymptotic stability for the tracking error of *all* transformed states but only boundedness for the full state vector that is required, it follows that if both control systems (tank-sided and load-sided valve opening, i.e.  $u_R \geq 0$  and  $u_R < 0$ ) can be shown to yield bounded tracking, then the system will show bounded tracking as a whole – the non-smoothness of the control input matrix hence is of no relevance for the functionality of the proposed control approach. In [91], an alternative theorem on the boundedness of tracking is proposed that is frequently drawn onto in the extant body of research. It does, however, require global

exponential stability of the zero dynamics – a condition that is not fulfilled here due to only locally exponentially stable zero dynamics. For such cases, theorem 1 due to Isidori [40] (see Appendix A) states sufficient conditions for bounded tracking (see also [97]).

According to this theorem, in order to show that the tracking is bounded in  $\xi, \eta$ , it has to be shown that  $\eta(t)$  is bounded and uniformly asymptotically stable upon excitation through  $\xi_R$  for both flow conditions. The assumption here is that for the external coordinates  $\xi$ , exact tracking is achieved so that  $\xi = \xi_R$  drive the internal dynamics. To show boundedness of the response of  $\eta_T$  and  $\eta_L$  with respect to their excitations by the reference signals theorem 3 from [53] is drawn onto (see Appendix A).

The first part of theorem 3 makes a statement on the conditions of boundedness while the second part provides correlating existence conditions that may in some cases allow calculating the bounds.

To show boundedness of

$$\eta_T = q_T(\xi_R, \eta_T),$$

the Lyapunov candidate

$$V = \frac{1}{2} C_{h1} \eta_T^2 \quad (8.70)$$

is assumed which is radially unbounded and positive definite. It thereby is guaranteed that  $\alpha_1$  and  $\alpha_2$  according to theorem 3 exist.

With  $\xi_R = [\xi_{1R} \ \xi_{2R} \ \xi_{3R}]^T$ , the time derivative of  $V$  will be then manipulated as follows:

$$\dot{V} = \eta_T (\hat{q}_P \xi_{1R} + A_{S2} \xi_{2R}) - |\eta_T| \sqrt{|\eta_T|} \gamma_F A_{OR1} \quad (8.71)$$

$$\leq |\eta_T| \underbrace{\sqrt{\xi_{1R}^2 + \xi_{2R}^2} \sqrt{(\hat{q}_P)^2 + (A_{S2})^2}}_{=: f_T(t)} - |\eta_T| \sqrt{|\eta_T|} \gamma_F A_{OR1} \quad (8.72)$$

$$= |\eta_T| f_T(t) - (1 - \theta) |\eta_T| \sqrt{|\eta_T|} \gamma_F A_{OR1} - \theta |\eta_T| \sqrt{|\eta_T|} \gamma_F A_{OR1} \quad (8.73)$$

$$\leq |\eta_T| K_{f_T} - (1 - \theta) |\eta_T| \sqrt{|\eta_T|} \gamma_F A_{OR1} - \theta |\eta_T| \sqrt{|\eta_T|} \gamma_F A_{OR1} \quad (8.74)$$

with  $K_{f_T}$  representing the upper bound on  $f_T$  resulting from bounded  $\xi_{1R}$  and  $\xi_{2R}$  and  $0 \leq \theta \leq 1$ . Hence,

$$\dot{V} \leq -(1 - \theta) |\eta_T| \sqrt{|\eta_T|} \gamma_F A_{OR1}, \quad \forall \sqrt{|\eta_T|} \geq \frac{K_{f_T}}{\theta} \frac{1}{\gamma_F A_{OR1}}. \quad (8.75)$$

Thus, for bounded reference signals  $\xi_{1R}$  and  $\xi_{2R}$  it follows that  $\eta_T$  is bounded.

The same approach can be used to show boundedness of  $\eta_L$  subject to excitation through the reference signal  $\xi_R$ .

With (8.58) and (8.63), the dynamics of  $\eta_L$  have the representation

$$\begin{aligned} \dot{\eta}_L = & \overbrace{\Psi_1 (\hat{q}_P \xi_{1R} + (A_{S2} - A_{S1}) \xi_{2R})}^{=: f(t)} \\ & - \gamma_F A_{OR1} \Psi_1 \text{sign}(\Psi_{3\xi}(t) + \Psi_{3\eta_L}(t) \eta_L) \sqrt{|\Psi_{3\xi}(t) + \Psi_{3\eta_L}(t) \eta_L|}. \end{aligned} \quad (8.76)$$

Now, with  $\Psi_{3\xi}(t) + \Psi_{3\eta_L}(t) \eta_L = \Psi_{3\eta_L}(t) \left( \frac{\Psi_{3\xi}(t)}{\Psi_{3\eta_L}(t)} + \eta_L \right)$  introducing a new coordinate  $\zeta$  is sensible:

$$\zeta = \frac{\overbrace{\Psi_{3\xi}(t)}^{=: \Psi_4(t)}}{\Psi_{3\eta_L}(t)} + \eta_L, \quad (8.77)$$

$$\dot{\zeta} = \dot{\Psi}_4(t) + \dot{\eta}_L. \quad (8.78)$$

This allows writing

$$\dot{\zeta} = f(t) + \dot{\Psi}_4(t) - \gamma_F A_{OR1} \Psi_1 \text{sign}(\Psi_{3\eta_L} \zeta) \sqrt{|\Psi_{3\eta_L} \zeta|} \quad (8.79)$$

and choosing the Lyapunov function candidate

$$V = \frac{1}{2} \zeta^2. \quad (8.80)$$

With (8.66), the Lyapunov function's time derivative then is

$$\dot{V} = \zeta \dot{\zeta} \quad (8.81)$$

$$= \zeta \left( f(t) + \dot{\Psi}_4(t) \right) - \frac{1}{\Psi_{3\eta_L}(t)} \text{sign}(\Psi_{3\eta_L}(t) \zeta) \sqrt{|\Psi_{3\eta_L}(t) \zeta|} (\Psi_{3\eta_L}(t) \zeta) \quad (8.82)$$

$$= \zeta \left( f(t) + \dot{\Psi}_4(t) \right) - \frac{1}{\Psi_{3\eta_L}(t)} |\Psi_{3\eta_L}(t) \zeta| \sqrt{|\Psi_{3\eta_L}(t) \zeta|} \quad (8.83)$$

$$\leq |\zeta| \left( |f(t)| + |\dot{\Psi}_4(t)| \right) - \frac{1}{\Psi_{3\eta_L}(t)} |\Psi_{3\eta_L}(t) \zeta| \sqrt{|\Psi_{3\eta_L}(t) \zeta|} \quad (8.84)$$

$$\leq |\zeta| \left( |K_f| + |K_{\dot{\Psi}_4}| \right) - \frac{1}{\Psi_{3\eta_L}(t)} |\Psi_{3\eta_L}(t) \zeta| \sqrt{|\Psi_{3\eta_L}(t) \zeta|} \quad (8.85)$$

$$\leq |\zeta| \left( |K_f| + |K_{\dot{\Psi}_4}| \right) - \frac{1}{K_{\Psi_{3\eta_L}}} |L_{\Psi_{3\eta_L}} \zeta| \sqrt{|L_{\Psi_{3\eta_L}} \zeta|} \quad (8.86)$$

$$= |\zeta| \left( |K_f| + |K_{\dot{\Psi}_4}| \right) - (1 - \theta) \frac{1}{K_{\Psi_{3\eta_L}}} |L_{\Psi_{3\eta_L}} \zeta| \sqrt{|L_{\Psi_{3\eta_L}} \zeta|} - \theta \frac{1}{K_{\Psi_{3\eta_L}}} |L_{\Psi_{3\eta_L}} \zeta| \sqrt{|L_{\Psi_{3\eta_L}} \zeta|}. \quad (8.87)$$

In the above derivations,  $K_f$ ,  $K_{\dot{\Psi}_4}$ ,  $K_{\Psi_{3\eta_L}}$  are the upper bounds on  $f(t)$ ,  $\dot{\Psi}_4(t)$  and  $\Psi_{3\eta_L}$ , respectively and  $L_{\Psi_{3\eta_L}}$  is the lower bound on  $\Psi_{3\eta_L}$ . The necessity of these functions to be bounded may impose restrictions on the choice of  $\xi_R$ . Ultimately, it follows that

$$\dot{V} \leq -(1 - \theta) \frac{1}{K_{\Psi_{3\eta_L}}} |L_{\Psi_{3\eta_L}} \zeta| \sqrt{|L_{\Psi_{3\eta_L}} \zeta|} \quad \forall \sqrt{|\zeta|} > \frac{K_{\Psi_{3\eta_L}} \left( |K_f| + |K_{\dot{\Psi}_4}| \right)}{\theta |L_{\Psi_{3\eta_L}}| \sqrt{|L_{\Psi_{3\eta_L}}|}}. \quad (8.88)$$

so that solutions for  $\zeta$  are bounded by the boundedness of the reference trajectories  $\xi_R$ ,  $\dot{\Psi}_4$ ,  $f(t)$  and  $\Psi_{3\eta_L}$ . Now, because  $\zeta$  is bounded, so is  $\eta_L$ .

In order to show uniform asymptotic stability, the dynamics of the difference between the actual trajectory  $\eta_T$  and the reference trajectory  $\eta_R = \eta_{TR}$  for the tank-sided internal dynamics  $\eta_T$  arising from perfect tracking of  $\xi_R$

$$\Delta\eta_T = \eta_T - \eta_{TR} \quad (8.89)$$

is considered locally through linearization about  $\eta_{TR}$ . The implication then is that disturbances imposed on the initial conditions in  $\eta_T$  or along the tracked trajectory are restricted in their magnitude in a way that a linearized system description remains feasible. For the tank-sided operating condition, the error dynamics from (8.89) read

$$\Delta\dot{\eta}_T = -\frac{\gamma_F A_{OR1}}{C_{h1}} \frac{1}{2\sqrt{|\eta_{TR}|}} \Delta\eta_T, \quad (8.90)$$

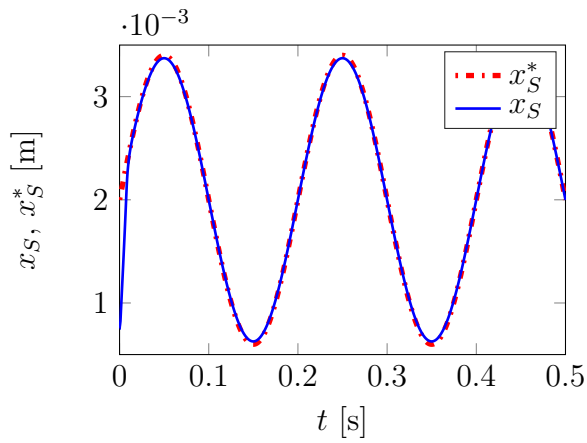
which are uniformly asymptotically stable for all times  $t \geq t_0$  according to theorem 2 (see Appendix A) by the boundedness for  $\eta_T$  (and  $\eta_{TR}$  as well) as shown above: with a Lyapunov candidate as in equation (8.70), it holds that

$$\dot{V} = -\gamma_F A_{OR1} \frac{1}{2\sqrt{|\eta_{TR}|}} \Delta\eta_T^2 \leq -\gamma_F A_{OR1} \frac{1}{2\sqrt{|K_{\eta_{TR}}|}} \Delta\eta_T^2, \quad (8.91)$$

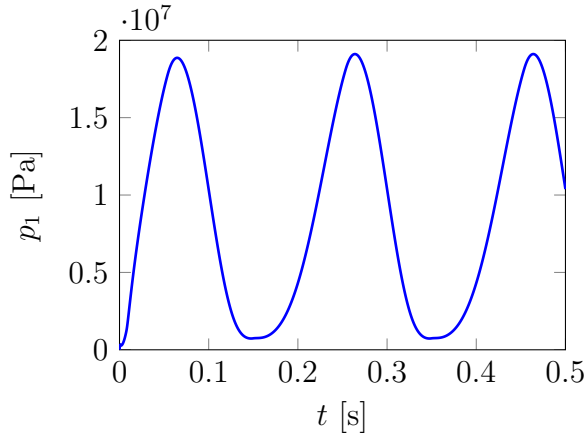
where  $K_{\eta_{TR}}$  is the bound on the tank-sided reference trajectory for  $\eta_T$  so that the internal dynamics are uniformly asymptotically stable. Considering the load-sided operating condition, the same approach can be applied accordingly, yielding the same result so that bounded tracking with uniformly asymptotically stable internal dynamics is ensured for both operating conditions from which bounded tracking follows for the system as a whole. Thus, because solutions for  $\eta_R$  are bounded and at least locally uniformly asymptotically stable, the control law devised by equations (8.36), (8.37) and (8.62) yields asymptotic output tracking with bounded states irrespective of the operating condition. Ultimately, the system as a whole can stably be controlled for trajectory tracking.

#### 8.4.4 Simulation Results

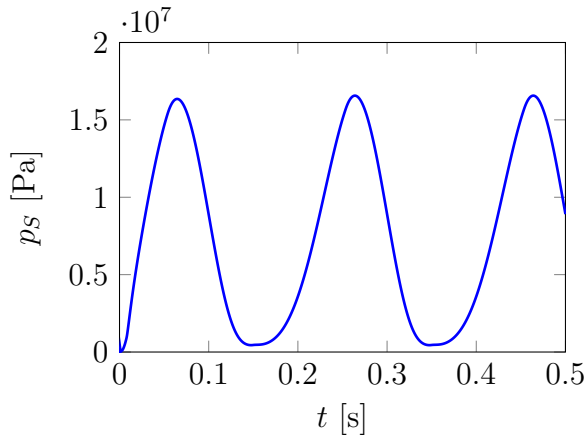
The simulation results in Figures 8.3 and 8.4 clearly show a high tracking performance for the pump eccentricity and thereby for volume flow control. Overshoots are marginal and subject to linear feedback design with valve dynamics showing a small effect on tracking behavior mainly in a transient phase. The simulation results thereby clearly indicate positive behavior of the input-output linearization.



(a) Pump displacement.

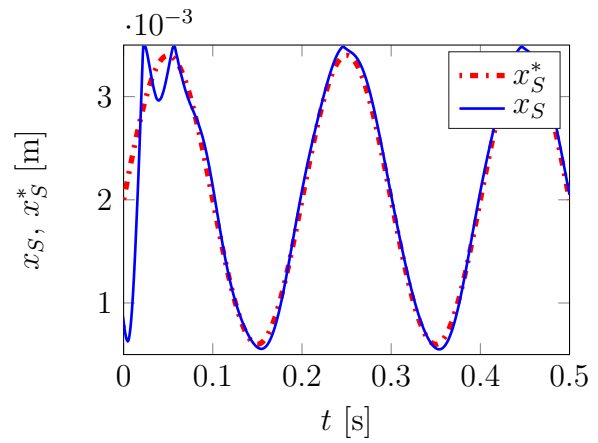


(b) Main chamber pressure.

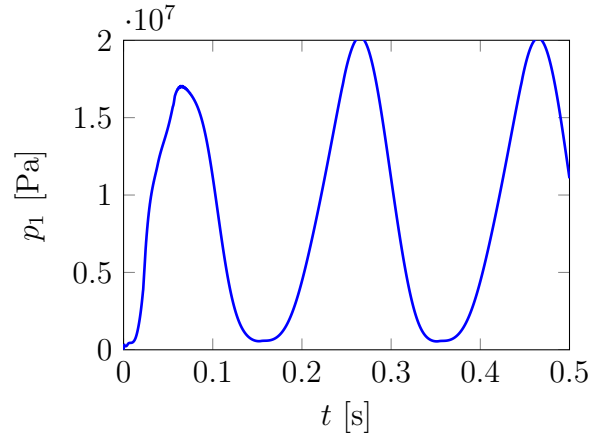


(c) Actuation chamber pressure.

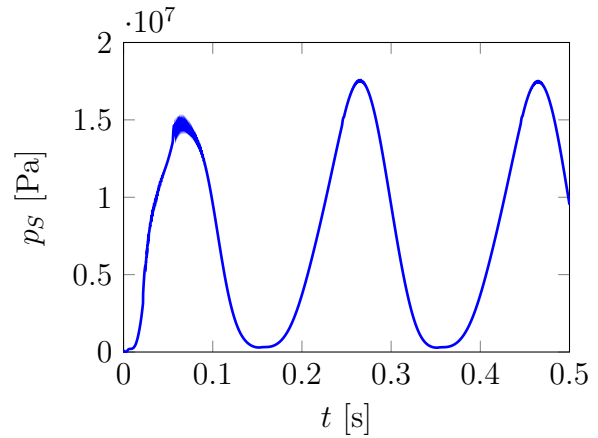
Figure 8.3: Without valve dynamics.



(a) Pump displacement.



(b) Main chamber pressure.



(c) Actuation chamber pressure.

Figure 8.4: With valve dynamics.

## 8.5 Adaptive Feedback-Linearizing Control

A remark on adaptive control techniques is in order. Up to this point, it was assumed that all system parameters are fully known. From a practical viewpoint, this assumption may not hold up well for system damping which may be subject to changes over operating time. It may therefore be asked if a control law adaption to damping is possible.

Another parameter varying over the life time of a valve is flow coefficient  $\gamma_F$  which – as is common in the extant body of research – in this thesis is generally assumed identical for all control edges. Relaxing this assumption and allowing for variations in  $\gamma_F$  over time, this should be done for each control edge separately as pressure differences across control edges typically are not identical so that effects of wear and soiling will differ among separate control edges. For parameter adaption, this entails switching parameters for which adaption is then sought. Because the scope of the methods drawn onto in this section does not allow for such a structural switching, only variations in damping  $d_{PS}$  will be considered.

However, even the problem of controlling linear systems with adaption algorithms is a complex task as by multiplicative parameter state coupling the corresponding system equations become nonlinear. Controlling nonlinear systems adaptively is a task of significant difficulty to which no generally applicable systematic solution has yet been found.

In general, two directions can be distinguished in classical adaptive control – indirect and direct adaptive control.

- Indirect adaptive control: here, one designs a control law (depending on unknown parameters) and then designs a method to update the parameters appropriately. Intuition then suggests that parameter estimates converging to the true parameter values will result in a control law asymptotically linearizing the input output behavior of the system. It should be emphasized that this is a heuristic approach – commonly referred to as certainty equivalence principle, see e.g. [110]. Indirect adaptive control approaches employ an observation error to update the plants instead of using an output error. Works in this field are [110] and references cited therein.
- Direct adaptive control: the parameter update law does not have to be such that parameters converge to their true values in order to achieve the desired control purpose. Prominent works in this field are [44, 93, 109]. For further reference and a discussion of different relevant approaches, see [110].

All the work available in feedback-linearization based adaptive control theory currently makes certain assumptions about the plant that the system at hand offends in at least one assumption. A standard assumption is linearity in the unknown parameters. Existing control schemes then impose either uncertainty constraints on the unknown parameters or restrictions on the nonlinearities in the scheme. Nonlinearity restrictions

typically are global Lipschitz properties. These are offended by the square root functions in the volume flow laws across orifices – while the underlying adaptive control may possibly converge nevertheless, [96] show that divergence can easily occur if the requirements for the control laws are offended. While for the square root functions a regularization scheme might be conceived to remedy this lack of Lipschitz continuity, higher order nonlinear models for the pump may possibly lead to a violation of the requirements.

In contrast, uncertainty constraining schemes impose geometric/structural conditions on the appearance of the unknown parameters in the systems. These constraints are commonly expressed in so-called matching conditions, amongst which exact and extended matching conditions can be distinguished. While exact matching conditions are met only by a small class of systems, the extended matching condition introduced in [44] for full-state feedback linearizable systems is somewhat less restrictive. It allows, for example, for the successful implementation of a MIMO adaptive control scheme for induction motor systems with non-full relative degree, as shown in [72]. Systems that do not fulfill a matching condition for the uncertainty will entail so-called over-parameterization in the adaptive control laws in order to account for higher order derivatives of the unknown parameter. This commonly complicates the control design which is why in general, designs based on matching conditions are preferable.

Among the available methods, only the approach outlined in [72] making use of an extended matching condition is applicable to the problem at hand. Here, too, the assumption is linearity in the unknown parameters which are assumed to be constant within the derivation of the adaptive control law but may actually vary with time. If the SISO system with  $p$  unknown parameters  $\boldsymbol{\theta} = [\theta_1, \dots, \theta_p]$  has the representation

$$\dot{\mathbf{x}} = \tilde{\mathbf{f}}_d(\mathbf{x}, \boldsymbol{\theta}) + \mathbf{g}(\mathbf{x}, \boldsymbol{\theta})u \quad (8.92)$$

$$= \mathbf{f}_d(\mathbf{x}) + \mathbf{g}_0(\mathbf{x})u + \sum_{i=1}^l \theta_i \mathbf{f}_i(\mathbf{x}) + \sum_{i=l+1}^p \theta_i \mathbf{g}_i(\mathbf{x})u \quad (8.93)$$

with  $\mathbf{f}_d$  representing the nominal drift term of the system and  $\mathbf{f}_i, \mathbf{g}_i$  representing the entry matrices of the  $i$ -th uncertain parameter in the drift and in the control input, respectively, then the exact matching condition for a fully state-feedback linearizable system reads [55]

$$\mathbf{f}_i, \mathbf{g}_j \in \text{span}\{\mathbf{g}_0\} \quad i = 1 \dots l, j = l + 1 \dots p, \quad (8.94)$$

while the extended matching condition is given by

$$\mathbf{f}_i \in \text{span}\{\mathbf{g}_0, \text{ad}_{\mathbf{f}_d} \mathbf{g}_0\} \quad i = 1 \dots l, \quad (8.95)$$

$$\mathbf{g}_j \in \text{span}\{\mathbf{g}_0\} \quad j = l + 1 \dots p \quad (8.96)$$

with  $\text{ad}_{\mathbf{f}_d} \mathbf{g}_0 = [\mathbf{f}_d, \mathbf{g}_0]$  representing the Lie bracket of  $\mathbf{f}_d$  and  $\mathbf{g}_0$  which is defined by

$$[\mathbf{f}_d, \mathbf{g}_0](\mathbf{x}) = \frac{\partial \mathbf{g}_0(\mathbf{x})}{\partial \mathbf{x}} \mathbf{f}_d(\mathbf{x}) - \frac{\partial \mathbf{f}_d(\mathbf{x})}{\partial \mathbf{x}} \mathbf{g}_0(\mathbf{x}). \quad (8.97)$$

The intuitive meaning of the matching condition is that the unknown parameters are at most “one integrator away” from the system inputs which can then counteract the parameter uncertainty, see also [28]. As a consequence of this condition, only first order derivatives of the unknown parameters will appear in the control designs which can be subjected to appropriate update laws.

In the majority of adaptive feedback designs and in the present context, too, Barbalat’s lemma (see Lemma 1 in Appendix) is of paramount importance.

From the lemma it follows that in case  $g \in \mathcal{L}_2$  and  $\frac{dg}{dt}$  is bounded,

$$\lim_{t \rightarrow \infty} g(t) = 0, \quad (8.98)$$

see e.g. [3, 92]. To show error convergence and parameter convergence, the lemma is typically invoked in the form of a deductive argument, as is here. From the boundedness of an error signal  $e$  and its time derivative  $\dot{e}$  it follows that

$$\lim_{t \rightarrow \infty} |e(t)| = 0 \quad (8.99)$$

so that asymptotic trajectory tracking is achieved.

Introducing unknown deviations from nominal damping  $d_{PS}$  in (8.18), (8.51) as parameter  $p$  to be adapted, the system description is

$$\dot{\mathbf{x}} = \mathbf{f}_d(\mathbf{x}) + p\mathbf{f}_1(\mathbf{x}) + \mathbf{g}_R(\mathbf{x})u_R. \quad (8.100)$$

The matrix through which  $p$  enters the system dynamics is

$$\mathbf{f}_1(\mathbf{x}) = \begin{bmatrix} 0 \\ -\frac{x_2}{m_{PS}} \\ 0 \\ 0 \end{bmatrix}. \quad (8.101)$$

Now the following transformation based on  $h(\mathbf{x}) = x_1 - x_S^{offset}$  and the *nominal* system ( $p = 0$ ) is defined:

$$y_1 = h(\mathbf{x}) = \Phi_1, \quad (8.102)$$

$$y_2 = \mathcal{L}_{\mathbf{f}_d} h(\mathbf{x}) = \Phi_2, \quad (8.103)$$

$$y_3 = \mathcal{L}_{\mathbf{f}_d}^2 h(\mathbf{x}) = \Phi_3, \quad (8.104)$$

$$y_4 = \Phi_4. \quad (8.105)$$

Here,  $\Phi_4$  represents the coordinate transformation for the internal dynamics of the system as in the case for ordinary, non-adaptive input-output-linearization.

Transforming the *nominal* system with the *nominal* transformation to Byrnes-Isidori normal form yields, as was already shown in section 8.4,

$$\dot{y}_1 = y_2, \quad (8.106)$$

$$\dot{y}_2 = y_3, \quad (8.107)$$

$$\dot{y}_3 = \mathcal{L}_{f_d}^3 \Phi_1 + \mathcal{L}_{g_R} \mathcal{L}_{f_d}^2 \Phi_1 u_R, \quad (8.108)$$

$$\dot{y}_4 = \mathcal{L}_{f_d} \Phi_4. \quad (8.109)$$

Now, the *nominal* transformation is applied to the *perturbed* system featuring the unknown parameter  $p \neq 0$ : That is, the perturbed system (8.100) is transformed with the coordinate transformation of the nominal system (8.102)-(8.105). Interpreting this step from another perspective, the transformed coordinates of the *nominal* system are derived along the trajectories of the *perturbed* system. With

$$(\dot{\cdot}) = \left[ \mathcal{L}_{f_d} + p\mathcal{L}_{f_1} + u_R \mathcal{L}_{g_R} \right] (\cdot) \quad (8.110)$$

one gets

$$\begin{aligned} \dot{y}_1 &= \left[ \mathcal{L}_{f_d} + p\mathcal{L}_{f_1} + u_R \mathcal{L}_{g_R} \right] \Phi_1 \\ &= \mathcal{L}_{f_d} \Phi_1 = x_2 = y_2, \end{aligned} \quad (8.111)$$

$$\begin{aligned} \dot{y}_2 &= \left[ \mathcal{L}_{f_d} + p\mathcal{L}_{f_1} + u_R \mathcal{L}_{g_R} \right] \mathcal{L}_{f_d} \Phi_1 \\ &= \mathcal{L}_{f_d}^2 \Phi_1 + p \mathcal{L}_{f_1} \mathcal{L}_{f_d} \Phi_1 \\ &= y_3 + p \mathcal{L}_{f_1} \mathcal{L}_{f_d} \Phi_1, \end{aligned} \quad (8.112)$$

$$\begin{aligned} \dot{y}_3 &= \left[ \mathcal{L}_{f_d} + p\mathcal{L}_{f_1} + u_R \mathcal{L}_{g_R} \right] \mathcal{L}_{f_d}^2 \Phi_1 \\ &= \mathcal{L}_{f_d}^3 \Phi_1 + p \mathcal{L}_{f_1} \mathcal{L}_{f_d}^2 \Phi_1 + u_R \mathcal{L}_{g_R} \mathcal{L}_{f_d}^2 \Phi_1, \end{aligned} \quad (8.113)$$

$$\begin{aligned} \dot{y}_4 &= \left[ \mathcal{L}_{f_d} + p\mathcal{L}_{f_1} + u_R \mathcal{L}_{g_R} \right] \Phi_4 \\ &= \mathcal{L}_{f_d} \Phi_4. \end{aligned} \quad (8.114)$$

From this, it can be seen that *ideally*, with perfect knowledge of  $p$ , the transformation for the perturbed system that depends on an estimate of parameter  $p$  should be

$$z_1 = y_1, \quad (8.115)$$

$$z_2 = y_2, \quad (8.116)$$

$$z_3 = y_3 + p \mathcal{L}_{f_1} \mathcal{L}_{f_d} \Phi_1, \quad (8.117)$$

$$z_4 = y_4. \quad (8.118)$$

If  $p = p(t)$  were known exactly, equations (8.115)–(8.118) would be identical with the transformations discussed in section 8.4. Since only an estimate  $\hat{p}$  is available for  $p$ , the following will be taken

$$z_3 = y_3 + \hat{p} \mathcal{L}_{f_1} \mathcal{L}_{f_d} \Phi_1. \quad (8.119)$$

Introducing the parameter estimate error  $e_p = p - \hat{p}$ , the system in  $z$ -coordinates based on the estimate  $\hat{p}$  reads

$$\dot{z}_1 = \dot{y}_1 = y_2 = z_2, \quad (8.120)$$

$$\begin{aligned}
 \dot{z}_2 = \dot{y}_2 &= [\mathcal{L}_{f_d} + p\mathcal{L}_{f_1} + u_R\mathcal{L}_{g_R}] \mathcal{L}_{f_d} \Phi_1 \\
 &= y_3 + p\mathcal{L}_{f_1} \mathcal{L}_{f_d} \Phi_1 \\
 &= y_3 + \hat{p}\mathcal{L}_{f_1} \mathcal{L}_{f_d} \Phi_1 + e_p \mathcal{L}_{f_1} \mathcal{L}_{f_d} \Phi_1 \\
 &= z_3 + e_p \mathcal{L}_{f_1} \mathcal{L}_{f_d} \Phi_1,
 \end{aligned} \tag{8.121}$$

$$\begin{aligned}
 \dot{z}_3 = \dot{y}_3 + \frac{d}{dt}(\hat{p}\mathcal{L}_{f_1} \mathcal{L}_{f_d} \Phi_1) \\
 &= [\mathcal{L}_{f_d} + p\mathcal{L}_{f_1} + u_R\mathcal{L}_{g_R}] \mathcal{L}_{f_d}^2 \Phi_1 + \hat{p} [\mathcal{L}_{f_d} + p\mathcal{L}_{f_1} + u_R\mathcal{L}_{g_R}] \mathcal{L}_{f_1} \mathcal{L}_{f_d} \Phi_1 \\
 &\quad + \dot{\hat{p}} \mathcal{L}_{f_1} \mathcal{L}_{f_d} \Phi_1
 \end{aligned} \tag{8.122}$$

$$\begin{aligned}
 &= \mathcal{L}_{f_d}^3 \Phi_1 + p\mathcal{L}_{f_1} \mathcal{L}_{f_d}^2 \Phi_1 + u_R \mathcal{L}_{g_R} \mathcal{L}_{f_d}^2 \Phi_1 + \hat{p} \mathcal{L}_{f_d} \mathcal{L}_{f_1} \mathcal{L}_{f_d} \Phi_1 \\
 &\quad + \hat{p} p \mathcal{L}_{f_1}^2 \mathcal{L}_{f_d} \Phi_1 + \dot{\hat{p}} \mathcal{L}_{f_1} \mathcal{L}_{f_d} \Phi_1,
 \end{aligned} \tag{8.123}$$

$$\dot{z}_4 = \dot{y}_4 = \mathcal{L}_{f_d} \Phi_4. \tag{8.124}$$

Now the nonlinearity compensating feedback-law based on the parameter estimate  $\hat{p}$  is derived from (8.122) as

$$\begin{aligned}
 u = \frac{1}{\mathcal{L}_{g_R} \mathcal{L}_{f_d}^2 \Phi_1} \left[ -\mathcal{L}_{f_d}^3 \Phi_1 - \hat{p} \mathcal{L}_{f_1} \mathcal{L}_{f_d}^2 \Phi_1 - \hat{p} \mathcal{L}_{f_d} \mathcal{L}_{f_1} \mathcal{L}_{f_d} \Phi_1 \right. \\
 \left. - \hat{p}^2 \mathcal{L}_{f_1}^2 \mathcal{L}_{f_d} \Phi_1 - \dot{\hat{p}} \mathcal{L}_{f_1} \mathcal{L}_{f_d} \Phi_1 + \nu \right]
 \end{aligned} \tag{8.125}$$

with the new input  $\nu$  chosen to be

$$\begin{aligned}
 \nu &= -k_1(z_1 - \xi_1^*) - k_2(z_2 - \xi_2^*) - k_3(z_3 - \xi_3^*) + \dot{\xi}_3^* \\
 &= k_1 e_1 + k_2 e_2 + k_3 e_3 + \dot{\xi}_3^*.
 \end{aligned} \tag{8.126}$$

For  $z_3$ , it then follows with the above control law

$$\begin{aligned}
 \dot{z}_3 &= (p - \hat{p}) \mathcal{L}_{f_1} \mathcal{L}_{f_d}^2 \Phi_1 + \hat{p}(p - \hat{p}) \mathcal{L}_{f_1}^2 \mathcal{L}_{f_d} \Phi_1 + k_1 e_1 + k_2 e_2 + k_3 e_3 + \dot{\xi}_3^* \\
 &= e_p \mathcal{L}_{f_1} \mathcal{L}_{f_d}^2 \Phi_1 + \hat{p} e_p \mathcal{L}_{f_1}^2 \mathcal{L}_{f_d} \Phi_1 + k_1 e_1 + k_2 e_2 + k_3 e_3 + \dot{\xi}_3^*.
 \end{aligned} \tag{8.127}$$

From this, the following error system is obtained:

$$\begin{aligned}
 \dot{\mathbf{e}} &= \begin{bmatrix} 0 & 1 & 0 \\ 0 & 0 & 1 \\ -k_1 & -k_2 & -k_3 \end{bmatrix} \mathbf{e} + \begin{bmatrix} 0 \\ \mathcal{L}_{f_1} \mathcal{L}_{f_d} \Phi_1 \\ \mathcal{L}_{f_1} \mathcal{L}_{f_d}^2 \Phi_1 + \hat{p} \mathcal{L}_{f_1}^2 \mathcal{L}_{f_d} \Phi_1 \end{bmatrix} e_p \\
 &= \mathbf{K} \mathbf{e} + \mathbf{W}(\mathbf{z}, \hat{p}) e_p.
 \end{aligned} \tag{8.128}$$

where  $\mathbf{W}(\mathbf{z}, \hat{p})$  is referred to as regressor. From this representation, a suitable parameter update law for the dynamics of  $\hat{p}$  can be deduced and the standard argument for parameter convergence in this context can be made.

To do so, it is assumed that  $\mathbf{P}$  is the positive definite, symmetric, solution to the Lyapunov equation

$$\mathbf{K}^T \mathbf{P} + \mathbf{P} \mathbf{K} = -\mathbf{Q} \tag{8.129}$$

with  $\mathbf{Q}$  positive definite.

Then the following Lyapunov-function candidate with  $\Gamma > 0$  is chosen:

$$V = \mathbf{e}^T \mathbf{P} \mathbf{e} + \Gamma e_p^2. \quad (8.130)$$

Its time derivative follows as

$$\dot{V} = \mathbf{e}^T \left( \mathbf{K}^T \mathbf{P} + \mathbf{P} \mathbf{K} \right) \mathbf{e} + 2e_p \mathbf{W}^T \mathbf{P} \mathbf{e} + 2\Gamma e_p \dot{e}_p. \quad (8.131)$$

To render  $\dot{V}$  at least negative semidefinite the parameter error update law

$$\dot{e}_p = -\frac{1}{\Gamma} \mathbf{W}^T \mathbf{P} \mathbf{e} \quad (8.132)$$

is chosen from which the parameter update law

$$\dot{\hat{p}} = -\frac{1}{\Gamma} \mathbf{W}^T \mathbf{P} \mathbf{e} \quad (8.133)$$

follows immediately since  $p$  is assumed constant.

With this choice of the parameter update law,

$$\dot{V} = -\mathbf{e}^T \mathbf{Q} \mathbf{e}. \quad (8.134)$$

Since  $\dot{V}$  is negative semidefinite, the trajectory error  $\mathbf{e}$  and the parameter error  $e_p$  are bounded. It also follows from this that  $\mathbf{e}$  is an  $\mathcal{L}_2$  signal, see [72]. Because  $e_p$  is bounded, so is  $\hat{p}$ . For a large class of tracking signals, the state  $\mathbf{z}$  then is bounded, too, due to the Hurwitz design of the trajectory error feedback with appropriately chosen  $k_1, k_2, k_3$ . Performing the respective calculations for the components of the regressor,

$$\mathcal{L}_{f_1} \mathcal{L}_{f_d} \Phi_1 = -\frac{1}{m_{PS}} z_2, \quad (8.135)$$

$$\mathcal{L}_{f_1} \mathcal{L}_{f_d}^2 \Phi_1 = -\frac{d_{PS}}{m_{PS}} z_2, \quad (8.136)$$

$$\mathcal{L}_{f_1}^2 \mathcal{L}_{f_d} \Phi_1 = \frac{1}{m_{PS}^2} z_2, \quad (8.137)$$

it can be seen that the regressor components are bounded by the boundedness of  $z_2$ . As in [72], it thus follows that  $\dot{\mathbf{e}}$  is bounded, too. Now with  $\mathbf{e}$  being a bounded signal with bounded derivative  $\dot{\mathbf{e}}$ , it follows from Barbalat's lemma that

$$\lim_{t \rightarrow \infty} \|\mathbf{e}(t)\| = 0 \quad (8.138)$$

so that asymptotic trajectory tracking based on the suggested control approach can be achieved.

In simulations, however, it is seen that the parameter  $d_{PS}$  has negligible impact on tracking quality. The input-output-linearization approach from section 8.4 is sufficiently robust with respect to even large variations in  $d_{PS}$  so that complicating the control law by inclusion of the parameter adaptive law (8.125) with (8.133) may not be required and unnecessarily complicate the control implementation.

## 8.6 Nonlinear Observer Design

While state space methods allow for control strategies in some cases superior to frequency space methods, they pose the problem of how to obtain knowledge of the system states. As measuring the states of a system comprehensively is not generally feasible, it is purposeful to design an observer to fulfill the task of estimating the respective system states. Even though observer theory is well developed for linear systems, results for nonlinear systems have remained particular to certain types of problems. In the following two sections, two such nonlinear observers – a high gain observer and a nonlinear local observer – shall be discussed with respect to their applicability to the problem of controlling the variable displacement pump system.

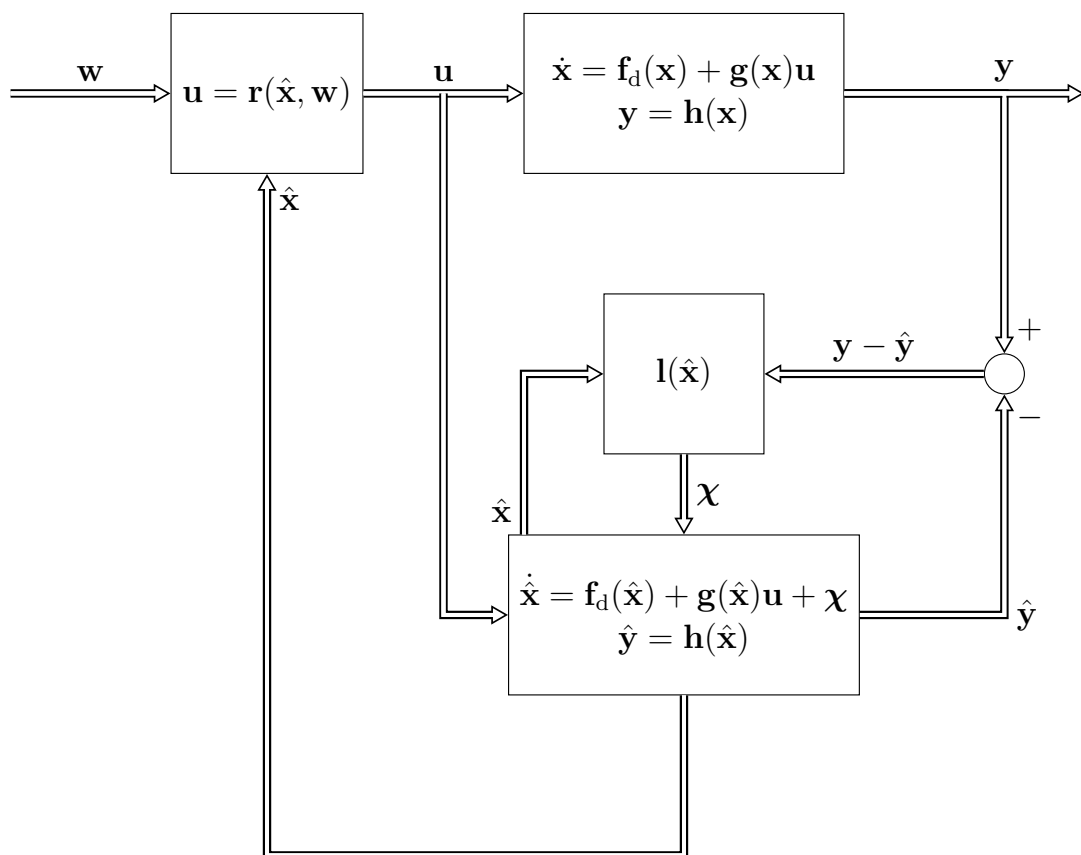


Figure 8.5: General structure for the nonlinear observers as treated in this chapter.

### 8.6.1 High Gain Observer

With the task of designing a nonlinear observer being comparatively straightforward for a nonlinear system with full relative degree (see e.g. [1]), a non-full relative degree system requires additional considerations due to the internal dynamics of the system.

Understanding the problem of observer design as a dual to the problem of nonlinear control, [42] approach the problem from a control based perspective. Their contribution has experienced several extensions, amongst which [85, 86] should be named for their relevance in the context treated here.

Under the assumption of a well-defined relative degree  $r$ , the generic SISO system

$$\dot{\mathbf{x}} = \mathbf{f}_d(\mathbf{x}) + \mathbf{g}(\mathbf{x})u, \quad (8.139)$$

$$y = h(\mathbf{x}) \quad (8.140)$$

can be transformed into either Byrnes-Isidori normal form or into a non-Byrnes-Isidori form as outlined in section 7.1:

$$\begin{bmatrix} \dot{\boldsymbol{\xi}} \\ \dot{\boldsymbol{\eta}} \end{bmatrix} = \mathbf{f}_{d\Phi}(\boldsymbol{\xi}, \boldsymbol{\eta}) + \mathbf{g}_{\Phi}(\boldsymbol{\xi}, \boldsymbol{\eta})u$$

or, equivalently,

$$\dot{\boldsymbol{\xi}} = \mathbf{A}\boldsymbol{\xi} + \mathbf{b}(\alpha(\boldsymbol{\xi}, \boldsymbol{\eta}) + \beta(\boldsymbol{\xi}, \boldsymbol{\eta})u), \quad y = \mathbf{c}^T \boldsymbol{\xi}, \quad (8.141)$$

$$\dot{\boldsymbol{\eta}} = \mathbf{q}(\boldsymbol{\xi}, \boldsymbol{\eta}) + \mathbf{p}(\boldsymbol{\xi}, \boldsymbol{\eta})u. \quad (8.142)$$

The above form implies that for the observer design, the transformation does not necessarily need to be the Byrnes-Isidori transformation as  $\mathbf{p}(\boldsymbol{\xi}, \boldsymbol{\eta}) \neq 0$  in (8.142). In equation (8.141),

$$\mathbf{A} = \begin{bmatrix} 0 & 1 & \dots & 0 \\ 0 & 0 & \ddots & 0 \\ \vdots & & \ddots & 1 \\ 0 & 0 & \dots & 0 \end{bmatrix}, \quad \mathbf{b} = \begin{bmatrix} 0 \\ \vdots \\ 0 \\ 1 \end{bmatrix}, \quad \mathbf{c} = \begin{bmatrix} 1 \\ 0 \\ \vdots \\ 0 \end{bmatrix}. \quad (8.143)$$

The triple  $\mathbf{A}, \mathbf{b}, \mathbf{c}$  associated with the external dynamics  $\boldsymbol{\xi}$  is in so-called Brunovsky-form. If an observer is to be constructed for a system that can be brought into the form of (8.141) and (8.142) the question of observability first has to be answered.

In the case of the external dynamics, observability is granted in any case, since all coordinates  $\xi_1, \dots, \xi_r$  are related by repeated differentiation with respect to time. Hence, if the system output is known, all these states can be reconstructed accordingly. By definition, the states  $\eta_1, \dots, \eta_{n-r}$  are unobservable from the system output for the control laws discussed here as the system output is not affected by these states. However, the high-gain observer suggested in [42] and extended in [85, 86] is of the form

$$\dot{\hat{\boldsymbol{\xi}}} = \mathbf{A}\hat{\boldsymbol{\xi}} + \mathbf{b} \left( \alpha(\hat{\boldsymbol{\xi}}, \hat{\boldsymbol{\eta}}) + \beta(\hat{\boldsymbol{\xi}}, \hat{\boldsymbol{\eta}})u \right) + \mathbf{k}(y - \mathbf{c}^T \hat{\boldsymbol{\xi}}), \quad (8.144)$$

$$\dot{\hat{\boldsymbol{\eta}}} = \mathbf{q}(\hat{\boldsymbol{\xi}}, \hat{\boldsymbol{\eta}}) + \mathbf{p}(\hat{\boldsymbol{\xi}}, \hat{\boldsymbol{\eta}})u \quad (8.145)$$

with  $\mathbf{k} \in \mathbb{R}^r$  subject to observer design. This observer consists of a high gain observer for the external dynamics  $\xi$  and a simulation-based estimation of the internal dynamics  $\eta$ . Noting that  $\xi_1 - \hat{\xi}_1 = y - h(\hat{\mathbf{x}})$  and transforming (8.144) back into  $\hat{\mathbf{x}}$ -coordinates via

$$\begin{bmatrix} \hat{\xi} \\ \hat{\eta} \end{bmatrix} = \Phi(\hat{\mathbf{x}}), \quad \begin{bmatrix} \dot{\hat{\xi}} \\ \dot{\hat{\eta}} \end{bmatrix} = \mathbf{f}_{d\Phi}(\Phi(\hat{\mathbf{x}})) + \mathbf{g}_{\Phi}(\Phi(\hat{\mathbf{x}}))u + \begin{pmatrix} \mathbf{k} \\ \mathbf{0}_{n-r} \end{pmatrix} (y - h(\hat{\mathbf{x}})) = \Phi'(\hat{\mathbf{x}})\dot{\hat{\mathbf{x}}} \quad (8.146)$$

$$\Rightarrow \dot{\hat{\mathbf{x}}} = (\Phi'(\hat{\mathbf{x}}))^{-1} \left( \mathbf{f}_{d\Phi}(\Phi(\hat{\mathbf{x}})) + \mathbf{g}_{\Phi}(\Phi(\hat{\mathbf{x}}))u + \begin{pmatrix} \mathbf{k} \\ \mathbf{0}_{n-r} \end{pmatrix} (y - h(\hat{\mathbf{x}})) \right), \quad (8.147)$$

the observer in  $\hat{\mathbf{x}}$ -coordinates is thus given by

$$\dot{\hat{\mathbf{x}}} = \mathbf{f}_d(\hat{\mathbf{x}}) + \mathbf{g}(\hat{\mathbf{x}})u + \underbrace{(\Phi'(\hat{\mathbf{x}}))^{-1} \begin{pmatrix} \mathbf{k} \\ \mathbf{0}_{n-r} \end{pmatrix}}_{=: \mathbf{l}(\hat{\mathbf{x}})} (y - h(\hat{\mathbf{x}})). \quad (8.148)$$

The original approach in [42] and of several of its successors requires globally exponentially stable zero dynamics. As was shown in section 8.4, this is not given with the system at hand. However, in [85, 86] an approach is proposed which requires the existence of an output-to-state Lyapunov function that allows for non-exponentially stable, but possibly only asymptotically stable zero dynamics, see the example given in [86]. In order for the suggested observer design to generate asymptotically stable observer error dynamics  $\tilde{\xi} = \hat{\xi} - \xi$  and  $\tilde{\eta} = \hat{\eta} - \eta$ , the following conditions ought to be fulfilled within the operating range of the system which is characterized by a set  $\mathcal{D}$  positively invariant under the flow of (8.139). Practically, this set can be assumed to exist and to be bounded for the vane pump system because of the end stops for cam ring displacement:  $0 \leq x_S \leq l_S$  and finite pump volume flow will yield finite pressures within the system if load flow through  $A_{OR1}$  is non-zero.

Specifically it ought to be ensured that

- the system given by (8.141) and (8.142) has a well-defined relative degree in  $\mathcal{D}$ ,
- the state transformation given by (7.15) is a global diffeomorphism in  $\mathcal{D}$ ,
- $\alpha$  and  $\beta$  are globally Lipschitz, which means that for bounded  $u$

$$|\alpha(\hat{\xi}, \hat{\eta}) + \beta(\hat{\xi}, \hat{\eta})u - \alpha(\xi, \eta) - \beta(\xi, \eta)u| \leq \gamma_1 \|\hat{\xi} - \xi\| + \gamma_2 \|\hat{\eta} - \eta\| \quad (8.149)$$

with  $\gamma_1, \gamma_2 > 0$ . This requirement is common in high-gain design, see also [85]. Roughly speaking, its meaning is that nonlinearities are such that their influence can be suppressed by choosing a sufficiently strong feedback of the signal of interest (measurement error in the case of observer design and control error in the case of controller design). This assumption is satisfied by many systems from a

practical viewpoint – even for the square root type of nonlinearity common in hydraulics – as Lipschitz-continuity depends on the operating range the system is designed for [82, 83, 84].

In the case of the pump system discussed here, the square root functions in  $\alpha(\boldsymbol{\xi}, \boldsymbol{\eta}), \beta(\boldsymbol{\xi}, \boldsymbol{\eta})$  with  $\boldsymbol{\eta} = \{\eta_T, \eta_L\}$  make it necessary to exclude  $x_3 - x_4 = 0$  and  $x_3 - p_C = x_4 = 0$  from the operating region of the observer in order to guarantee Lipschitz properties of the mappings  $\alpha(\boldsymbol{\xi}, \boldsymbol{\eta})$  and  $\beta(\boldsymbol{\xi}, \boldsymbol{\eta})$ . Ideally,  $x_4$  will always remain sufficiently far away from  $x_3$ . This is no severe restriction as  $x_3 - x_4 = 0$  has already been excluded from admissible working points due to generating an ill-defined relative degree. The other exclusions  $x_3 - p_C = x_4 = 0$  are not a problem either as the pump is not supposed at this working point as these configurations imply zero pump flow. Again,  $\mathcal{D}$  should be bounded, thereby requiring a bounded operating region in order for  $\alpha(\boldsymbol{\xi}, \boldsymbol{\eta}), \beta(\boldsymbol{\xi}, \boldsymbol{\eta})$  to be Lipschitz. Further discussion of the physical aspects of these requirements will be given below.

- There exist a positive definite matrix  $\mathbf{P}_2 \in \mathbb{R}^{(n-r) \times (n-r)}$  and constants  $\gamma_3, \gamma_4 > 0$  for the system given by (8.141) and (8.142) so that for the Lyapunov candidate  $V_2(\tilde{\boldsymbol{\eta}}) = \tilde{\boldsymbol{\eta}}^T \mathbf{P}_2 \tilde{\boldsymbol{\eta}}$  it holds that

$$\frac{\partial V_2(\tilde{\boldsymbol{\eta}})}{\partial \tilde{\boldsymbol{\eta}}} \left( \mathbf{q}(\hat{\boldsymbol{\xi}}, \hat{\boldsymbol{\eta}}) + \mathbf{p}(\hat{\boldsymbol{\xi}}, \hat{\boldsymbol{\eta}})u - \mathbf{q}(\boldsymbol{\xi}, \boldsymbol{\eta}) - \mathbf{p}(\boldsymbol{\xi}, \boldsymbol{\eta})u \right) \leq \gamma_3 \|\tilde{\boldsymbol{\xi}}\|^2 - \gamma_4 \|\tilde{\boldsymbol{\eta}}\|^2. \quad (8.150)$$

This Lyapunov function can be interpreted as an output-to-state Lyapunov function. Finding such a function is difficult in general. In the present case, such a function can, however, be found as internal dynamics are one-dimensional. Naturally, higher order internal dynamics significantly complicate the problem of finding a Lyapunov function candidate. The constant  $\gamma_3$  can be interpreted as a measure of how strongly the external observer error dynamics influence the internal dynamics error system. It therefore has to be bounded to allow for a functional observer – a requirement fulfilled in many practical circumstances.

The purpose of the following section is to assess if the observer problem has a solution for volume flow control of the pump system despite the switching behavior of the system's control input matrix  $\mathbf{g}_R$ . To do so, the same coordinate transformation will be applied to both system descriptions, yielding transformed system dynamics whose observation errors can be investigated. Because identical transformations are applied to (8.18) and (8.51), the transformed coordinates have the same meaning for both operating conditions. This is required in order to conclude stability of the system with switched input matrices. For transforming the system, the tank-sided transformation (8.31) will be employed.

### 8.6.1.1 Tank side valve opening

For the tank-side flow condition, the internal dynamics read

$$\dot{\eta}_T = \frac{1}{C_{h1}} \left( \underbrace{(\hat{q}_P \mathbf{R}_1^T + A_{S2} \mathbf{R}_2^T)}_{=: \mathbf{R}_T^T} \boldsymbol{\xi} - \gamma_F A_{OR1} \text{sign}(\eta_T) \sqrt{|\eta_T|} \right) \quad (8.151)$$

with  $\mathbf{R}_1^T = [1 \ 0 \ 0]$  and  $\mathbf{R}_2^T = [0 \ 1 \ 0]$ .

Building the nonlinear observer error  $\tilde{\eta}_T = \hat{\eta}_T - \eta_T$ , one obtains

$$\dot{\tilde{\eta}}_T = \frac{1}{C_{h1}} \left( \mathbf{R}_T^T \tilde{\boldsymbol{\xi}} - \gamma_F A_{OR1} \left( \text{sign}(\hat{\eta}_T) \sqrt{|\hat{\eta}_T|} - \text{sign}(\eta_T) \sqrt{|\eta_T|} \right) \right). \quad (8.152)$$

Applying the mean value theorem,

$$f(x_2) - f(x_1) = f'(x_\lambda)(x_2 - x_1) \quad (8.153)$$

with  $x_\lambda = x_1(1 - \lambda) + x_2\lambda$  and  $\lambda \in (0, 1)$ , one can write

$$\dot{\tilde{\eta}}_T = \frac{1}{C_{h1}} \left( \mathbf{R}_T^T \tilde{\boldsymbol{\xi}} - \tilde{\gamma}_{OR1T} \tilde{\eta}_T \right), \quad \eta_{T\lambda} = \eta_T(1 - \lambda) + \hat{\eta}_T\lambda, \quad \lambda \in (0, 1). \quad (8.154)$$

Here,

$$\tilde{\gamma}_{OR1T} := \frac{\gamma_F A_{OR1}}{2\sqrt{|\eta_{T\lambda}|}}. \quad (8.155)$$

Before continuing it is noted that

$$\begin{aligned} & \left( \sqrt{\mu_T} \tilde{\eta}_T - \frac{1}{\sqrt{\mu_T}} \tilde{\boldsymbol{\xi}}^T \mathbf{R}_T \right)^2 \geq 0 \\ & \Rightarrow \mu_T \tilde{\eta}_T^2 + \frac{1}{\mu_T} \tilde{\boldsymbol{\xi}}^T \mathbf{R}_T \mathbf{R}_T^T \tilde{\boldsymbol{\xi}} \geq 2 \tilde{\eta}_T \mathbf{R}_T^T \tilde{\boldsymbol{\xi}} \\ & \Rightarrow \frac{1}{2} \left( \mu_T \tilde{\eta}_T^2 + \frac{1}{\mu_T} \|\mathbf{R}_T\|^2 \|\tilde{\boldsymbol{\xi}}\|^2 \right) \geq |\tilde{\eta}_T| \|\mathbf{R}_T^T \tilde{\boldsymbol{\xi}}\| \end{aligned} \quad (8.156)$$

holds for any  $\mu_T > 0$ .

Now the Lyapunov function candidate

$$V_2 = \frac{C_{h1}}{2} \tilde{\eta}_T^2 \quad (8.157)$$

yields the following time derivative along error trajectories

$$\dot{V}_2 = C_{h1} \tilde{\eta}_T \dot{\tilde{\eta}}_T \quad (8.158)$$

$$= \tilde{\eta}_T \mathbf{R}_T^T \tilde{\boldsymbol{\xi}} - \tilde{\gamma}_{OR1T} \tilde{\eta}_T^2 \quad (8.159)$$

$$\leq |\tilde{\eta}_T| \|\mathbf{R}_T^T \tilde{\boldsymbol{\xi}}\| - \tilde{\gamma}_{OR1T} \tilde{\eta}_T^2 \quad (8.160)$$

$$\leq \frac{1}{2\mu_T} \|\mathbf{R}_T\|^2 \|\tilde{\boldsymbol{\xi}}\|^2 - \left( \tilde{\gamma}_{OR1T} - \frac{1}{2}\mu_T \right) \tilde{\eta}_T^2 \quad (8.161)$$

for any  $\mu_T > 0$ .

### 8.6.1.2 Load side valve opening, alternative coordinate transformation

While the coordinate transformation leading to Byrnes-Isidori normal form certainly is advantageous in many cases, in the context of a high gain observer with switched system dynamics it is more purposeful to employ the same coordinate transformations for both flow conditions of the system. This is needed in order to show asymptotic stability of the observer error.

Essentially, through (8.148) the coordinate transformation employed defines the state dependent component of the observer gain. Drawing on (8.31) and applying it to the load side flow condition, one finds the internal coordinate now depending on the system input  $u_R$ , however noting that  $u_R < 0$  so that  $u_R = -|u_R|$ . The inverse coordinate transformation leads to the following representation

$$\begin{aligned}
 x_4 &= -\frac{k_S l_S + F_{S0}}{A_{S1}} + \frac{k_S}{A_{S1}} \xi_1 + \frac{d_{PS}}{A_{S1}} \xi_2 + \frac{m_{PS}}{A_{S1}} \xi_3 \\
 &\quad + (\eta + p_C) \frac{1}{A_{S1}} \left( A_{S2} - f_{P1}(\xi_1 + x_S^{offset}) \right) - \frac{1}{A_{S1}} f_{P2}(\xi_1 + x_S^{offset}) \\
 &= -\frac{k_S l_S + F_{S0}}{A_{S1}} + \mathbf{R}_{L2}^T \boldsymbol{\xi} + (\eta + p_C) \frac{1}{A_{S1}} \left( A_{S2} - f_{P1}(\xi_1 + x_S^{offset}) \right) \\
 &\quad - \frac{1}{A_{S1}} f_{P2}(\xi_1 + x_S^{offset}) \tag{8.162}
 \end{aligned}$$

of  $x_4$  where

$$\mathbf{R}_{L2}^T = \begin{bmatrix} \frac{k_S}{A_{S1}} & \frac{d_{PS}}{A_{S1}} & \frac{m_{PS}}{A_{S1}} \end{bmatrix}. \tag{8.163}$$

For the benefit of a clear presentation of the following analysis, a hybrid notation will be pursued in the beginning for the representation of the internal coordinate's dynamics which will feature simultaneous use of  $\mathbf{x}$  and  $\boldsymbol{\xi}, \eta_T$  coordinates.

With  $u_R = -|u_R|$ , the dynamics of the internal coordinate  $\eta_T$  for the load side flow condition become

$$\begin{aligned}
 \dot{\eta}_T &= \frac{1}{C_{h1}} \left( \underbrace{\left( \hat{q}_P \mathbf{R}_1^T + (A_{S2} - A_{S1}) \mathbf{R}_2^T \right)}_{=: \mathbf{R}_{L1}^T} \boldsymbol{\xi} - \gamma_F A_{OR1} \text{sign}(\eta_T) \sqrt{|\eta_T|} \right. \\
 &\quad \left. - |u_R| \gamma_F b_{Reg} \text{sign}(\eta_T + p_C - x_4) \sqrt{|\eta_T + p_C - x_4|} \right). \tag{8.164}
 \end{aligned}$$

When building the observer error dynamics for the internal coordinate  $\eta_T$ , the manipulation

$$\begin{aligned}
 \text{sign}(\hat{\eta}_T + p_C - \hat{x}_4) \sqrt{|\hat{\eta}_T + p_C - \hat{x}_4|} &- \text{sign}(\eta_T + p_C - x_4) \sqrt{|\eta_T + p_C - x_4|} \\
 &= \frac{1}{2 \sqrt{|\eta_{T\lambda_1} + p_C - x_{4\lambda_1}|}} (\tilde{\eta}_T - \tilde{x}_4) \tag{8.165}
 \end{aligned}$$

with

$$\begin{aligned} \tilde{x}_4 = & \mathbf{R}_{L2}^T \tilde{\boldsymbol{\xi}} - \frac{1}{A_{S1}} \left( f_{P2}(\hat{\xi}_1 + x_S^{offset}) - f_{P2}(\xi_1 + x_S^{offset}) \right) + \frac{A_{S2}}{A_{S1}} \tilde{\eta}_T \\ & - \frac{1}{A_{S1}} \left( (\hat{\eta}_T + p_C) f_{P1}(\hat{\xi}_1 + x_S^{offset}) - (\eta_T + p_C) f_{P1}(\xi_1 + x_S^{offset}) \right). \end{aligned} \quad (8.166)$$

and repeated use of the mean value theorem (8.153) will be needed. In the above derivations, the index  $i = 1$  in  $\lambda_i$  signifying the first application of the mean value theorem. Applying the mean value theorem again, one finds

$$f_{P2}(\hat{\xi}_1 + x_S^{offset}) - f_{P2}(\xi_1 + x_S^{offset}) = \left. \frac{\partial f_{P2}}{\partial \xi_1} \right|_{\lambda_2} \mathbf{R}_1^T \tilde{\boldsymbol{\xi}} \quad (8.167)$$

and

$$\begin{aligned} & (\hat{\eta}_T + p_C) f_{P1}(\hat{\xi}_1 + x_S^{offset}) - (\eta_T + p_C) f_{P1}(\xi_1 + x_S^{offset}) \\ = & \left[ \left. \frac{\partial f_{P1}}{\partial \xi_1} \right|_{\lambda_2} (\eta_T \lambda_2 + p_C) \quad 0 \quad 0 \quad f_{P1} \Big|_{\lambda_2} \right] \cdot \begin{bmatrix} \tilde{\boldsymbol{\xi}} \\ \tilde{\eta}_T \end{bmatrix} \\ = & \left. \frac{\partial f_{P1}}{\partial \xi_1} \right|_{\lambda_2} (\eta_T \lambda_2 + p_C) \mathbf{R}_1^T \tilde{\boldsymbol{\xi}} + f_{P1} \Big|_{\lambda_2} \tilde{\eta}_T. \end{aligned} \quad (8.168)$$

In the above manipulations, the abbreviated form

$$\left. \frac{\partial f_{Pi}}{\partial \xi_1} \right|_{\lambda_2} = \left. \frac{\partial f_{Pi}}{\partial \xi_1} \right|_{\xi_{1\lambda_2}} \quad i = 1, 2 \quad (8.169)$$

was used.

The error  $\tilde{x}_4$  thus is ultimately given by

$$\begin{aligned} \tilde{x}_4 = & \mathbf{R}_{L2}^T \tilde{\boldsymbol{\xi}} + \frac{A_{S2}}{A_{S1}} \tilde{\eta}_T - \frac{1}{A_{S1}} \left. \frac{\partial f_{P2}}{\partial \xi_1} \right|_{\lambda_2} \mathbf{R}_1^T \tilde{\boldsymbol{\xi}} \\ & - \frac{1}{A_{S1}} \left( \left. \frac{\partial f_{P1}}{\partial \xi_1} \right|_{\lambda_2} (\eta_T \lambda_2 + p_C) \mathbf{R}_1^T \tilde{\boldsymbol{\xi}} + f_{P1} \Big|_{\lambda_2} \tilde{\eta}_T \right). \end{aligned} \quad (8.170)$$

Now building the observer error dynamics with

$$\tilde{\gamma}_{OR1L} := \frac{\gamma_F A_{OR1}}{2\sqrt{|\eta_T \lambda_1|}} > 0, \quad (8.171)$$

$$\tilde{\gamma}_R := \frac{\gamma_F |u_R| b_{Reg}}{2\sqrt{|\eta_T \lambda_1 + p_C - x_{4\lambda_1}|}} > 0 \quad (8.172)$$

for the internal coordinate  $\eta_T$ , one obtains

$$\begin{aligned} \dot{\tilde{\eta}}_T = \frac{1}{C_{h1}} \left( \mathbf{R}_{L1}^T \tilde{\boldsymbol{\xi}} - \tilde{\gamma}_{OR1L} \tilde{\eta}_T - \tilde{\gamma}_R \left( \frac{1}{A_{S1}} \frac{\partial f_{P2}}{\partial \xi_1} \Big|_{\lambda_2} \mathbf{R}_1^T + \frac{1}{A_{S1}} \frac{\partial f_{P1}}{\partial \xi_1} \Big|_{\lambda_2} (\eta_T \lambda_2 + p_C) \mathbf{R}_1^T - \mathbf{R}_{L2}^T \right) \tilde{\boldsymbol{\xi}} \right. \\ \left. - \tilde{\gamma}_R \left( 1 - \frac{A_{S2}}{A_{S1}} + \frac{1}{A_{S1}} f_{P1} \Big|_{\lambda_2} \right) \tilde{\eta}_T \right). \end{aligned} \quad (8.173)$$

Because asymptotic stability is to be shown for the switched system, the Lyapunov function candidate

$$V_2 = \frac{C_{h1}}{2} \tilde{\eta}_T^2 \quad (8.174)$$

is again assumed, this time as a common Lyapunov function candidate. For the tank-sided operating condition, it could already be shown that the system (8.18) has property (8.150) with this Lyapunov function. In order to show property (8.150) is fulfilled for the load sided operating condition, too, the time derivative of  $V_2$  along trajectories for the load sided operating condition has to be investigated:

$$\begin{aligned} \dot{V}_2 &= C_{h1} \tilde{\eta}_T \dot{\tilde{\eta}}_T \\ &= \overbrace{\left( \mathbf{R}_{L1}^T + \tilde{\gamma}_R \mathbf{R}_{L2}^T - \tilde{\gamma}_R \left( \frac{1}{A_{S1}} \frac{\partial f_{P2}}{\partial \xi_1} \Big|_{\lambda_2} \mathbf{R}_1^T + \frac{1}{A_{S1}} \frac{\partial f_{P1}}{\partial \xi_1} \Big|_{\lambda_2} (\eta_T \lambda_2 + p_C) \mathbf{R}_1^T \right) \right)}{=: \mathbf{R}_L^T(\lambda_1, \lambda_2)} \tilde{\boldsymbol{\xi}} \tilde{\eta}_T \\ &\quad - \tilde{\gamma}_R \left( 1 - \frac{A_{S2}}{A_{S1}} + \frac{1}{A_{S1}} f_{P1} \Big|_{\lambda_2} \right) \tilde{\eta}_T^2 - \tilde{\gamma}_{OR1L} \tilde{\eta}_T^2. \end{aligned} \quad (8.175)$$

Since no magnitude comparison of  $\tilde{\gamma}_{OR1L}$  and  $\tilde{\gamma}_R$  can be made per se, in order to make a statement about the positiveness or negativeness of  $\dot{\tilde{\eta}}_T^2$  in equation (8.175) it has to hold that

$$1 - \frac{A_{S2}}{A_{S1}} + \frac{1}{A_{S1}} f_{P1} \Big|_{\lambda_2} \geq 0. \quad (8.176)$$

This requirement translates into

$$A_{S1} - A_{S2} + f_{P1} \Big|_{\lambda_2} \geq 0, \quad (8.177)$$

which practically holds as a result of pump design, as otherwise the pump could not be displaced in positive direction because for typical situations  $p_S < p_1$ .

As a result,

$$\begin{aligned} \dot{V}_2 &= C_{h1} \tilde{\eta}_T \dot{\tilde{\eta}}_T \\ &= \tilde{\eta}_T \mathbf{R}_L^T \tilde{\boldsymbol{\xi}} - \left( \tilde{\gamma}_{OR1L} + \tilde{\gamma}_R \left( 1 - \frac{A_{S2}}{A_{S1}} + \frac{1}{A_{S1}} f_{P1} \Big|_{\lambda_2} \right) \right) \tilde{\eta}_T^2 \end{aligned}$$

$$\begin{aligned}
 &\leq |\tilde{\eta}_T| \|\mathbf{R}_L^T \tilde{\boldsymbol{\xi}}\| - \tilde{\gamma}_{OR1L} \tilde{\eta}_T^2 \\
 &\leq \frac{1}{2\mu_L} \|\mathbf{R}_L\|^2 \|\tilde{\boldsymbol{\xi}}\|^2 - \left( \tilde{\gamma}_{OR1L} - \frac{1}{2}\mu_L \right) \tilde{\eta}_T^2
 \end{aligned} \tag{8.178}$$

for any  $\mu_L > 0$ .

### 8.6.1.3 Asymptotic stability of the switched error system

Upon consideration of (8.161), (8.178) and noting that within the operating range  $\mathcal{D}$

$$\min(\tilde{\gamma}_{OR1T}) = \min(\tilde{\gamma}_{OR1L}) =: \tilde{\gamma}_{OR1}, \tag{8.179}$$

it holds that

$$\dot{V}_2 \leq \begin{cases} \frac{1}{2\mu} \|\mathbf{R}_T\|^2 \|\tilde{\boldsymbol{\xi}}\|^2 - (\tilde{\gamma}_{OR1} - \frac{1}{2}\mu) \tilde{\eta}_T^2 & \text{for } u_R \geq 0, \\ \frac{1}{2\mu} \|\mathbf{R}_L\|^2 \|\tilde{\boldsymbol{\xi}}\|^2 - (\tilde{\gamma}_{OR1} - \frac{1}{2}\mu) \tilde{\eta}_T^2 & \text{for } u_R < 0 \end{cases} \tag{8.180}$$

for a choice of  $\mu = \mu_T = \mu_L$  with  $\mu \in (0, 2\tilde{\gamma}_{OR1})$ . Thus,

$$\dot{V}_2 \leq \frac{1}{2\mu} (\|\mathbf{R}_T\|^2 + \|\mathbf{R}_L\|^2) \|\tilde{\boldsymbol{\xi}}\|^2 - \left( \tilde{\gamma}_{OR1} - \frac{1}{2}\mu \right) \tilde{\eta}_T^2. \tag{8.181}$$

However,  $\mathbf{R}_L = \mathbf{R}_L(\lambda_1, \lambda_2)$  and thereby a function of the interval the system is assumed to operate on, i.e.  $\mathcal{D}$ . Hence, for an unbounded operating range and operating points for which  $x_3 = x_4$  and/or  $x_3 = p_C$  hold,  $\mathbf{R}_L$  may theoretically assume infinite values. In order for

$$\frac{1}{2\mu} (\|\mathbf{R}_T\|^2 + \|\mathbf{R}_L\|^2) \leq \gamma_3 = \text{const} \tag{8.182}$$

and thus to fulfill (8.150), the operating range of the system needs to be bounded and exclude  $x_3 = x_4$ . This was already required in the context of Lipschitz continuity for  $\alpha(\boldsymbol{\xi}, \eta), \beta(\boldsymbol{\xi}, \eta)$  with  $\eta = \{\eta_T, \eta_L\}$  and does not pose a practical problem either since, from physical reasoning, finite pump flow from  $0 \leq x_1 \leq l_S$  will generate finite system pressure contingent upon non-zero consumer flow so that  $\mathcal{D}$  is bounded.

In many cases, the operating range of the system will indeed be known in advance. Situations with  $x_3 = x_4$  will not be encountered when the system is at any point  $0 < x_S = x_1 < l_S$  and  $u_R < 0$  (with  $x_1 - x_S^{offset}$  being the system output) because of condition (8.177) and the flow dynamics generated by the piston flow  $x_2 A_{S2}$ . Because of (8.177), as soon as  $x_3 - x_4$  becomes smaller than some value depending on the actual geometry parameters  $A_{S1}, A_{S2}$ , cam ring radius  $r_C$ , pump width  $h_P$  and the port angles, the combined spring force and pressure force acting on  $A_{S1}$  will exceed the counteracting internal force of the pump and pressure force on  $A_{S2}$  and thereby displace the pump

in positive direction, resulting in a volume flow  $x_2 A_{S1}$  which will reduce  $x_4$  and thereby restore the pressure difference  $x_3 - x_4$ . In addition, due to increased  $x_1$ ,  $x_3$  undergoes an increase as well. It is notable that because of condition (8.177), the situation  $x_1 = l_S$  can nevertheless be reached without  $x_3 = x_4$ . For  $x_1 = l_S$ , however, system input  $u_R$  must be decreased to zero then in order to prevent  $x_3$  to become equal to  $x_4$  for  $t \rightarrow \infty$ . Thus, excluding these points from  $\mathcal{D}$  and dismissing the corresponding inputs  $u_R = \text{const} < 0$  leading to such a situation is no restriction either (see [84], where a related problem is discussed).

It is noteworthy that because  $\gamma_3$  depends on the specific operating range of the system through (8.182), so will observer gain. Ultimately, one obtains

$$\dot{V}_2 \leq \gamma_3 \|\tilde{\boldsymbol{\xi}}\|^2 - \gamma_4 |\tilde{\eta}_T|^2. \quad (8.183)$$

Then, from

$$\begin{aligned} & \left| \alpha(\hat{\boldsymbol{\xi}}, \hat{\eta}_T) + \beta(\hat{\boldsymbol{\xi}}, \hat{\eta}_T)u_R - \alpha(\boldsymbol{\xi}, \eta_T) - \beta(\boldsymbol{\xi}, \eta_T)u_R \right| \\ & \leq \begin{cases} \gamma_{1T} \|\tilde{\boldsymbol{\xi}}\| + \gamma_{2T} |\tilde{\eta}_T| & \text{for } u_R \geq 0, \\ \gamma_{1L} \|\tilde{\boldsymbol{\xi}}\| + \gamma_{2L} |\tilde{\eta}_T| & \text{for } u_R < 0 \end{cases} \end{aligned} \quad (8.184)$$

it follows that

$$\begin{aligned} & \left| \alpha(\hat{\boldsymbol{\xi}}, \hat{\eta}_T) + \beta(\hat{\boldsymbol{\xi}}, \hat{\eta}_T)u_R - \alpha(\boldsymbol{\xi}, \eta_T) - \beta(\boldsymbol{\xi}, \eta_T)u_R \right| \\ & \leq \underbrace{(\gamma_{1T} + \gamma_{1L})}_{=: \gamma_1} \|\tilde{\boldsymbol{\xi}}\| + \underbrace{(\gamma_{2T} + \gamma_{2L})}_{=: \gamma_2} |\tilde{\eta}_T|. \end{aligned} \quad (8.185)$$

The above relationships are subject to the same line of reasoning about the system operating range as for the constant  $\gamma_3$ . With these considerations in mind, the proof for asymptotic stability of the observer from [86] can be applied to showing the asymptotic stability of the switched observer error system.

The common Lyapunov function candidate for both flow conditions is assumed to be

$$V(\tilde{\boldsymbol{\xi}}, \tilde{\eta}_T) = \tilde{\boldsymbol{\xi}}^T \mathbf{P} \tilde{\boldsymbol{\xi}} + \frac{C_{h1}}{2} \tilde{\eta}_T^2, \quad (8.186)$$

where  $\mathbf{P}$  is the positive definite, symmetric solution to the following Ricatti-like inequality:

$$\left( \mathbf{A} - \mathbf{k} \mathbf{c}^T \right)^T \mathbf{P} + \mathbf{P} \left( \mathbf{A} - \mathbf{k} \mathbf{c}^T \right) + \nu \mathbf{P} \mathbf{b} \mathbf{b}^T \mathbf{P} + \rho \mathbf{I} < 0. \quad (8.187)$$

A positive definite, symmetric solution for  $\mathbf{P}$  is guaranteed if  $\mathbf{A} - \mathbf{k} \mathbf{c}^T$  has real negative eigenvalues, while  $\nu$  and  $\rho$  are arbitrary positive real constants. In the context of

the switched system treated here,  $V(\tilde{\boldsymbol{\xi}}, \tilde{\eta}_T)$  shall be considered as a common Lyapunov function candidate.

With [85], it can then be seen that the Lyapunov function's time derivative is less than zero irrespective of which flow condition holds:

$$\begin{aligned} \dot{V}(\tilde{\boldsymbol{\xi}}, \tilde{\eta}_T) &= \tilde{\boldsymbol{\xi}}^T \left[ \left( \mathbf{A} - \mathbf{k}\mathbf{c}^T \right)^T \mathbf{P} + \mathbf{P} \left( \mathbf{A} - \mathbf{k}\mathbf{c}^T \right) \right] \tilde{\boldsymbol{\xi}} + C_{h1} \tilde{\eta}_T \dot{\tilde{\eta}}_T \\ &\quad + 2\tilde{\boldsymbol{\xi}}^T \mathbf{P}\mathbf{b} \left[ \alpha(\hat{\boldsymbol{\xi}}, \hat{\eta}_T) + \beta(\hat{\boldsymbol{\xi}}, \hat{\eta}_T)u_R - \alpha(\boldsymbol{\xi}, \eta_T) - \beta(\boldsymbol{\xi}, \eta_T)u_R \right] \\ &\leq \tilde{\boldsymbol{\xi}}^T \left[ \left( \mathbf{A} - \mathbf{k}\mathbf{c}^T \right)^T \mathbf{P} + \mathbf{P} \left( \mathbf{A} - \mathbf{k}\mathbf{c}^T \right) \right] \tilde{\boldsymbol{\xi}} + \gamma_3 \|\tilde{\boldsymbol{\xi}}\|^2 - \gamma_4 |\tilde{\eta}_T|^2 \\ &\quad + 2\tilde{\boldsymbol{\xi}}^T \mathbf{P}\mathbf{b} \left[ \alpha(\hat{\boldsymbol{\xi}}, \hat{\eta}_T) + \beta(\hat{\boldsymbol{\xi}}, \hat{\eta}_T)u_R - \alpha(\boldsymbol{\xi}, \eta_T) - \beta(\boldsymbol{\xi}, \eta_T)u_R \right]. \end{aligned} \quad (8.188)$$

Then, from (8.149), (8.185)

$$\begin{aligned} &2\tilde{\boldsymbol{\xi}}^T \mathbf{P}\mathbf{b} \left[ \alpha(\hat{\boldsymbol{\xi}}, \hat{\eta}_T) + \beta(\hat{\boldsymbol{\xi}}, \hat{\eta}_T)u_R - \alpha(\boldsymbol{\xi}, \eta_T) - \beta(\boldsymbol{\xi}, \eta_T)u_R \right] \\ &\leq 2\gamma_1 |\tilde{\boldsymbol{\xi}}^T \mathbf{P}\mathbf{b}| \cdot \|\tilde{\boldsymbol{\xi}}\| + 2\gamma_2 |\tilde{\boldsymbol{\xi}}^T \mathbf{P}\mathbf{b}| \cdot |\tilde{\eta}_T| \\ &\leq \left( \gamma_1^2 + \frac{\gamma_2^2}{\mu} \right) \tilde{\boldsymbol{\xi}}^T \mathbf{P}\mathbf{b}\mathbf{b}^T \mathbf{P}\tilde{\boldsymbol{\xi}} + \tilde{\boldsymbol{\xi}}^T \tilde{\boldsymbol{\xi}} + \mu \tilde{\eta}_T^2, \end{aligned} \quad (8.189)$$

follows where a manipulation similar to those in (8.158) and (8.161) was used in the last step.

Ultimately, using the bound estimate (8.189) in (8.188) and taking  $\nu = \gamma_1^2 + \gamma_2^2/\mu$  and  $\rho = \gamma_3 + 1$  yields

$$\dot{V}(\tilde{\boldsymbol{\xi}}, \tilde{\eta}_T) \leq \tilde{\boldsymbol{\xi}}^T \left[ \left( \mathbf{A} - \mathbf{k}\mathbf{c}^T \right)^T \mathbf{P} + \mathbf{P} \left( \mathbf{A} - \mathbf{k}\mathbf{c}^T \right) + \nu \mathbf{P}\mathbf{b}\mathbf{b}^T \mathbf{P} + \rho \mathbf{I} \right] \tilde{\boldsymbol{\xi}} - (\gamma_4 - \mu) \tilde{\eta}_T^2, \quad (8.190)$$

which is negative definite by the choice of  $\mathbf{P}$ . The Lyapunov function candidate therefore is a common Lyapunov function, proving the observer error to asymptotically approach zero for the switched system with an appropriate choice of  $\mathbf{k}$ . This result fundamentally rests on the relative degree and the transformation for the external coordinates being identical for both flow conditions. The result should however only be understood in the sense that the observer problem does have a solution for the system treated here – no precise statement is made on how to specifically choose the observer gain to ensure stability. In [86], it is remarked that  $\mathbf{k}$  will commonly be chosen via pole placement.

The switched system has an interesting geometrical interpretation with respect to observer gain computation. In [85, 86], a simplified computation of the observer gain is suggested under certain additional assumptions. Because in many cases the internal dynamics can be difficult to derive analytically, the ability to compute an appropriate observer gain without explicit knowledge of the internal dynamics is highly feasible. In [85], a choice for the observer gain relying only on the known transformation for the

external coordinates is presented which guarantees asymptotic stability under certain additional assumptions. To do so, a Moore-Penrose-Inverse based observer gain computation is performed. The idea is to separate the Jacobian of the transformation matrix' external and internal coordinates

$$\Phi'(\mathbf{x}) = \begin{bmatrix} \mathbf{Q}(\mathbf{x}) \\ \mathbf{R}(\mathbf{x}) \end{bmatrix}, \quad (8.191)$$

where  $\mathbf{Q}(\mathbf{x})$  is the so called reduced observability matrix, associated with the external coordinates and thereby unique and  $\mathbf{R}(\mathbf{x})$  is not, representing the Jacobian of the coordinate transformation for the internal coordinates:

$$\mathbf{Q}(\mathbf{x}) = \begin{bmatrix} \tau_1^T(\mathbf{x}) \\ \vdots \\ \tau_r^T(\mathbf{x}) \end{bmatrix} = \begin{bmatrix} \text{grad}(h(\mathbf{x})) \\ \vdots \\ \text{grad}(\mathcal{L}_{f_d}^{r-1}h(\mathbf{x})) \end{bmatrix}, \quad \mathbf{R}(\mathbf{x}) = \begin{bmatrix} \text{grad}(\Phi_{r+1}(\mathbf{x})) \\ \vdots \\ \text{grad}(\Phi_n(\mathbf{x})) \end{bmatrix}. \quad (8.192)$$

The suggested observer gain is then proposed as

$$\mathbf{l}(\mathbf{x}) = \mathbf{Q}^T(\mathbf{x}) \left( \mathbf{Q}(\mathbf{x})\mathbf{Q}^T(\mathbf{x}) \right)^{-1} \mathbf{k}. \quad (8.193)$$

This simplified design rule is restricted to cases where the span of the reduced observability matrix is involutive. The span of the reduced observability matrix

$$\Delta(\mathbf{x}) = \text{span} \{ \tau_1(\mathbf{x}), \dots, \tau_r(\mathbf{x}) \} \quad (8.194)$$

is a so-called distribution which is characterized by a mapping of a point  $\mathbf{x} \in \mathbb{R}^n$  to a vector space  $\Delta\mathbf{x} \subseteq \mathbb{R}^n$ . Involutivity can be understood as a generalized principle of commutativity of partial derivatives and requires the Lie brackets of

$$[\tau_i, \tau_j](\mathbf{x}) = \frac{\partial \tau_j(\mathbf{x})}{\partial \mathbf{x}} \tau_i(\mathbf{x}) - \frac{\partial \tau_i(\mathbf{x})}{\partial \mathbf{x}} \tau_j(\mathbf{x}) \quad i, j = 1 \dots r \quad (8.195)$$

to lie within the span of  $\Delta(\mathbf{x})$  [40]. It is to be noted that the rows of  $\mathbf{Q}(\mathbf{x})$  are linearly independent by (7.16) so that (8.194) is regular. The proof in [86] for the applicability of a Moore-Penrose-Inverse based observer gain computation relies on the Frobenius theorem (see e.g. [40] for reference) which essentially states that if  $\Delta(\mathbf{x})$  is involutive, then it is integrable so that there exist functions  $\Phi_{r+1}(\mathbf{x}), \dots, \Phi_n(\mathbf{x})$  for which

$$\text{grad}(\Phi_i(\mathbf{x})) \cdot \tau(\mathbf{x}) = 0 \quad \forall \tau(\mathbf{x}) \in \Delta(\mathbf{x}) \quad i = r + 1, \dots, n. \quad (8.196)$$

This is a restriction for the system structure. For the pump system,  $\mathbf{Q}(\mathbf{x})$  is the same irrespective of the flow condition and it holds that

$$[\tau_1(\mathbf{x}), \tau_2(\mathbf{x})] = \begin{bmatrix} 0 & 0 & 0 & 0 \end{bmatrix}^T, \quad (8.197)$$

$$[\boldsymbol{\tau}_1(\mathbf{x}), \boldsymbol{\tau}_3(\mathbf{x})] = \frac{1}{m_{PS}} \left[ \frac{\partial^2 f_P(x_1, x_3)}{\partial x_1^2} \quad 0 \quad \frac{\partial^2 f_P(x_1, x_3)}{\partial x_1 \partial x_3} \quad 0 \right]^T, \quad (8.198)$$

$$[\boldsymbol{\tau}_2(\mathbf{x}), \boldsymbol{\tau}_3(\mathbf{x})] = \begin{bmatrix} 0 & 0 & 0 & 0 \end{bmatrix}^T. \quad (8.199)$$

It can easily be checked that

$$\text{Rank} \left( \begin{bmatrix} \boldsymbol{\tau}_1(\mathbf{x}) & \boldsymbol{\tau}_2(\mathbf{x}) & \boldsymbol{\tau}_3(\mathbf{x}) & [\boldsymbol{\tau}_1(\mathbf{x}), \boldsymbol{\tau}_2(\mathbf{x})] & [\boldsymbol{\tau}_1(\mathbf{x}), \boldsymbol{\tau}_3(\mathbf{x})] & [\boldsymbol{\tau}_2(\mathbf{x}), \boldsymbol{\tau}_3(\mathbf{x})] \end{bmatrix} \right) = 4, \quad (8.200)$$

implying that the distribution  $\Delta(\mathbf{x})$  is not involutive in a strict sense of meaning so that a computation of the observer gain based on  $\mathbf{Q}(\mathbf{x})$  alone is not formally admissible. However, equation (8.196) can be interpreted geometrically as a scalar product, thereby essentially yielding an orthogonality statement. That is, in order to see how strongly the distribution (8.194) violates the orthogonality statement with the internal dynamics for tank-side and load-side flow condition of the valve, the scalar product and the corresponding angle between  $\text{grad}\Phi_4(\mathbf{x})$  and the  $\boldsymbol{\tau}_i$ ,  $i = 1, 2, 3$  can be computed. For the tank-side flow condition with  $u_R \geq 0$ , the gradient of  $\Phi_4(\mathbf{x})$  is given by

$$\text{grad}(\Phi_4(\mathbf{x})) = \begin{bmatrix} 0 & 0 & C_{h1} & 0 \end{bmatrix}. \quad (8.201)$$

Due to the structure of  $\boldsymbol{\tau}_1$  and  $\boldsymbol{\tau}_2$ , the corresponding angles with  $\text{grad}\Phi_4$  are orthogonal. For  $\boldsymbol{\tau}_3$ , the angle with  $\text{grad}\Phi_4$  is given by

$$\cos(\angle(\boldsymbol{\tau}_3, \text{grad}(\Phi_4))) = \frac{-A_{S2} + \frac{\partial f_P}{\partial x_3}}{\sqrt{\left(-k_S + \frac{\partial f_P}{\partial x_1}\right)^2 + \left(-A_{S2} + \frac{\partial f_P}{\partial x_3}\right)^2 + A_{S1}^2 + d_{PS}^2}}. \quad (8.202)$$

For the load side flow condition the transformation for the internal coordinate  $\eta_L$  yields a gradient

$$\text{grad}(\Phi_4(\mathbf{x})) = \begin{bmatrix} 0 & 0 & \Psi_1 C_{h1} & \Psi_1 C_{hS} \end{bmatrix} \quad (8.203)$$

and the corresponding angle computed from the scalar product between  $\boldsymbol{\tau}_3$  and  $\text{grad}\Phi_4$  is

$$\cos(\angle(\boldsymbol{\tau}_3, \text{grad}(\Phi_4))) = \frac{C_{h1} \left(-A_{S2} + \frac{\partial f_P}{\partial x_3}\right) + C_{hS} A_{S1}}{\sqrt{C_{h1}^2 + C_{hS}^2} \sqrt{\left(-k_S + \frac{\partial f_P}{\partial x_1}\right)^2 + \left(-A_{S2} + \frac{\partial f_P}{\partial x_3}\right)^2 + A_{S1}^2 + d_{PS}^2}}. \quad (8.204)$$

A numerical evaluation of these quantities for representative parameters shows that the scalar product between  $\text{grad}\Phi_4$  and  $\boldsymbol{\tau}_3$  typically lies in the range of  $\mathcal{O}(1 \times 10^{-8})$  so that from a practical perspective, the involutivity condition required for (8.193) to be an

admissible approach to observer gain computation can be considered as given. The implication of this with respect to the observer gain computation for the switched system is that essentially, the switching behavior is of no relevance for the calculation of the observer gain since it can be computed based on the Moore-Penrose-Inverse. Reconsidering the demonstration that the observer problem has a solution for the switched system at hand as outlined above, the same observation can be made because the system here was transformed by the same coordinate transformation irrespective of the sign of  $u_R$ . Intuitively, the “practical” applicability of the Moore-Penrose-Inverse based observer gain calculation therefore suggests observer stability for the switched system if stability can be shown for the systems separately.

#### 8.6.1.4 Simulation Results

The simulation results in Figures 8.6, 8.7 show that the observer has excellent convergence properties. Initial conditions for the observer  $\hat{\mathbf{x}}_0$  were set close to zero, the observer converges in very short time nevertheless. This holds well for the simulation results with valve dynamics, too. Here, the observer even seems to alleviate transients from valve dynamics when comparing the results with Figure 8.6.

### 8.6.2 Nonlinear Local Observer

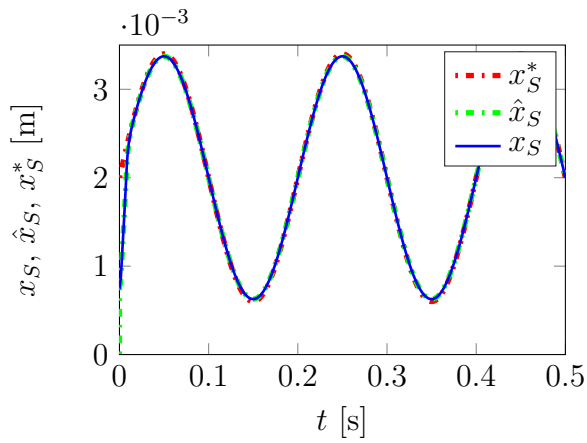
The observer presented in the previous section prominently lends itself to the implementation of an observer for the variable displacement vane pump system. However, exploring other observer concepts is worthwhile with regard to practical questions such as the measurability of the system output  $y = x_1$ . As an alternative to the high gain observer presented in the preceding section, a nonlinear local tracking observer based on linearization of the system dynamics about a desired or nominal trajectory in state space  $\mathbf{x}^*$  can be constructed. The idea behind the corresponding observer is to choose the observer gain  $\mathbf{l}(\mathbf{x})$  such that the linearized error dynamics are asymptotically stable. The observer gain is chosen according to a pole-placement technique for time-varying systems. The concept is extensively discussed in [87, 88, 89, 132] in the context of differentially flat systems to which it can be applied in the most straightforward fashion. In physical state coordinates  $\mathbf{x}$ , the observer has the representation

$$\dot{\hat{\mathbf{x}}} = \mathbf{f}_d(\hat{\mathbf{x}}) + \mathbf{g}(\hat{\mathbf{x}})\hat{u} + \mathbf{l}(t)(y - h(\hat{\mathbf{x}})), \quad (8.205)$$

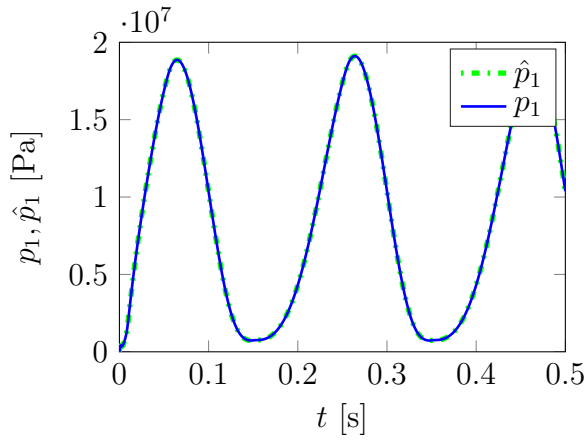
where in contrast to the high gain form observer presented before  $y = h(\hat{\mathbf{x}})$  does not need to be cam ring displacement but can be any other state variable in agreement with the observability criterion.

Combining (8.205) with the system dynamics given by (7.1), (7.2) yields dynamics for the observation error  $\tilde{\mathbf{x}} = \hat{\mathbf{x}} - \mathbf{x}$  which are of the following form:

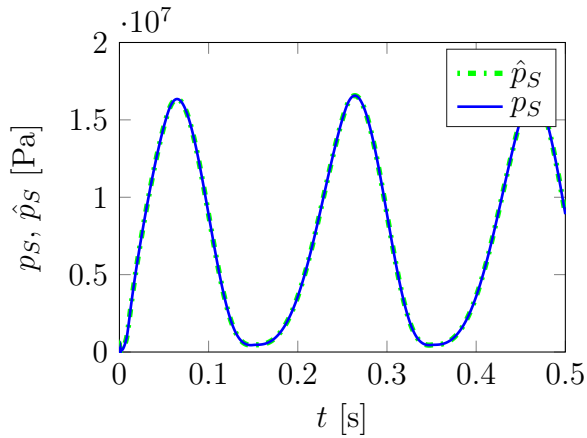
$$\dot{\tilde{\mathbf{x}}} = \mathbf{f}_d(\hat{\mathbf{x}}) + \mathbf{g}(\hat{\mathbf{x}})\hat{u} - \mathbf{f}_d(\mathbf{x}) - \mathbf{g}(\mathbf{x})\hat{u} + \mathbf{l}(t) (h(\mathbf{x}) - h(\hat{\mathbf{x}})), \quad (8.206)$$



(a) Pump displacement.

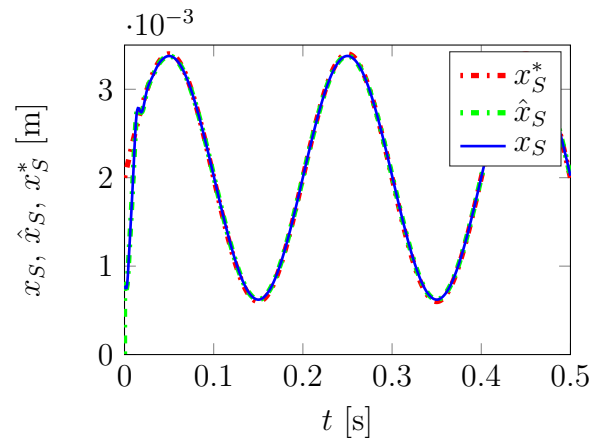


(b) Main chamber pressure.

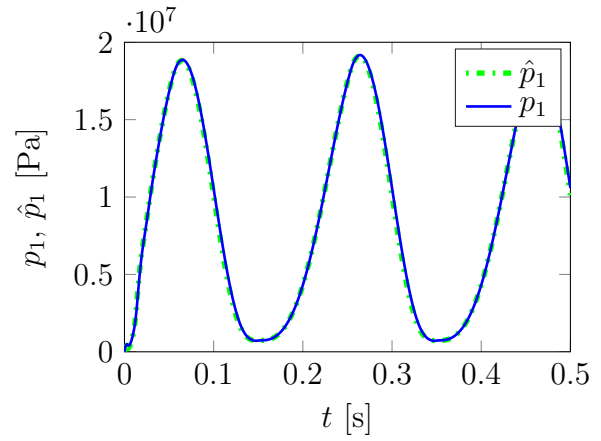


(c) Actuation chamber pressure.

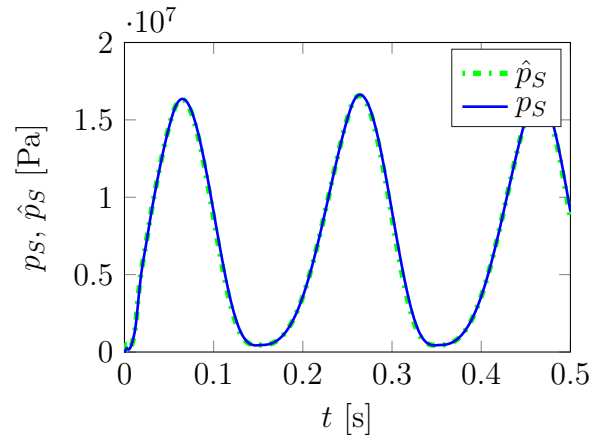
Figure 8.6: Without valve dynamics.



(a) Pump displacement.



(b) Main chamber pressure.



(c) Actuation chamber pressure.

Figure 8.7: With valve dynamics.

$$\tilde{\mathbf{x}}(0) = \hat{\mathbf{x}}_0 - \mathbf{x}_0. \quad (8.207)$$

It is to be emphasized that the above representation of the observer error dynamics expresses the fact that the system input  $u = \hat{u}$  is synthesized as a function of the state estimates provided by the observer.

Now linearizing about  $\mathbf{x}^* = \mathbf{x}^*(t)$ ,  $u^* = u^*(t)$  yields

$$\begin{aligned} \Delta \dot{\tilde{\mathbf{x}}} &= \underbrace{\left[ \mathbf{A}(t)\Delta \hat{\mathbf{x}} + \mathbf{B}(t)\Delta \hat{u} + \mathbf{l}(t) \left( \mathbf{c}^T(t)\Delta \mathbf{x} - \mathbf{c}^T(t)\Delta \hat{\mathbf{x}} \right) \right]}_{\text{observer}} - \underbrace{\left[ \mathbf{A}(t)\Delta \mathbf{x} + \mathbf{B}(t)\Delta \hat{u} \right]}_{\text{plant}} \\ &= \left( \mathbf{A}(t) - \mathbf{l}(t)\mathbf{c}^T(t) \right) \Delta \tilde{\mathbf{x}}. \end{aligned} \quad (8.208)$$

Here, the time varying matrices are

$$\mathbf{A}(t) = \left. \frac{\partial(\mathbf{f}_d(\mathbf{x}) + \mathbf{g}(\mathbf{x})\hat{u})}{\partial \mathbf{x}} \right|_{\mathbf{x}^*, u^*}, \quad \mathbf{B}(t) = \left. \frac{\partial(\mathbf{f}_d(\mathbf{x}) + \mathbf{g}(\mathbf{x})\hat{u})}{\partial \hat{u}} \right|_{\mathbf{x}^*, u^*}, \quad \mathbf{c}^T(t) = \left. \frac{\partial \mathbf{h}(\mathbf{x})}{\partial \mathbf{x}} \right|_{\mathbf{x}^*}.$$

Introducing the operator

$$M_{\mathbf{A}}^0 \circ (\cdot) = (\cdot), \quad (8.209)$$

$$M_{\mathbf{A}}^1 \circ (\cdot) = \frac{d}{dt} (\cdot) + (\cdot) \mathbf{A} \quad (8.210)$$

$$M_{\mathbf{A}}^i \circ (\cdot) = M_{\mathbf{A}}^1 \left( M_{\mathbf{A}}^{i-1} \circ (\cdot) \right) \quad (8.211)$$

with  $\mathbf{v} = \mathbf{v}(t)$  and  $\mathbf{A} = \mathbf{A}(t)$ , the time-varying observability map for a system with  $n$  states can be defined as follows:

$$\mathbf{O}(\mathbf{c}^T(t), \mathbf{A}(t)) = \begin{bmatrix} M_{\mathbf{A}}^0 \mathbf{c}^T(t) \\ M_{\mathbf{A}}^1 \mathbf{c}^T(t) \\ \vdots \\ M_{\mathbf{A}}^{n-1} \mathbf{c}^T(t) \end{bmatrix}. \quad (8.212)$$

The system

$$\Delta \dot{\mathbf{x}} = \mathbf{A}(t)\Delta \mathbf{x} + \mathbf{B}(t)\Delta u, \quad (8.213)$$

$$\Delta y = \mathbf{c}^T(t)\Delta \mathbf{x} \quad (8.214)$$

is called observable if  $\text{rank}(\mathbf{O}(\mathbf{c}^T(t), \mathbf{A}(t))) = n$ . For the SISO system considered at this stage, this is equivalent to showing the determinant of the observability matrix does not become zero along the desired trajectory  $\mathbf{x}^*, u^*$ . It can easily be seen that applying the definition for the observability of a time-varying system to a time-invariant system yields the observability matrix well known from linear time invariant theory. If observability is given, the system can be transformed to so called observability normal form. To do so, another operator first requires introduction. The operator

$$N_{\mathbf{A}}^0 \circ (\cdot) = (\cdot), \quad (8.215)$$

$$N_{\mathbf{A}}^1 \circ (\cdot) = -\frac{d}{dt}(\cdot) + \mathbf{A}(\cdot), \quad (8.216)$$

$$N_{\mathbf{A}}^i \circ (\cdot) = N_{\mathbf{A}}^1 \left( N_{\mathbf{A}}^{i-1} \circ (\cdot) \right) \quad (8.217)$$

allows for the construction of the inverse of matrix transforming the system to observability normal form.

The inverse of the transformation matrix is computed as

$$\mathbf{V}^{-1}(t) = [N_{\mathbf{A}}^0 \mathbf{v}(t) \quad N_{\mathbf{A}}^1 \mathbf{v}(t) \dots \quad N_{\mathbf{A}}^{n-1} \mathbf{v}(t)] \quad (8.218)$$

with

$$\mathbf{v}(t) = \mathbf{O}^{-1}(\mathbf{c}^T(t), \mathbf{A}(t)) \begin{bmatrix} 0 \\ \vdots \\ 0 \\ \tilde{c}_{n-1}(t) \end{bmatrix} \quad (8.219)$$

and  $\tilde{c}_{n-1}(t)$  constituting a degree of freedom in the design of the observer. It ought to be chosen in such a way that  $\mathbf{v}(t)$  assumes the simplest form. Typically, an effort will be made to choose  $\tilde{c}_{n-1}(t)$  in such a way that it will render the representation for  $\mathbf{v}(t)$  constant, if possible. Applying the transformation  $\mathbf{z}(t) = \mathbf{V}(t)\Delta\mathbf{x}(t)$  yields the observability normal form

$$\begin{bmatrix} \dot{z}_1 \\ \dot{z}_2 \\ \vdots \\ \dot{z}_{n-1} \\ \dot{z}_n \end{bmatrix} = \begin{bmatrix} 0 & 0 & \dots & 0 & -\tilde{a}_0(t) \\ 1 & 0 & \dots & 0 & -\tilde{a}_1(t) \\ \vdots & & \ddots & & \vdots \\ 0 & 0 & \dots & 0 & -\tilde{a}_{n-2}(t) \\ 0 & 0 & \dots & 1 & -\tilde{a}_{n-1}(t) \end{bmatrix} \begin{bmatrix} z_1 \\ z_2 \\ \vdots \\ z_{n-1} \\ z_n \end{bmatrix} + \begin{bmatrix} \tilde{b}_1(t) \\ \tilde{b}_2(t) \\ \vdots \\ \tilde{b}_{n-2}(t) \\ \tilde{b}_{n-1}(t) \end{bmatrix} u, \quad \mathbf{z}(t=0) = \mathbf{z}_0, \quad (8.220)$$

$$\Delta y = [0 \quad 0 \quad \dots \quad 0 \quad \tilde{c}_{n-1}(t)] \begin{bmatrix} z_1 \\ z_2 \\ \vdots \\ z_{n-1} \\ z_n \end{bmatrix}. \quad (8.221)$$

Transforming the linearized error dynamics to observability normal form with  $\zeta(t) = \mathbf{V}(t)\Delta\tilde{\mathbf{x}}(t)$ , one gets

$$\frac{d}{dt}\zeta(t) = \underbrace{\begin{bmatrix} 0 & 0 & \dots & 0 & -\tilde{a}_0(t) - \tilde{l}_0(t) \\ 1 & 0 & \dots & 0 & -\tilde{a}_1(t) - \tilde{l}_1(t) \\ \vdots & & \ddots & & \vdots \\ 0 & 0 & \dots & 0 & -\tilde{a}_{n-2}(t) - \tilde{l}_{n-2}(t) \\ 0 & 0 & \dots & 1 & -\tilde{a}_{n-1}(t) - \tilde{l}_{n-1}(t) \end{bmatrix}}_{=: \mathbf{E}(t)} \zeta(t), \quad \zeta(t=0) = \zeta_0. \quad (8.222)$$

The idea then is to chose  $\tilde{\mathbf{I}}(t)$  in a way that renders the matrix  $\mathbf{E}(t)$  time invariant and assigns poles with strictly negative real parts to  $\mathbf{E}(t) = \mathbf{E}$ . Transforming back to  $\Delta\tilde{\mathbf{x}}$  coordinates, the observer gain required for asymptotic stabilization of the observer error is  $\mathbf{l}(t) = \mathbf{V}^{-1}(t)\tilde{\mathbf{I}}(t)$ .

In the case of the present variable displacement vane pump system, one obtains

$$\mathbf{A}(t) = \begin{cases} \mathbf{A}_T(t) & \text{for } u_R \geq 0, \\ \mathbf{A}_L(t) & \text{for } u_R < 0 \end{cases} \quad (8.223)$$

with

$$\mathbf{A}_T(t) = \begin{bmatrix} 0 & 1 & 0 & 0 \\ \frac{x_3^* \frac{\partial f_{P1}}{\partial x_1} \Big|_{x_1^*} + \frac{\partial f_{P2}}{\partial x_1} \Big|_{x_1^*} - k_S}{m_{PS}} & -\frac{d_{PS}}{m_{PS}} & \frac{f_{P1}(x_1^*) - A_{S2}}{m_{PS}} & \frac{A_{S1}}{m_{PS}} \\ \frac{\hat{q}_P}{C_{h1}} & \frac{A_{S2}}{C_{h1}} & -\frac{1}{2} \frac{\gamma_F A_{OR1}}{C_{h1} \sqrt{|x_3^*(t) - p_C|}} & 0 \\ 0 & -\frac{A_{S1}}{C_{hS}} & 0 & -\frac{1}{2} \frac{\gamma_F u_R^*(t) b_{Reg}}{C_{hS} \sqrt{|x_4^*(t) - p_0|}} \end{bmatrix}, \quad (8.224)$$

$$\mathbf{A}_L(t) = \begin{bmatrix} 0 & 1 & 0 & 0 \\ \frac{x_3^* \frac{\partial f_{P1}}{\partial x_1} \Big|_{x_1^*} + \frac{\partial f_{P2}}{\partial x_1} \Big|_{x_1^*} - k_S}{m_{PS}} & -\frac{d_{PS}}{m_{PS}} & \frac{f_{P1}(x_1^*) - A_{S2}}{m_{PS}} & \frac{A_{S1}}{m_{PS}} \\ \frac{\hat{q}_P}{C_{h1}} & \frac{A_{S2}}{C_{h1}} & A_{L33} & -\frac{1}{2} \frac{\gamma_F u_R^*(t) b_{Reg}}{C_{h1} \sqrt{|x_3^*(t) - x_4^*(t)|}} \\ 0 & -\frac{A_{S1}}{C_{hS}} & -\frac{1}{2} \frac{\gamma_F u_R^*(t) b_{Reg}}{C_{hS} \sqrt{|x_3^*(t) - x_4^*(t)|}} & \frac{1}{2} \frac{\gamma_F u_R^*(t) b_{Reg}}{C_{hS} \sqrt{|x_3^*(t) - x_4^*(t)|}} \end{bmatrix} \quad (8.225)$$

and

$$A_{L33} = \frac{1}{2C_{h1}} \left( \frac{\gamma_F u_R^*(t) b_{Reg}}{\sqrt{|x_3^*(t) - x_4^*(t)|}} - \frac{\gamma_F A_{OR1}}{\sqrt{|x_3^*(t) - p_C|}} \right). \quad (8.226)$$

The control input matrix for the linearized system is

$$\mathbf{B}(t) = \begin{cases} \mathbf{B}_T(t) & \text{for } u_R \geq 0, \\ \mathbf{B}_L(t) & \text{for } u_R < 0 \end{cases} \quad (8.227)$$

with

$$\mathbf{B}_T(t) = \begin{bmatrix} 0 \\ 0 \\ 0 \\ -\frac{1}{C_{hS}} \text{sign}(x_4^* - p_0) \gamma_F b_{Reg} \sqrt{|x_4^* - p_0|} \end{bmatrix}, \quad (8.228)$$

$$\mathbf{B}_L(t) = \begin{bmatrix} 0 \\ 0 \\ \frac{1}{C_{h1}} \text{sign}(x_3^* - x_4^*) \gamma_F b_{Reg} \sqrt{|x_3^* - x_4^*|} \\ -\frac{1}{C_{h5}} \text{sign}(x_3^* - x_4^*) \gamma_F b_{Reg} \sqrt{|x_3^* - x_4^*|} \end{bmatrix} \quad (8.229)$$

and

$$\mathbf{c}^T = [0 \quad 0 \quad 1 \quad 0]. \quad (8.230)$$

To evaluate the above matrices, the nominal trajectory  $\mathbf{x}^*$  which is being linearized about has to be generated. As a differentially flat output is not available for the system, the generation of a nominal trajectory requires the integration of the internal dynamics as excited by the external dynamics  $\boldsymbol{\xi}^*$ . This integration is complicated by the switching behavior of the internal dynamics as a function of valve input  $u_R$ . Given a desired trajectory  $\mathbf{x}^* \in \mathbb{R}^4$ , however, the corresponding nominal control input  $u_R^*$  can be computed as well so that linearization of the system dynamics about  $\mathbf{x}^*$ ,  $u_R^*$  can be performed. It is to be remarked at this point that the approach outlined above and applied to the system with switched control input matrix is expected to yield asymptotically stable error dynamics as the eigenvalues of the error dynamics are identically placed for both tank-sided and load-sided operating conditions. While this is intuitive, the observer gain calculation depends on each system configuration's normal form. These normal forms are different for tank-side and load-side flow condition, as  $\mathbf{A}_T \neq \mathbf{A}_L$ . Therefore,  $\mathbf{z}(t)$  will not have the same meaning when applied to the tank-side and the load-side flow condition, respectively, so that in fact one obtains  $\mathbf{z}_T(t)$  and  $\mathbf{z}_L(t)$ , respectively. Ultimately, each system configuration will yield asymptotically stable error dynamics as derived from the corresponding normal form – this will, however, not generally guarantee asymptotic stability of the switched error system in a strict sense as is easily demonstrated by the example from Branicky presented in the introduction as stability will also depend on the switching law that switches between the tank-side and load-side flow condition. Because the switching behavior up to this stage of analysis has not yet shown any dysfunctional properties, it is likely that the observer approach based on system linearization will work and should therefore be investigated.

In the next two subsections, two nonlinear local observers based on system linearization about the desired trajectory are thus presented. Observer I makes use of two separate pressure measurements,  $p_1$  and  $p_S$ , or  $x_3$  and  $x_4$  in state space coordinates. Observer II is constructed as a full observer and requires measurement of only  $p_1 = x_3$  for the estimation of all states.

### 8.6.2.1 Nonlinear Local Observer I

Assuming the availability of an additional measurement of  $x_4$ , it is possible to construct a reduced observer for which only an estimation of  $x_1, x_2$  and  $x_3$  needs then to be performed as  $x_4$  is taken to be known from measurement – it is the very knowledge of  $x_4$

that allows for the construction of this reduced observer only partially estimating states. The matrices (8.224) and (8.225) can thereby be reduced by the fourth column and row each, allowing for a simplified observer design. This additional measurement may not only improve the observer performance in general, but can possibly be relevant in case the capacitance  $C_{hS}$  can not be taken constant. Because the associated volume is smaller than that of the main capacitance,  $C_{hS}$  is much more prone to showing a dependence on pump displacement than is  $C_{h1}$ . With an appropriate choice of the design parameter  $\tilde{c}_{n-1}(t)$ , the simplest structure of  $\mathbf{v}(t)$  is the same for both flow conditions:

$$\mathbf{v}(t) = \mathbf{v}_T(t) = \mathbf{v}_L(t) = \begin{bmatrix} -\frac{A_{S2}}{\hat{q}_P} \\ 1 \\ 0 \end{bmatrix}. \quad (8.231)$$

The length of  $\tilde{c}_{n-1}(t) = \{\tilde{c}_{n-1,T}(t), \tilde{c}_{n-1,L}(t)\}$  makes it unsuitable for stating it here explicitly – in its derivation, the symbolic computation abilities of MAPLE were intensely used. From this vector, the repeated application of the  $N$ -operator allows the derivation of the three-component error-stabilizing observer gain also known as time-variant Ackermann formula

$$\mathbf{l}_T(t) = \frac{1}{\tilde{c}_{n-1,T}(t)} \left[ a_0 N_{\mathbf{A}_T}^0 \mathbf{v}(t) + a_1 N_{\mathbf{A}_T}^1 \mathbf{v}(t) + a_2 N_{\mathbf{A}_T}^2 \mathbf{v}(t) + N_{\mathbf{A}_T}^3 \mathbf{v}(t) \right], \quad (8.232)$$

$$\mathbf{l}_L(t) = \frac{1}{\tilde{c}_{n-1,L}(t)} \left[ a_0 N_{\mathbf{A}_L}^0 \mathbf{v}(t) + a_1 N_{\mathbf{A}_L}^1 \mathbf{v}(t) + a_2 N_{\mathbf{A}_L}^2 \mathbf{v}(t) + N_{\mathbf{A}_L}^3 \mathbf{v}(t) \right], \quad (8.233)$$

where the  $a_i$ ,  $i = 0, 1, 2$  are the coefficients of the characteristic polynomial defining the desired pole locations for the observer.

### 8.6.2.2 Nonlinear Local Observer II

If only a measurement of  $p_1 = x_3$  can be made and the displacement dependence of  $C_{hS}$  is negligible for the linearization quality about  $\mathbf{x}^*$ ,  $u_R^*$ , a full observer can be constructed in similar fashion as described above for a reduced observer.

Here, the respective operators are applied to the full linearization matrices from (8.224) and (8.225), starting from a vector  $\mathbf{v}(t)$  for the tank side which, through an appropriate choice of  $\tilde{c}_{n-1}(t)$  assumes the form

$$\mathbf{v}_T(t) = \begin{bmatrix} -A_{S1}A_{S2}^2 \\ \hat{q}_P A_{S1}A_{S2} \\ 0 \\ A_{S2}^2 \frac{\partial f_P}{\partial x_1} - m_{PS} \hat{q}_P^2 + d_{PS} A_{S2} \hat{q}_P - A_{S2}^2 k_S \end{bmatrix}. \quad (8.234)$$

The structural similarity of this vector in its first three components with (8.231) is evident. As for the corresponding vector  $\mathbf{v}_L(t)$ , its length is prohibitive for stating it explicitly. The resulting observer gains for each flow condition, however, are

$$\mathbf{l}_T(t) = \frac{1}{\tilde{c}_{n-1,T}(t)} \left[ a_0 N_{\mathbf{A}_T}^0 \mathbf{v}_T(t) + a_1 N_{\mathbf{A}_T}^1 \mathbf{v}_T(t) + a_2 N_{\mathbf{A}_T}^2 \mathbf{v}_T(t) + a_3 N_{\mathbf{A}_T}^3 \mathbf{v}_T(t) + N_{\mathbf{A}_T}^4 \mathbf{v}_T(t) \right], \quad (8.235)$$

$$\mathbf{l}_L(t) = \frac{1}{\tilde{c}_{n-1,L}(t)} \left[ a_0 N_{\mathbf{A}_L}^0 \mathbf{v}_L(t) + a_1 N_{\mathbf{A}_L}^1 \mathbf{v}_L(t) + a_2 N_{\mathbf{A}_L}^2 \mathbf{v}_L(t) + a_3 N_{\mathbf{A}_L}^3 \mathbf{v}_L(t) + N_{\mathbf{A}_L}^4 \mathbf{v}_L(t) \right] \quad (8.236)$$

with  $a_i$ ,  $i = 0, \dots, 3$  again being the coefficients of the desired characteristic polynomial for the observer.

### 8.6.2.3 Simulation Results

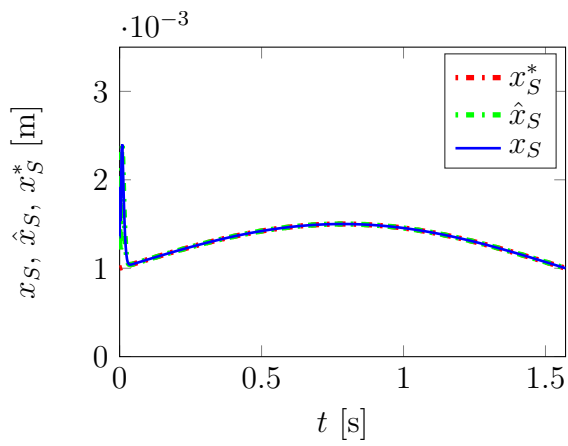
Simulation results for the reduced observer are shown in Figure 8.8.

The results indicate that in principle, state estimation with the reduced observer is possible. A closer look at the results in Figure 8.9 reveal, however, that the convergence behavior of the observer featuring valve dynamics is not ideal as a comparatively extensive transient is evident in the simulation results. While convergence was achieved in the example here, other trajectories to be tracked yielded non-converging results. In addition, extensive simulations revealed that the observer is sensitive with respect to observer initial conditions and numerically sensitive, too.

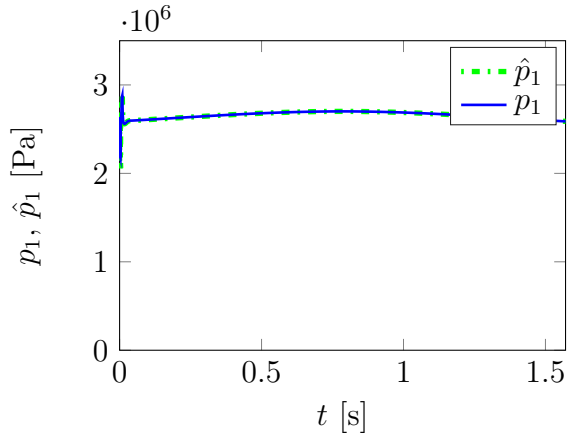
For the full observer, simulation results are shown in Figures 8.10 and 8.11.

While observer and control convergence was achieved, it should be pointed out that this rests heavily upon a significantly increased mass  $m_{PS}$  for these simulations: instead of 0.32kg as in all other simulations, a total mass of 1kg had to be chosen in order to achieve the results shown in Figure 8.10. This makes the applicability of the full nonlinear local tracking observer questionable. As for both reduced and full nonlinear local tracking observer, numerical instability and sensitivity towards observer initial conditions are an issue frequently encountered during simulation, see Figure 8.12 for an example of a non-converging solution.

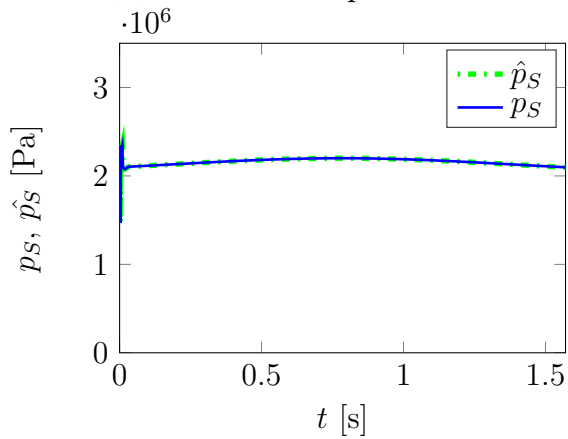
Ultimately, this observer type is far from being implemented easily. To conclude, even though theoretically applicable in some cases, the nonlinear local tracking observers can not be expected to generally yield satisfactory results in the context of this system so that only state estimation based on cam ring displacement appears to be a feasible observer approach.



(a) Pump displacement.

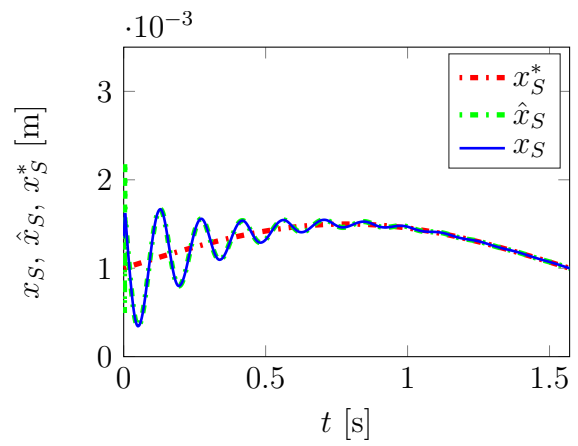


(b) Main chamber pressure.

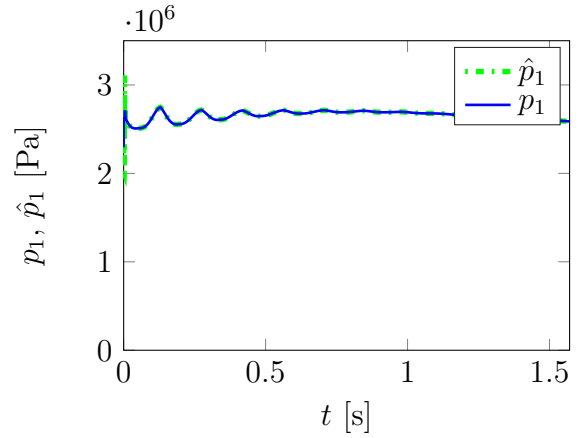


(c) Actuation chamber pressure.

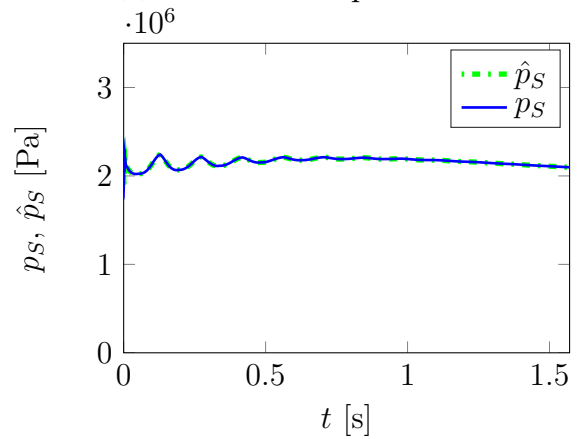
Figure 8.8: Reduced observer: Without valve dynamics.



(a) Pump displacement.

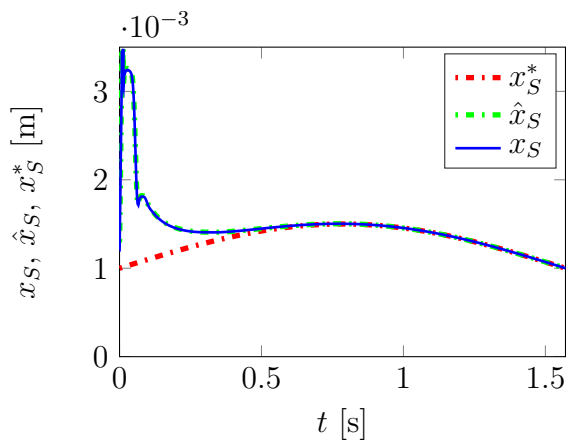


(b) Main chamber pressure.

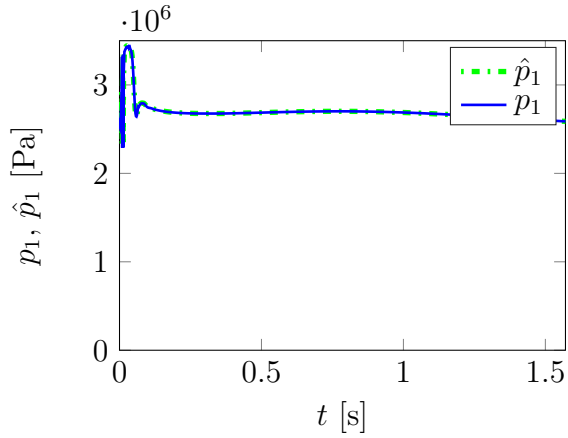


(c) Actuation chamber pressure.

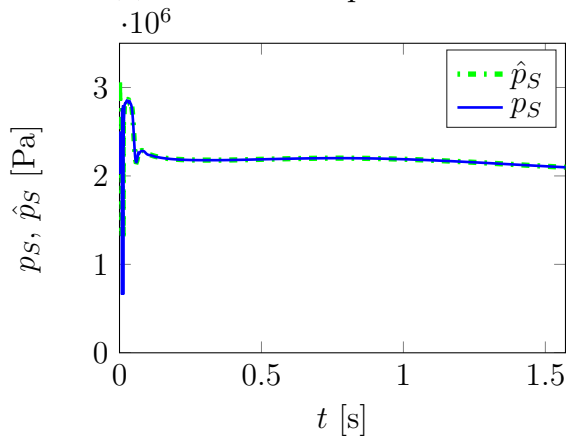
Figure 8.9: Reduced observer: With valve dynamics.



(a) Pump displacement.

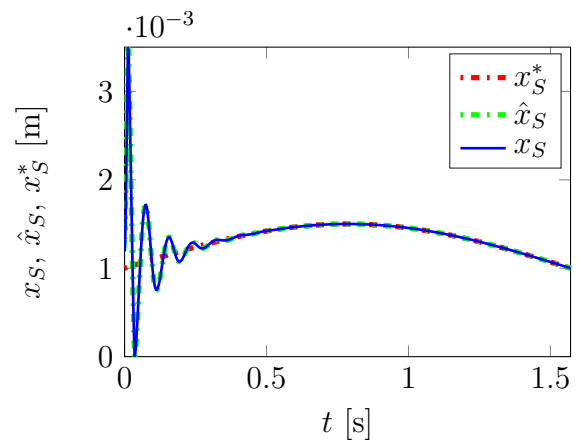


(b) Main chamber pressure.

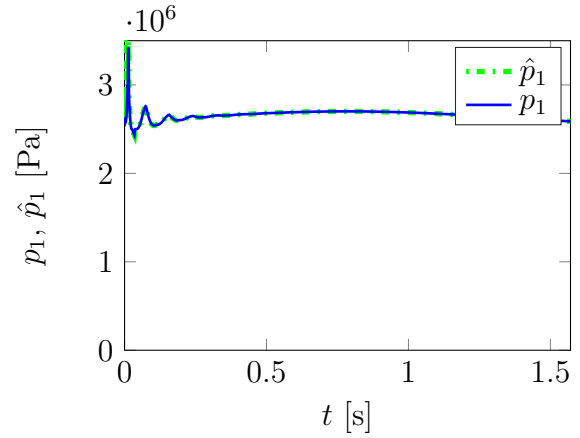


(c) Actuation chamber pressure.

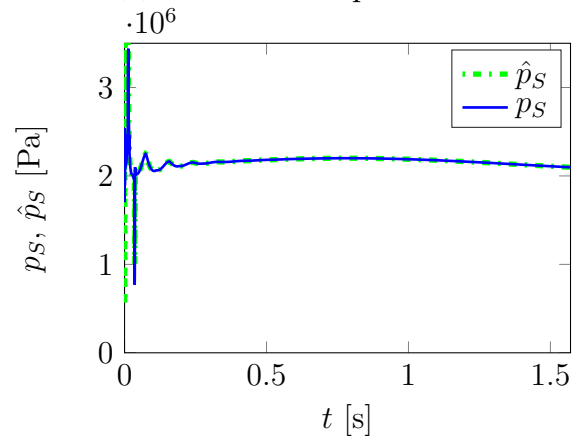
Figure 8.10: Full observer: Without valve dynamics.



(a) Pump displacement.



(b) Main chamber pressure.



(c) Actuation chamber pressure.

Figure 8.11: Full observer: With valve dynamics.

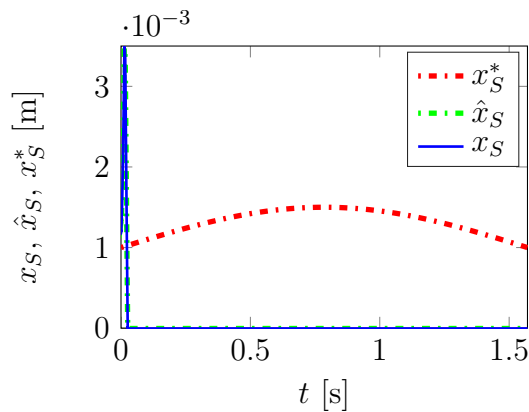


Figure 8.12: Pump displacement for non-convergent simulation – non-zero consumer pressure  $p_C > 0$ .

## 8.7 Feedforward-Linearizing Control

The nonlinear control strategy presented in section 8.4 is suitable for the system at hand in so far that it imposes a linear system behavior by feedback compensation of the nonlinearities of the system. Its functionality rests on a sufficiently accurate model of the system. Unmodeled dynamics or modeling errors of different kinds may prevent the nonlinearity compensation inherent to input-output linearization from functioning well. Even though the control strategies discussed so far show robust behavior, investigating alternative approaches to controlling the system may be worthwhile. As an alternative to input-output-linearizing strategies, it is possible to construct a feedforward control in accordance with the desired output trajectory. The problem with pure feedforward control, however, is a sensitivity to disturbances and initial condition errors which cannot be compensated and therefore may lead to deviations from the desired trajectory or even destabilize the system. Therefore, control effectiveness is typically enhanced by superposing a possibly linear feedback controller whose purpose it is to stabilize the system about the desired output trajectory, see Figure 8.13. This is known as two-degree-of-freedom control design as the feedforward control is conceived independently from the feedback control.

The determination of the feedforward control nominally yielding the desired output trajectory is related to system inversion. The problem of determining the control signal(s) required for a certain desired output trajectory is easy to answer for fully actuated systems which can be inverted directly with the computed torque method. Fundamental results treating the question of system inversion have been presented in [35], addressing the question of system inversion for underactuated systems, too.

In the recent past, it has been found that the same differential-geometrical considerations allowing for a nonlinearity-compensating input-output-linearizing control of nonlinear systems can also be used to construct feedforward control laws. Practically, the

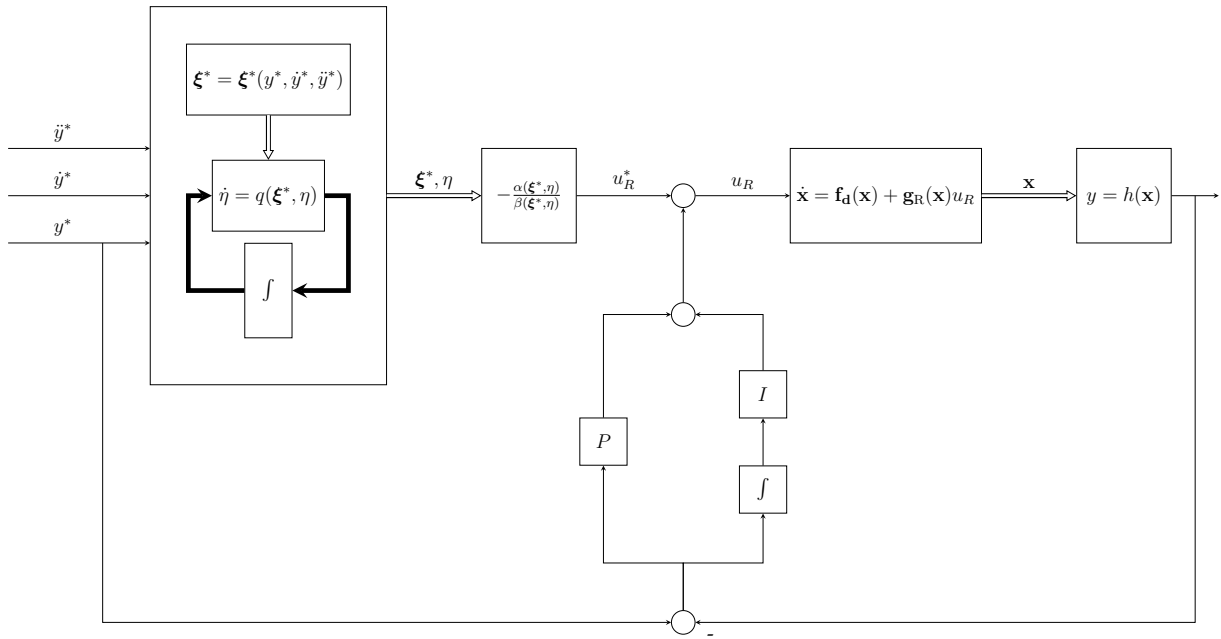


Figure 8.13: Feedforward-linearizing control approach with  $PI$  output feedback.

nominal control input for a non-flat SISO system to follow a desired output trajectory  $y^*$  can be computed from [91]

$$u^* = \frac{y^{*,(r)} - \alpha(\xi^*, \eta)}{\beta(\xi^*, \eta)}. \quad (8.237)$$

From this it can be seen that a SISO system is invertible only if it has a strict relative degree. The  $\eta$  dynamics can be computed from

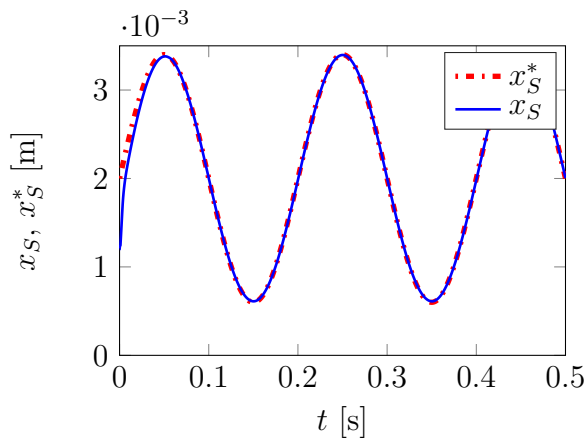
$$\dot{\eta} = q(\xi^*, \eta) \quad (8.238)$$

with arbitrary initial conditions. Now in order for the system to perfectly track the desired output trajectory, it has to hold that

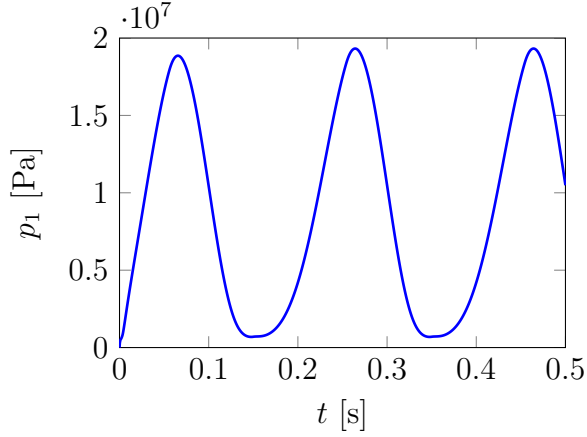
$$\xi(0) = \xi^*(0). \quad (8.239)$$

As this will not practically be fulfilled in many cases which is why for exact output tracking this feedforward control will be superposed with an appropriate feedback controller. Most popularly, this is the well-known  $PID$  control or one of its phenotypes, i.e.  $PI$  or  $PD$  control etc. For differentially flat systems, this approach has become widely treated in the literature as in e.g. [31, 89, 131].

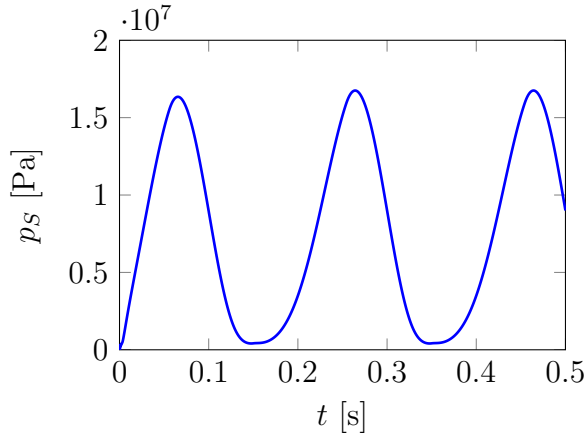
Applying this approach to the vane pump system at hand yields the advantage that in case a simple  $PI$  controller works for stabilizing the system about the desired trajectory  $\xi^*$ , the problem of state estimation is resolved in that essentially an output-feedback technique is used.



(a) Pump displacement.

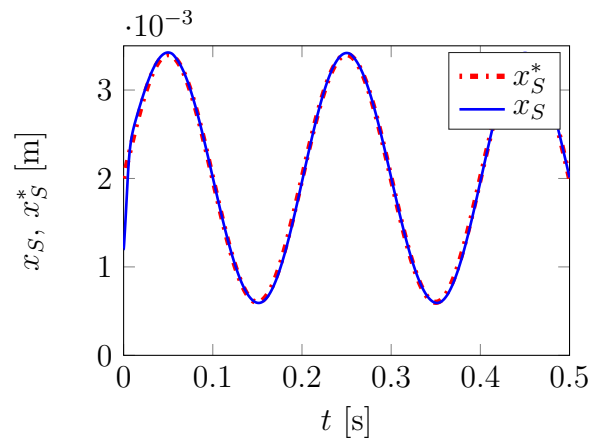


(b) Main chamber pressure.

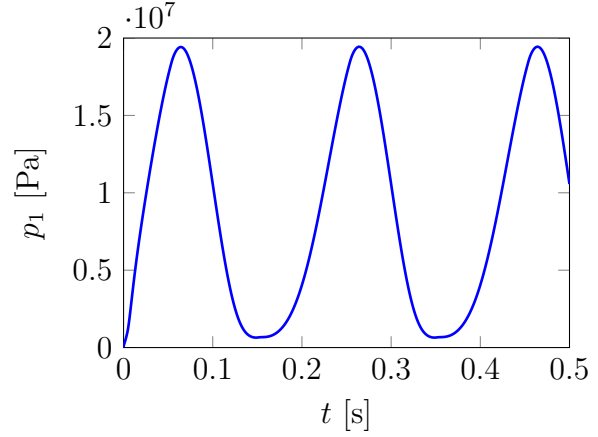


(c) Actuation chamber pressure.

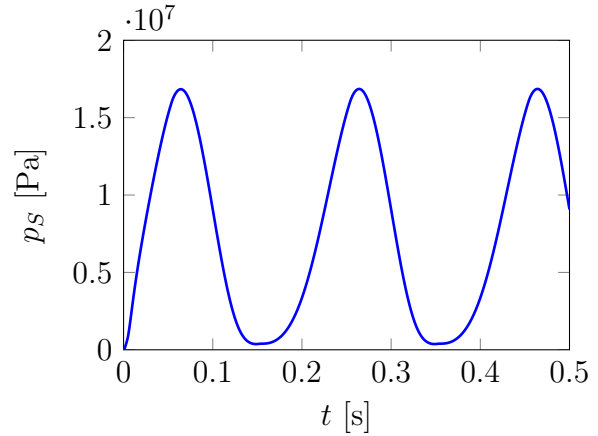
Figure 8.14: Feedforward control: without valve dynamics.



(a) Pump displacement.



(b) Main chamber pressure.



(c) Actuation chamber pressure.

Figure 8.15: Feedforward control: with valve dynamics.

**Simulation results** Simulation results for the feedforward-linearizing control featuring *PI* feedback control are shown in Figure 8.14 for a system with an ideal valve and in Figure 8.15 for a system with a non-ideal valve. The results show that stable trajectory tracking with negligible error can be achieved. Transients from valve dynamics show minor influence.

## 8.8 Intermediate Conclusion

In this chapter, a feedback-linearizing control approach for the nonlinear volume flow control of a variable displacement vane pump system was suggested under the assumption of perfect actuator dynamics, i.e. an ideal servo valve.

With the system behavior showing switching behavior in the control input matrix because, it was shown that the internal dynamics of the system feature a switching behavior accordingly. Stability of the internal dynamics was discussed within the available frameworks, indicating stable system behavior as essentially the external coordinates that are asymptotically stabilized about a desired output trajectory do not have switching properties.

Simulation results show excellent tracking performance of the system, even when actuating the system with the inclusion of valve dynamics and the input derived from a system without valve dynamics.

To account for the need of state availability within the control approach suggested, two different observer types were assessed with respect to their applicability within this context. A high-gain nonlinear observer effectively dominating system nonlinearities yielded very good observation and tracking results too. In addition, a nonlinear local tracking observer was investigated. While results here indicate that this observer can in principle be applied to the observation problem at hand, numerical simulations showed severe sensitivity in terms of observer initialization and physical parameters, so that overall, this observer type is likely to remain a theoretical concept.

The investigation of a feedforward-linearizing control law was shown to bear the potential to remedy the disadvantages of full state control. With the feedforward control law computable offline, a simple stabilizing *PI* output feedback was shown to yield very good results for trajectory tracking.

As for the assumption of a static valve in the derivation of the control laws in this section, inclusion of valve dynamics is no promising approach for two reasons: Firstly, as pointed out in [32], inclusion of valve dynamics significantly complicates the control law and secondly and more importantly, inclusion of the valve dynamics in the plant model for control law derivation can easily be shown to result in switching *external* coordinates. In the control approach suggested here, only the one-dimensional internal

dynamics show switching behavior as a consequence of the switching input matrix  $g_R$  while the external coordinate errors are stabilized. Control laws with switching external coordinates can, if at all, not in general be expected to yield stable tracking behavior. Stability proofs here are expected to be of significant difficulty as the switching system's stability will have to be analyzed for all six states so that the inclusion of valve dynamics in this problem is advised against for future research.

# 9 Nonlinear Control of a Transmission Featuring a Variable Displacement Vane Pump

## 9.1 Background

With ever increasing needs to reduce energy consumption in automotive transmissions, a variable displacement vane pump is a means to do so by adapting volume flow to varying needs of the hydraulic consumer(s). In order to investigate the SISO control approach suggested in chapter 8 in the context of a clutch actuation circuit, the pump needs to be integrated in an according hydraulic circuit conceptually so that an appropriate model of the system can be derived. Naturally, the interaction of the pump dynamics with potentially a multitude of dynamically responding elements makes nonlinear control within automotive transmissions a challenging task. Until now, control concepts for hydraulic control units in automotive transmissions have largely remained linear which is partly due to the use of mainly solenoid valves with pressure feedback. The concept presented in this chapter demonstrates the possibility of alternative control approaches based on purely servo-valve-based control for pressures and pump volume flow.

## 9.2 System Description

The clutch actuation system to be controlled with multiple inputs is shown in Figure 9.1. The pump is again to provide the volume flow for the system whose pressures are controlled through the inputs to the servo valves with inputs  $u_M$  and  $u_C$ . The main pressure valve is to maintain the system pressure whereas the clutch valve is to control the clutch which represents the main hydraulic consumer. The secondary hydraulic consumer is modeled as an ideal consumer with consumer pressure  $p_C$ . As with  $u_R$  in the preceding chapter, inputs  $u_M$  and  $u_C$  will be taken as nominal valve openings.

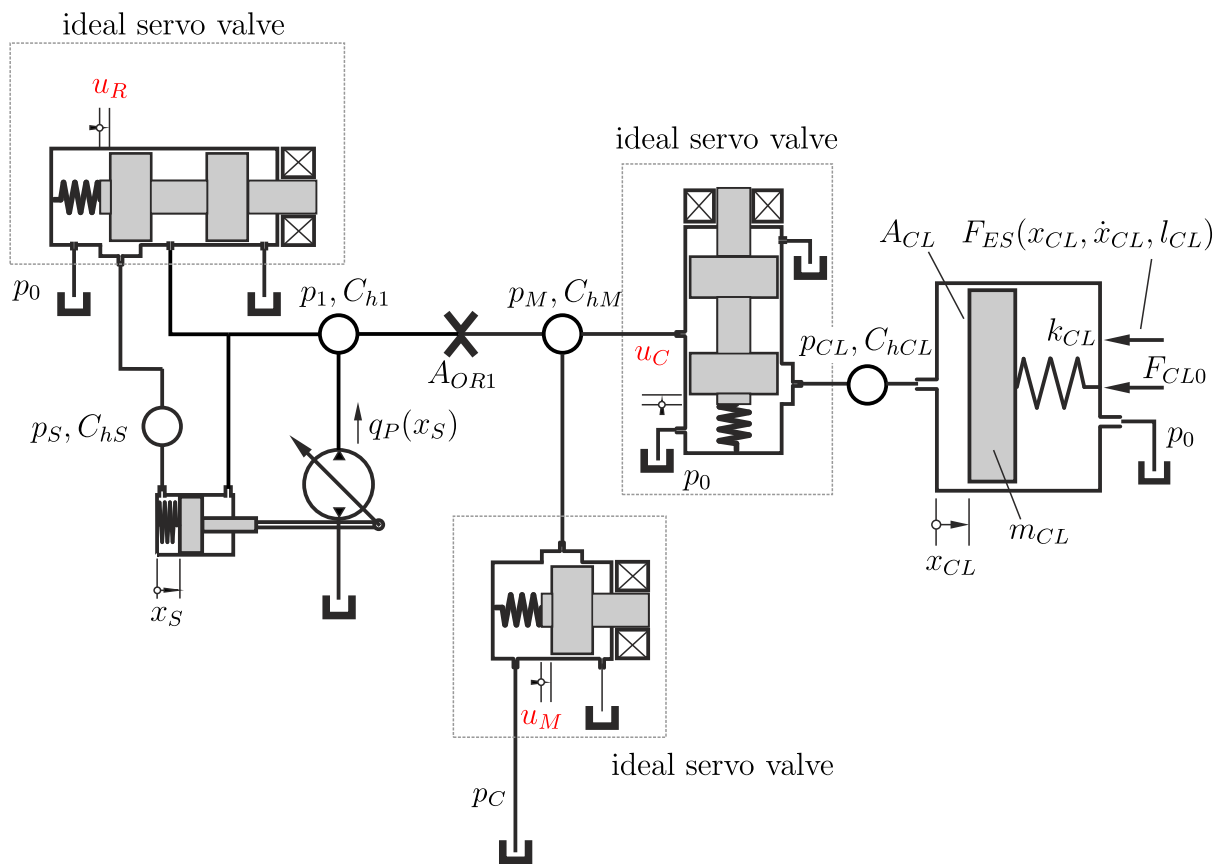


Figure 9.1: Clutch actuation system with servo valves.

### 9.3 MIMO Model

The following model is assumed for the dynamics of the clutch:

$$m_{CL}\ddot{x}_{CL} + d_{CL}\dot{x}_{CL} + k_{CL}x_{CL} = p_{CL}A_{CL} - F_{CL0} - F_{ES}(x_{CL}, \dot{x}_{CL}, l_{CL}). \quad (9.1)$$

The clutch spring is pre-stressed by  $F_{CL0}$  so that in order to actuate the clutch, this pre-stress has to be overcome. End stop forces are again described by (4.5). As in the case of the SISO control problem, the hydraulic balance equations of the system can be stated as

$$\mathbf{C}_h \dot{\mathbf{p}} = \mathbf{Q}\mathbf{q} + \mathbf{A}\dot{\mathbf{x}}_m, \quad (9.2)$$

where

$$\mathbf{C}_h = \begin{bmatrix} C_{h1} & 0 & 0 & 0 \\ 0 & C_{hS} & 0 & 0 \\ 0 & 0 & C_{hM} & 0 \\ 0 & 0 & 0 & C_{hCL} \end{bmatrix}, \quad \mathbf{Q} = \begin{bmatrix} 1 & -1 & 0 & -1 & 0 & 0 & 0 \\ 0 & 1 & -1 & 0 & 0 & 0 & 0 \\ 0 & 0 & 0 & 1 & -1 & 1 & 0 \\ 0 & 0 & 0 & 0 & 0 & -1 & -1 \end{bmatrix},$$

$$\mathbf{A} = \begin{bmatrix} A_{S2} & 0 \\ -A_{S1} & 0 \\ 0 & 0 \\ 0 & -A_{CL} \end{bmatrix}, \quad (9.3)$$

and the mechanical and hydraulic degrees of freedom

$$\mathbf{x}_m = [x_S \quad x_{CL}]^T, \quad \mathbf{p} = [p_1 \quad p_S \quad p_M \quad p_{CL}]^T. \quad (9.4)$$

The volume flows appearing in equation (9.2) are

$$\mathbf{q} = [q_P \quad q_R \quad q_T \quad q_{OR1} \quad q_M \quad q_{CLPA} \quad q_{CLAT}]^T. \quad (9.5)$$

The volume flows  $q_R$  and  $q_T$  are known from (8.11) and (8.12), respectively. The other volume flows are governed by the equations

$$q_{OR1} = \text{sign}(p_1 - p_M) \gamma_F A_{OR1} \sqrt{|p_1 - p_M|}, \quad (9.6)$$

$$q_M = \begin{cases} \text{sign}(p_M - p_C) \gamma_F b_M u_M \sqrt{|p_M - p_C|} & \text{for } u_M \geq 0, \\ 0 & \text{for } u_M < 0, \end{cases} \quad (9.7)$$

$$q_{CLPA} = \begin{cases} 0 & \text{for } u_C \geq 0, \\ \text{sign}(p_M - p_{CL}) \gamma_F b_{CL} u_C \sqrt{|p_M - p_{CL}|} & \text{for } u_C < 0, \end{cases} \quad (9.8)$$

$$q_{CLAT} = \begin{cases} \text{sign}(p_{CL} - p_0)\gamma_F b_{CL} u_C \sqrt{|p_{CL} - p_0|} & \text{for } u_C \geq 0, \\ 0 & \text{for } u_C < 0. \end{cases} \quad (9.9)$$

The capacitances are computed from (6.8) and (6.9) and read

$$C_{hM} = \frac{V_{M0}}{E_{fl}}, \quad C_{hCL} = \frac{V_{CL0} + A_{CL}x_{CL}}{E_{fl}}. \quad (9.10)$$

The parameters related to the modeling of the elements new to this chapter are given in table 9.1.

Table 9.1: Parameters of the transmission system.

Parameter	Symbol	Value	Unit
Clutch mass	$m_{CL}$	3	kg
Clutch damping	$d_{CL}$	60	Ns/m
Clutch stiffness	$k_{CL}$	$10 \times 10^5$	N/m
Clutch cylinder area	$A_{CL}$	$\pi/4 \times 0.05^2$	m
Main volume	$V_{M0}$	$5 \times 10^{-4}$	m <sup>3</sup>
Clutch volume	$V_{CL0}$	$5 \times 10^{-4}$	m <sup>3</sup>

In the situation at hand, the purpose is to synthesize a control law controlling the system by means of three system inputs. One input,  $u_R$  is to act on the regulator valve as outlined in section 8.4. The two other inputs are applied to the main pressure control valve and the clutch valve:  $u_M$  is to act on the main pressure valve in order to ensure the line pressure is kept at the desired level and  $u_C$  to the clutch valve. Again assuming servo valves with ideal, i.e. static behavior, the state space formulation of the plant model derived from equation (9.1) et sqq. reads

$$\dot{\mathbf{x}} = \mathbf{f}_d(\mathbf{x}) + \mathbf{g}_R(\mathbf{x})u_R + \mathbf{g}_C(\mathbf{x})u_C + \mathbf{g}_M(\mathbf{x})u_M \quad (9.11)$$

with the state space vector

$$\mathbf{x} = \begin{bmatrix} x_S & \dot{x}_S & p_1 & p_S & p_M & p_{CL} & x_{CL} & \dot{x}_{CL} \end{bmatrix}^T \quad (9.12)$$

$$= \begin{bmatrix} x_1 & x_2 & x_3 & x_4 & x_5 & x_6 & x_7 & x_8 \end{bmatrix}^T. \quad (9.13)$$

The drift term for the model thus is

$$\mathbf{f}_d(\mathbf{x}) = \begin{bmatrix} x_2 \\ \frac{1}{m_{PS}} [k_S l_S + F_{S0} - k_S x_1 - d_{PS} x_2 - A_{S2} x_3 + A_{S1} x_4 + f_P(x_1, x_3)] \\ \frac{1}{C_{h1}} [\hat{q}_P(x_1 - x_S^{offset}) - \text{sign}(x_3 - x_5) \gamma_F A_{OR1} \sqrt{|x_3 - x_5|} + A_{S2} x_2] \\ -\frac{A_{S1}}{C_{hS}} x_2 \\ \frac{1}{C_{hM}} \text{sign}(x_3 - x_5) \gamma_F A_{OR1} \sqrt{|x_3 - x_5|} \\ -\frac{A_{CL}}{C_{hCL}} x_8 \\ x_8 \\ \frac{1}{m_{CL}} [-F_{CL0} + A_{CL} x_6 - k_{CL} x_7 - d_{CL} x_8] \end{bmatrix}. \quad (9.14)$$

The input matrices are

$$\mathbf{g}_R(\mathbf{x}) = \begin{bmatrix} 0 \\ 0 \\ \frac{1}{C_{h1}} \delta_L \tilde{q}_R \\ \frac{1}{C_{hS}} [-\delta_L \tilde{q}_R - \delta_T \tilde{q}_T] \\ 0 \\ 0 \\ 0 \\ 0 \end{bmatrix}, \quad (9.15) \quad \mathbf{g}_M(\mathbf{x}) = \begin{bmatrix} 0 \\ 0 \\ 0 \\ 0 \\ -\frac{\delta_M}{C_{hM}} \tilde{q}_M \\ 0 \\ 0 \end{bmatrix}, \quad (9.16)$$

$$\mathbf{g}_C(\mathbf{x}) = \begin{bmatrix} 0 \\ 0 \\ 0 \\ 0 \\ \frac{1}{C_{hM}} \delta_{CLPA} \tilde{q}_{CLPA} \\ \frac{1}{C_{hCL}} (-\delta_{CLPA} \tilde{q}_{CLPA} - \delta_{CLAT} \tilde{q}_{CLAT}) \\ 0 \\ 0 \end{bmatrix}, \quad (9.17)$$

with

$$\tilde{q}_R = \text{sign}(x_3 - x_4) \gamma_F b_{Reg} \sqrt{|x_3 - x_4|}, \quad (9.18)$$

$$\tilde{q}_T = \text{sign}(x_4 - p_0) \gamma_F b_{Reg} \sqrt{|x_4 - p_0|}, \quad (9.19)$$

$$\tilde{q}_M = \text{sign}(x_5 - p_C) \gamma_F b_M \sqrt{|x_5 - p_C|}, \quad (9.20)$$

$$\tilde{q}_{CLPA} = \text{sign}(x_5 - x_6) \gamma_F b_{CL} \sqrt{|x_5 - x_6|}, \quad (9.21)$$

$$\tilde{q}_{CLAT} = \text{sign}(x_6 - p_0) \gamma_F b_{CL} \sqrt{|x_6 - p_0|}. \quad (9.22)$$

In (9.15) – (9.17), dummy variables  $\delta_i$  were made use of to allow for a concentrated notation. Specifically,

$$\delta_L = \begin{cases} 1 & \text{if } u_R < 0, \\ 0 & \text{else} \end{cases} \quad \delta_T = 1 - \delta_L, \quad (9.23)$$

$$\delta_M = \begin{cases} 1 & \text{if } u_M \geq 0, \\ 0 & \text{else} \end{cases} \quad (9.24)$$

$$\delta_{CLPA} = \begin{cases} 1 & \text{if } u_C < 0, \\ 0 & \text{else} \end{cases} \quad \delta_{CLAT} = 1 - \delta_{CLPA}. \quad (9.25)$$

To complete the system description, the system outputs, according to controlling volume flow via  $x_S - x_S^{offset} = x_1 - x_S^{offset}$ , main pressure  $p_M = x_5$  and clutch pressure  $p_{CL} = x_6$ , are taken as

$$h_1(\mathbf{x}) = x_1 - x_S^{offset}, \quad (9.26)$$

$$h_2(\mathbf{x}) = x_5, \quad (9.27)$$

$$h_3(\mathbf{x}) = x_6. \quad (9.28)$$

## 9.4 Feedback-Linearizing Control

With the input-affine state space representation (9.14) et sqq. of the system dynamics, the system is now in the form to be subjected to the feedback-linearizing control technique outlined in chapter 7.

### 9.4.1 Control Synthesis

**Determining the relative degree** Performing the Lie derivations for the first system output, the pump displacement  $x_1 - x_S^{offset}$ , shows that (8.24) to (8.29) yield the respective expressions for the Lie derivatives of the system  $h_1(\mathbf{x}) = x_1 - x_S^{offset}$  and of  $\mathcal{L}_{f_d}^j h_1(\mathbf{x})$  along  $\mathbf{g}_R$  for  $j = 0, 1, 2$ . Building the derivatives of  $\mathcal{L}_{f_d}^j h_1(\mathbf{x})$  along  $\mathbf{g}_R, \mathbf{g}_M, \mathbf{g}_C$  for  $j = 0, 1$  shows that

$$\mathcal{L}_{\mathbf{g}_R} h_1(\mathbf{x}) = 0, \quad \mathcal{L}_{\mathbf{g}_M} h_1(\mathbf{x}) = 0, \quad \mathcal{L}_{\mathbf{g}_C} h_1(\mathbf{x}) = 0, \quad (9.29)$$

$$\mathcal{L}_{\mathbf{g}_R} \mathcal{L}_{f_d} h_1(\mathbf{x}) = 0, \quad \mathcal{L}_{\mathbf{g}_M} \mathcal{L}_{f_d} h_1(\mathbf{x}) = 0, \quad \mathcal{L}_{\mathbf{g}_C} \mathcal{L}_{f_d} h_1(\mathbf{x}) = 0 \quad (9.30)$$

and, for  $j = 2$ ,

$$\begin{aligned} \mathcal{L}_{\mathbf{g}_R} \mathcal{L}_{\mathbf{f}_d}^2 h_1(\mathbf{x}) = & \left[ \delta_L \left( - \left( A_{S2} + A_{S1} \frac{C_{h1}}{C_{hS}} \right) \right. \right. \\ & \left. \left. + \frac{\partial f_P(x_1, x_3)}{\partial x_3} \right) \text{sign}(x_3 - x_4) \gamma_F b_{Reg} \sqrt{|x_3 - x_4|} \right. \\ & \left. - \delta_T A_{S1} \frac{C_{h1}}{C_{hS}} \text{sign}(x_4 - p_0) \gamma_F b_{Reg} \sqrt{|x_4 - p_0|} \right] \frac{1}{m_{PS} C_{h1}}, \end{aligned} \quad (9.31)$$

$$\mathcal{L}_{\mathbf{g}_M} \mathcal{L}_{\mathbf{f}_d}^2 h_1(\mathbf{x}) = 0, \quad (9.32)$$

$$\mathcal{L}_{\mathbf{g}_C} \mathcal{L}_{\mathbf{f}_d}^2 h_1(\mathbf{x}) = 0, \quad (9.33)$$

so that the relative degree of output  $h_1(\mathbf{x})$  is  $r_1 = 3$ .

For system output  $h_2(\mathbf{x}) = x_5$ , the following expressions can be derived:

$$\mathcal{L}_{\mathbf{g}_R} h_2(\mathbf{x}) = 0, \quad (9.34)$$

$$\mathcal{L}_{\mathbf{g}_M} h_2(\mathbf{x}) = -\frac{\delta_M}{C_{hM}} \text{sign}(x_5 - p_C) \gamma_F b_M \sqrt{|x_5 - p_C|}, \quad (9.35)$$

$$\mathcal{L}_{\mathbf{g}_C} h_2(\mathbf{x}) = \frac{1}{C_{hM}} \delta_{CLPA} \text{sign}(x_5 - x_6) \gamma_F b_{CL} \sqrt{|x_5 - x_6|}. \quad (9.36)$$

The relative degree of output  $h_2(\mathbf{x})$  therefore is  $r_2 = 1$ .

Ultimately, the relative degree of the third output,  $h_3(\mathbf{x}) = x_6$  is computed from

$$\mathcal{L}_{\mathbf{g}_R} h_3(\mathbf{x}) = 0, \quad (9.37)$$

$$\mathcal{L}_{\mathbf{g}_M} h_3(\mathbf{x}) = 0, \quad (9.38)$$

$$\begin{aligned} \mathcal{L}_{\mathbf{g}_C} h_3(\mathbf{x}) = & -\frac{1}{C_{hCL}} \left( \delta_{CLPA} \text{sign}(x_5 - x_6) \gamma_F b_{CL} \sqrt{|x_5 - x_6|} \right. \\ & \left. + \delta_{CLAT} \text{sign}(x_6 - p_0) \gamma_F b_{CL} \sqrt{|x_6 - p_0|} \right), \end{aligned} \quad (9.39)$$

so that  $r_3 = 1$ , too.

**Transforming into normal form** The internal dynamics for the pump unit and its control valve are equivalent to those of the SISO-case. As now a hydraulic consumer model is connected to the pump outlet, the internal dynamics have to be investigated. From physical considerations, these can be linked with the dynamics of the clutch mass, thus leading to a choice of  $x_7, x_8$  for the internal dynamics associated with the third

system output,  $h_3(\mathbf{x})$ . From this it follows that the transformation law for the change of coordinates can be stated as

$$\begin{bmatrix} \xi \\ \eta \end{bmatrix} = \begin{bmatrix} \xi_{1,1} \\ \xi_{1,2} \\ \xi_{1,3} \\ \xi_{2,1} \\ \xi_{3,1} \\ \eta_{1,1} \\ \eta_{2,1} \\ \eta_{2,2} \end{bmatrix} = \Phi(\mathbf{x}) = \begin{bmatrix} h_1(\mathbf{x}) \\ \mathcal{L}_{f_d} h_1(\mathbf{x}) \\ \mathcal{L}_{f_d}^2 h_1(\mathbf{x}) \\ h_2(\mathbf{x}) \\ h_3(\mathbf{x}) \\ \delta_L(\Psi_1(C_{h_1}x_3 + C_{h_S}x_4) + \Psi_2) + \delta_T x_3 \\ x_7 \\ x_8 \end{bmatrix} \quad (9.40)$$

$$= \begin{bmatrix} x_1 - x_S^{offset} \\ x_2 \\ -\frac{1}{m_{PS}}(k_S x_1 - A_{S1}x_4 + A_{S2}x_3 + d_{PS}x_2 - f_P(x_1, x_3) - k_S l_S - F_{S0}) \\ x_5 \\ x_6 \\ \delta_L(\Psi_1(C_{h_1}x_3 + C_{h_S}x_4) + \Psi_2) + \delta_T x_3 \\ x_7 \\ x_8 \end{bmatrix}. \quad (9.41)$$

Its Jacobian,

$$\frac{d\Phi(\mathbf{x})}{d\mathbf{x}} = \begin{bmatrix} 1 & 0 & 0 & 0 & 0 & 0 & 0 & 0 \\ 0 & 1 & 0 & 0 & 0 & 0 & 0 & 0 \\ J_{31} & -\frac{d_{PS}}{m_{PS}} & J_{33} & \frac{A_{S1}}{m_{PS}} & 0 & 0 & 0 & 0 \\ 0 & 0 & 0 & 0 & 1 & 0 & 0 & 0 \\ 0 & 0 & J_{53} & J_{54} & 0 & 0 & 0 & 0 \\ 0 & 0 & 0 & 0 & 0 & 1 & 0 & 0 \\ 0 & 0 & 0 & 0 & 0 & 0 & 1 & 0 \\ 0 & 0 & 0 & 0 & 0 & 0 & 0 & 1 \end{bmatrix} \quad (9.42)$$

with

$$J_{31} = \frac{-k_S + \frac{\partial f_P}{\partial x_1}}{m_{PS}}, \quad J_{33} = \frac{-A_{S2} + \frac{\partial f_P}{\partial x_3}}{m_{PS}},$$

$$J_{53} = \delta_L \Psi_1 C_{h1} + \delta_T, \quad J_{54} = \delta_L \Psi_1 C_{hS},$$

fulfills the invertibility condition, so that (9.40) constitutes a diffeomorphism in  $\mathcal{D}$  irrespective of the flow condition of the regulator valve, i.e. whether  $u_R \geq 0$  or  $u_R < 0$ .

Using the diffeomorphism found, the Byrnes-Isidori normal form becomes

$$\begin{bmatrix} \dot{\xi}_{1,1} \\ \dot{\xi}_{1,2} \\ \dot{\xi}_{1,3} \\ \dot{\xi}_{2,1} \\ \dot{\xi}_{3,1} \\ \dot{\eta}_{1,1} \\ \dot{\eta}_{2,1} \\ \dot{\eta}_{2,2} \end{bmatrix} = \begin{bmatrix} \xi_{1,2} \\ \xi_{1,3} \\ a_1(\Phi^{-1}(\xi, \eta)) + B_{11}(\Phi^{-1}(\xi, \eta))u_R \\ a_2(\Phi^{-1}(\xi, \eta)) + B_{22}(\Phi^{-1}(\xi, \eta))u_M + B_{23}(\Phi^{-1}(\xi, \eta))u_C \\ a_3(\Phi^{-1}(\xi, \eta)) + B_{33}(\Phi^{-1}(\xi, \eta))u_C \\ \dot{\Phi}_6(\mathbf{x}) \\ \dot{\Phi}_7(\mathbf{x}) \\ \dot{\Phi}_8(\mathbf{x}) \end{bmatrix} \quad (9.43)$$

with the inverse of the decoupling matrix which in physical coordinates is

$$\begin{aligned} \mathbf{B}(\Phi^{-1}(\xi, \eta)) = \mathbf{B}(\mathbf{x}) &= \begin{bmatrix} B_{11} & B_{12} & B_{13} \\ B_{21} & B_{22} & B_{23} \\ B_{31} & B_{32} & B_{33} \end{bmatrix} \\ &= \begin{bmatrix} \mathcal{L}_{\mathbf{g}_R} \mathcal{L}_{\mathbf{f}_d}^2 h_1(\mathbf{x}) & 0 & 0 \\ 0 & \mathcal{L}_{\mathbf{g}_M} h_2(\mathbf{x}) & \mathcal{L}_{\mathbf{g}_C} h_2(\mathbf{x}) \\ 0 & 0 & \mathcal{L}_{\mathbf{g}_C} h_3(\mathbf{x}) \end{bmatrix}, \end{aligned} \quad (9.44)$$

making use of (9.31) to (9.39) and with the transformed plant nonlinearities which in physical coordinates can be given as

$$\begin{aligned} \mathbf{a}(\Phi^{-1}(\xi, \eta)) = \mathbf{a}(\mathbf{x}) &= \begin{bmatrix} \mathcal{L}_{\mathbf{f}_d}^3 h_1(\mathbf{x}) \\ \mathcal{L}_{\mathbf{f}_d} h_2(\mathbf{x}) \\ \mathcal{L}_{\mathbf{f}_d} h_3(\mathbf{x}) \end{bmatrix} \\ &= \begin{bmatrix} \frac{1}{m_{PS}} \left( \left( \frac{\partial f_P}{\partial x_1} - k_S - \frac{A_{S1}^2}{C_{hS}} \right) f_{d1}(\mathbf{x}) - \frac{d_{PS}}{m_{PS}} f_{d2}(\mathbf{x}) - \frac{A_{S2}}{C_{h1}} \frac{\partial f_P}{\partial x_3} f_{d3}(\mathbf{x}) \right) \\ \frac{1}{C_{hM}} \text{sign}(x_3 - x_5) \gamma_F A_{OR1} \sqrt{|x_3 - x_5|} \\ -\frac{1}{C_{hCL}} A_{CL} x_8 \end{bmatrix}. \end{aligned} \quad (9.45)$$

Here,  $f_{d1}(\mathbf{x})$ ,  $f_{d2}(\mathbf{x})$ ,  $f_{d3}(\mathbf{x})$  are the first three entries of the drift matrix (9.14), respectively. Unsurprisingly, the first entry in  $\mathbf{a}$  is identical with expression (8.36) from chapter 8 when substituting  $p_C$  for  $x_5$ .

**Synthesizing the control law** The corresponding plant- or drift-nonlinearity compensating control is determined by expression (9.45). Thus, with equation (7.44), the control law is

$$\mathbf{u} = \mathbf{B}^{-1}(\Phi^{-1}(\xi, \eta))(\boldsymbol{\nu} - \mathbf{a}(\Phi^{-1}(\xi, \eta)))$$

featuring matrix  $\mathbf{B}(\Phi^{-1}(\xi, \eta))$  given by (9.44) and with the new input  $\nu$  chosen as

$$\nu = \begin{bmatrix} -k_{11}(\xi_{1,1} - \xi_{1,1}^*) - k_{12}(\xi_{1,2} - \dot{\xi}_{1,1}^*) - k_{13}(\xi_{1,3} - \ddot{\xi}_{1,1}^*) + \ddot{\xi}_{1,1}^* \\ -k_{21}(\xi_{2,1} - \xi_{2,1}^*) + \dot{\xi}_{2,1}^* \\ -k_{31}(\xi_{3,1} - \xi_{3,1}^*) + \dot{\xi}_{3,1}^* \end{bmatrix} \quad (9.46)$$

in order to stabilize the system about the desired trajectory  $\xi^*$  by appropriate choice (pole placement design) of the factors  $k_{ij}$  with  $i, j \in [1, 3]$ .

**Investigating the zero dynamics** The internal dynamics  $\eta_{1,1}$  are essentially identical with the internal dynamics discussed in section 8.4. As for  $\eta_{2,1}, \eta_{2,2}$ , the dynamics are given by the clutch dynamics

$$\dot{\eta}_{2,1} = \eta_{2,2}, \quad (9.47)$$

$$\dot{\eta}_{2,2} = \frac{1}{m_{CL}} (\xi_{3,1} A_{CL} - d_{CL} \eta_{2,2} - k_{CL} \eta_{2,1} - F_{CL0} - F_{ES}(\eta_{2,1}, \eta_{2,2}, l_{CL})) \quad (9.48)$$

and, by setting  $\xi = \mathbf{0}$ , the following globally exponentially stable zero dynamics

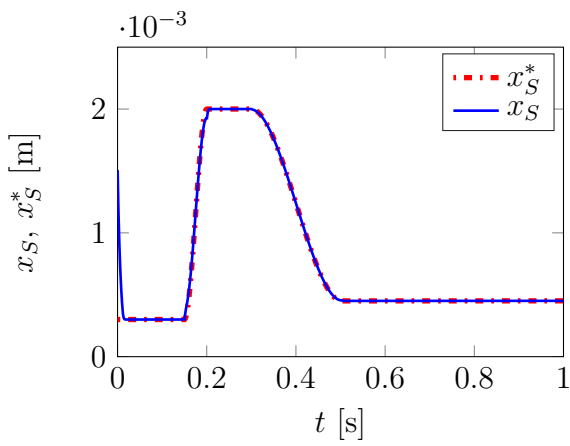
$$\dot{\eta}_{2,1} = \eta_{2,2}, \quad (9.49)$$

$$\dot{\eta}_{2,2} = \frac{1}{m_{CL}} (-d_{CL} \eta_{2,2} - k_{CL} \eta_{2,1} - F_{CL0} - F_{ES}(\eta_{2,1}, \eta_{2,2}, l_{CL})). \quad (9.50)$$

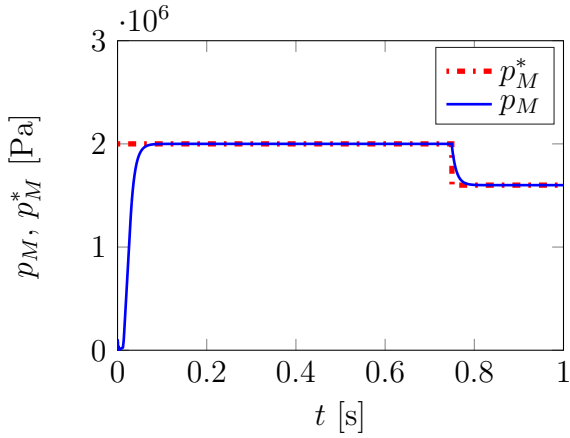
## 9.4.2 Simulation Results

The simulation results in Figures 9.2 and 9.3 demonstrate that a nonlinear multiple input, multiple output control approach yields potential for real life application in the context of clutch actuation.

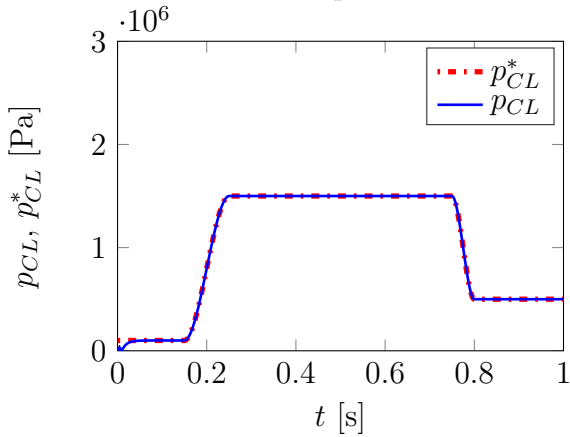
The simulation results show trajectory tracking for an increase in pump flow needed for clutch actuation. Main pressure is to be held constant with a step change at  $t = 0.75\text{s}$  while the clutch pressure shall track a signal leading to clutch actuation. For a system with an ideal valve, very good trajectory tracking results are achieved. Figure 9.3 shows, however, that transients from valve dynamics may play a more significant role than in a SISO-system. While transients from valve dynamics are known to possibly play a role (e.g. [41]) in hydraulic servo systems, to the best of this thesis' author's knowledge transients from valve dynamics have not been researched thoroughly in the context of multiple input systems. The results in Figure 9.3 indicate that transient interaction within multiple input system is detrimental to system performance. It stands to reason that this type of effect will also be observed in experiments.



(a) Pump displacement.

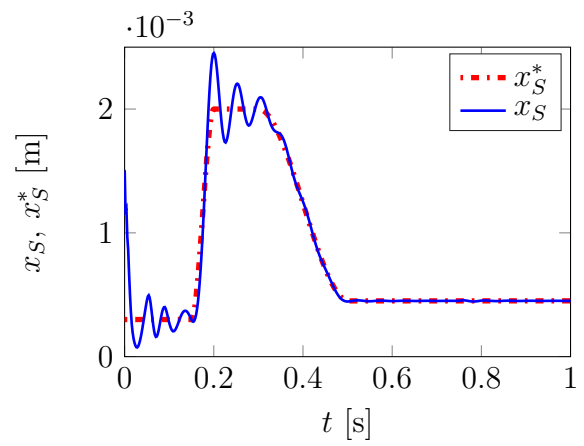


(b) Main circuit pressure.

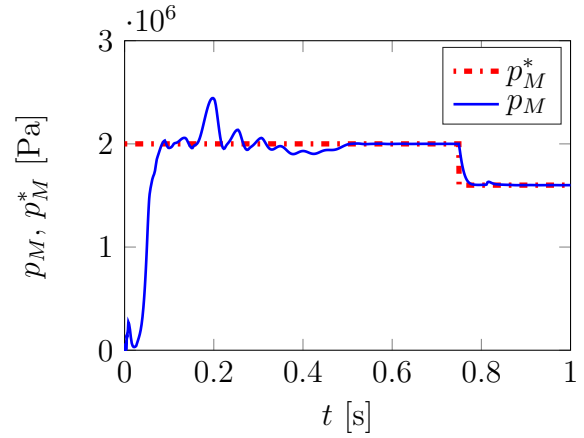


(c) Clutch pressure.

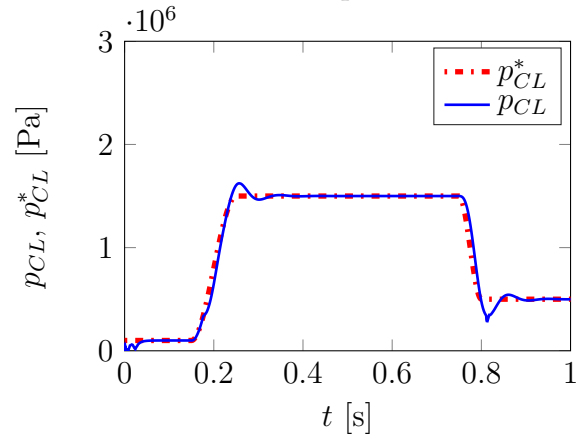
Figure 9.2: Control outputs: without valve dynamics.



(a) Pump displacement.

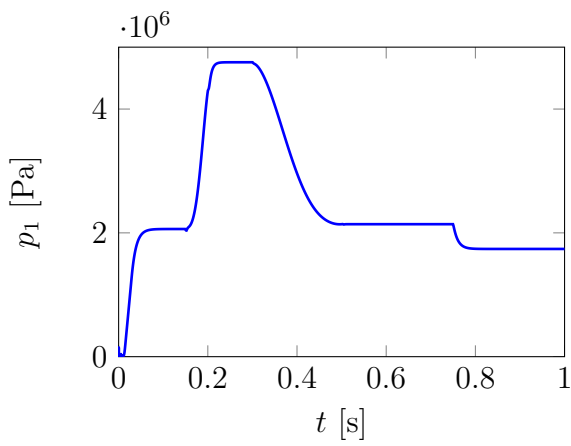


(b) Main circuit pressure.

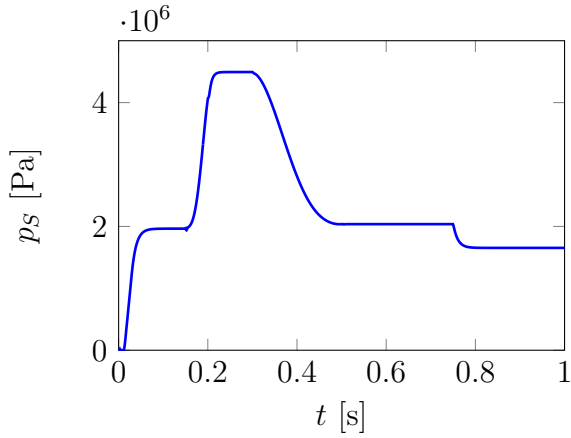


(c) Clutch pressure.

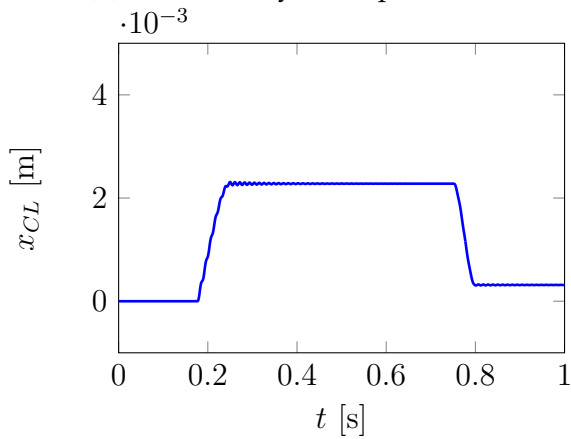
Figure 9.3: Control outputs: with valve dynamics.



(a) Pressure in capacitance  $C_{h1}$ .

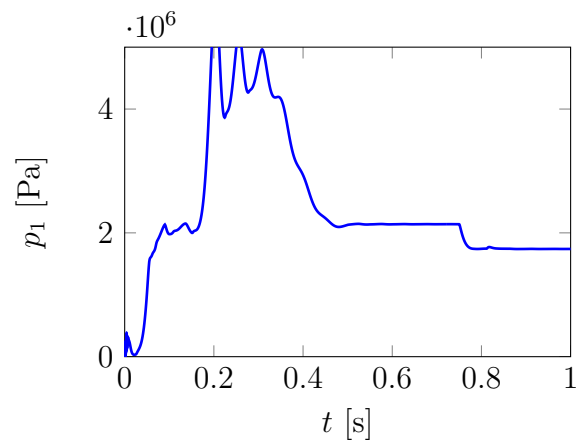


(b) Actuation cylinder pressure.

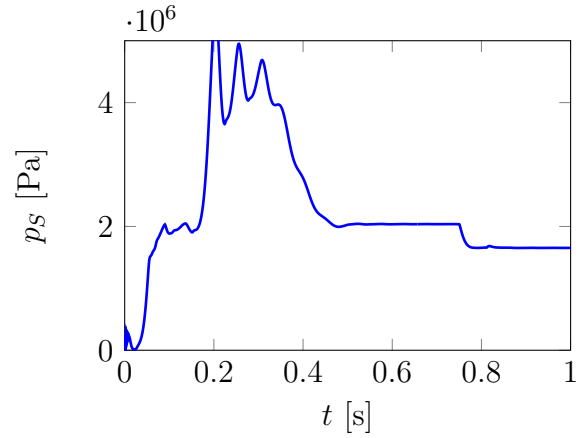


(c) Clutch displacement.

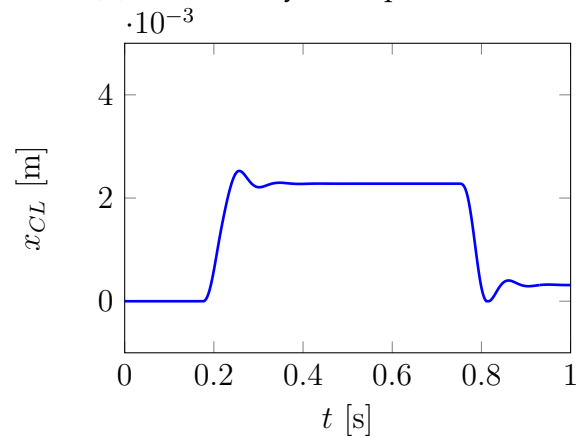
Figure 9.4: Auxiliary states: without valve dynamics.



(a) Pressure in capacitance  $C_{h1}$ .



(b) Actuation cylinder pressure.



(c) Clutch displacement.

Figure 9.5: Auxiliary states: with valve dynamics.

## 9.5 Observer Designs for Clutch Actuation

The control approach presented is to provide the clutch cylinders with pressure so that synchronization in the transmission can take place according to the specification at hand. With the MIMO input-output-linearizing control being a state space method, an obvious question to ask how to implement the clutch actuation control law  $u_C$  as it features the clutch displacement velocity  $\dot{x}_{CL} = x_8$ , see equation (9.45). The proposed control law features and thus requires knowledge of not only the current clutch pressure, but also the volume flow generated from  $\dot{x}_{CL}$ . While this may be measured under test-rig conditions, measurement of clutch displacement is not feasible in mass production because sensors would have to be placed on transmission components with very high revolution speeds. Therefore, methods for the estimation of the volume flow from clutch velocity ought to be investigated. A natural approach is to devise an observer reconstructing not only the axial clutch cylinder displacement velocity, but clutch displacement, too. Such a full state observer will, however, be confronted with uncertainty about the cylinder damping which may be subject to slow, but significant changes over the operating timeframe. This will likely affect the estimation quality for both transient and stationary processes and in turn decrease control performance. Two approaches to overcome this difficulty are thus presented in this section.

The first approach is a disturbance observer, for which asymptotic stability can be established analytically. The other approach is a Proportional-Integral observer which in different settings has proven to be robust against parameter uncertainties to a certain extent. In both cases, the volume flow generated from clutch displacement velocity will be considered as a disturbance  $d(t)$  of the nominal system consisting of a simple volume to be filled with fluid. In the interest of an eased discussion of the methods, the clutch cylinder will be considered as an independent subsystem of the hydraulic circuit. With the system pressure controlled by the main pressure valve, the net volume flow into the clutch can be controlled by knowledge of  $p_M = x_5$  and  $p_{CL} = x_6$ , so that the following model of the clutch is sufficient to represent the clutch dynamics:

$$\dot{p}_{CL} = \frac{1}{C_{hCL}} (q_{CL} - A_{CL}\dot{x}_{CL}) , \quad (9.51)$$

$$\dot{x}_{CL} = v_{CL} , \quad (9.52)$$

$$\dot{v}_{CL} = \frac{1}{m_{CL}} (p_{CL}A_{CL} - F_{CL0} - F_{ES}(x_{CL}, v_{CL}, l_{CL}) - k_{CL}x_{CL} - d_{CL}v_{CL}) \quad (9.53)$$

with  $q_{CL} = -q_{CLPA} + q_{CLAT}$ , i.e.  $q_{CL}$  representing the control input related volume flow into and out of the clutch.

Within the scope of the above model, the input-output-linearizing control law for clutch pressure control can be represented as

$$q_{CL} = \underbrace{A_{CL}\dot{x}_{CL}}_{=:-d(t)} - C_{hCL}k_{31}(p_{CL} - p_{CL}^*) + C_{hCL}\dot{p}_{CL}^* \quad (9.54)$$

with  $k_{31}$  being chosen as in equations (9.46) such that asymptotic reference tracking of  $p_{CL}^*$  is ensured. Interpreting the term  $A_{CL}\dot{x}_{CL}$  as a disturbance  $d(t)$ , the control is to counteract this disturbance.

### 9.5.1 Disturbance Observer

Disturbance observers are an important and comparatively novel concept in control engineering. Relevant publications in the field, among others, are [14, 15]. Generally, two approaches can be distinguished. The first approach relies on a disturbance model, in many cases linear, generating the disturbance to be observed. Then, by pole-placement-like techniques observer gains are derived that guarantee asymptotic stability of the disturbance error. This approach is not applicable here because even though a model for the disturbance behavior could be stated in the form of the clutch dynamics, the uncertain damping parameter  $d_{CL}$  will feature in the equation and therefore again cause a misrepresentation of the actual disturbance behavior in the plant. The second approach relies on the construction of an internal disturbance-observer-related variable whose dynamics are designed in such a way that the sum of the internal variable and another function to be devised which is driven by the available measurement signal guarantee disturbance error convergence. This is the approach chosen for the problem at hand. General approaches to the design of the required functions do not seem to be available as of yet – in the case at hand it certainly is beneficial that the pressure dynamics in the clutch are essentially linear in  $q_{CL}$  for zero disturbance.

From

$$\dot{p}_{CL} = \frac{1}{C_{hCL}} (q_{CL} + d(t)) , \quad (9.55)$$

the disturbance can be expressed as

$$d(t) = C_{hCL}\dot{p}_{CL} - q_{CL}. \quad (9.56)$$

The observer is then taken as

$$\dot{\hat{d}}(t) = -\Theta(p_{CL})\hat{d}(t) + \Theta(p_{CL}) (C_{hCL}\dot{p}_{CL} - q_{CL}) \quad (9.57)$$

$$= -\Theta(p_{CL}) (\hat{d}(t) - d(t)) \quad (9.58)$$

$$= -\Theta(p_{CL})\tilde{\delta}(t). \quad (9.59)$$

Here,  $\Theta(p_{CL})$  is a function yet unknown, but to be designed according to the convergence requirement for the disturbance error  $\tilde{\delta} = \hat{d} - d$ . It is driven by the available measurement(s), clutch pressure  $p_{CL}$  in this case. In a lack of knowledge of the exact disturbance dynamics,  $\dot{d} = 0$  is now assumed in order to derive the disturbance error dynamics. This assumption is made in [15], too, along with the reasoning that in order for this assumption to be plausible, the observer dynamics simply have to be much

faster than the disturbance dynamics. Whether this is given depends on the very structure of  $\Theta(p_{CL})$ . While in some cases the freedom to design this function is restricted or not given at all, it will be seen that in the present case it can be chosen in such a way that the assumption of sufficiently fast disturbance error dynamics is fulfilled. With  $\dot{d} = 0$ , it follows that

$$\dot{\tilde{\delta}} = -\Theta(p_{CL})\tilde{\delta}. \quad (9.60)$$

Now, the following internal observer variable  $\sigma$  is defined:

$$\sigma := \hat{d} - \Lambda(p_{CL}). \quad (9.61)$$

In the above expression,  $\Lambda(p_{CL})$  is a second function also depending on measurable output  $p_{CL}$  that has to be devised so that the disturbance observation error will converge. Here, it is chosen to fulfill

$$\Theta(p_{CL}) = \frac{\partial \Lambda(p_{CL})}{\partial p_{CL}} \frac{1}{C_{hCL}}. \quad (9.62)$$

The internal observer variable's dynamics thus are

$$\dot{\sigma} = \dot{\hat{d}} - \frac{d\Lambda(p_{CL})}{dt} = \dot{\hat{d}} - \frac{\partial \Lambda(p_{CL})}{\partial p_{CL}} \dot{p}_{CL} \quad (9.63)$$

$$= -\Theta(p_{CL})\dot{\hat{d}} + \Theta(p_{CL})\dot{d} - \Theta(p_{CL})C_{hCL}\dot{p}_{CL} \quad (9.64)$$

$$= -\Theta(p_{CL})(\sigma + \Lambda(p_{CL})) + \Theta(p_{CL})(C_{hCL}\dot{p}_{CL} - q_{CL}) - \Theta(p_{CL})C_{hCL}\dot{p}_{CL} \quad (9.65)$$

$$= -\Theta(p_{CL})(\sigma + \Lambda(p_{CL})) - \Theta(p_{CL})q_{CL}. \quad (9.66)$$

Hence, the dynamics of the disturbance observer are

$$\dot{\sigma} = -\Theta(p_{CL})\sigma + \Theta(p_{CL})(-q_{CL} - \Lambda(p_{CL})), \quad (9.67)$$

$$\hat{d} = \sigma + \Lambda(p_{CL}). \quad (9.68)$$

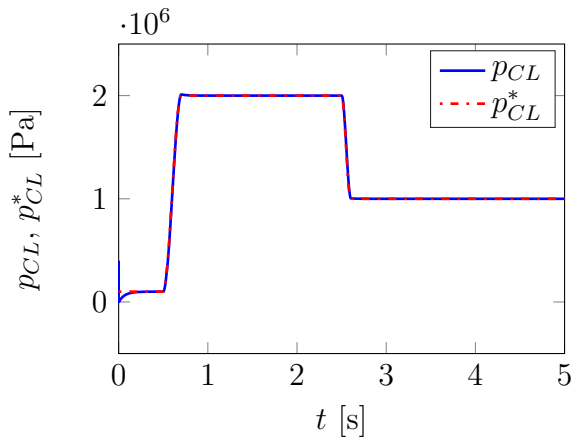
With the error dynamics given by (9.60), the following choice for  $\Theta(p_{CL})$  makes the disturbance observer error dynamics linear and time-invariant with an arbitrary convergence rate  $c$ :

$$\Theta(p_{CL}) = c. \quad (9.69)$$

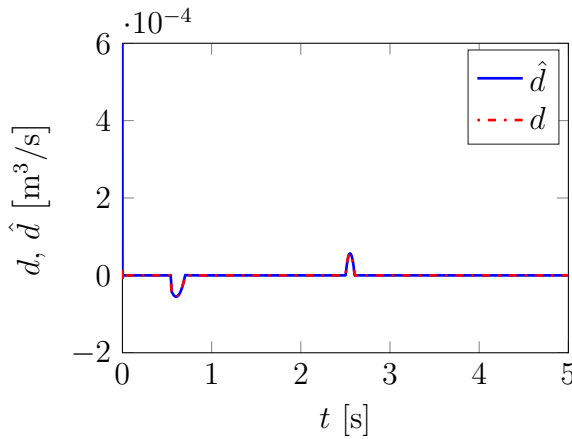
As for  $\Lambda(p_{CL})$ , it follows as

$$\Lambda(p_{CL}) = cC_{hCL}p_{CL}. \quad (9.70)$$

In order to employ  $\Lambda(p_{CL})$  in a concrete control law,  $C_{hCL}$  is taken as a fixed quantity, i.e. its clutch displacement dependence will be ignored. It thus is to be expected that the observer will yield good results only as long as the change in clutch capacitance is not significant. Simulations show, however, that this is given even for comparatively small clutch cylinder volumes of  $1 \times 10^{-4} \text{m}^3$ . Results for the estimation of disturbance and the related control are shown in Figures 9.6, 9.7. The simulation results suggest overall good performance of the observer, both without and with valve dynamics so that it can be seen as a sensible approach to estimating the volume flow generated through clutch displacement velocity.

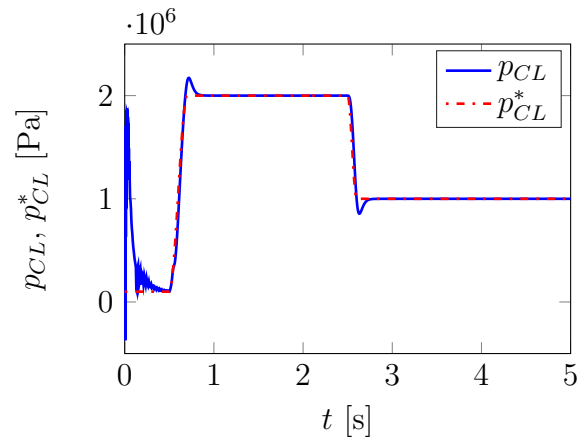


(a) Clutch pressure.

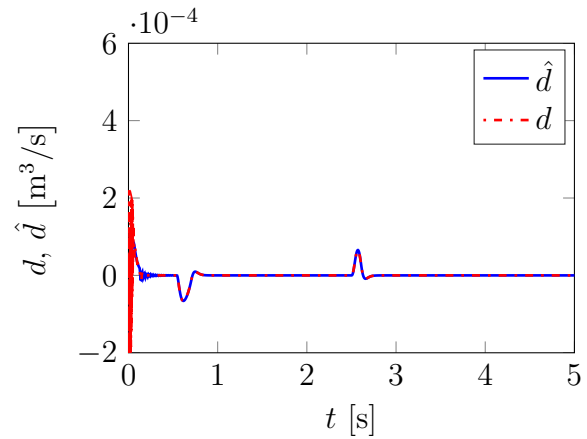


(b) Disturbance induced by clutch displacement.

Figure 9.6: Disturbance observer: without valve dynamics.



(a) Clutch pressure.



(b) Disturbance induced by clutch displacement.

Figure 9.7: Disturbance observer: with valve dynamics.

### 9.5.2 PI-Observer

In [64], a proportional-integral (“PI”) observer is suggested for the robust observation and control of input-output-linearizable systems. Based on the Byrnes-Isidori normal form of a system a pole placement technique can be applied to the estimation of both unknown disturbances and states. This being a fairly recent contribution, its appeal lies especially in the applicability to general, possibly MIMO input-output-linearizable systems featuring disturbances. Considering the clutch as a SISO system, the core idea is to transform a general system perturbed by bounded, but unknown disturbances  $\mathbf{d}(\mathbf{x}, t)$  which enter the system dynamics through a matrix  $\mathbf{E}$

$$\dot{\mathbf{x}} = \mathbf{f}_d(\mathbf{x}) + \mathbf{g}(\mathbf{x})u + \mathbf{E}\mathbf{d}(\mathbf{x}, t), \quad (9.71)$$

$$y = h(\mathbf{x}) \quad (9.72)$$

via the coordinate transformation associated with the Lie derivatives of the system output into

$$\begin{aligned} \dot{\xi}_1 &= \xi_2, \\ &\vdots \end{aligned} \quad (9.73)$$

$$\dot{\xi}_{r-1} = \xi_r \quad (9.74)$$

$$\dot{\xi}_r = \alpha(\boldsymbol{\xi}, \boldsymbol{\eta}) + \beta(\boldsymbol{\xi}, \boldsymbol{\eta})u + \delta(\mathbf{x}, t) \quad (9.75)$$

in its external coordinates  $\boldsymbol{\xi}$ . Here,  $\delta(\mathbf{x}, t)$  are the transformed unknown disturbances. For a system with relative degree  $r = 1$  as is the case with the clutch actuation system here and with  $\xi_1$  according to equation (9.73) corresponding to  $\xi_{3,1}$  in the transformation defined in (9.40), the transformed system (with  $\alpha(\boldsymbol{\xi}, \boldsymbol{\eta}) = 0$  in the present special case) reads

$$\begin{aligned} \dot{p}_{CL} &= \frac{1}{C_{hCL}}q_{CL} + \frac{1}{C_{hCL}}d(t) \\ &= \dot{\xi}_{3,1} = \beta(\xi_{3,1})u_C + \delta(\mathbf{x}, t), \end{aligned} \quad (9.76)$$

which, after performing input-output linearization can be stated as

$$\dot{\xi}_{3,1} = \nu + \delta(\mathbf{x}, t) \quad (9.77)$$

with the new input  $\nu$ . As pointed out before, the external dynamics are observable and controllable. The *PI*-observer then assumes the form [64, 104]

$$\begin{bmatrix} \dot{\hat{\xi}}_{3,1} \\ \dot{\hat{\delta}} \end{bmatrix} = \underbrace{\begin{bmatrix} 0 & 1 \\ 0 & 0 \end{bmatrix}}_{=: \mathbf{A}_e} \begin{bmatrix} \hat{\xi}_{3,1} \\ \hat{\delta} \end{bmatrix} + \begin{bmatrix} 1 \\ 0 \end{bmatrix} \nu + \begin{bmatrix} l_1 \\ l_2 \end{bmatrix} (y - \hat{y}), \quad (9.78)$$

$$\hat{y} = \underbrace{\begin{bmatrix} 1 & 0 \end{bmatrix}}_{=: \mathbf{c}_e} \begin{bmatrix} \hat{\xi}_{3,1} \\ \hat{\delta} \end{bmatrix}. \quad (9.79)$$

The observability criterion is fulfilled for the extended pair  $(\mathbf{A}_e, \mathbf{c}_e)$ . Because the above observer not only proportionally feeds back the observer error  $\hat{y} - y$  but also feeds back  $\hat{\delta}$  to the dynamics of  $\hat{\xi}_{3,1}$  (see also Figure 9.8), it features an integral component, thus being referred to as a *PI*-observer. This integral component is advantageous in that it is commonly associated with certain robustness properties towards plant uncertainties not only beneficially exploited here, but in other contexts as well [5, 118].

The corresponding observer error dynamics  $\tilde{\xi}_{3,1} = \hat{\xi}_{3,1} - \xi_{3,1}$  and  $\tilde{\delta} = \hat{\delta} - \delta$  thus are

$$\begin{bmatrix} \dot{\tilde{\xi}}_{3,1} \\ \dot{\tilde{\delta}} \end{bmatrix} = \begin{bmatrix} -l_1 & 1 \\ -l_2 & 0 \end{bmatrix} \begin{bmatrix} \tilde{\xi}_{3,1} \\ \tilde{\delta} \end{bmatrix} - \begin{bmatrix} 0 \\ \dot{\delta} \end{bmatrix}. \quad (9.80)$$

Now, for bounded  $\dot{\delta}$ , the observation errors  $\tilde{\xi}_{3,1}$  and  $\tilde{\delta}$  can be reduced to a non-zero, but arbitrarily small value through an appropriate, high-gain choice for  $l_1$  and  $l_2$ , see [64, 104]. The *PI*-observer therefore estimates not only the external coordinate  $\xi_{3,1}$ , but also the disturbance  $\delta$ . Since the disturbance  $d$  physically is a volume flow generated from a clutch cylinder moving with finite velocity and subject to finite, i.e. bounded acceleration, boundedness of  $d = d(t)$  can be considered as given so that disturbance estimation with this approach should be feasible. In Figure 9.10, simulation results are shown, both for an ideal valve and a non-ideal valve with a valve frequency of 250Hz. While only an arbitrarily small, but non-zero tracking error can be expected from the *PI*-observer, its robustness property leads to a control performance superior to the performance of the disturbance observer when taking into account valve dynamics, even though asymptotic stability is guaranteed for the disturbance observer from section 9.5.1.

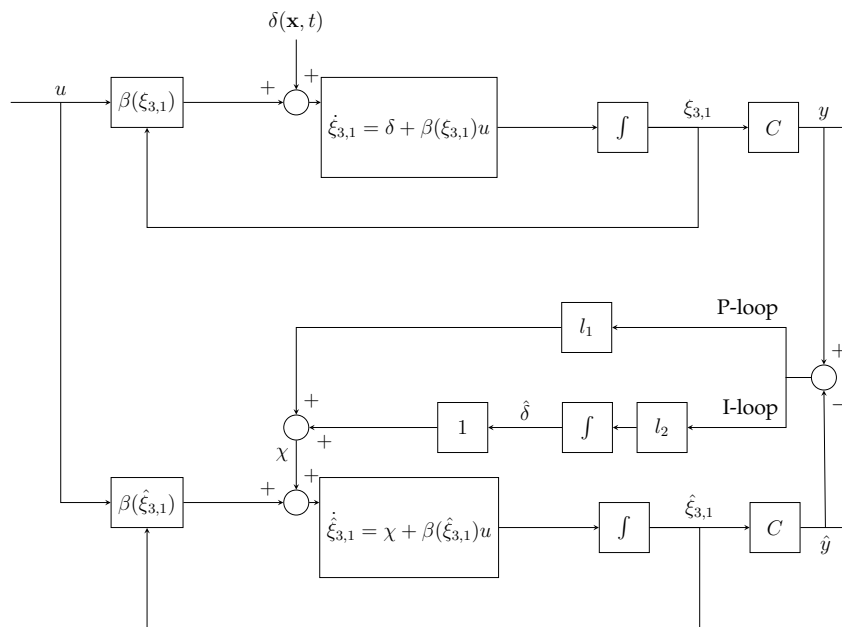
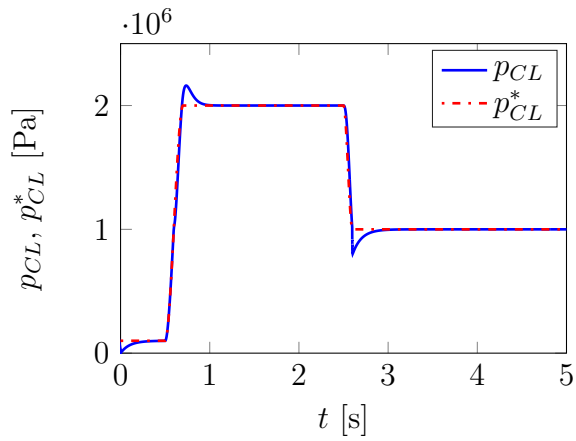
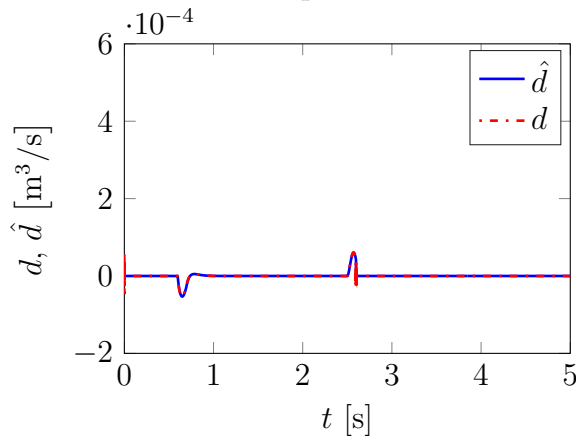


Figure 9.8: *PI*-observer for the clutch actuation system.

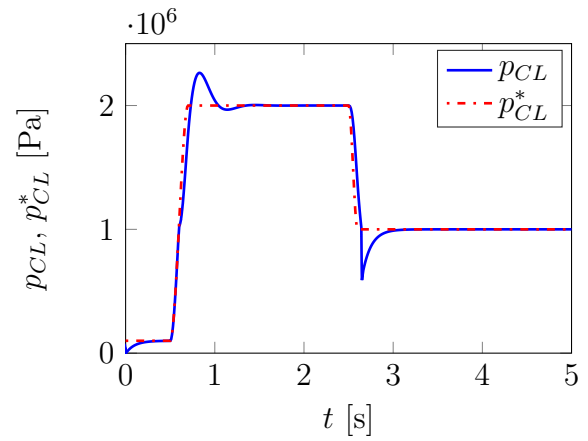


(a) Clutch pressure.

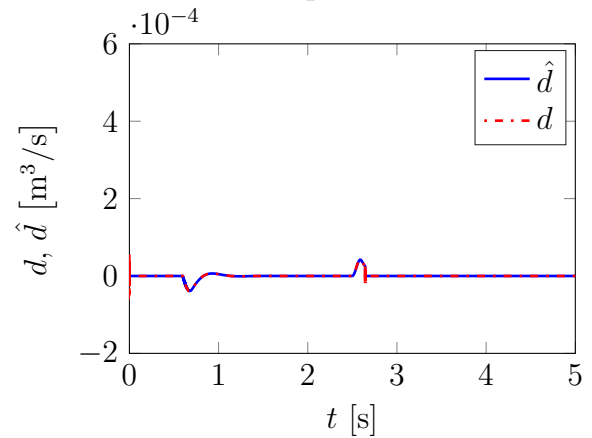


(b) Disturbance induced by clutch displacement.

Figure 9.9: *PI*-observer results: without valve dynamics.



(a) Clutch pressure.



(b) Disturbance induced by clutch displacement.

Figure 9.10: *PI*-observer results: with valve dynamics.

## 9.6 Intermediate Conclusion

Building on the results for SISO nonlinear volume flow control from chapter 8, a nonlinear MIMO control approach for a clutch actuation circuit featuring a variable displacement pump was suggested.

The nonlinear control laws were generated under the assumption of ideal servo valve behavior. Simulations with the generated control laws for a system featuring valve dynamics were benchmarked against simulation results without valve dynamics and showed satisfactory behavior, however pointing to possibly complex transient interaction between various capacitances that allegedly can be attributed to dynamic imperfections of real world valves.

In order to account for unknown and practically unmeasurable volume flow generated from clutch cylinder displacement, two novel observer concepts were suggested – a disturbance observer with asymptotic convergence properties and a robust *PI*-observer that yields arbitrarily small bounded tracking error. Both observers provide a possible solution to the disturbance estimation problem.

# 10 Identification of a Hydraulic Consumer

## 10.1 Background

In many technical applications, detailed knowledge about system parameters is required in order to model the system adequately. With large numbers of parameters commonly unavailable to systems engineers, the question of parameter identification and estimation is of utmost practical importance. In this chapter, a feasibility study for an approach to identifying system parameters and parameter-free state maps of a nonlinear clutch system as treated in [137, 138] is presented.

The method makes use of the well-known Kalman filter technique and applies its state estimation approach to the estimation of the system parameters and state maps of the system. As the functionality of the Kalman filter is subject to system observability and its potential for parameter estimation is presumably constrained by system complexity, a strategy how to structurally break down a complex system into subsystems to which the filter technique can be applied will need to be devised. In the present chapter, such an approach shall be made for a minimal model of a clutch actuation mechanism as encountered in automatic transmissions. The purpose of this chapter is to evaluate the potential of a Kalman-Filter based identification routine in this context.

A standard filtering tool in control systems theory with significant industrial relevance, the Kalman filter was originally conceived as an observer with the core purpose to provide optimal state estimates for a system whose measurements are corrupted by measurement noise. While the original Kalman filter was designed for linear systems exclusively, its conceptual approach has found an extension to nonlinear systems in the form of the extended Kalman filter which today is the most frequently drawn onto observation approach in an industrial context. With the extended Kalman filter – similarly to the pole placement technique based on system linearization about a trajectory as discussed in section 8.6.2 – the observer gain law is based on the linearization about a trajectory. The trajectory that is being linearized about, however, is not the desired or actual trajectory, but the observed trajectory. As with other classic observation concepts, a state estimate  $\hat{\mathbf{x}}$  is computed by feeding back the observation error  $\mathbf{h}(\hat{\mathbf{x}}) - \mathbf{h}(\mathbf{x})$  multiplied by an observer gain  $\mathbf{l}(\hat{\mathbf{x}})$  whose computation is at the core of the observer design:

$$\dot{\hat{\mathbf{x}}} = \mathbf{f}(\hat{\mathbf{x}}, \hat{\mathbf{u}}) + \mathbf{l}(\hat{\mathbf{x}})(\mathbf{y} - \mathbf{h}(\hat{\mathbf{x}})) = \mathbf{f}_d(\hat{\mathbf{x}}) + \mathbf{g}(\hat{\mathbf{x}})\hat{\mathbf{u}} + \mathbf{l}(\hat{\mathbf{x}})(\mathbf{y} - \mathbf{h}(\hat{\mathbf{x}})).$$

Since its inception, the Kalman filter has also found application in the field of parameter identification. The idea behind this step is to introduce unknown parameters as additional states which the Kalman filter is to generate an estimate for. Due to its conceptual

origin in least square minimization, it is sometimes also presented in a systems identification context such as in [76], where its similarity with the recursive least squares algorithm, a prominent system identification technique, is pointed out. The Kalman filter has been successfully applied to numerous identification problems, albeit theoretically so in most cases. In [38], the identification of mass and stiffness of a chain of oscillators is presented, whereas in [52], an approach to the non-parametric identification of possibly non-smooth restoring forces and damping forces for different mechanical systems is exemplified.

As pointed out, Kalman filtering is contingent on system observability. In the case of a nonlinear SISO system, to compute the observability map, the same intuition is followed as in linear time-invariant or line time-varying systems, namely to consider whether the map obtained from building the time derivatives of the system output up to  $n - 1$ -th order

$$\mathbf{q} = \begin{bmatrix} h(\mathbf{x}) \\ \mathcal{L}_f h(\mathbf{x}) \\ \vdots \\ \mathcal{L}_f^{n-1} h(\mathbf{x}) \end{bmatrix}$$

yields full rank information. Building the gradient of  $\mathbf{q}$ , local nonlinear observability is given (see e.g. [1]) if the observability matrix

$$\mathbf{O} = \frac{d\mathbf{q}}{d\mathbf{x}} \tag{10.1}$$

has full rank

$$\text{rank}(\mathbf{O}) = n \quad \forall \mathbf{x} \in \mathcal{D}, \tag{10.2}$$

over the full domain  $\mathcal{D}$  of  $\mathbf{x}$ . This is the formulation for the nonlinear (local) observability criterion in contrast to the linear (time varying) formulation presented in equation (8.212).

Conceptually summarizing the Kalman filter approach to state estimation, the concept is to use the last best possible estimate for state and state covariance to predict the next best estimate taking into account the known control input and an uncertain but quantifiable noise disturbance of both plant and measurement. For additional background on the concepts of Kalman filtering see e.g. [25, 26, 101].

The gain computation for the extended Kalman filter comprises several steps which shall briefly be outlined in the following.

In this chapter, the system and the measurements are synchronized in discrete time by an algorithm for the extended Kalman filter from [101] suitable for discrete systems given as follows:

$$\mathbf{x}_k = \mathbf{f}_{k-1}(\mathbf{x}_{k-1}, \mathbf{u}_{k-1}, \mathbf{w}_{k-1}), \quad (10.3)$$

$$\mathbf{y}_k = \mathbf{h}_k(\mathbf{x}_k, \mathbf{v}_k), \quad (10.4)$$

$$\mathbf{w}_k \sim (\mathbf{0}, \mathbf{Q}_k), \quad (10.5)$$

$$\mathbf{v}_k \sim (\mathbf{0}, \mathbf{R}_k). \quad (10.6)$$

Here, the signals  $\mathbf{w}$  and  $\mathbf{v}$  represent process and measurement noise with zero mean each and covariance  $\mathbf{Q}_k$  and  $\mathbf{R}_k$ , respectively. To apply the Kalman filter to the system, in a first step the state estimate  $\hat{\mathbf{x}}$  and the estimate for the state covariance matrix  $\mathbf{P}$  are initialized with their respective expected values:

$$\hat{\mathbf{x}}_0^+ = E(\mathbf{x}_0), \quad (10.7)$$

$$\mathbf{P}_0^+ = E\left[(\mathbf{x}_0 - \hat{\mathbf{x}}_0^+)(\mathbf{x}_0 - \hat{\mathbf{x}}_0^+)^T\right]. \quad (10.8)$$

This initialization, along with the choice for  $\mathbf{Q}_k$ , is crucial to the results the Kalman filter gives. Because in Kalman filtering a distinction between pre- and post-measurement quantities is necessary, the superscripts “+” and “-” are used to indicate post-measurement and pre-measurement estimates, respectively.

For  $k = 1, 2, \dots$ , the following are then to be computed:

$$\mathbf{F}_{k-1} = \left. \frac{\partial \mathbf{f}_{k-1}}{\partial \mathbf{x}} \right|_{\hat{\mathbf{x}}_{k-1}^+}, \quad \mathbf{L}_{k-1} = \left. \frac{\partial \mathbf{f}_{k-1}}{\partial \mathbf{w}} \right|_{\hat{\mathbf{x}}_{k-1}^+}. \quad (10.9)$$

Clearly,  $\mathbf{F}_{k-1}$  is the system Jacobian and  $\mathbf{L}_{k-1}$  is the Jacobian with respect to the process noise. In that the Jacobian is evaluated about  $\hat{\mathbf{x}}_{k-1}^+$  it becomes evident that linearization about the *estimated* state is performed. The time update of the state estimate and the estimation error covariance for the next time step before availability of a measurement update can then be computed as

$$\mathbf{P}_k^- = \mathbf{F}_{k-1} \mathbf{P}_{k-1}^+ \mathbf{F}_{k-1}^T + \mathbf{L}_{k-1} \mathbf{Q}_{k-1} \mathbf{L}_{k-1}^T, \quad (10.10)$$

$$\hat{\mathbf{x}}_k^- = \mathbf{f}_{k-1}(\hat{\mathbf{x}}_{k-1}^+, \mathbf{u}_{k-1}, \mathbf{0}). \quad (10.11)$$

The following partial derivative matrices constituting measurement equation Jacobians with respect to system state  $\mathbf{x}$  and noise  $\mathbf{v}$ , respectively,

$$\mathbf{H}_k = \left. \frac{\partial \mathbf{h}_k}{\partial \mathbf{x}} \right|_{\hat{\mathbf{x}}_k^-}, \quad \mathbf{M}_k = \left. \frac{\partial \mathbf{h}_k}{\partial \mathbf{v}} \right|_{\hat{\mathbf{x}}_k^-}, \quad (10.12)$$

then allow for the computation of the measurement-driven update of the state estimate and estimation-error covariance as follows:

$$\mathbf{K}_k = \mathbf{P}_k^- \mathbf{H}_k^T \left( \mathbf{H}_k \mathbf{P}_k^- \mathbf{H}_k^T + \mathbf{M}_k \mathbf{R}_k \mathbf{M}_k^T \right)^{-1}, \quad (10.13)$$

$$\hat{\mathbf{x}}_k^+ = \hat{\mathbf{x}}_k^- + \mathbf{K}_k [\mathbf{y}_k - \mathbf{h}_k(\hat{\mathbf{x}}_k^-, \mathbf{0})], \quad (10.14)$$

$$\mathbf{P}_k^+ = (\mathbf{I} - \mathbf{K}_k \mathbf{H}_k) \mathbf{P}_k^-. \quad (10.15)$$

After performing the respective updates, the state estimates are available for manipulation by control laws. Notably, the Kalman filter requires a valid system model and quantitative knowledge of the measurement and process noise.

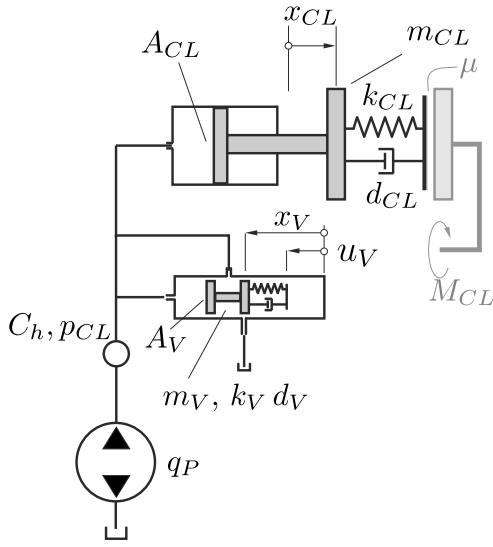
The core purpose of Kalman filtering is to provide valid state estimates for noise-corrupted measurements. When in need for parameter estimates and willing to sacrifice the filter's original purpose for the sake of the parameter estimates needed, the Kalman filter can be altered as such: In the state space formulation of the system model, the state space is augmented by the parameters to be estimated. The right hand side of these (formally parameter) states is set equal to zero, assuming constant parameters. Then the Kalman filter is initialized accordingly and used to estimate all system states including the parameters to be estimated. As the parameter to be identified was introduced to the state space formulation of the system, so it is estimated.

This routine is fairly well-known in control systems and identification theory. However, it should be emphasized once more that this principle cannot be extended to an arbitrary degree. In any case, fulfilling the observability criterion (which clearly depends on the structure of the system and thus on the number of parameters to be estimated) is a necessary, but not sufficient requirement for the filter to deliver meaningful results. An important aspect when initializing the respective matrices in order to obtain parameter or state map estimates of non-smooth forces or volume flow therefore is to allow for process noise in the model and to introduce a non-zero matrix  $\mathbf{Q}_k$  capturing model uncertainty. This matrix is an important tuning parameter of the filter in order to fulfill its parameter estimation function. Increasing values for the entries of  $\mathbf{Q}_k$  imply that the filter has room for adjusting the respective state variable according to the updated measurements – matrix  $\mathbf{Q}_k$ 's entries can be thus be understood as the strength of time variance of the respective states [76].

## 10.2 System Description

Figure 10.1 shows the reduced model of a reduced clutch actuating system. The purpose of the mechanism is to provide a system pressure such that a certain clutch force in the spring-damper-combination is achieved by which clutch torque  $M_{CL}$  is transmitted via friction with coefficient  $\mu$ .

To do so, a flow source provides a specified and adjustable volume flow  $q_P$ , causing the pressure in the system to rise with dynamics specified by system capacitance  $C_h$ . By increasing pressure, the clutch mass is moved in positive  $x_{CL}$ -direction. The system pressure is limited by the pressure limitation valve. Once the maximum pressure is reached, the valve opens so that the fluid flowing through the valve is equal to the flow provided by the pressure source.



Parameter	Symbol	Value	Unit
Piston area	$A_{CL}$	$\frac{\pi}{4} \times 0.045^2$	$\text{m}^2$
Clutch mass	$m_{CL}$	3	kg
Clutch damping	$d_{CL}$	30	Ns/m
Clutch stiffness	$k_{CL}$	$10^5$	N/m
Valve area	$A_V$	$\frac{\pi}{4} \times 0.01^2$	$\text{m}^2$
Valve mass	$m_V$	0.015	kg
Valve damping	$d_V$	2	Ns/m
Valve stiffness	$k_V$	2000	N/m
Valve overlap	$u$	0.005	m
Capacitance	$C_h$	$8 \times 10^{-11}$	$\text{m}^3/\text{bar}$

Figure 10.1: Clutch system.

Table 10.1: System parameters.

## 10.3 System Model

In order to account for the purpose of a conceptual assessment of the proposed identification approach, a most simple model of the clutch system is drawn on – the system is thus modeled as follows:

$$m_{CL}\ddot{x}_{CL} = -k_{CL}x_{CL} - d_{CL}\dot{x}_{CL} + A_{CL}p_{CL}, \quad (10.16)$$

$$m_V\ddot{x}_V = -k_V(x_V - u_V) - d_V(\dot{x}_V - \dot{u}_V) + A_V p_{CL}, \quad (10.17)$$

$$C_h\dot{p}_{CL} = q_P - q_V - A_{CL}\dot{x}_{CL} - A_V\dot{x}_V, \quad (10.18)$$

with the volume flow  $q_V$  governed by the nonlinear law

$$q_V = \begin{cases} 0 & \text{if } x_V \leq u, \\ \gamma_F b_V (x_V - u) \sqrt{p_{CL} - p_0} & \text{else.} \end{cases} \quad (10.19)$$

Here,  $u$  is the valve overlap and  $u_V$  an imposed spring displacement yielding a spring pre-stress or valve actuation force. Notably, end stop forces are ignored in this model to keep the model as simple as possible.

The hydraulic components are a source of significant nonlinearity, thereby certainly challenging the Extended Kalman filtering approach. First, the flow through any orifice (in this case, the valve) is a nonlinear function of the pressure of the system. In addition, due to a positive overlap of the valve, there is a dead band  $u$  implying that the valve does not open before a threshold valve displacement is exceeded. In the course of the identification approach, it is assumed that system pressure  $p_{CL}$  and clutch force

$F_{CL} = k_{CL}x_{CL} + d_{CL}\dot{x}_{CL}$  can be measured, so that the measurement equation is given by

$$\mathbf{y} = \begin{bmatrix} p_{CL} \\ k_{CL}x_{CL} + d_{CL}\dot{x}_{CL} \end{bmatrix}. \quad (10.20)$$

## 10.4 Identification Approach

The identification comprises several steps: First, system capacitance is identified from a simple consideration of the pressure dynamics while the clutch is blocked and the valve closed. Then, with a blocked valve, an effort is made to identify relevant parameters of the clutch, i.e. clutch mass, stiffness and damping. Once these are determined, in a next step the valve can be identified. Here, an approach with two substeps is used: To keep the system as simple as possible for the identification of valve mass and stiffness, an effort is made to exploit the valve-inherent overlap by exciting the valve without permitting fluid outflow. The idea is that the valve translation reveals information on the dynamic behavior of the valve without involvement of the nonlinear flow behavior that would otherwise make a simultaneous identification difficult. Once the valve stiffness and mass are known, the system is excited in such a way that the valve opens, thereby revealing information about the flow characteristic of the valve.

### 10.4.1 Identification of the System Capacitance

In an initial step, the capacity of the system is to be determined. By means of a known and constant volume flow excitation  $q_P$  considered as input, the measurement of the system pressure allows for a determination of the capacity by noting that the pressure increase over time is linear with  $q_P = \text{const.}$  It is assumed that both clutch mass and valve mass are blocked, i.e. their position is fixed. Considering pressure differences in the system as measured over a time period sufficiently long to prevent errors from measurement noise to have a significant influence, the capacity can be computed from:

$$\dot{p}_{CL} = \frac{q_P}{C_h}, \quad (10.21)$$

yielding, upon integration,

$$p_{CL} = p_0 + \frac{q_P}{C_h}t, \quad (10.22)$$

from which an estimate of the capacitance may be computed by algebraic manipulation.

### 10.4.2 Identification of the Clutch

For the identification of the clutch, in a first step it is assumed that the pressure control valve is pre-stressed by so large a force that it will not open and not even move within

the time interval considered. This reduces the system to the following state-space representation of the remaining dynamics:

$$\dot{\mathbf{x}} = \begin{bmatrix} x_2 \\ -\frac{k_{CL}}{m_{CL}}x_1 - \frac{d_{CL}}{m_{CL}}x_2 + \frac{A_{CL}}{m_{CL}}x_3 \\ -\frac{A_{CL}}{C_h}x_2 + \frac{q_P}{C_h} \end{bmatrix}, \quad (10.23)$$

$$\mathbf{y} = \mathbf{h}(\mathbf{x}) = \begin{bmatrix} x_3 \\ k_{CL}x_1 + d_{CL}\dot{x}_2 \end{bmatrix} + \begin{bmatrix} v_1 \\ v_2 \end{bmatrix} \quad (10.24)$$

with  $\mathbf{x} = [x_{CL} \ \dot{x}_{CL} \ p_{CL}]^T = [x_1 \ x_2 \ x_3]^T$ . With respect to the estimation of the parameters  $k_{CL}$  and  $d_{CL}$ , these are introduced as states  $x_4$  and  $x_5$  with trivial dynamics in the corresponding slave model

$$\dot{\mathbf{x}} = \begin{bmatrix} x_2 \\ -\frac{x_4}{m_{CL}}x_1 - \frac{x_5}{m_{CL}}x_2 + \frac{A_{CL}}{m_{CL}}x_3 \\ -\frac{A_{CL}}{C_h}x_2 + \frac{q_P}{C_h} \\ 0 \\ 0 \end{bmatrix}, \quad (10.25)$$

$$\mathbf{y} = \mathbf{h}(\mathbf{x}) = \begin{bmatrix} x_3 \\ x_4x_1 + x_5x_2 \end{bmatrix} + \begin{bmatrix} v_1 \\ v_2 \end{bmatrix}. \quad (10.26)$$

For this first step of the identification approach, the observability matrix for the first output  $x_3$  shall be given. It can be computed as

$$\mathbf{O} = \begin{bmatrix} 1 & 0 & 0 & 0 & 0 \\ 0 & 1 & 0 & 0 & 0 \\ -\frac{x_4}{m_{CL}} & -\frac{x_5}{m_{CL}} & \frac{A_{CL}}{m_{CL}} & -\frac{x_1}{m_{CL}} & -\frac{x_2}{m_{CL}} \\ \frac{x_5x_4}{m_{CL}^2} & O_{42} & -\frac{x_5A_{CL}}{m_{CL}^2} & \frac{-x_2m_{CL} + x_1x_5}{m_{CL}^2} & O_{44} \\ O_{51} & O_{52} & O_{53} & O_{54} & O_{55} \end{bmatrix}, \quad (10.27)$$

with

$$O_{42} = \frac{C_h(x_5^2 - x_4m_{CL}) - A_{CL}^2m_{CL}}{m_{CL}^2C_h}, \quad (10.28)$$

$$O_{44} = \frac{-A_{CL}x_3 + 2x_5x_2 + x_4x_1}{m_{CL}^2}, \quad (10.29)$$

$$O_{51} = \frac{(A_{CL}^2m_{CL} - C_hx_5^2 + C_hx_4m_{CL})x_4}{m_{CL}^3C_h}, \quad (10.30)$$

$$O_{52} = \frac{(2A_{CL}^2m_{CL} - C_hx_5^2 + 2C_hx_4m_{CL})x_5}{m_{CL}^3C_h}, \quad (10.31)$$

$$O_{53} = \frac{(x_4m_{CL}C_h + x_5^2C_h - A_{CL}^2m_{CL})A_{CL}}{m_{CL}^3C_h}, \quad (10.32)$$

$$O_{54} = \frac{((-A_{CL}x_3 + 2x_5x_2 + 2x_4x_1)m_{CL} - x_5^2x_1)C_h + A_{CL}^2m_{CL}x_1}{m_{CL}^3C_h}, \quad (10.33)$$

$$O_{55} = \frac{\left(2x_4x_2m_{CL} + 2x_5\left(A_{CL}x_3 - \frac{3}{2}x_5x_2 - x_4x_1\right)\right)C_h}{m_{CL}^3C_h} + \frac{A_{CL}m_{CL}(2A_{CL}x_2 - q_P)}{m_{CL}^3C_h}. \quad (10.34)$$

As can be seen from its determinant

$$\det(\mathbf{O}) = -\frac{A_{CL}}{m_{CL}^5C_h} \left( A_{CL}^2C_hx_3^2 + A_{CL}^2m_{CL}x_2^2 - A_{CL}C_hx_5x_2x_3 - 2A_{CL}C_hx_4x_1x_3 + C_hx_5x_4x_1x_2 + C_hx_4^2x_1^2 - C_hx_4m_{CL}x_2^2 - A_{CL}m_{CL}x_2q_P \right), \quad (10.35)$$

the system can be expected to be locally observable from output  $h_1 = x_3$  alone, at least for some trajectories. From this perspective, the additional measurement of the clutch torque or clutch force can be interpreted as an additional measurement made with the prospect of easing the convergence process of the filter.

The state estimate is then initialized with

$$\hat{\mathbf{x}}_0^+ = \begin{bmatrix} 0 & 0 & x_{30} & 0.5k_{CL} & 0.5d_{CL} \end{bmatrix}^T, \quad (10.36)$$

so that estimates for the unknown parameters  $k_{CL}$  and  $d_{CL}$  are as good as fifty percent of their true values.

The filter is initialized with

$$\hat{\mathbf{P}}_0^+ = \mathbf{diag} \left( [0.001^2 \quad 0.0002^2 \quad 0.1^2 \quad (0.1k_{CL})^2 \quad (0.1d_{CL})^2] \right) \quad (10.37)$$

$$\mathbf{Q}_0 = \mathbf{diag} \left( [0.001^2 \quad 0.0002^2 \quad 0.1^2 \quad 3(0.1k_{CL})^2 \quad 3(0.1d_{CL})^2] \right). \quad (10.38)$$

Results are shown in Figure 10.2. As can be seen, convergence behavior is good and the true values of both  $k_{CL}$  and  $d_{CL}$  are met with satisfactory precision in comparatively short time. The convergence pattern in this case is even better than is the case for textbook illustrative examples from nonlinear adaptive observer theory, e.g. [133, 134], where, despite *proven* convergence for the observer formulation for state-affine nonlinear systems the convergence rate cannot be prescribed arbitrarily. It is worth to point out that in order to identify clutch damping, volume flow excitation through  $q_P$  needs to be such that the clutch performs oscillatory motion.

As an alternate approach,  $m_{CL}$  could have been identified instead of  $d_{CL}$ . Efforts to simultaneously identify  $m_{CL}$ ,  $d_{CL}$  and  $k_{CL}$  however did not yield converging results.

### 10.4.3 Identification of the Valve

The simplest method to determine further parameters of the system is to allow valve displacement for a given  $q_P > 0$ , but to suppress the volume flow related to an open

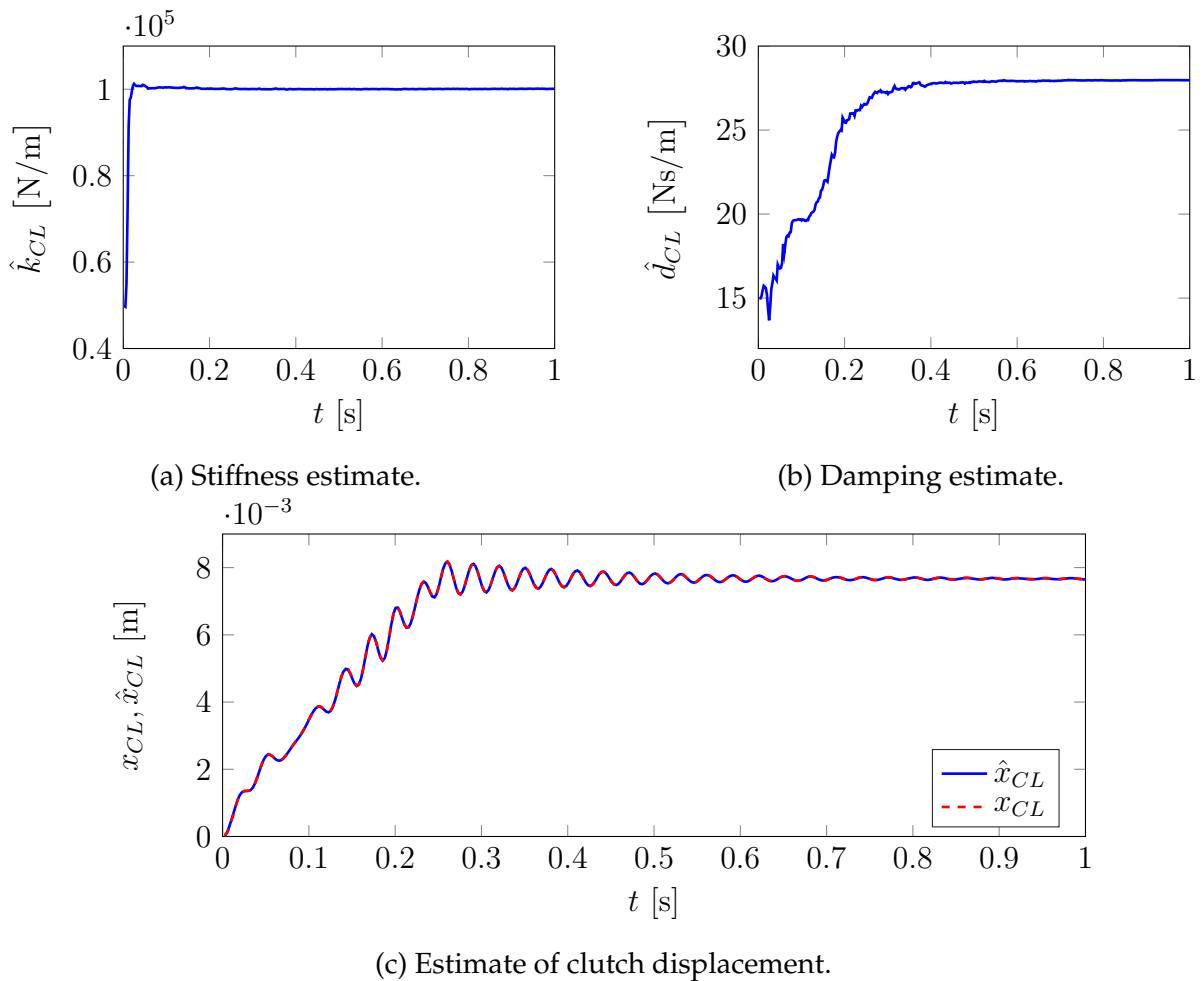


Figure 10.2: Clutch estimates.

valve. This will allow for valve dynamics to show in the measurements without the complicating effects from fluid outflow across an open valve. Essentially, this undermines the pressure limitation functionality of the valve. While this is possible theoretically, it should not be done in a real-world system as an (even artificially so) disabled pressure limitation valve will increase the risk of irreversible system failure. Instead, the valve shall be actuated in such a way that it can be identified within the time interval during which it translates in the overlap region without opening. Even for large valve overlap, this demands rather short convergence intervals and a large number of available measurement data points for the Kalman Filter.

The system dynamics including the valve have the following state-space representation and fully represent the system shown in Figure 10.1:

$$\dot{\mathbf{x}} = \begin{bmatrix} x_2 \\ -\frac{k_{CL}}{m_{CL}}x_1 - \frac{d_{CL}}{m_{CL}}x_2 + \frac{A_{CL}}{m_{CL}}x_5 \\ x_4 \\ -\frac{k_V}{m_V}(x_3 - u_V) - \frac{d_V}{m_V}(x_4 - \dot{u}_V) + \frac{A_V}{m_V}x_5 \\ -\frac{A_{CL}}{C_h}x_2 - \frac{A_V}{C_h}x_4 - \frac{q_V}{C_h} + \frac{q_P}{C_h} \end{bmatrix}, \quad (10.39)$$

$$\mathbf{y} = \mathbf{h}(\mathbf{x}) = \begin{bmatrix} x_5 \\ k_{CL}x_1 + d_{CL}\dot{x}_2 \end{bmatrix} + \begin{bmatrix} v_1 \\ v_2 \end{bmatrix} \quad (10.40)$$

with  $\mathbf{x} = [x_{CL} \ \dot{x}_{CL} \ x_V \ \dot{x}_V \ p_{CL}]$  and  $q_V$  from equation (10.19).

The valve is pre-stressed by  $u_V$ . In the course of the present investigation, it is assumed that this pre-stress can be manipulated in order to prevent the valve from opening.

The system dynamics (10.39) feature the volume outflow  $q_V$  across the pressure limitation valve. In the corresponding slave model, this volume outflow will not be included as the valve is, by assumption, actuated in such a way that it does not open. While the slave model will exhibit the same dynamical behavior as the system for zero valve outflow  $q_V = 0$ , there will be a significant model mismatch once the valve opens so that a Kalman filter based on the mismatched slave model can not be expected to show convergent behavior anymore.

From the viewpoint of parameter identification, the slave model can be used for identification purposes only as long as the valve translates within the overlap region, yielding a zero opening area for the valve and thus zero outflow  $q_V = 0$ . The slave model featuring the unknown parameters  $k_V$  and  $m_V$  as states  $x_6$  and  $x_7$ , respectively, therefore is assumed as

$$\dot{\mathbf{x}} = \begin{bmatrix} x_2 \\ -\frac{k_{CL}}{m_{CL}}x_1 - \frac{d_{CL}}{m_{CL}}x_2 + \frac{A_{CL}}{m_{CL}}x_5 \\ x_4 \\ -\frac{x_6}{x_7}(x_3 - u_V) - \frac{d_V}{x_7}(x_4 - \dot{u}_V) + \frac{A_V}{x_7}x_5 \\ -\frac{A_{CL}}{C_h}x_2 - \frac{A_V}{C_h}x_4 + \frac{q_P}{C_h} \\ 0 \\ 0 \end{bmatrix}, \quad (10.41)$$

$$\mathbf{y} = \mathbf{h}(\mathbf{x}) = \begin{bmatrix} x_5 \\ k_{CL}x_1 + d_{CL}\dot{x}_2 \end{bmatrix} + \begin{bmatrix} v_1 \\ v_2 \end{bmatrix}. \quad (10.42)$$

It is to be noted here that  $d_{CL}$  and  $k_{CL}$  are assumed to be known from section 10.4.2, therefore they appear as known parameters in the model.

The filter is initialized with

$$\hat{\mathbf{P}}_0^+ = \mathbf{diag} \left( [0.001^2 \ 0.0002^2 \ 0.0001^2 \ 0.00002^2 \ 0.1^2 \ (0.1k_V)^2 \ (0.1m_V)^2] \right), \quad (10.43)$$

$$\mathbf{Q}_0 = \mathbf{diag} \left( [0.001^2 \quad 0.0002^2 \quad 0.0001^2 \quad 0.00002^2 \quad 0.1^2 \quad (0.1k_V)^2 \quad (0.1m_V)^2] \right), \quad (10.44)$$

$$\hat{\mathbf{x}}_0^+ = [0 \quad 0 \quad 0 \quad 0 \quad x_{50} \quad 0.5k_V \quad 0.8m_V]^T. \quad (10.45)$$

Exciting the full system with volume flow  $q_P$ , for certain choices of  $u_V$  the valve will show oscillations and displacement during a short time while not permitting fluid outflow. This is due to the valve overlap and shall here be exploited for the estimation of the valve parameters. Because the valve exhibits dynamics relevant for parameter estimation while not permitting fluid outflow for only a short time, it is important to generate sufficiently many measurement points during this time interval relevant for parameter estimation. In Figure 10.3 the estimation results are shown. In contrast to the estimation results shown before, the time interval shown in the Figure is only 0.1s, i.e. one tenth of the intervals considered before. The filter provides a good estimate of the true valve parameters even though the results suggest the estimation routine would have profited from a longer time interval during which the valve remains closed. The simulations also demonstrate the aforementioned effect of model mismatching: once the valve opens at  $\approx 0.05s$ , the slave model no longer matches the master model and the filter diverges.

While the simulation results in principle indicate feasibility of the approach presented, it should be stressed that in practice, the identification of mass and stiffness properties of the valve is expected to be highly cumbersome, if possible at all. The reason for this lies in small overlaps leaving little room for filter convergence and only minor influence of the volume flow  $A_V \dot{x}_V$  generated by valve motion on the overall system pressure, especially relative to the volume flow from clutch motion. Hence, the revelatory relevance of valve motion and corresponding volume flow  $A_V \dot{x}_V$  in a real-world setting likely is very limited.

Ultimately, the knowledge of valve mass and stiffness may be employed in an effort to determine the flow characteristic of the valve. The system dynamics are given by (10.39) while the slave model with  $q_V = x_6$  reads

$$\dot{\mathbf{x}} = \begin{bmatrix} -\frac{k_{CL}}{m_{CL}}x_1 - \frac{d_{CL}}{m_{CL}}x_2 + \frac{A_{CL}}{m_{CL}}x_5 \\ \frac{x_4}{m_V}(x_3 - u_V) - \frac{d_V}{m_V}(x_4 - \dot{u}_V) + \frac{A_V}{m_V}x_5 \\ -\frac{A_{CL}}{C_h}x_2 - \frac{A_V}{C_h}x_4 - \frac{1}{C_h}x_6 + \frac{q_P}{C_h} \\ 0 \end{bmatrix}, \quad (10.46)$$

$$\mathbf{y} = \mathbf{h}(\mathbf{x}) = \begin{bmatrix} x_5 \\ k_{CL}x_1 + d_{CL}\dot{x}_2 \end{bmatrix} + \begin{bmatrix} v_1 \\ v_2 \end{bmatrix}. \quad (10.47)$$

While the structure of the governing law for the volume flow across a valve is known and could in theory be substituted in the estimation problem above (with the purpose

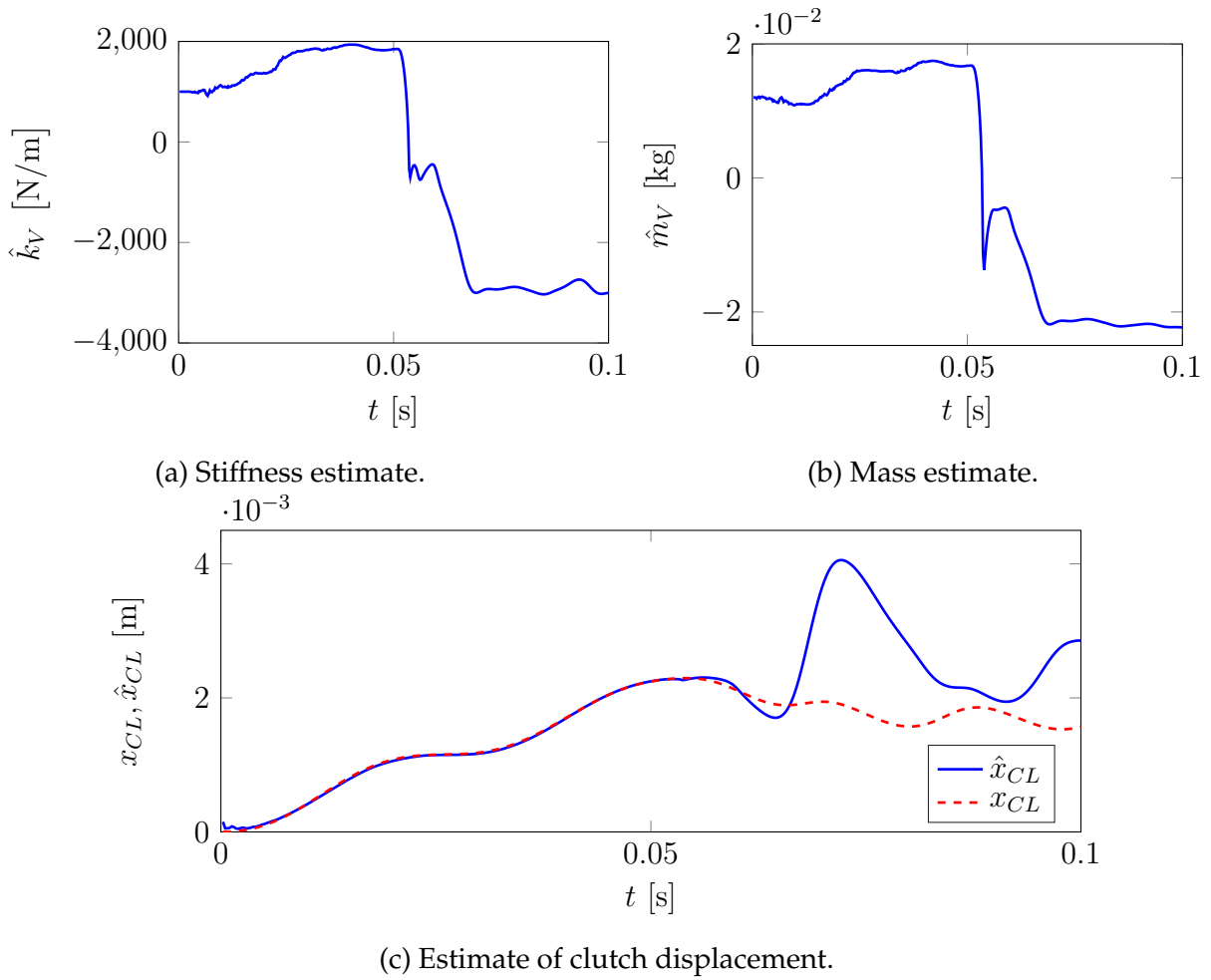


Figure 10.3: Valve estimates.

of determining the flow coefficient), the distinct nonlinearity and the coupling of states in (10.19) would significantly complicate the estimation problem. With an eye towards robustness of the estimation procedure, the volume flow across the valve is therefore modeled as an aggregate state  $x_6$ . Since estimates for the valve displacement and system pressure obtained (as of all other states) are obtained from the Kalman filter, it is possible to plot the flow through the valve as a function of these two states, yielding a parameter free state-volume-flow map. In order to cover as large a domain as possible for the state-volume-flow map (i.e. as many different triples  $\{\hat{x}, \hat{p}_{CL}, \hat{q}_V\}$  over as wide a range as possible), the pressure limitation valve is subjected to an oscillatory excitation with increasing amplitude and frequency:

$$u_V = \begin{cases} 0 & \text{if } t \leq t_1, \\ \hat{u}_V \sin(2\pi f_V(t - t_1)) (t - t_1) & \text{else.} \end{cases} \quad (10.48)$$

The filter is then initialized with

$$\hat{\mathbf{P}}_0^+ = \mathbf{diag} \left( [0.001^2 \quad 0.0002^2 \quad 0.0001^2 \quad 0.00002^2 \quad 5 \times 10^4 \quad 2 \times 10^{-4}] \right), \quad (10.49)$$

$$\mathbf{Q}_0 = \mathbf{diag} \left( [0.001^2 \quad 0.0002^2 \quad 0.0001^2 \quad 0.00002^2 \quad 1 \times 10^2 \quad 1 \times 10^6] \right), \quad (10.50)$$

$$\hat{\mathbf{x}}_0^+ = [0 \quad 0 \quad 0 \quad 0 \quad x_{50} \quad 0]^T. \quad (10.51)$$

Figures 10.4 – 10.6 show the estimation results of the volume flow as a function of valve displacement and system pressure.

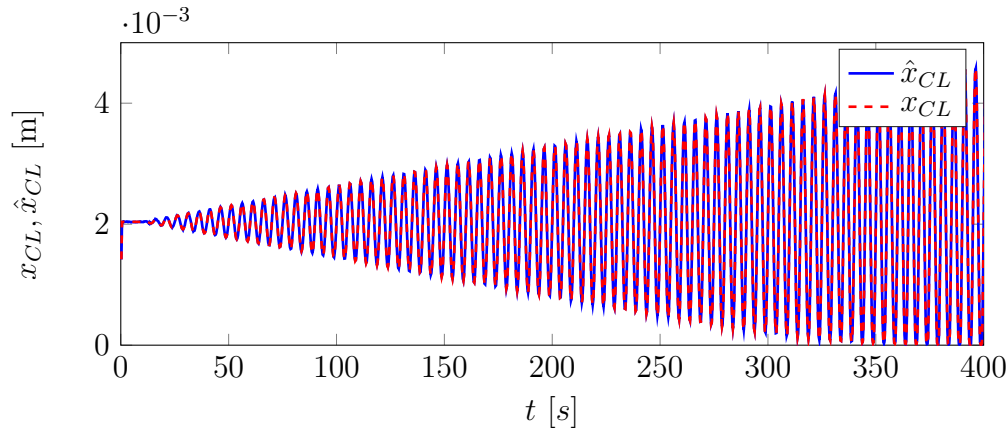


Figure 10.4: Estimate of clutch displacement.

Displaying estimated volume flow over estimates of valve displacement and system pressure eliminates the time dependency of these state variables from the estimation results. For each estimation triple  $(\hat{x}_V, \hat{p}_{CL}, \hat{q}_V)$  at some point in time, a blue dot is shown in Figures 10.5 and 10.6, the blue dots hence are the unprocessed estimation results. In contrast, the black dots are processed data generated from the blue points through a partitioning of the blue points into parcels along linearly spaced intervals of  $\hat{x}_V$  and  $\hat{p}_{CL}$ . Within these parcels, available data is partitioned further into sub-parcels, averaged within the sub-parcels, checked for sufficiency of information content on parcel level and then subjected to a parcel-wide linear regression over the averaged sub-parcel data. This allows the extrapolation of available estimation data at specified sampling points within whose proximity estimation data may not be available. The evaluation of the parcel-wide regression data at the sampling points yields the data represented by the black dots. The procedure is motivated by the problem that excitation through an input of choice for the system may not necessarily yield sufficiently finely sampled estimation data along the intervals of  $\hat{x}_V$  and  $\hat{p}_{CL}$ , a property that is difficult to control through a choice of system inputs.

All parameters of the system were assumed to be known, i.e. the sole estimation purpose was the state map for the valve flow. Under these (ideal) circumstances for the numerical experiment, the results are satisfying. The valve overlap causing a zero vol-

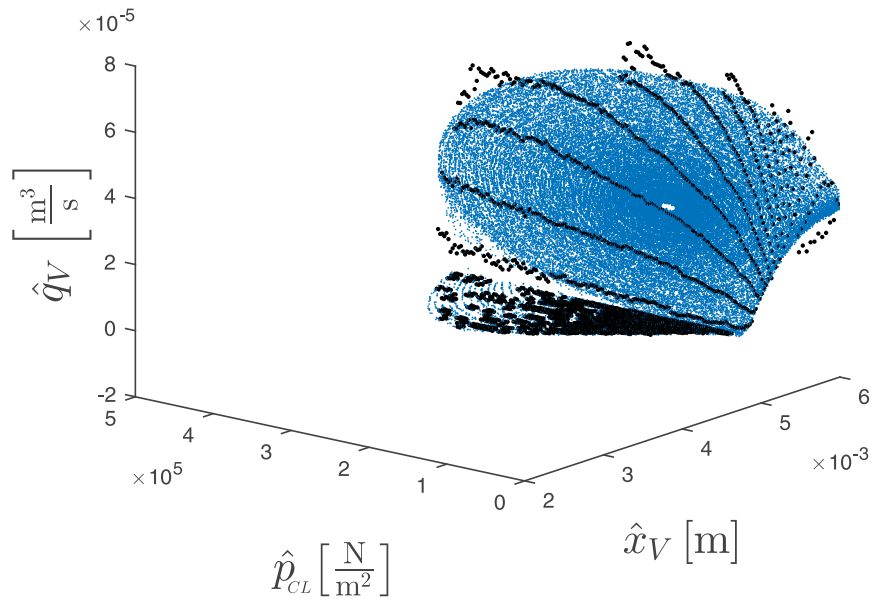


Figure 10.5: Identified volume flow across valve, view 1.

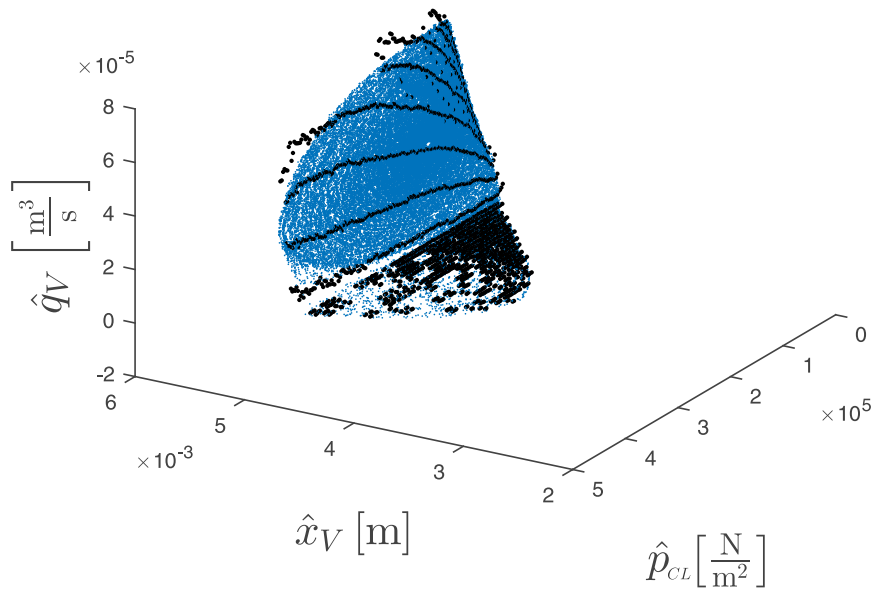


Figure 10.6: Identified volume flow across valve, view 2.

ume flow unless the valve displacement exceeds the overlap can clearly be seen, so can the pressure difference square root law once the valve is open.

## 10.5 Intermediate Conclusion

In this chapter, an approach for the systematic identification of a hydraulic consumer in the context of an automatic transmission was presented.

As there is no universally applicable procedure for the initialization of the Kalman filter, significant tuning effort and expert knowledge is to be expected as a requirement when a system needs to be identified in a real world setting. To the best of this thesis' author's knowledge, the Kalman filter works satisfyingly well for simple estimation problems not involving any state maps. Here, the results indicate a good overall estimation quality for unknown parameters. The potential of the filtering method can possibly be enhanced by combining it with other forms of parameter estimation in order to obtain good approximations of the parameter values to initialize the Kalman filter with. Naturally, the better the filter initialization – i.e. the initial estimates for the unknown parameters – the better the identification result. In this context, some authors have suggested an iterative procedure for filtering in combination with parameter estimation problems, see [38] for example.

The major formal and mathematically concise limitation to the proposed method is the observability criterion. Generally, one would expect that the number of parameters that can be estimated increases with the number of sensors applied to the system in order to prevent the observability matrix to lose full rank. In the context of unknown-input observers, [12, 13] discuss structural restrictions as to where unknown quantities may enter the system dynamics. It stands to reason that similar structural restrictions may exist for Kalman filter based identification.

It also has been found in this study that the estimation of highly nonlinear physical relationships does pose a problem to Kalman filtering, an issue well-known to practitioners. This does not come as a surprise insofar that the extended Kalman filter employs an observer gain computation principle that is based upon the linearization of the system about the observed trajectory. It cannot be expected in general that a linearization-based estimation routine will be a suitable approach for a system with nonlinearities of arbitrary degree. Here, the unscented Kalman filter as suggested in [43, 117] which takes the Kalman filtering approach to truly nonlinear problems may provide a promising alternative. Additionally, in [145] an approach based on a homotopy method suggested in [116] is discussed, showing positive indication for applicability in the present setting. To conclude, the positive indication for the applicability of this chapter's approach should be seen in the light of the simplifying assumptions made for the present minimal model. It is to be expected that in a real world setting, a more realistic model will complicate the identification task.



## Conclusion and Outlook

In the present thesis, selected problems of hydraulic modeling and simulation, analysis and control were discussed. The thesis' context relates most closely to applications in automotive engineering but is general in its overall scope. With a view towards the research questions outlined in the introduction, the findings can be summarized as follows.

Variable displacement vane pumps of translational type can sensibly be modeled based on elementary physical and kinematic considerations. The pump cam ring is subject to three force components listed in the sequence of decreasing relevance for the validity of a pump model: forces from line pressure exposure, forces from dead volume compression and forces from dead volume expansion. The autonomous model derived in the present thesis allows for a simple integration in hydraulic circuits for the purpose of stability analysis and control design.

Prominent examples of passive hydraulic circuits with a variable displacement vane pump feature a modified pressure regulator valve which yields switched system behavior. From the perspective of stability, two aspects are relevant:

- from a macro perspective, the pressure regulator valve structurally introduces an unstable limit cycle to the system that possibly prevents the system from reaching an otherwise stable equilibrium position. This type of limit cycle has been observed in isolated pressure regulators before. It is of utmost importance to choose a parameter constellation for the respective system that moves this limit cycle into a region in state space that is not relevant for the intended operating scenarios.
- from a micro perspective, system equilibrium stability depends on operating point, the choice of notch geometry in the regulator valve and valve leakage. For almost critically lapped regulator valves with different notch geometries, larger loads tend to yield stable operating points – *ceteris paribus*. Too low a regulator spring stiffness (and thus operating pressure) may be detrimental to system stability – higher stiffnesses appear to have a beneficial effect for equilibrium stability. Increasing operating pressure through increased regulator valve pre-stress, however, increases regions of instability. Increasing regulator valve damping may destabilize equilibria irrespective of the underlying notch geometry. Pump leakage does not significantly affect equilibrium stability. Increasing valve leakage via decreasing viscosity increases regions of instability. At the cost of losing set-point

regulation accuracy and load adaption time, increasing regulator valve overlap can help stabilize the system equilibrium by reducing leakage.

As to novel concepts for the nonlinear volume flow control of a variable displacement vane pump, analysis showed that

- Nonlinear SISO feedback-linearizing control can theoretically be employed in conjunction with a servo valve to obtain stable high-performance volume flow trajectory tracking for a variable displacement vane pump. In order to achieve full state knowledge, a nonlinear state observer may be made use of. Alternatively, feedforward-linearizing control with a simple *PI*-output-feedback control can achieve stable trajectory tracking without the need for full state estimation.
- The nonlinear feedback-linearizing control can be extended to a comprehensive clutch actuation circuit by making use of MIMO feedback-linearizing control. Pressure regulation for clutch actuation by means of a servo valve may require the employment of a disturbance observer. Here, both asymptotic disturbance observer and *PI*-observer are promising approaches.

The aforementioned key results were supported by the following background analyses and extended in different directions:

- Hydraulic pressure regulators with sufficiently large overlap yield stable equilibria within the overlap-related dead band for zero load flow. For a valve with sufficiently small overlap (or an unsuitable combination of pressure differences across its control edges) at given viscosity, a rectangular notch geometry and zero load flow, leakage may cause the equilibrium position to move towards a nominally open valve position, thereby destabilizing the equilibrium. No such effect was observed for triangular or circular notches.

For non-zero load flow and an open control edge, equilibrium stability depends largely on notch geometry, valve damping and pressure difference across the respective control edge. Larger pressure differences tend to destabilize equilibria requiring an open control edge.

- Kalman filtering bears potential for identification of hydraulic systems. While application to a clutch actuation unit requires extensive expert knowledge for filter initialization and the approach may not be robust in all circumstances, results obtained in this study indicate a positive outlook in principle.

Relating to these findings, several points may be worth addressing in future research, deriving both from assumptions made for the models discussed in the present work and from conceptual extensions to what has been covered here:

- Future research may address problems of pressure-depending bulk modulus. While fluid bulk modulus in hydraulics can in many cases be assumed constant, significant bulk modulus variations may contribute to system stability to an extent unforeseen by the models outlined in the present work.

With regard to the control approaches discussed, bulk modulus variations from pressure differences are expected to not fundamentally alter the effectiveness of the control designs. The reason lies in the systems' relative degrees: Pressure dynamics enter the Lie derivatives at  $r$ -th order in all cases discussed here – thereby system capacitances enter the control laws as parameters which no further derivatives are needed for. As a consequence, bulk modulus variations can – in theory – be compensated for by the control laws accordingly. Selected numerical experiments conducted in this context support this expectation as the control designs have shown to be robust with respect to bulk modulus variations.

- Damping in hydraulic valves was modeled with a simple viscous damping element in the present work. Thereby, damping was implicitly taken as a system parameter of its own without any explicit relation to operating conditions, most importantly temperature. As laid out in chapter 1, damping in hydraulic elements derives from fluid shear forces acting on valve spools subject to displacement to a large extent. While the modeling approach pursued in this thesis allowed for a separate consideration of leakage and damping effects on equilibrium stability especially in chapter 6 and thereby for regulator valve or dashpot design recommendations, a refined model for damping from fluid viscosity in ring gaps may be worth pursuing.
- Other modeling aspects possibly worth incorporating in future models of hydraulic systems are friction elements capturing valve spool friction. This is an additional nonlinearity with the potential to introduce complex effects to the dynamics of hydraulic systems. In addition, effects from flow forces may be investigated.
- Another aspect whose relevance for dynamic phenomena in hydraulic systems has remained largely ignored in the research community is the effect of pressure and volume flow pulsations stemming from a finite number of pump chambers. Incorporating this into dynamic analysis necessitates a Floquet theory approach. Given the significant number of physical parameters in hydraulic systems, the numerical stiffness and non-smoothness that stands to qualitatively characterize such systems on macro scale even after leakage regularization, the success of such effort is uncertain, however.
- While the theoretical assessment and the simulation results of the control designs proposed in this work are a positive indication, questions of robustness with respect to unmodeled dynamics, noisy measurements or time delays to be expected

in real-world actuation hardware are an important issue to be addressed when implementing the designs on a test-rig. Here, future research may shed further light on these aspects. In addition, refined trajectory planning may be needed.

- Conceptually, the control concepts discussed in the second part of this work may be extended in the direction of a data-driven identification and control implementation approach, i.e. grey box modeling. This will likely be required in order to respond to changes in operating conditions – most commonly due to temperature changes – and otherwise unknown parameters or parasitic dynamics. While this was the original research intent of FFG-Project 850729, the system topology proposed in the second part of the present work proved too complex to build on a test-rig from scratch after project kick-off, making a stepwise approach based on the system modeled in chapter 4 necessary.

# Appendix



# A Theorems

**Theorem 1.** [40]: Suppose  $y_R(t), \dot{y}_R(t), \dots, y_R^{(r-1)}(t)$  are defined for all  $t \geq 0$  and bounded. Let  $\boldsymbol{\eta}_R(t)$  denote the solution of

$$\dot{\boldsymbol{\eta}} = \mathbf{q}(\boldsymbol{\xi}_R(t), \boldsymbol{\eta}) \quad (\text{A.1})$$

satisfying  $\boldsymbol{\eta}_R(0) = \mathbf{0}$ . Suppose this solution is defined for all  $t \geq 0$ , bounded and uniformly asymptotically stable. Finally, suppose the roots of the polynomial

$$s^r + c_{r-1}s^{r-1} + \dots + c_1s + c_0 = 0 \quad (\text{A.2})$$

all have negative real part. Then, for sufficiently small  $a > 0$ , if

$$|\xi_i(t^0) - y_R^{(i-1)}(t^0)| < a, \quad 1 \leq i \leq r, \quad \|\boldsymbol{\eta}(t^0) - \boldsymbol{\eta}_R(t^0)\| < a \quad (\text{A.3})$$

the corresponding response  $\xi_i(t), \boldsymbol{\eta}(t), t \geq t^0 \geq 0$ , of the closed loop system (7.1), (7.24), (7.26) is bounded. More precisely, for all  $\varepsilon > 0$ , there exists  $\delta > 0$  such that

$$|\xi_i(t^0) - y_R^{(i-1)}(t^0)| < \delta \Rightarrow |\xi_i(t) - y_R^{(i-1)}(t^0)| < \varepsilon \quad \text{for all } t \geq t^0 \geq 0, \quad (\text{A.4})$$

$$\|\boldsymbol{\eta}(t^0) - \boldsymbol{\eta}_R(t^0)\| < \delta \Rightarrow \|\boldsymbol{\eta}(t) - \boldsymbol{\eta}_R(t)\| < \varepsilon \quad \text{for all } t \geq t^0 \geq 0. \quad (\text{A.5})$$

**Theorem 2.** [53]: Let  $\mathbf{x} = \mathbf{0}$  be an equilibrium point for  $\dot{\mathbf{x}} = \mathbf{f}(t, \mathbf{x})$  and  $\mathcal{D} \subset \mathbb{R}^n$  be a domain containing  $\mathbf{x} = \mathbf{0}$ . Let  $V : [0, \infty) \times \mathcal{D} \rightarrow \mathbb{R}$  be a continuously differentiable function such that

$$W_1(\mathbf{x}) \leq V(t, \mathbf{x}) \leq W_2(\mathbf{x}), \quad (\text{A.6})$$

$$\frac{\partial V}{\partial t} + \frac{\partial V}{\partial \mathbf{x}} \mathbf{f}(t, \mathbf{x}) \leq -W_3(\mathbf{x}) \quad (\text{A.7})$$

$\forall t \geq 0, \forall \mathbf{x} \in \mathcal{D}$ , where  $W_1(\mathbf{x}), W_2(\mathbf{x})$  and  $W_3(\mathbf{x})$  are continuous positive definite functions on  $\mathcal{D}$ . Then  $\mathbf{x} = \mathbf{0}$  is uniformly asymptotically stable.

**Theorem 3.** [53]: Let  $D \subset \mathbb{R}^n$  be a domain that contains the origin and  $V : [0, \infty) \times D \rightarrow \mathbb{R}$  be a continuously differentiable function such that

$$\alpha_1(\|\mathbf{x}\|) \leq V(t, \mathbf{x}) \leq \alpha_2(\|\mathbf{x}\|), \quad (\text{A.8})$$

$$\frac{\partial V}{\partial t} + \frac{\partial V}{\partial \mathbf{x}} \mathbf{f}(t, \mathbf{x}) \leq -W_3(\mathbf{x}), \quad \forall \|\mathbf{x}\| \geq \mu > 0 \quad (\text{A.9})$$

$\forall t \geq 0$  and  $\forall \mathbf{x} \in \mathcal{D}$ , where  $\alpha_1$  and  $\alpha_2$  are class  $\mathcal{K}$  functions and  $W_3(\mathbf{x})$  is a continuous positive definite function. Take  $r > 0$  such that  $B_r \subset \mathcal{D}$  and suppose that

$$\mu < \alpha_2^{-1}(\alpha_1(r)). \quad (\text{A.10})$$

Then, there exists a class  $\mathcal{KL}$  function  $\beta$  and for every initial state  $\mathbf{x}(t_0)$ , satisfying  $\|\mathbf{x}(t_0)\| < \alpha_2^{-1}(\alpha_1(r))$ , there is  $T \geq 0$  (dependent on  $\mathbf{x}(t_0)$  and  $\mu$ ) such that the solution of

$$\dot{\mathbf{x}} = \mathbf{f}(t, \mathbf{x}) \quad (\text{A.11})$$

satisfies

$$\|\mathbf{x}(t)\| \leq \beta(\|\mathbf{x}(t_0)\|, t - t_0), \quad \forall t_0 \leq t \leq t_0 + T, \quad (\text{A.12})$$

$$\|\mathbf{x}(t)\| \leq \alpha_2^{-1}(\alpha_1(r)), \quad \forall t \geq t_0 + T. \quad (\text{A.13})$$

Moreover, if  $\mathcal{D} = \mathbb{R}^n$  and  $\alpha_1$  belongs to  $\mathcal{K}_\infty$ , then (A.12) and (A.13) hold for any initial state  $\mathbf{x}(t_0)$ , with no restriction on how large  $\mu$  is.

**Lemma 1. (Barbalat's Lemma) [3]**: If  $g$  is a real function of a real variable  $t$ , defined and uniformly continuous for  $t \geq 0$  and if the limit of the integral

$$\int_0^t g(s) ds \quad (\text{A.14})$$

exists as  $t$  tends to infinity and if it is a finite number, then

$$\lim_{t \rightarrow \infty} g(t) = 0. \quad (\text{A.15})$$

A much used consequence of Barbalat's lemma (see also [3]) is that if  $g \in \mathcal{L}_2$  and  $dg/dt$  is bounded, then

$$\lim_{t \rightarrow \infty} g(t) = 0. \quad (\text{A.16})$$

## Bibliography

- [1] ADAMY, J. *Nichtlineare Regelungen*. Springer-Verlag Berlin Heidelberg, 2009.
- [2] AKERS, A., GASSMAN, M., AND SMITH, R. *Hydraulic Power System Analysis*. CRC press, 2006.
- [3] ÅSTRÖM, K., AND WITTENMARK, B. *Adaptive Control*. Dover, 2008.
- [4] BAUER, G. *Ölhydraulik*. 9. Vieweg, 2009.
- [5] BEALE, S., AND SHAFAI, B. Robust control system design with a proportional integral observer. *International Journal of Control* 50, 1 (1989), 97–111.
- [6] BEATER, P. *Entwurf hydraulischer Maschinen: Modellbildung, Stabilitätsanalyse und Simulation hydrostatischer Antriebe und Steuerungen*. Springer-Verlag, 2013.
- [7] BORCHSENIUS, F. *Simulation ölhydraulischer Systeme*. VDI-Verlag, 2003.
- [8] BOSCH REXROTH AG. *Verstellbare Flügelzellenpumpe, vorgesteuert*.
- [9] BRANICKY, M. Multiple Lyapunov functions and other analysis tools for switched and hybrid systems. *IEEE Transactions on Automatic Control* 43, 4 (1998), 475–482.
- [10] BRYSON, A., AND HO, Y. *Applied Optimal Control: Optimization, Estimation and Control*. CRC Press, 1975.
- [11] CAVALLARI, M. *A Lumped Parameter Model for the Pressure and Vibration Analysis of Variable Displacement Vane Pumps*. PhD thesis, Università degli Studi di Ferrara, 2011.
- [12] CHEN, J., AND PATTON, R. *Robust Model-Based Fault Diagnosis for Dynamic Systems*. Springer Science & Business Media, 2012.
- [13] CHEN, J., PATTON, R., AND ZHANG, H. Design of unknown input observers and robust fault detection filters. *International Journal of Control* 63, 1 (1996), 85–105.
- [14] CHEN, W. Disturbance-observer-based control for nonlinear systems. *IEEE/ASME Transactions on Mechatronics* 9, 4 (2004), 706–710.
- [15] CHEN, W., BALLANCE, D., GAWTHROP, P., AND O'REILLY, J. A nonlinear disturbance observer for robotic manipulators. *IEEE Transactions on Industrial Electronics* 47, 4 (2000), 932–938.

- [16] CHIRIBOGA, J., THEIN, M., AND MISAWA, E. Input-output feedback linearization control of a load-sensing hydraulic servo system. In *Proceedings of the 4th IEEE Conference on Control Applications* (1995), IEEE, pp. 910–915.
- [17] COX, C., AND FRENCH, I. Limit cycle prediction conditions for a class of hydraulic control systems. *Journal of Dynamic Systems, Measurement and Control* 108, 1 (1986), 17–23.
- [18] CUNDIFF, J. *Fluid Power Circuits and Controls: Fundamentals and Applications*. CRC Press, 2001.
- [19] DI BERNARDO, M., BUDD, C., CHAMPNEYS, A., AND KOWALCZYK, P. *Piecewise-Smooth Dynamical Systems: Theory and Applications*. Springer Science & Business Media, 2008.
- [20] DI BERNARDO, M., BUDD, C., CHAMPNEYS, A., KOWALCZYK, P., NORDMARK, A., TOST, G., AND PIROINEN, P. Bifurcations in nonsmooth dynamical systems. *SIAM Review* 50, 4 (2008), 629–701.
- [21] ELLMAN, A. Leakage behaviour of four-way servo valve. In *ASME Fluid Power Systems and Technology Division, International Mechanical Engineering Congress and Exposition* (1998), vol. 5, pp. 163–167.
- [22] ERYILMAZ, B., AND WILSON, B. Combining leakage and orifice flows in a hydraulic servo valve model. *Journal of Dynamic Systems, Measurement and Control* 122, 3 (2000), 576–579.
- [23] FINDEISEN, D. *Ölhydraulik*. Springer-Verlag, 2006.
- [24] FISCHER, R., KÜCÜKAY, F., JÜRGENS, G., NAJORK, R., AND POLLAK, B. *Das Getriebebuch*. Springer-Verlag Wien, 2012.
- [25] FRIEDLAND, B. *Control System Design: An Introduction to State-Space Methods*. Courier Corporation, 2012.
- [26] GEERING, H. *Regelungstechnik: Mathematische Grundlagen, Entwurfsmethoden, Beispiele*. Springer-Verlag, 2013.
- [27] GEIST, B., AND RESH, W. Dynamic modeling of a variable displacement vane pump within an engine oil circuit. In *ASME 2011 Internal Combustion Engine Division Fall Technical Conference* (2011), American Society of Mechanical Engineers, pp. 857–870.
- [28] GHANADAN, R. *Adaptive Control of Nonlinear Systems with Applications to Flight Control Systems and Suspension Dynamics*. PhD thesis, University of Maryland, 1993.

- [29] GROSS, D., HAUGER, W., SCHNELL, W., AND WRIGGERS, P. *Technische Mechanik 4*. Springer-Verlag, 2002.
- [30] GÜCKER, J. *Experimentelle Identifikation und nichtlineare Regelung eines einachsigen servohydraulischen Antriebs*. PhD thesis, Universität Kassel, 2006.
- [31] HAGENMEYER, V., AND DELALEAU, E. Exact feedforward linearization based on differential flatness. *International Journal of Control* 76, 6 (2003), 537–556.
- [32] HAHN, H., PIEPENBRINK, A., AND LEIMBACH, K. Input-output linearization control of an electro-servo-hydraulic actuator. In *Proceedings of the Third IEEE Conference on Control Applications* (1994), IEEE, pp. 995–1000.
- [33] HEISEL, U., FIEBIG, W., AND MATTEN, N. Betrachtungen zum dynamischen Verhalten druckgeregelter Flügelzellenpumpen. *Ölhydraulik und Pneumatik* 34 (1990), 429–432.
- [34] HEISEL, U., FIEBIG, W., AND MATTEN, N. Druckwechsellvorgänge in druckgeregelten Flügelzellenpumpen. *Ölhydraulik und Pneumatik* 35 (1991), 906–913.
- [35] HIRSCHORN, R. Invertibility of multivariable nonlinear control systems. *IEEE Transactions on Automatic Control* 24 (1979), 855–865.
- [36] HO, D., AND HEDRICK, J. Control of nonlinear non-minimum phase systems with input-output linearization. In *American Control Conference (ACC), 2015* (2015), IEEE, pp. 4016–4023.
- [37] HOFFMANN, W. *Dynamisches Verhalten hydraulischer Systeme, automatischer Modelaufbau und digitale Simulation*. PhD thesis, RWTH Aachen, 1981.
- [38] HOSHIYA, M., AND SAITO, E. Structural identification by extended kalman filter. *Journal of Engineering Mechanics* 110, 12 (1984), 1757–1770.
- [39] INEICHEN, L. *Konzeptvergleich zur Bekämpfung der Torsionsschwingungen im Antriebsstrang eines Kraftfahrzeugs*. PhD thesis, Karlsruher Institut für Technologie, 2013.
- [40] ISIDORI, A. *Nonlinear Control Systems*. Springer-Verlag, 1995.
- [41] JELALI, M., AND KROLL, A. *Hydraulic Servo-Systems: Modelling, Identification and Control*. Springer Science & Business Media, 2012.
- [42] JO, N.H. AND SEO, J. Input-output linearization approach to state observer design for nonlinear systems. *IEEE Transactions on Automatic Control* 45, 12 (2000), 2388–2393.

- [43] JULIER, S., AND UHLMANN, J. A new extension of the Kalman filter to nonlinear systems. In *AeroSense'97* (1997), International Society for Optics and Photonics, pp. 182–193.
- [44] KANELLAKOPOULOS, I., KOKOTOVIC, P., AND MARINO, R. An extended direct scheme for robust adaptive nonlinear control. *Automatica* 27, 2 (1991), 247–255.
- [45] KARMEL, A. A study of the internal forces in a variable-displacement vane-pump—part i: A theoretical analysis. *Journal of Fluids Engineering* 108, 2 (1986), 227–232.
- [46] KARMEL, A. A study of the internal forces in a variable-displacement vane-pump—part ii: A parametric study. *Journal of Fluids Engineering* 108, 2 (1986), 233–237.
- [47] KARMEL, A. Stability and regulation of a variable-displacement-vane-pump. In *American Control Conference* (1987), pp. 347–354.
- [48] KARMEL, A. Modeling and analysis of the dynamics of a variable-displacement vane-pump with a pivoting cam. *Journal of Dynamic Systems, Measurement and Control* 110, 2 (1988), 197–202.
- [49] KARMEL, A. Stability and regulation of a variable-displacement vane-pump. *Journal of Dynamic Systems, Measurement and Control* 110, 2 (1988), 203–209.
- [50] KAVANAGH, G. The dynamic modelling of an axial piston hydraulic pump. Master's thesis, University of Saskatchewan, 1987.
- [51] KEMMETMÜLLER, W., FUCHSHUMER, F., AND KUGI, A. Nonlinear pressure control of self-supplied variable displacement axial piston pumps. *Control Engineering Practice* 18, 1 (2010), 84–93.
- [52] KENDERI, G., AND FIDLIN, A. Nonparametric identification of nonlinear dynamic systems using a synchronisation-based method. *Journal of Sound and Vibration* 333, 24 (2014), 6405–6423.
- [53] KHALIL, H., AND GRIZZLE, J. *Nonlinear Systems*. Prentice Hall, 1996.
- [54] KIM, S., CHO, H., AND LEE, C. A parameter sensitivity analysis for the dynamic model of a variable displacement axial piston pump. *Proceedings of the Institution of Mechanical Engineers, Part C: Journal of Mechanical Engineering Science* 201, 4 (1987), 235–243.
- [55] KOKOTOVIĆ, P., KANELLAKOPOULOS, I., AND MORSE, A. Adaptive feedback linearization of nonlinear systems. In *Foundations of adaptive control*. Springer Berlin Heidelberg, 1991, pp. 309–346.

- 
- [56] KREMER, E. About absolute stability of control valves. In *ENOC 2008* (2008).
- [57] KREMER, G., AND THOMPSON, D. A bifurcation-based procedure for designing and analysing robustly stable non-linear hydraulic servo systems. *Proceedings of the Institution of Mechanical Engineers, Part I: Journal of Systems and Control Engineering* 212, 5 (1998), 383–394.
- [58] KRUS, P. *On Load Sensing Fluid Power Systems*. PhD thesis, Linköping University, 1988.
- [59] KUGI, A. *Nonlinear Control Based on Physical Models: Electrical, Hydraulic, and Mechanical Systems*. Springer-Verlag New York, Inc., 2001.
- [60] KWAKERNAAK, H., AND SIVAN, R. *Linear Optimal Control Systems*. Wiley Interscience New York, 1972.
- [61] LIBERZON, D. *Switching in Systems and Control*. Springer Science & Business Media, 2012.
- [62] LIBERZON, D., AND MORSE, A. Basic problems in stability and design of switched systems. *IEEE Control systems* 19, 5 (1999), 59–70.
- [63] LICSKÓ, G., CHAMPNEYS, A., AND HÓS, C. Dynamical analysis of a hydraulic pressure relief valve. In *Proceedings of the World Congress on Engineering* (2009), vol. 2.
- [64] LIU, Y., AND SÖFFKER, D. Robust control approach for input-output linearizable nonlinear systems using high-gain disturbance observer. *International Journal of Robust and Nonlinear Control* 24, 2 (2014), 326–339.
- [65] LUNZE, J. *Regelungstechnik 2: Mehrgrößensysteme – Digitale Regelung*. Springer-Verlag, 2012.
- [66] LYNCH, S. *Dynamical Systems with Applications Using MATLAB*. Springer, 2004.
- [67] MAGORIEN, V. Effects of air on hydraulic systems. *Hydraulics & Pneumatics* 20, 10 (1967), 128.
- [68] MAITI, R., SAHA, R., AND WATTON, J. The static and dynamic characteristics of a pressure relief valve with a proportional solenoid-controlled pilot stage. *Proceedings of the Institution of Mechanical Engineers, Part I: Journal of Systems and Control Engineering* 216, 2 (2002), 143–156.
- [69] MANCO, S., NERVEGNA, N., RUNDO, M., AND ARMENIO, G. Modelling and simulation of variable displacement vane pumps for ic engine lubrication. Tech. Rep. 2004-01-1601, SAE Technical Paper, 2004.
- [70] MANRING, N. *Hydraulic Control Systems*. Wiley, 2005.

- [71] MANRING, N., AND JOHNSON, R. Modeling and designing a variable-displacement open-loop pump. *Journal of Dynamic Systems, Measurement and Control* 118, 2 (1996), 267–271.
- [72] MARINO, R., PERESADA, S., AND VALIGI, P. Adaptive input-output linearizing control of induction motors. *IEEE Transactions on Automatic Control* 38, 2 (1993), 208–221.
- [73] MERRITT, H. *Hydraulic Control Systems*. John Wiley & Sons, 1967.
- [74] MISRA, A., BEHDINAN, K., AND CLEGHORN, W. Self-excited vibration of a control valve due to fluid–structure interaction. *Journal of Fluids and Structures* 16, 5 (2002), 649–665.
- [75] MURRENHOFF, H. *Grundlagen der Fluidtechnik, Teil 1: Hydraulik*. Shaker, 2001.
- [76] NELLES, O. *Nonlinear System Identification: From Classical Approaches to Neural Networks and Fuzzy Models*. Springer Science & Business Media, 2001.
- [77] PARKER, T., AND CHUA, L. *Practical Numerical Algorithms for Chaotic Systems*. Springer Science & Business Media, 2012.
- [78] PELETIES, P., AND DECARLO, R. Asymptotic stability of m-switched systems using Lyapunov functions. In *Proceedings of the 31st IEEE Conference on Decision and Control* (1992), IEEE, pp. 3438–3439.
- [79] PERKO, L. *Differential Equations and Dynamical Systems*. Springer Science & Business Media, 2013.
- [80] PETERSSON, H., KRUS, P., JANSSON, A., AND PALMBERG, J. The design of pressure compensators for load sensing hydraulic systems. In *Control'96, UKACC International Conference on (Conf. Publ. No. 427)* (1996), vol. 2, IET, pp. 1456–1461.
- [81] PFEIFFER, F. *Mechanical System Dynamics*. Springer Science & Business Media, 2008.
- [82] RAJAMANI, R. Observers for Lipschitz nonlinear systems. *IEEE Transactions on Automatic Control* 43, 3 (1998), 397–401.
- [83] RAJAMANI, R., AND CHO, Y. Existence and design of observers for nonlinear systems: Relation to distance to unobservability. *International Journal of Control* 69, 5 (1998), 717–731.
- [84] RAJAMANI, R., AND HEDRICK, J. Adaptive observers for active automotive suspensions: Theory and experiment. *Control Systems Technology, IEEE Transactions on* 3, 1 (1995), 86–93.

- [85] RÖBENACK, K. Zum High-Gain-Beobachterentwurf für eingangsausgangslinearisierte SISO-Systeme. *at-Automatisierungstechnik* 52 (2004), 481–488.
- [86] RÖBENACK, K. Observer design for a class of nonlinear systems with non-full relative degree. *Nonlinear Dynamics and Systems Theory* 7, 4 (2007), 399–408.
- [87] ROTHFUSS, R. *Anwendung der flachheitsbasierten Analyse und Regelung nichtlinearer Mehrgrößensysteme*. PhD thesis, Universität Stuttgart, 1997.
- [88] ROTHFUSS, R., RUDOLPH, J., AND ZEITZ, M. Flatness-based control of a nonlinear chemical reactor model. *Automatica* 32, 10 (1996), 1433–1439.
- [89] ROTHFUSS, R., RUDOLPH, J., AND ZEITZ, M. Flachheit: ein neuer Zugang zur Steuerung und Regelung nichtlinearer Systeme. *at-Automatisierungstechnik* 45, 11 (1997), 517–525.
- [90] RUNDO, M., AND NERVEGNA, N. Geometry assessment of variable displacement vane pumps. *Journal of Dynamic Systems, Measurement and Control* 129, 4 (2007), 446–455.
- [91] SASTRY, S. *Nonlinear Systems: Analysis, Stability and Control*. Springer New York, 1999.
- [92] SASTRY, S., AND BODSON, M. *Adaptive control: stability, convergence and robustness*. Courier Corporation, 2011.
- [93] SASTRY, S., AND ISIDORI, A. Adaptive control of linearizable systems. *IEEE Transactions on Automatic Control* 34, 11 (1989), 1123–1131.
- [94] SCHOENAU, G., BURTON, R., AND KAVANAGH, G. Dynamic analysis of a variable displacement pump. *Journal of Dynamic Systems, Measurement and Control* 112, 1 (1990), 122–132.
- [95] SCHOLZ, D. *Proportionalhydraulik*. Springer, 1997.
- [96] SCHWARTZ, C., AND MAREELS, I. Comments on "Adaptive control of linearizable systems" by S. Sastry and A. Isidori. *IEEE Transactions on Automatic Control* 37, 5 (1992), 698–701.
- [97] SEIFRIED, R. *Dynamics of Underactuated Multibody Systems*. Springer, 2014.
- [98] SEO, J., VENUGOPAL, R., AND KENNÉ, J. Feedback linearization based control of a rotational hydraulic drive. *Control Engineering Practice* 15, 12 (2007), 1495–1507.
- [99] SHORTEN, R., WIRTH, F., MASON, O., WULFF, K., AND KING, C. Stability criteria for switched and hybrid systems. *SIAM Review* 49, 4 (2007), 545–592.

- [100] SHUKLA, A., AND THOMPSON, D. Bifurcation stability of servo-hydraulic systems. In *American Control Conference, 2001. Proceedings of the 2001* (2001), vol. 5, IEEE, pp. 3943–3948.
- [101] SIMON, D. *Optimal State Estimation: Kalman, H-infinity and Nonlinear Approaches*. John Wiley & Sons, 2006.
- [102] SINGH, A. An analytical study of the dynamics and stability of a spring loaded safety valve. *Nuclear Engineering and Design* 72, 2 (1982), 197–204.
- [103] SLOTINE, J., AND LI, W. *Applied Nonlinear Control*, vol. 199. Prentice-Hall Englewood Cliffs, NJ, 1991.
- [104] SÖFFKER, D., YU, T., AND MÜLLER, P. State estimation of dynamical systems with nonlinearities by using proportional-integral observer. *International Journal of Systems Science* 26, 9 (1995), 1571–1582.
- [105] SOHL, G., AND BOBROW, J. Experiments and simulations on the nonlinear control of a hydraulic servo system. *Control Systems Technology, IEEE Transactions on* 7, 2 (1999), 238–247.
- [106] SPURK, J. *Strömungslehre: Einführung in die Theorie der Strömungen*. Springer-Verlag, 2013.
- [107] STEINBOECK, A., KEMMETMÜLLER, W., LASSL, C., AND KUGI, A. Model-based condition monitoring of an electro-hydraulic valve. *Journal of Dynamic Systems, Measurement and Control* 135, 6 (2013), 1–9.
- [108] SVARICEK, F. Nulldynamik linearer und nichtlinearer Systeme: Definitionen, Eigenschaften und Anwendungen. *at-Automatisierungstechnik* 54, 7/2006 (2006), 310–322.
- [109] TAYLOR, D., KOKOTOVIC, P., MARINO, R., AND KANNELLAKOPOULOS, I. Adaptive regulation of nonlinear systems with unmodeled dynamics. *IEEE Transactions on Automatic Control* 34, 4 (1989), 405–412.
- [110] TEEL, A., KADIYALA, R., KOKOTOVIC, P., AND SASTRY, S. Indirect techniques for adaptive input-output linearization of nonlinear systems. *International Journal of Control* 53, 1 (1991), 193–222.
- [111] THOMPSON, D., AND KREMER, G. Quantitative feedback design for a variable displacement hydraulic vane pump. In *American Control Conference, 1997. Proceedings of the 1997* (1997), vol. 2, IEEE, pp. 1061–1065.
- [112] THOMPSON, D., AND KREMER, G. Quantitative feedback design for a variable-displacement hydraulic vane pump. *Optimal Control Applications & Methods* 19, 2 (1998), 63–92.

- 
- [113] VAUGHAN, N., AND GAMBLE, J. The modeling and simulation of a proportional solenoid valve. *Journal of Dynamic Systems, Measurement and Control* 118, 1 (1996), 120–125.
- [114] VIERSMA, T. *Analysis, Synthesis and Design of Hydraulic Servo Systems and Pipelines*. Elsevier, 1980.
- [115] VOSSOUGH, G., AND DONATH, M. Dynamic feedback linearization for electrohydraulically actuated control systems. *Journal of Dynamic Systems, Measurement and Control* 117, 4 (1995), 468–477.
- [116] VYASARAYANI, C., UCHIDA, T., CARVALHO, A., AND MCPHEE, J. Parameter identification in dynamic systems using the homotopy optimization approach. *Multibody System Dynamics* 26, 4 (2011), 411–424.
- [117] WAN, E., AND VAN DER MERWE, R. The unscented Kalman filter for nonlinear estimation. In *Adaptive Systems for Signal Processing, Communications, and Control Symposium 2000*. (2000), IEEE, pp. 153–158.
- [118] WEINMANN, A. *Uncertain Models and Robust Control*. Springer Science & Business Media, 2012.
- [119] WEY, T. *Nichtlineare Regelungssysteme*. Springer, 2002.
- [120] WIDMANN, R. *Geräuschminderung bei druckgeregelten Flügelzellenpumpen: Fördervorgang, Schallerregungsmechanismen und konstruktive Massnahmen zur Lärminderung*. Technischer Verlag Grossmann, 1985.
- [121] WIGGINS, S. *Introduction to Applied Nonlinear Dynamical Systems and Chaos*. Springer Science & Business Media, 2003.
- [122] WILL, D., AND GEBHARDT, N. *Hydraulik*. Springer, 2011.
- [123] WOWRIES, A. Der theoretische Förderstrom regelbarer Flügelzellenpumpen. *Ölhydraulik und Pneumatik* 2 (1964), 58–60.
- [124] WU, D. *Modeling and Experimental Evaluation of a Load-Sensing and Pressure Compensated Hydraulic System*. PhD thesis, University of Saskatchewan, 2003.
- [125] WU, D., BURTON, R., AND SCHOENAU, G. An empirical discharge coefficient model for orifice flow. *International Journal of Fluid Power* 3, 3 (2002), 13–19.
- [126] WU, D., BURTON, R., SCHOENAU, G., AND BITNER, D. Establishing operating points for a linearized model of a load sensing system. *International Journal of Fluid Power* 3, 2 (2002), 47–54.
- [127] WU, D., BURTON, R., SCHOENAU, G., AND BITNER, D. Modelling of orifice flow rate at very small openings. *International Journal of Fluid Power* 4, 1 (2003), 31–39.

- [128] WU, D., BURTON, R., SCHOENAU, G., AND BITNER, D. Analysis of a pressure-compensated flow control valve. *Journal of Dynamic Systems, Measurement and Control* 129, 2 (2007), 203–211.
- [129] WULFF, K. *Quadratic and Non-Quadratic Stability Criteria for Switched Linear Systems*. PhD thesis, National University of Ireland-Maynooth, 2004.
- [130] ZEIGER, G., AND AKERS, A. Torque on the swashplate of an axial piston pump. *Journal of Dynamic Systems, Measurement and Control* 107, 3 (1985), 220–226.
- [131] ZEITZ, M. Differenzielle Flachheit: Eine nützliche Methodik auch für lineare SISO-Systeme. *at-Automatisierungstechnik* 58, 1 (2010), 5–13.
- [132] ZEITZ, M. Flachheitsbasierter Entwurf linearer zeitvarianter SISO-Systeme. *at-Automatisierungstechnik* 58, 7 (2010), 351–360.
- [133] ZHANG, Q. Adaptive observer for MIMO linear time varying systems. Tech. rep., INRIA, 2001.
- [134] ZHANG, Q. Adaptive observer for multiple-input-multiple-output (MIMO) linear time-varying systems. *IEEE Transactions on Automatic Control* 47, 3 (2002), 525–529.

## Publications

- [135] FIDLIN, A. ; KÖSTER, M.: CPA - Developing a Simulink model and integrating it into a Simulink Drivetrain Model. *Project report for AVL List GmbH*, unpublished, 2012
- [136] KÖSTER, M. ; FIDLIN, A.: Nonlinear dynamics of a hydraulic pressure control valve. In: *Proceedings of the 11th International Conference on Vibration Problems*, 2013
- [137] FIDLIN, A.; JEHLE, G.; KÖSTER, M.: Kalman filtering as a method to identify system parameters. *Project report for AVL List GmbH*, unpublished, 2013
- [138] KÖSTER, M. ; JEHLE, G. ; FIDLIN, A.: System identification based on model synchronization. In: *Proc. Appl. Math. Mech.* 14 (2014), pp. 929-930
- [139] JEHLE, G. ; KÖSTER, M. ; FIDLIN, A. ; FRIDRICH, A.: On the influence of the fluid pipe on the stability of a mechanical system subjected to friction-induced vibrations. In: *Proceedings of ENOC 2014* (2014)
- [140] KÖSTER, M. ; FIDLIN, A.: Nonlinear volume flow control of a variable displacement vane pump. In: *Proc. Appl. Math. Mech.* 15 (2015), pp. 635-636
- [141] KOESTER, M.; FIDLIN, A.: Nonlinear volume flow control of a variable displacement vane pump. *Project report for AVL List GmbH*, unpublished, 2015
- [142] KÖSTER, M. ; FIDLIN, A.; SCHRÖDERS, S.: Modeling and simulating a variable displacement vane pump. In: *Proc. Appl. Math. Mech.* 16 (2016), pp. 281-282
- [143] KÖSTER, M.; FIDLIN, A.: A minimal model for a variable displacement vane pump and a nonlinear local observer for a hydraulic control system. *Project report for AVL List GmbH*, unpublished, 2016



## Supervision of student thesis assignments

- [144] PROBST, M.: *Identifikation dynamischer Systeme mit einer homotopischen Methode: Potentiale und Grenzen*, Karlsruher Institut für Technologie, Bachelor's-Thesis, 2014
- [145] GUNNARSSON, G.S.: *Identification of dynamical systems with a homotopy method: applications*, Karlsruher Institut für Technologie, Bachelor's-Thesis, 2014
- [146] ENGELHORN, F.: *Synthese eines Verstellpumpensystems*, Karlsruher Institut für Technologie, Bachelor's-Thesis, 2015
- [147] SCHRÖDERS, S.: *Modellbildung, numerische Simulation und Stabilitätsuntersuchung eines selbstregelnden hydraulischen Systems*, Karlsruher Institut für Technologie, Master's-Thesis, 2016
- [148] WANG, T.: *Co-Simulation eines TMC-Pumpenmodells*, Karlsruher Institut für Technologie, Master's-Thesis, 2016